OSAME, P.U. 2024. *Hydrodynamic characterisation of soil subsurface flows for water conservation purposes*. Robert Gordon University, PhD thesis. Hosted on OpenAIR [online]. Available from: https://doi.org/10.48526/rgu-wt-2795739

Hydrodynamic characterisation of soil subsurface flows for water conservation purposes.

OSAME, P.U.

2024

HYDRODYNAMIC CHARACTERISATION OF SOIL SUBSURFACE FLOWS FOR WATER CONSERVATION PURPOSES

Peter Uloho Osame

PhD 2024

HYDRODYNAMIC CHARACTERISATION OF SOIL SUBSURFACE FLOWS FOR WATER CONSERVATION PURPOSES

Peter Uloho Osame

A thesis submitted in partial fulfilment of the requirements of the

Robert Gordon University

For the award of the degree of Doctor of Philosophy

(School of Engineering)

October 2024

HYDRODYNAMIC CHARACTERISATION OF SOIL SUBSURFACE FLOWS FOR WATER CONSERVATION PURPOSES

PhD Candidate

Peter Uloho Osame

Supervisory Team

Dr Taimoor Asim (Principal supervisor)

Dr Sheikh Zahidul Islam

Dr Dallia Ali

School of Engineering, Robert Gordon University, The Sir Ian Wood Building, Riverside East, Garthdee Road, Aberdeen, AB10 7GJ, United Kingdom

Funding Organisation

Tertiary Education Trust Fund, Abuja, Nigeria

Declaration

I hereby declare that the research report in this thesis is original and that I, Peter Uloho Osame, performed it independently under the supervision of Dr Taimoor Asim, Dr Sheikh Zahidul Islam and Dr Dallia Ali. This thesis has not been submitted for consideration for any other degree or professional qualification.

Dedication

To my father, Late **Mr Lawrence Fati Osame** who promised to sponsor me to any level in education when I emerged in the first position in primary school leaving certificate year, but he passed away the same year. This promise has been my inspiration whenever I cry to my God.

And to all those who are driven by inspiration to move on in life.

Acknowledgements

I am most grateful to my principal supervisor, **Dr Taimoor Asim**, who opened the book of fluid dynamics and freely granted me unlimited access to it, teaching me to see things in four dimensions. He practically steered the research with open access to internal funding to enable procurement of every equipment needed for standard results. I am also very grateful to other members of the supervisory team: Dr Sheikh Zahidul Islam for his invaluable role in my exposure to the Ansys fluent software, and Dr Dalia Ali for her strong advice on the structure of the research. Dr Nazmi Sellami groomed me and seamlessly took me through the initial complex stages of the research journey. I am grateful to the entire members of the school of engineering in general, and the following members of the school with whom I had personal encounter in the course of this research: Prof Nadimul Haque Faisal who was readily available whenever I needed help, and freely granted me access to the metallurgical samples and materials preparation lab to use as my work station; Prof Radhakrishna Prabhu and Prof Mamdud Hossain for their invaluable advice and encouragement; Dr Gbenga Oluyemi for his very important advice on the texture and structure of the soil samples; Dr Clare O'Farrel and Dr Aditya Karnik whom I worked with as Demonstrator; Dr Judith Abolle-Okoyeagu and Dr Russein Mahon for their words of encouragement.

I deeply appreciate the technical team headed by the Engineering Services manager, Phil Chaplain, Allan McLean; Alan McPherson for his suggestion of aluminium box section to build the rig; Alexander Laing for practically constructing the rig; David Howie and Patrick Kayne for always assisting whenever I raised a complaint in the workshop. I also thank Dr Roslyn Shanks, Kirsty, Kiall, Tracey who readily tackled my administrative issues, and RGU Reslife for sorting out accommodation issues for me.

I am grateful to my colleagues in the engineering research hub with whom I shared the fun and the stress while it lasted; Ebikapaye, Sani, Florence, Ayatte, Amina, Idris, Vinooth, Hareesh, Obinna, Maria, Evans, MaryJane and my friend Stella Mukolu.

With a deep sense of love, I appreciate my lovable children; Nicholas, Liberty, Reginald, Theodora and Xavier the youngest, who joined my family back home during the pandemic in August 2020 while I was already away from them in a lockdown for the quest for knowledge. I sincerely appreciate my wife, Patience Osame, who bore the "sweetness" of childbirth at such a time all alone.

My sincere thanks to my two Professors, James Asalor and Godwin Ovuworie, who provided references for me to secure the admission and my former Vice Chancellor at the Delta State University, Abraka, Nigeria, Prof Victor Peretomode, who did not only run the race to provide the funding for the research, but also visited RGU with his wife, Dr (Mrs) Otaroghene Peretomode in the course of the research to see how we were faring. I am grateful to the Delta State University, Abraka, Nigeria and my sponsor, Tertiary Education Trust Fund (TETFund) Abuja, Nigeria, for the sponsorship of this research.

I thank Dr John Newstead and Stephen Williams of Delta-T Devices for supplying the logging equipment and constantly giving their support throughout the research.

Above all, the mighty presence of the Almighty God is deeply acknowledged.

Peter Uloho Osame
October 2024

Abstract

This study focuses on the hydrodynamic characterisation of soil subsurface flows using developed new soil column experimental setup to assess the hydraulic parameters of unsaturated soil in the laboratory. The soils in the inland valley of Nigeria's Niger Delta, where agriculture uses more than one-third of the clean water available, is the subject of the study. The Nigerian agriculture industry needs more effective water management as, when it comes to irrigation, flood irrigation being the most widely used technique, farmers primarily rely on experience rather than empirical data. The study seeks to provide a better understanding of the complex hydrodynamics of water flow through soil subsurface. A purpose-built cylindrical vertical soil column rig is constructed, and the volumetric soil water content θ (%) and soil matric potential Ψ (kPa) are measured using precision sensors. The soil water characteristics curve is obtained as a relationship between the volumetric soil water content and the soil matric potential. Gravity-driven flow experiments are conducted on two distinct monoliths of undisturbed soil samples from Ivrogbo and Oleh in the Niger Delta inland valley of Nigeria, and a homogeneous packed sample of the soil from Aberdeen in the United Kingdom for comparative purposes. Experiments are carried out on the monoliths of undisturbed soil samples once in each case, whereas experiment is conducted on the packed sample before it is further agitated to simulate ploughing and subsequent infiltration experiments are carried out on it, making four samples on the whole.

The Van Genuchten model of the soil water characteristics curve has been used for the verification of the experimental data. The volumetric soil water contents and soil matric potentials of the four samples are compared at different depths, which reveal a marked difference in their behaviour. Nonetheless, the range of values is smaller than the predicted curve. At 200 mm depth, the value of n is noticed to be 15 with θ_r of 0.046 and θ_s of 0.23 for the packed soil sample, giving a percentage difference of 86.7 % compared to n equal to 2 in the Van Genuchten curve. Also, for the ploughed sample, n equals 10 giving a percentage difference of 80 % but θ_r = 0.03 while θ_s = 0.23. For the Ivrogbo sample and Oleh samples, the range of the matric potential is relatively too small for the comparison. The pre-experiment moisture content of the soil samples is part of the cause of this,

in addition to differences in the soil type. Furthermore, the findings demonstrate a strong agreement between the measured behaviour and the predicted technique of the soil water characteristics curve. The results also show that ploughing improves soil homogeneity and uniform flow, which makes it more suitable for irrigation in agricultural settings. Additionally, the Oleh region soil sample needs less water to reach field capacity (i.e., the EU standard for crop comfort zone) and has the lowest negative matric potential (good water retention capabilities). Based on these results, farmers in the Oleh region can readily implement drip micro-irrigation.

Key Words: Hydrodynamics characterisation, Hydraulic parameters, Soil water content, Soil matric potential, Soil water retention, Soil subsurface flows, Soil column experiments.

Table of Contents

Declaration iv
Dedication v
Acknowledgements vi
Abstract viii
Table of Contents x
List of Figures xiv
List of Tables xix
Nomenclature xx
Chapter 1 Introduction 1
1.1 Background 2
1.2 Soil Classification and Flow Types 5
1.3 Consideration for Soil Subsurface Hydrodynamics Characterization 7
1.4 Soil Hydraulic Properties 9
1.4.1 Permeability 9
1.4.2 Soil Water Content 11
1.4.3 Soil Matric Potential 12
1.4.4 Soil Hydraulic Conductivity 14
1.4.5 Soil Water Diffusivity 15
1.4.6 Soil Water Characteristic Curve (SWCC) 17
1.4.7 Soil Pore Water Electrical Conductivity 20
1.5 Crops and Comfort Zones 22
1.6 Motivation 23
1.7 Research Aims 25
1.8 Thesis Outline 25
Chapter 2 Literature Review 28
2.1 Water Flow Processes Through Saturated and Unsaturated Soils 29
2.2 Models of Fluid Flow Through Variably Saturated Soils 34
2.2.1 Single Porosity Model 34
2.2.2 Dual Porosity Models 36
2.2.3 Dual Permeability Models 36
2.2.4 Multiple Porosity/Permeability Models 37
2.3 Experimental Measurement of Soil Hydraulic Properties 38

2.3.1 Field Measurement of Soil Hydraulic Properties 40
2.3.2 Soil Column Laboratory Measurement of Soil Hydraulic Properties. ... 43
2.4 Research Gaps in Knowledge 58
2.4.1 Research Objectives 59
Chapter 3 Methodology 60
3.1 Apparatus for The Experiments 61
3.1.1 The Aluminium Support Structure 63
3.1.2 The Supply Tank 65
3.1.3 The Soil Column 66
3.1.4 The Receiver Tank 67
3.1.5 Weighing Scales 67
3.1.6 Soil Water Content Recording System 68
3.1.7 Soil Matric Potential Recording System 69
3.1.8 Data Logging and Monitoring Devices 71
3.1.9 Application of Software 73
3.2 Test Materials 74
3.2.1 Packed Soil Samples from Aberdeen 74
3.2.2 Monolith of Undisturbed Soil Sample from Ivrogbo 75
3.2.3 Monolith of Undisturbed Soil Sample from Oleh 76
3.3 Experimental Procedure and Sequence 76
3.4 Correlation of Soil Water Retention Curve 78
3.4.1 Brooks and Corey Correlation 78
3.4.2 Van Genuchten Correlation 78
3.4.3 Fredlund and Xing Correlation 79
3.5 Technical Challenges 79
3.6 Scope of the Research 80
Chapter 4 Soil Water Content based Hydrodynamic Characterisation of Different Soil Types 82
4.1 Test Conditions 83
4.1.1 Packed Soil Sample 83
4.1.2 Monolith of Undisturbed Soil Sample from Ivrogbo 83
4.1.3 Monolith of Undisturbed Soil Sample from Oleh 84
4.2 Test Results 84
4.2.1 Packed Soil Sample 84
4.2.2 Ploughed Soil Sample 86

4.2.3 Test Results for Sieve Analysis of Monolith of Undisturbed Soil Sample from Ivrogbo 87
4.2.4 Test Results of Infiltration Experiment for Monolith of Soil Sample from Ivrogbo 93
4.2.5 Test Results for Sieve Analysis of Monolith of Undisturbed Soil Sample from Oleh 95
4.2.6 Test Results of Infiltration Experiment for Monolith of Soil Sample from Oleh 101
4.3 Soil Water Content 102
4.3.1 Measured Soil Water Content for the Packed Soil Sample from Aberdeen 102
4.3.2 Measured Soil Water Content for the Ploughed Soil Sample from Aberdeen 105
4.3.3 Measured Soil Water Content for Monolith of Undisturbed Soil Sample from Ivrogbo 107
4.3.4 Measured Soil Water Content for Monolith of Undisturbed Soil Sample from Oleh 110
4.3.5 Comparison of the Soil Water Content in the Soil Types 113
4.4 Summary of Key Findings 116
Chapter 5 Matric Potential based Hydrodynamic Characterisation of Different Soil Types 117
5.1 Soil Matric Potential 118
5.1.1 Measured Soil Matric Potential for Packed Soil Sample from Aberdeen 118
5.1.2 Measured Soil Matric Potential for Ploughed Soil Sample from Aberdeen 119
5.1.3 Measured Soil Matric Potential for Monolith of Soil Sample from Ivrogbo 121
5.1.4 Measured Soil Matric Potential for Monolith of Soil Sample from Oleh 123
5.1.5 Comparison of Soil Matric Potential in the Different Soil Types 125
5.2 Summary of key findings 128
Chapter 6 Hydrodynamic Characterisation of Different Soil Types based on Soil Water Characteristics Curve 129
6.1 Soil Water Characteristic Curve 130
6.1.1 Measured Soil Water Characteristic Curve (SWCC) For Packed Soil Sample 130
6.1.2 Measured Soil Water Characteristic Curve (SWCC) for Ploughed Soil Sample from Aberdeen 133

6.1.3 Measured Soil Water Characteristic Curve (SWCC) For Monolith of Soil Sample from Ivrogbo 136
6.1.4 Measured Soil Water Characteristic Curve (SWCC) For Monolith of Soil Sample from Oleh 139
6.2 Comparison of the Soil Water Characteristics Curves in the Soil types .. 144
6.3 Development of Smart Drip Micro-Irrigation System Based on Hydrodynamics Characterisation of Soils 146
6.4 Summary of Key Findings 148
Chapter 7 Conclusions 149
7.1 Research Problem Synopsis 150
7.2 Thesis Conclusion 151
7.3 Contribution to Knowledge 153
7.4 Recommendations for Future Work 154
References 155
Appendix 1. Simulated data for soil water characteristic curve (Van Genuchten 1980) 166
Appendix 2. Logged Data Generated from the soil column infiltration experiment for the Aberdeen packed soil sample 169
Appendix 3. Logged Data Generated from ploughed Aberdeen Soil Column Experiment 180
Appendix 4. Logged Data Generated from the Ivrogbo Soil Column Experiment 189
Appendix 5. Logged Data Generated from the Oleh Soil Column Experiment. 195

List of Figures

Figure 1.1. Global Water Availability (UNESCO World Water Assessment Programme 2022) 2
Figure 1.2. Household water consumption across some continents and countries of the earth (UNESCO World Water Assessment Programme 2022) 3
Figure 1.3. AASHTO classification chart for fine-grained soil (Moreno-Maroto, Alonso-Azcárate and O'Kelly 2021b) 6
Figure 1.4. Typical profile of the soil water retention curve (van Genuchten 1980) 8
Figure 1.8. Water potential scale for some crops (Taylor and Ashcroft 1972)... 23
Figure 2.1. (a) Coring of an undisturbed lysimeter core, (b) installed lysimeter, (c) instrumentation, and (d) view of a lysimeter setup with underground access (Pütz, Fank and Flury 2018) 39
Figure 2.2. Estimation of soil hydraulic conductivity (a) double ring infiltrometer (b) CSIRO positive-head tension permeameter, and (c) GUELPH constant head permeameter (Morbidelli et al. 2017) 41
Figure 2.3. (a) Sketch (b) Picture of the modified hood infiltrometer (Moret-Fernández et al. 2015) 43
Figure 2.4. Novel permeameter for laboratory measurement of unsaturated hydraulic conductivity (Gallage, Kodikara and Uchimura 2013)........ 44
Figure 2.5. (a) the schematic and (b) soil column for novel hydrogeophysical probe (Bienvenue, Xie and Niu 2022) 45
Figure 2.6. Soil column for water flow in unsaturated soil (Hou, Xiaokun, Vanapalli and Li 2019) 46
Figure 2.7. SWCC for the loess test (Hou, Xiaokun, Vanapalli and Li 2019)..... 47
Figure 2.8. Effect of volume change on soil water retention curve. (a) K-8 (b) Takeda (c) Sasaguri (d) Fukuchi (Liu, Q. et al. 2012) 48
Figure 2.9. (a) Soil column laboratory set-up for volcanic soil monolith (Ritter et al. 2004) 49
Figure 2.9. (b) Soil moisture retention curves observed in the monolith. Measured data (symbols) and fitted van Genuchten curves (lines) (Ritter et al. 2004) 50

Figure 2.10a. Soil column experiment for studying macropore flow processes: (a) column with instrumentation and (b) complete setup (Köhne, J. and Mohanty 2005) 52
Figure 2.10b. Hydraulic van Genuchten functions for matrix and macropore obtained by inverse parameter estimation of approach ARE for drainage, infiltration, and upward infiltration experiments: (a) water retention and (b) hydraulic conductivity (Köhne, J. and Mohanty 2005) 53
Figure 2.11. Soil column experiment for the determination of soil pore water electrical conductivity (Aljoumani, Sanchez-Espigares and Wessolek 2018) 54
Figure 3.1 (a) CAD model of the soil column test rig (b) Fabricated experimental setup used as workstation for the soil column experiment. 63
Figure 3.2. (a) CAD model of rig frame 64
Figure 3.2.(b) photo image of the rig frame with castor wheels 65
Figure 3.3. Supply tank 66
Figure 3.4. (a) Samples of soil column (b) Soil column instrumented with sensors 67
Figure 3.5. photo image of the weighing scale 68
Figure 3.6. WET150 sensor for soil water measurement. 69
Figure 3.7. EQ3 Equitensiometer 71
Figure 3.8. GP2 Data Logger 72
Figure 3.9. DeltaLINK 3.9 interface for the GP2 Data Logger. 74
Figure 3.10. Unsaturated soil column with sensors before experiment 77
Figure 4.1. Test output graph for Ivrogbo soil 89
Figure 4.2. Atterberg Limit Test Output Graph for Ivrogbo 90
Figure 4.3. Weight of Ivrogbo soil column and sensors before the experiment . 94
Figure 4.4. Arrangement for the experiment of the Ivrogbo soil sample 94
Figure 4.5. Test Output Graph for Oleh Soil 96
Figure 4.6. Atterberg Limit Test Output Graph for Oleh Soil 97
Figure 4.7. Domain-specific volumetric soil water content at 100 mm depth for Aberdeen packed soil sample 103
Figure 4.8. Domain-specific volumetric soil water content at 200 mm depth for Aberdeen packed soil sample 104
Figure 4.9. Domain-specific volumetric soil water content at 300mm depth for Aberdeen packed soil sample 104

Figure 4.10. Infiltration experiment showing domain-specific water content at depths of (a) 100 mm (b) 200 mm (c) 300 mm for packed soil sample 105
Figure 4.11. Domain-specific volumetric soil water content at 100mm depth for Aberdeen ploughed soil sample 106
Figure 4.12. Domain-specific volumetric soil water content at 200mm depth for Aberdeen ploughed soil sample 106
Figure 4.13. Domain-specific volumetric soil water content at 300mm depth for Aberdeen ploughed soil sample 107
Figure 4.14. Infiltration experiment showing domain specific water content at depths of (a) 100 mm (b) 200 mm (c) 300 mm using the Aberdeen ploughed soil sample 107
Figure 4.15. Domain-specific volumetric soil water content at 100mm depth for Ivrogbo soil sample infiltration experiment 108
Figure 4.16. Domain-specific volumetric soil water content at 200mm depth for Ivrogbo soil sample infiltration experiment 109
Figure 4.17. Domain-specific volumetric soil water content at 300mm depth for Ivrogbo soil sample infiltration experiment 109
Figure 4.18. Domain-specific volumetric soil water content for average of 200mm and 300mm depth for Ivrogbo soil sample infiltration experiment..... 110
Figure 4.19. Infiltration experiment showing domain specific water content at depths of (a) 100 mm (b) 200 mm (c) 300 mm using the monolith of Ivrogbo soil sample... 110
Figure 4.20. Domain-specific volumetric soil water content at 100mm depth for Oleh soil sample infiltration experiment 111
Figure 4.21. Domain-specific volumetric soil water content at 200mm depth for Oleh soil sample infiltration experiment 111
Figure 4.22. Domain-specific volumetric soil water content at 300mm depth for Oleh soil sample infiltration experiment 112
Figure 4.23. Domain-specific volumetric soil water content for average of 200mm and 300mm depth for Oleh soil sample infiltration experiment 112
Figure 4.24. Infiltration experiment showing domain specific water content at depths of (a) 100 mm (b) 200 mm (c) 300 mm using the monolith of Oleh soil sample 113
Figure 4.25 Domain-specific soil water content for the different soil types (a) 100 mm depth (b) 200 mm depth (c) 300 mm depth...................................... 115

Figure 5.1. Domain-specific matric suction at 200 mm depth using Aberdeen packed soil infiltration experiment 119
Figure 5.2. Domain-specific matric suction at 300 mm depth using Aberdeen packed soil infiltration experiment 119
Figure 5.3. Domain-specific matric suction at 200 mm and 300 mm depths using Aberdeen ploughed soil infiltration experiment 121
Figure 5.4. Domain-specific matric suction at 200 mm depth using monolith of soil sample from Ivrogbo in the infiltration experiment 122
Figure 5.5. Domain-specific matric suction at 300 mm depth using monolith of soil sample from Ivrogbo in the infiltration experiment 122
Figure 5.6. Average matric suction for 200 and 300 mm depth for Ivrogbo soil 123
Figure 5.7. Domain-specific matric suction at 200 mm depth using monolith of soil sample from Oleh in the infiltration experiment 124
Figure 5.8. Domain-specific matric suction at 300 mm depth using monolith of soil sample from Oleh in the infiltration experiment 124
Figure 5.9. Average matric suction for 200 and 300 mm depth for Oleh soil .. 125
Figure 5.10 Domain-specific Soil Matric Potential in the Soil Types (a) 200 mm (b) 300 mm 127
Figure 6.1. Infiltration experiment at 200 mm depth for Aberdeen packed soil column showing the soil water characteristic curve 132
Figure 6.2. Infiltration experiment at 300 mm depth for Aberdeen packed soil column showing the soil water characteristic curve 132
Figure 6.3. Predicted and measured soil water characteristic curve (a) Predicted Van Genuchten SWCC (b) Measured SWCC at 200 mm for the packed soil sample 133
Figure 6.4. Infiltration experiment at 200 mm depth for Aberdeen ploughed soil column showing the soil water characteristic curve 134
Figure 6.5. Infiltration experiment at 300 mm depth for Aberdeen ploughed soil column showing the soil water characteristic curve 135
Figure 6.6. Predicted and measured soil water characteristic curve (a) Predicted Van Genuchten SWCC (b) Measured SWCC at 200 mm for the ploughed soil sample 136

Figure 6.7. Predicted and measured soil water characteristic curve (a) Predicted Van Genuchten SWCC (b) Measured SWCC at 200 mm for the Ivrogbo soil sample infiltration experiment 138
Figure 6.8. Infiltration experiment at 300 mm depth for Ivrogbo soil column showing the soil water characteristic curve 139
Figure 6.9. Average measured soil water characteristic curve for Ivrogbo soil 139
Figure 6.10. Infiltration experiment at 200 mm depth for Oleh soil column showing the soil water characteristic curve 141
Figure 6.11. Infiltration experiment at 300 mm depth for Oleh soil column showing the soil water characteristic curve 142
Figure 6.12. Average measured soil water characteristic curve for Oleh soil... 142
Figure 6.13. Predicted and measured soil water characteristic curve (a) Predicted Van Genuchten SWCC (b) Measured SWCC at 200 mm for the Oleh soil sample infiltration experiment 143
Figure 6.14 Domain-specific Soil Water Characteristics Curve for the Different Soil Types (a) 200 mm (b) 300 mm... 146

List of Tables

Table 2.1. Theoretical expression for the finger radius (Rf) derived through linear stability analysis or dimensional analysis/experimentation (de Rooij, G. H. 2000) 31
Table 2.2 Summary of Literature Reports on Flow through Variably Saturated Soils 55
Table 4.1. Mass balance during infiltration experiment of packed soil sample ... 85
Table 4.2. Mass balance consideration of water flow processes for infiltration experiment of Aberdeen ploughed soil sample 87
Table 4.3. Determination of Particle Size for Ivrogbo Soil Sample 88
Table 4.4. Atterberg Limit for Ivrogbo Soil Sample 89
Table 4.5. Bulk density test for Ivrogbo soil sample 90
Table 4.6. Gaseous analysis for the Ivrogbo soil sample 90
Table 4.7. Soil Classification 92
Table 4.8. Mass balance consideration of water flow processes for the infiltration experiment using the Ivrogbo soil sample 95
Table 4.9. Determination Of Particle Size for Oleh Soil Sample 96
Table 4.10. Atterberg Limit for Oleh Soil Sample 97
Table 4.11. Bulk Density Test For Oleh Soil Sample 98
Table 4.12. Gaseous analysis for the Oleh soil sample 99
Table 4.13. Soil Classification for Oleh soil sample 100
Table 4.14. Mass balance consideration of water flow processes 102

Nomenclature

Abbreviations	
AASHTO	American Association of State Highway and Transportation Officials
ARE	axisymmetric Richards' equation
CHP	constant-head well permeameter
CSIRO-TP	CSIRO version of the tension permeameter
DI	disc infiltrometer
DLM	dynamic linear model
DRI	double ring infiltrometer
EC	electrical conductivity
ECb	electrical conductivity of soil
EDL	electrical double layer
EPM	equivalent porous medium
GUELPH-CHP	Guelph version of the constant-head well permeameter
GWT	groundwater table
H1-H4	heterogeneities in the soil profile, where four layers
ISSS	International Society of Soil Science
LL	liquid limit
LSA	linear stability analysis
MHI	modified hood infiltrometer
PI	plasticity index
PL	plastic limit
PTFs	pedotransfer functions
REV	representative elementary volume
RPDE	Richards partial differential equation
RS	rainfall simulator
RSV	residual suction value
SCM	soil core method
SDI-12	serial digital interface at 1200 baud
SMP	soil matric potential
SWCC	soil water characteristic curve
SWCC	soil water characteristics curves
SWRC	soil water retention curve
TDR	time domain reflectometry
TOC	total organic carbon
TP	tension permeameter
USCS	Unified Soil Classification System
WEV	water-entry value

Greek Symbols	**Description**	**Units**
θ	soil water content	%
Ψ	matric potential	kPa
σ	soil pore water electrical conductivity	mS/m
ρ	density	kg/m^3
ε	relative dielectric permittivity	
γ	surface tension of water	N/m
α	water contact angle	(°)
τ	Equilibration time constant	

Chapter 1
Introduction

Water conservation is an important concept in agricultural development. As a result, there are now several ways that water is used in agriculture, with drip micro-irrigation emerging as one of the most effective techniques for achieving water efficiency. But to be able to apply drip micro-irrigation and obtain optimum water use efficiency, it is necessary to have an understanding of the complex hydrodynamics of water flow through the soil subsurface. This chapter introduces key concepts involved in hydrodynamics characterisation of soil subsurface flows, and highlights the aims and motivation for this research.

1.1 Background

Crop production through agricultural operations is essential in a world where population growth is constant. Water, however, is a basic requirement for plants that are soil-dwelling. Figure 1.1 depicts the distribution of water resources globally. Even while water covers more than 70% of the planet, the seas contain 97% of all water, which is salty, dangerous to drink, and generally unsuitable for growing crops. Just 3% of the water on Earth is fresh. Furthermore, 97.5% of the fresh water on Earth is frozen and therefore inaccessible. There is only about 2.5% of fresh water on Earth that can be used. The distribution of this extremely rare freshwater is quite irregular. It is clear from the figure that freshwater lakes, rivers, and the atmosphere—which together make up the smaller proportions—are responsible for available fresh water for farming.

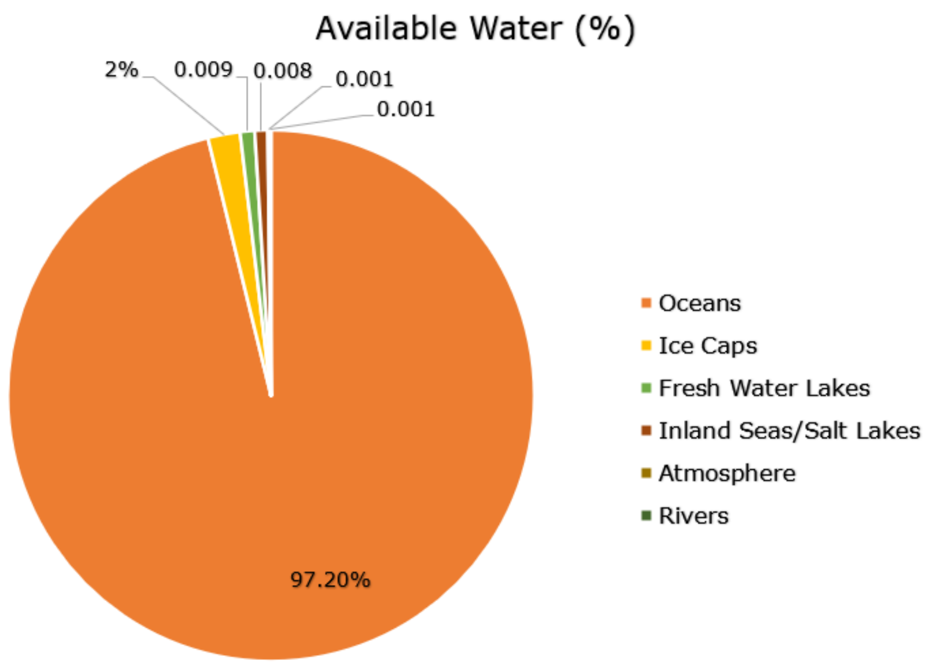

Figure 1.1. Global Water Availability (UNESCO World Water Assessment Programme, 2022)

The fact that freshwater availability fluctuates with consumption around the world is also notable. The water use per family on some continents and countries is shown in Figure 1.2. Physical and economic factors, fast population increase, and the impact of climate change on the water cycle are the main reasons of water scarcity in Africa. Sub-Saharan Africa experiences sporadic and highly variable rainfall, which frequently results in flooding and dry spells. Water-saving methods are clearly needed, as rain-dependent agriculture is practised in the majority of African countries. The evolution of water demand is largely location-specific, which reflects a varying pattern of use across the three primary sectors that use water - municipalities, industries, and agriculture, according to the United Nations World Water Development Report, 2023 (UNESCO World Water Assessment Programme, 2023). Because of variations in climate and geology, water availability varies greatly on a local and regional scale. Another major factor influencing the demand for water storage is seasonal variations in water availability. Furthermore, there is concerning occurrence of drought, which consistently has a detrimental impact on crop yield.

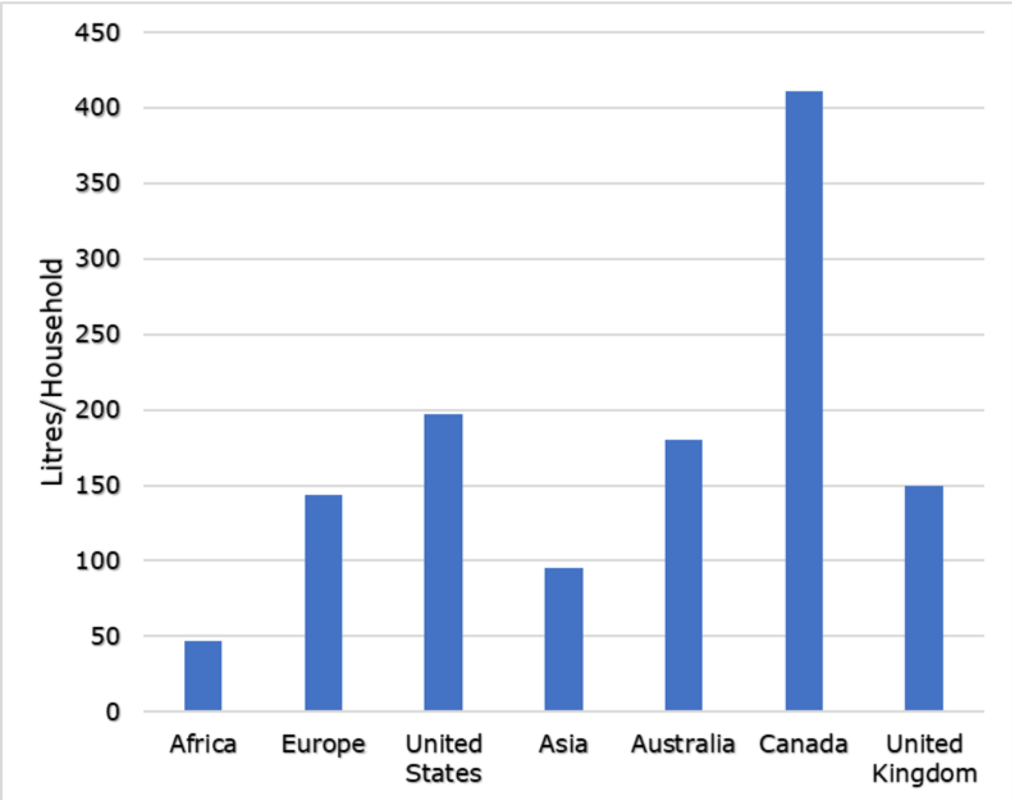

Figure 1.2. Household water consumption across some continents and countries of the earth (UNESCO World Water Assessment Programme, 2022)

According to the United Nations World Water Development Report 2023 (UNESCO World Water Assessment Programme, 2023), droughts impacted 1.43 billion people between 2000 and 2019, resulting in estimated losses of around US$130 billion. A combination of the different scenarios below can be referred to as an environmental drought, an agricultural drought (low soil moisture), a hydrological drought (low water levels in rivers, lakes, and groundwater), and a meteorological drought (far below average precipitation) (Bates et al., 2008; Clarke et al., 2022). Drought trends are more difficult to define, but most regions should expect a rise in the frequency or intensity of droughts and "heat extremes" as a direct result of climate change. Droughts have an impact on domestic, industrial, and agricultural water supplies as well as rain-fed agricultural productivity. There have been more severe and recurring droughts in a few semi-arid and sub-humid areas, such as the Sahel, the western USA, southern Canada, and Australia. Because there aren't many high-quality water resources in arid and semi-arid regions, and even in sub-sahara Africa, low-quality water is used instead. This results in soil salinization, which would lower agricultural productivity, and result in a loss of overall revenue (Aljoumani et al., 2018; Selim et al., 2013). According to the Palmer Drought Severity Index (PDSI), more places are experiencing droughts as a result of reduced land precipitation and rising temperatures, which increase evapotranspiration and decrease soil moisture. By 2030, all people should have access to and be able to manage their water and sanitation in a sustainable manner, according to Sustainable Development Goal 6 of the United Nations World Water Development Report 2023. All of SDG 6's (clean water and sanitation) targets are not being met at the current rate, and in some regions, implementation rates need to be increased by at least four times (UNESCO World Water Assessment Programme, 2023).

The inadequate rate of advancement in water and sanitation emphasises the necessity of seeking joint ventures and cooperative alternatives. The topic of partnerships and collaboration for water is examined in the United Nations World Water Development Report 2023, covering many regions and its implications for agriculture, the environment, human settlements, industry, health, and climate change. With a focus on increased agricultural productivity in mind, it is therefore necessary to explore research that will lead to water conservation in agricultural soils. The soils in the interior valley of Nigeria's Niger Delta, where agriculture uses more than one-third of the clean water available, are the subject of the study. The Nigerian agriculture industry needs more effective water management as, when it comes to irrigation, flood irrigation being the most widely used technique, farmers primarily rely on experience rather than empirical data. This study has been undertaken to provide insight into the complex hydrodynamics of water flow through the soil subsurface for agricultural water conservation.

1.2 Soil Classification and Flow Types

Because of the interaction of several solid, liquid, and gas phases, soil exhibits a high degree of complexity that makes its behaviour unpredictable. The amount of soil water that is available influences the management choices that farmers make all year long. Soil classification is therefore crucial because it helps with decision-making regarding management since it provides some insight into the physical characteristics of the soil and how it relates to soil moisture. Water permeability, water-holding capacity, and infiltration are significantly influenced by the texture and structure of the soil. According to (Prakash & Sridharan, 2012) a soil classification does not involve a description; rather, it is a systematic method of classifying and subclassifying soils according to their anticipated engineering behaviour. Many soil classification systems are currently used but the Unified Soil Classification System (USCS) and the American Association of State Highway and Transportation Officials (AASHTO) are the most popular. According to (Daryati et al., 2019; Prakash & Sridharan, 2012), soil on USCS is divided into two groups: 1) Less than 50% of the total weight of the soil sample that passed the N0.200 sieve is composed of coarse-grained soil, which includes sand and gravel. 2) Fine-grained soil, defined as soil that passes the No. 200 sieve with at least 50% of its entire weight. The USCS classifies soil into two categories: fine soils, such as silt (M) or clay (C), and coarse soils, such as gravel (G) or sand (S). The subdivide of coarse soils is either well-graded (W) or poorly graded (P), while the subdivide of fine soils is either low plasticity (L) for LL<50% or high plasticity (H) for LL> 50%. The seven primary classes (A-1 to A-7) that make up the AASHTO textural-plasticity categorization are further divided into further subgroups, for a total of twelve (Moreno-Maroto et al., 2021a). Groups A-4, A-5, A-6, and A-7 comprise the fine-grained soils, which contain more than 35 weight percent of material with a particle size of less than 75 μm as shown in Figure 1.3. Whether the plasticity index (PI) is below 10 (silt) or above this value (clay), that is the criterion used to classify silts and clays. Consequently, silts would be represented by groups A-4 and A-5 and clays by groups A-6 and A-7. A-7-5 and A-7-6 are the two subgroups that make up the A-7 grouping; the former is less flexible and changes in volume more than the latter.

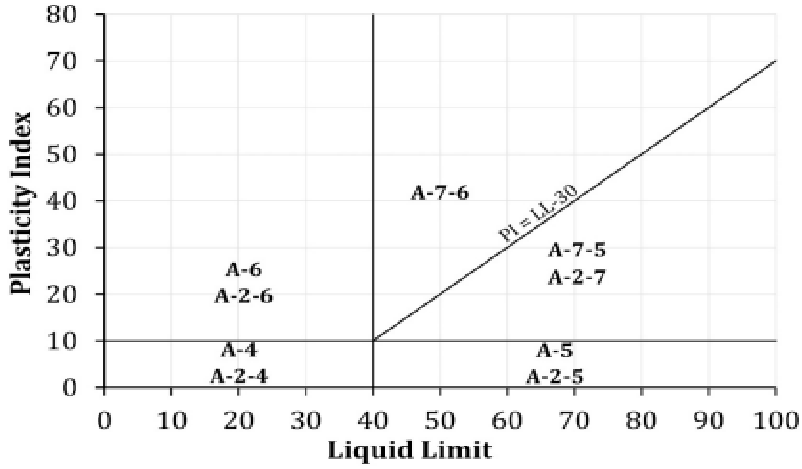

Figure 1.3. AASHTO classification chart for fine-grained soil (Moreno-Maroto et al., 2021b)

Based on the properties of their flexibility and particle sizes, soils are classified into multiple classes by the AASHTO classification system. Particle size distribution and Atterberg limits, which evaluate the soil's flexibility, are the two main variables taken into account in the classification. The Atterberg limits are a basic measure of the critical water contents of a fine-grained soil: its shrinkage limit, plastic limit, and liquid limit. The shrinkage limit (SL) is the water content where further loss of moisture will not result in more volume reduction. The shrinkage limit is much less commonly used than the liquid and plastic limits. The gravimetric moisture level at which the thread splits at a diameter of 3.2 mm, or roughly 1/8 inch, is known as the plastic limit. If a thread cannot be rolled out to 3.2 mm at any wetness, the soil is deemed non-plastic. The water concentration at which clayey soil behaves differently from its plastic state to its liquid state is known as the liquid limit (LL). The soil's shear strength is not truly zero at the liquid limit; rather, the change from plastic to liquid behaviour is progressive throughout a range of water concentrations. The difference between the plastic and liquid limits is known as the plasticity index, PI (PI = LL-PL). Clay-containing soils have a high PI, silt-containing soils have a lower PI, and neither silt nor clay are present in large amounts in non-plastic soils (PI of 0).

According to (Gerke, Horst H., 2006), soils can have either a uniform or nonuniform water flow. Nonuniform flow produces spatially uneven wetting of the soil profile, whereas uniform flow produces stable wetting fronts that move downward into the soil as a comparatively homogeneous front and essentially parallel to the infiltration soil surface. Preferential flow is the term used to describe the phenomena where water moves more quickly and in greater quantities at specific spots within the soil than at others because of uneven flow patterns. The methodological ramifications of preferential flow for computing soil element budgets and solute fluxes are significant. It seems dubious to interpret point data without understanding the flow pathways and soil structure. Gerke (2006) presents the term preferential flow as comprising all phenomena where water and solutes move along certain pathways. In well-structured, primarily fine-textured soils, macropore flow is a term used to describe preferential flow in continuous root channels, earthworm tunnels, fissures, or cracks. It is typically found in coarse-textured soils that unstable flow occurs. Water repellency can cause distribution flow to start in the topsoil, which can eventually result in the "finger"-like flow patterns that are seen in a lot of soils.

1.3 Consideration for Soil Subsurface Hydrodynamic Characterisation

To effectively describe and quantify the movement of water in the vadose zone (which is the area of the ground between the water table and the land surface, sometimes known as the unsaturated zone), a knowledge of the soil water retention curve (SWRC), also known as soil water characteristic curve (SWCC) which bears a relationship between soil water matric potential (Ψ) and soil water volumetric content (θ) is essential and prerequisite (Fu et al., 2021; Karup et al., 2017). (Fu et al., 2021; He et al., 2021) reported that the soil water retention curve is also a fundamental soil hydraulic property for estimating the water that is available for the plant, scheduling irrigation and watershed runoff prediction. Other soil hydraulic properties include soil hydraulic conductivity and coefficient of diffusion or moisture diffusivity (Gallage et al., 2013) and soil pore water electrical conductivity. A typical profile of the soil water retention curve (Fredlund & Xing, 1994; van Genuchten, 1980) is shown in figure 1.4 below. It shows the relationship between the soil water content and the soil matric potential which is represented by the pressure head. It has the features of the residual zone, the transition zone and the saturation zone which are described under the soil water characteristic curve as a hydraulic property.

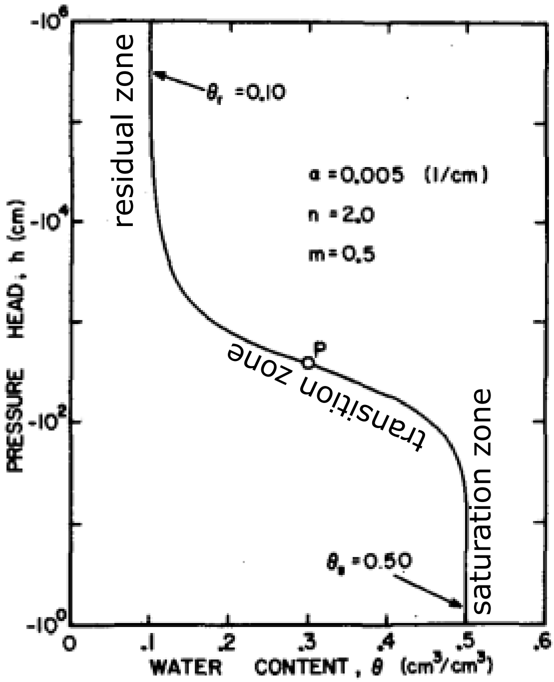

Figure 1.4. Typical profile of the soil water retention curve (van Genuchten, 1980)

To determine the soil water retention curve, two primary methods are typically employed. The first is the "direct method," sometimes known as experimental measurement. Field (in-situ) measurements or laboratory measurements can be used for this. The second approach, known as the indirect method, uses publicly accessible data to estimate the soil water retention curve, either directly or through the pedotransfer function process (ABBASI et al., 2011; Bienvenue et al., 2022; Haghverdi, Amir et al., 2018; Obi et al., 2014; Rudiyanto et al., 2021; Tian et al., 2021; Tomasella et al., 2000; Vereecken et al., 1989) or another process known as artificial neural network (Bayat et al., 2013; Haghverdi, A. et al., 2012). This study focuses on understanding the complex hydrodynamics of water flow through the soil subsurface by carrying out laboratory measurement of unsaturated soil hydraulic properties through a series of infiltration experiments using gravity-driven flow of water in ambient conditions of temperature. The soil hydraulic properties determined through measurement and analysis in this study are the soil water content, soil matric potential, and the soil water characteristics curve.

1.4 Soil Hydraulic Properties

The soil hydraulic properties such as hydraulic conductivity, soil water retention, available water capacity and infiltration are mostly affected by different existing soil properties including porosity, bulk density, surface and subsurface crusting, organic matter, soil structure and soil texture. It has been reported that most of the soil functions indirectly or directly rely on soil hydraulic properties, which explain their importance for soil processes under different climate conditions. The increasing temperature directly affects the soil hydraulic properties and indirectly it's associated soil chemical and biological properties. Soil hydraulic properties reflect the structure of the soil porous system comprising pores of different geometry, sizes and connectivity (Kutilek & Jendele, 2008; Othmer et al., 1991). These properties also reflect on the soil texture, surface crust and sealing, and soil temperature (Abd El-Ghany et al., 2010). Optimum soil hydraulic properties are important for crop production for minimizing environmental pollution arising from preferential flow (Jarvis, N. et al., 2013). The soil hydraulic properties have been a field of intensive research in many disciplines such as agricultural engineering, soil science, civil engineering, petroleum engineering, chemical engineering, hydrogeology and hydrology (Kargas et al., 2022; Mualem, 1976; Wang, X. et al., 2020), and the methodology will continue to be open because of the issue of simple rapid and reliable procedures. The important properties relevant to the solid matrix of the soil include pore size distribution, pore shape, tortuosity, specific surface area, and porosity. In relation to the soil fluid, the important properties include fluid density and fluid viscosity.

Soil hydraulic properties relevant to this study are presented below:

1.4.1 Permeability

Permeability is a function of the flow path geometry of the medium, (Claisse, 2016; Tiab & Donaldson, 2016; Woessner & Poeter, 2020). There are two different parameters that are used to define the permeability. The coefficient of permeability is commonly used in geotechnology, but only applies to water. The intrinsic permeability is used for the science of materials and can be applied to any fluid because it includes a term for viscosity. Intrinsic permeability is an inseparable property of a porous material because it depends only on properties such as surface area, pore size and tortuosity. A porous material is one that allows the flow of fluid through it as a result of pore spaces it contains. A material or medium is homogeneous if the permeability is constant from point to point over the medium while it is heterogeneous if the permeability changes from point to point in the medium. (Keller & Simmons, 2005) conceptualize the intrinsic permeability from Poiseuille's law as follows:

$$Q = \frac{\pi . r^4 \, \rho \, g \, \Delta P}{8 \mu . L} \tag{1.1}$$

where Q is volumetric flow rate (m^3/s), ρ = fluid density (kg/m^3), ΔP/L = pressure drop per unit length, μ = fluid dynamic viscosity (Ns/m^2). While the cross-sectional area of a pore is proportional to the radius, r^2, from Equation (1.1), the flow rate through a pore is proportional to r^4. The result is that a single large pore with the same cross-sectional area of numerous small pores will conduct more water. This can be explained by the fact that a single large pore will promote less viscous drag along the pore wall than numerous small pores will. Because coarse-textured soils are generally composed of pores of larger radius than fine-textured soils, intrinsic permeability can be related to soil texture with coarser soils, such as sands having a larger intrinsic permeability than finer clay and silt soils. Intrinsic permeability varies by order of magnitude, depending on the soils being considered, resulting in conditions in which large volumes of fluid are easily transmitted into the soil or conditions in which very little infiltration occurs.

The coefficient of permeability, k (m/s), is the measure of the flow conductance of the porous medium and it is defined by Darcy's law (Scheidegger, 1974):

$$k = \left(\frac{\varepsilon}{\tau}\right)^2 \frac{\varepsilon dp^2 p_{eff}}{36(1-\varepsilon)^2 k_c} \tag{1.2}$$

where ε is the porosity of the porous media (%), τ the tortuosity factor and k_c is the Kozeny's constant (Kozeny, 1927), and is dependent on the porosity for packing, d_p is the particle diameter and P_{eff} is the effective permeability which is the ability of a fluid phase to flow in the presence of other fluid phases. (Kozeny, 1927) has also expressed the permeability as:

$$k = c\frac{\varepsilon^3}{S^2\tau} \tag{1.3}$$

where C is a proportionality parameter, which depends on the shape of the channels, and S is granular surface area. The Kozeny equation has been largely applied and modified by other researchers. (Carman, 1997) introduced the surface exposed to the fluid S_b=(S-1) and set the constant c to 1/5 which gave the best fit to his experimental results. The result is known as the Kozeny-Carman equation (Richardson et al., 2002):

$$k = \frac{\varepsilon^3}{5(S_b)^2(1-\varepsilon)^2} \tag{1.4}$$

Blake-Kozeny equation related permeability to the void fraction and primary particle size and introduced a correction factor derived from experimental results, giving the permeability k as follows (MacDonald et al., 1991; Richardson et al., 2002):

$$k = \frac{{d_p}^2\varepsilon^3}{180(1-\varepsilon)^2} \tag{1.5}$$

The Blake-Kozeny equation provides a more explicit relationship to the Darcy's equation but is limited to a class of flow in porous media and not applicable to those made up of multisized particles.

1.4.2 Soil Water Content

Water contained in the soil, known as soil water content, can be measured as the gravimetric soil water content or volumetric soil water content. Gravimetric soil water content (θ_g)is the mass of water in the soil which is measured as the difference between the moist soil and the soil dried at 105^{o}C.

$$\theta_g = \frac{m_W}{m_t} \tag{1.6}$$

where m_w is the mass of water in the sample, and m_t is the total mass of the dry sample.

Measurements of gravimetric soil water content are destructive and not suitable for further chemical analysis.

Volumetric soil water content is the volume of water per unit volume of soil.

$$\theta_v = \frac{V_w}{V_s} \tag{1.7}$$

where V_w is the volume of water contained in the sample, V_s is the total volume of the soil sample.

The preferred unit for this ratio is $m^3.m^{-3}$, though % vol is frequently used. Soil water content varies from approximately 0.02 $m^3.m^{-3}$ for sandy soils at the permanent wilting point, through 0.04 $m^3.m^{-3}$ for clay soils at their field capacity, up to values as high as 0.85 $m^3.m^{-3}$ in saturated peat soils.

1.4.3 Soil Matric Potential

Matric potential is the amount of water bound to the matrix of a plant via hydrogen bond and is always negative to zero. The soil matric potential (SMP) stands for the quantity of water that is relatively available and held in the soil profile for plant uptake and use. It shows how much energy plants will have to apply to extract the water molecules from particles. The matric potential is always negative because the water attracted by the soil matrix has an energy state lower than that of pure water. Matric potential only occurs in unsaturated soil above the water table. Matric potential is measured either directly through a pressure transducer in tensiometers or through soil moisture measurements in an equivalent porous medium (EPM) with known soil water retention properties. Typical ranges are 0 to 10,000,000 hpa (hectopascal, also called millibars). The drier the soil the more energy it takes to pull water from it. Because of the wide ranges of pressure that can be observed from very wet to very dry conditions, matric potential is often expressed as the common logarithm of the pressure in hPa. The log of the pressure is called pF. For example, 1,000,000 hPa is equal to a pF of 6. (Passioura, 1980; Whalley et al., 2013) defines matric potential as the difference in water potential between a system and its equilibrium dialysate when both are at the same height and temperature, and are subjected to the same external pressure. The equilibrium dialysate is a solution in equilibrium with the soil solution, separated by a semi-permeable membrane or barrier, one which allows the movement of water but not solutes or soil particles. The matric potential bears a relationship with the total water potential.

According to Lu et al.(2002), the Terminology Committee of Commission I of the International Society of Soil Science (ISSS) first provided a terminology report in 1963 in which total water potential was formally defined to express the energy state of water in the soil as follows:

The amount of work that must be done per unit quantity of pure water in order to transport reversibly and isothermally an infinitesimal quantity of water from a pool of pure water at a specified elevation at atmospheric pressure to the soil water (at a point under consideration).

The total potential, Ψ_t of soil water expressed using the notation and terminology of mechanics is as follows (Lu, 2019; Luo et al., 2022a):

$$\begin{aligned}\Psi_t &= -\int F_g \cdot dx - \int F_{op} \cdot dx - \int F_p \cdot dx - \int F_{ad} \cdot dx \\ &= -g\int dy - v\int d\pi - v\int dp - \frac{\varepsilon-1}{8\pi} v\int d(\nabla\emptyset)^2 \qquad (1.8)\end{aligned}$$

where dx is a displacement vector; F_g, F_{op}, F_p and F_{ad} are the force vectors corresponding to four components of total potential (gravitational, osmotic, pressure and adsorptive potentials, respectively); y is the direction pointing to the centre of the Earth; g is acceleration due to gravity; v is the reciprocal density or specific volume of water; π and p are osmotic and gauge pressures respectively; ε is the dielectric constant of water; and ∅ is the electric potential within the electrical double layer (EDL) formed at external surfaces of the soil particles.

The matric potential has been universally defined in literature as the negative capillary pressure with magnitude depicted in the Young Laplace equation:

$$\Psi_m = P_w - P_{air} = \frac{2\gamma\cos\alpha}{r} \qquad (1.9)$$

where P_w and P_{air} are pore water and air pressures (Pa), respectively; α is a soil water contact angle (°); γ is the surface tension of water (Nm^{-1}); and r is the mean principal radius of curvature at the air-water interface (m). However, most modern literature combines the capillary pressure and adsorptive potential (i.e. the last two terms of equation 1.8) into a single term (the matric potential), such that Ψ_t is divided into three major components (Lu, 2019; Or & Tuller, 1999; Tuller et al., 1999):

$$\Psi_t = \Psi_g + \Psi_o + \Psi_m \tag{1.10}$$

where Ψ_g is gravitational potential due to the gravitational force field; Ψ_o represents the osmotic potential which is caused by the dissolved electrolytes in the water; Ψ_m is the matric potential which arises from the soil-water interactions. (Lu, 2019) argues that although the term matric potential used to be called the negative capillary potential, it covers phenomena beyond capillarity because as the water content decreases in a porous material, water that is held in pores due to capillarity becomes negligibly small when compared to the water held directly on particle surfaces. (Or & Tuller, 1999; Tuller et al., 1999) argue that the common definition of matric potential as depicted by equation (1.10) is incorrect due to the fact that the adsorptive component is either incorrectly excluded or has been deliberately ignored due to oversimplification.

A unitary definition of matric potential has been provided by (Luo et al., 2022b; Zhang & Lu, 2019) using a mathematical description on the basis of gravimetric soil water content during either the wetting or drying process as follows:

$$\Psi_m(\theta) = \Psi_{cap}(\theta) + \Psi(x, \theta) \tag{1.11}$$

Equation (1.11) bears a similar outlook with a combination of the last two terms of equation (1.8).

1.4.4 Soil Hydraulic Conductivity

Hydraulic conductivity (k, in SI units of ms^{-1}), is a property of porous materials, soils and rocks, which describes the ease with which a fluid (usually water) can move through the pore space, or fractures network (Keller & Simmons, 2005; Kool et al., 2019; Radinja et al., 2019; Schuhmann et al., 2011; Shackelford, 2013). The hydraulic conductivity of natural soils in place varies from about 30 m/day for a silty clay loam to 0.05 m/day for a clay soil. The hydraulic conductivity for disturbed soil materials varies from about 600 m/day for gravel to 0.02 m/day for silt and clay.

The soil hydraulic conductivity is the coefficient of permeability in Darcy's law given as (Atangana, 2018; Dukhan et al., 2014; Shackelford, 2013):

$$q = \frac{Q}{A} = -ki \tag{1.12}$$

where q is the fluid flux or flow rate (LT^{-1}), Q is the volumetric flow rate of the liquid (L^3T^{-1}), A is the total cross sectional area of the soil (soil plus voids) perpendicular to the direction of flow (L^2), k is the hydraulic conductivity or coefficient of permeability (LT^{-1}) and i is the hydraulic gradient (dimensionless). The hydraulic conductivity is among the most variable material properties in all of engineering (Shackelford, 2013; van Genuchten, 1980). (Koorevaar et al., 1991) explain that the hydraulic conductivity varies greatly between soils because the forces acting on the flowing water are dependent more on the geometry of the liquid-filled pore space than on the total amount of water in the soil. The hydraulic conductivity depends on the soil grain size, the structure of the soil matrix, the type of fluid, and the relative amount of soil fluid (saturation) present in the soil matrix.

1.4.5 Soil Water Diffusivity

Soil water diffusivity characterizes soil water movement under unsaturated conditions. Diffusivity is the ratio of the transport coefficient and the differential capacity. The soil water diffusivity is defined as (Koorevaar et al., 1991):

$$D = \frac{K}{C} = \frac{K}{\frac{d\theta}{dp_m}} = k\frac{dp_m}{d\theta} \tag{1.13}$$

where D is the diffusivity, k is the hydraulic conductivity, θ is the volumetric soil water content and p_m is the matric pressure head.

The Richards partial differential equation (RPDE) (Richards, L. A., 1931) is always the governing equation that needs to be solved in order to apply the approximation of the analytical approach. In the absence of gravity, the process of water infiltration is reduced to a horizontal diffusion equation by RPDE. Researchers have created techniques for calculating the soil moisture diffusivity based on this horizontal diffusion equation since it is simple to solve and provides some insight into the characteristics of infiltration, despite the limitation of disregarding the effects of gravity. The Richard's equation, which has the space coordinate x and the time t, is for horizontal absorption or, more generally, for water flow where the gradient of the gravitational component of soil water can be ignored and is stated below (Koorevaar et al., 1991; Li, J. et al., 2022; Villarreal et al., 2019):

$$\frac{\partial \theta}{\partial t} = \frac{\partial}{\partial x}\underbrace{\left[D(\theta)\frac{\partial \theta}{\partial x}\right]}_{\text{flux}} \tag{1.14}$$

Given the starting and boundary conditions having the initial water content, θ_0, and the surface water content, θ_s, and the soil water diffusivity, $D(\theta)$, expressed as a function of the water content, θ.

$$\begin{array}{lll} \theta = \theta_0 & t = 0 & x \geq 0 \\ \theta = \theta_0 & t > 0 & x \to \infty \\ \theta = \theta_s & t > 0 & x = 0 \end{array} \tag{1.15}$$

The theoretical analysis basically involves applying the Boltzmann transformation $\lambda = \lambda(\theta)$, to convert the partial differential equation of diffusivity (Eq. (1.14)) to an ordinary differential equation. This is given as

$$\lambda = x t^{-1/2} \tag{1.16}$$

where the function of θ is λ. If the water content θ is a single-valued function of λ, then Eq. (1.14)'s usage of the Boltzmann transformation λ from Eq. (1.16) makes this assumption. The applicability of Darcy's law to unsaturated water flow forms the foundation of the diffusivity Equation (1.14). (Li, J. et al., 2022) determines the important diffusivity parameters analytically using the Brooks-Corey empirical water diffusion equation (Brooks et al., 1964). The stationary action concept serves as the foundation for the solution. This avoids the necessity of the Boltzmann-transformation, which is frequently needed in conventional techniques.

1.4.6 Soil Water Characteristic Curve (SWCC)

The soil water characteristic curve (SWCC) is a fundamental concept in soil science and hydrology, providing crucial insights into the relationship between soil water content and soil water potential. This curve plays a pivotal role in understanding soil behaviour, water movement in the vadose zone, and its impact on various environmental and engineering processes. The soil water characteristic curve has implications for agriculture, geotechnical engineering, and environmental management. In agriculture, the SWCC is essential for understanding soil moisture dynamics, plant-water relationships, and irrigation management. It helps farmers determine the available water-holding capacity of different soil types, enabling them to make informed decisions regarding crop selection, irrigation scheduling, and soil amendment practices. By utilising the information derived from the SWCC, farmers can optimize water use efficiency, minimize water stress in crops, and prevent soil degradation due to over-irrigation or water logging. In geotechnical engineering, the SWCC is critical for assessing the behaviour of unsaturated soils in engineering projects such as slope stability analysis, foundation design, and landfill cover systems. The curve provides insights into the shear strength, compressibility, and volume change characteristics of unsaturated soils, aiding engineers in making accurate predictions about soil behaviour under different moisture conditions. From an environmental perspective, the SWCC influences the movement of water and contaminants in the vadose zone, impacting groundwater recharge, pollutant transport, and the remediation of contaminated sites. Understanding the SWCC is essential for designing effective strategies for groundwater protection, land reclamation, and the sustainable management of natural resources. Additionally, it plays a role in assessing the potential for soil erosion, landslides, and the impact of land use changes on hydrological processes. A link between the volume fraction of water and a suitable component of the water potential is necessary to address issues with water flow in unsaturated soils. The link between the mass of moisture in a soil and the related energy state, or suction, within the pore water defines the soil water characteristic curve (SWCC) distinctively (Brooks et al., 1964; Eyo et al., 2022; Fredlund & Xing, 1994; Koorevaar et al., 1991; van Genuchten, 1980). It is frequently referred to as the "soil water characteristic" since it is typical for various soil types. The term "soil water retentivity curve" or "function" is more apt. The relationship between soil suction and moisture content is described by the SWCC, which has a sigmoidal form for most soils as represented in figure 1.5 below (Eyo et al., 2022; Vanapalli et al., 1996). From figure 1.5, (Eyo et al., 2022) describe the SWCC as follows: The transition stage, boundary effect stage, and residual stage are its three separate phases. Two essential elements are distinguished by the slope of the curve that contains the inflexion point: residual conditions (also known as residual suction or residual water content) and the air entry value (AEV) suction. The suction value at which air starts to enter the greatest voids in the soil is known as the AEV, or bubbling pressure. The suction that corresponds to the residual moisture content at the residual condition is known as the residual suction value (RSV) or residual soil suction. The lowest moisture content, known as the residual moisture content, is the point at which suction causes no discernible change in moisture content. Note that the suction at which there is a noticeable increase in the water content as the wetting goes on is known as the water-entry value (WEV), if the wetting curve is taken into account.

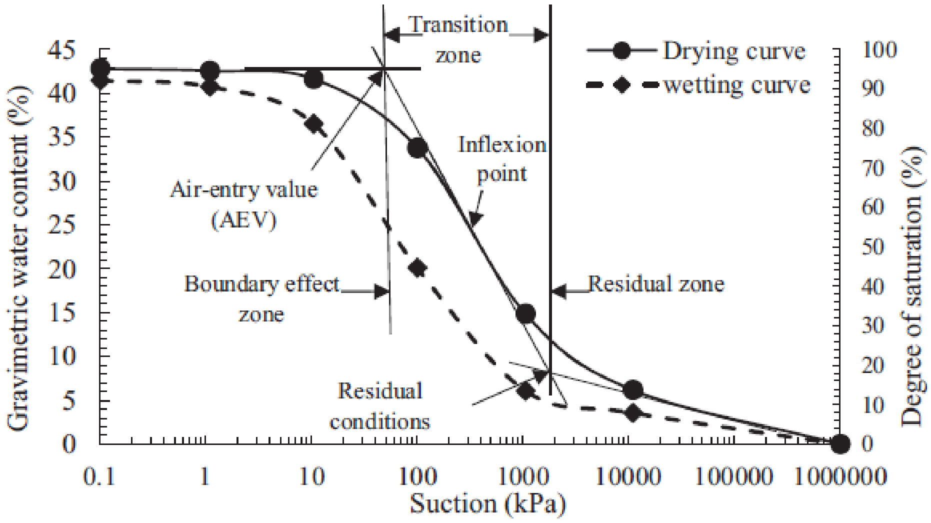

Figure 1.5. Features of the soil-water characteristic curve (Eyo et al., 2022)

A plot of the soil-water retention curve is shown in Figure 1.6 (Koorevaar et al., 1991). Here, the volumetric soil water content, θ, is plotted on the abscissa while the matric head, $h_{m,}$ is plotted on the ordinate. When the matric head is lowered from $h_m = 0$ to $h_m \approx -10^4$ m, one observes a more progressive release of water in soils with a wider variety of grain sizes. Plotting the entire soil water characteristic on a single graph in these situations is challenging unless h_m is shown on a logarithmic scale. The pF value is defined as the value of $^{10}\log(-h_m/\text{cm})$, where $h_m < 0$. The pF curve of soil is the graph that illustrates the relationship between the pF value and θ as shown in Figure 1.7. It should be observed that the abscissa of figure 1.5 is also plotted on a logarithmic scale for this reason.

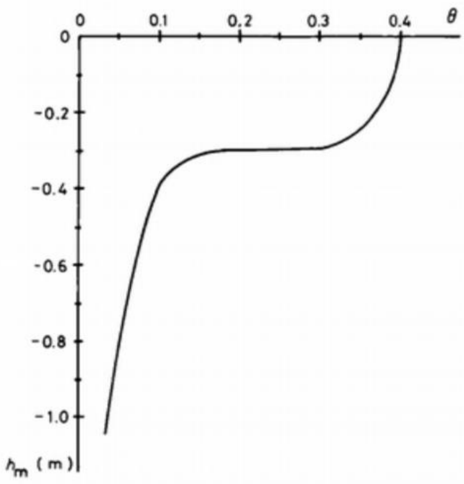

Figure 1.6. Soil-water retention curve of a coarse sandy soil (Koorevaar et al., 1991)

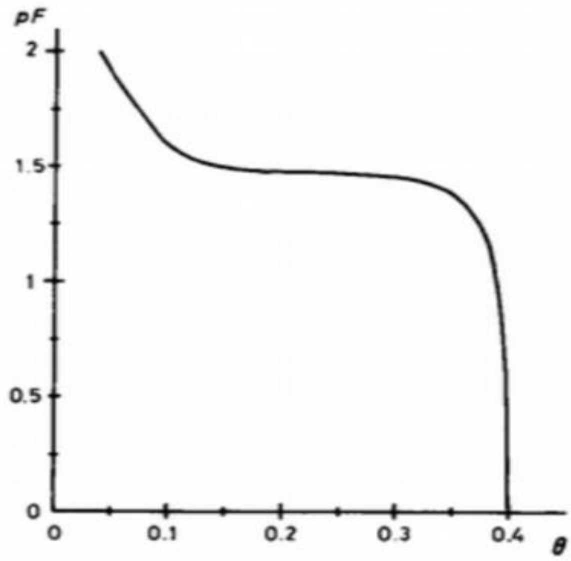

Figure 1.7. Relationship between pF values and θ (Koorevaar et al., 1991)

1.4.7 Soil Pore Water Electrical Conductivity

Soil pore water electrical conductivity (σ_p) is a measure of the ability of water in the soil pores to conduct an electrical current. Because it can reveal details about the salinity, nutrient content, and soil's capacity to hold and transfer water, it is a crucial parameter in soil research and agriculture. The amount of dissolved ions, such as salts and nutrients, in the soil water has an impact on electrical conductivity. Plant growth and the general health of the soil can be impacted by the higher concentrations of dissolved ions seen in soils with high electrical conductivity. For agricultural applications, measurements of (σ_p) are frequently used to evaluate the salinity, nutrient content, and general health of the soil. Farmers can use this knowledge to make well-informed decisions on soil management techniques such as fertilisation and irrigation. The electrical conductivity of soil pore water (σ_p) is highly dependent on the soil water content, θ. The pore holes in the soil fill with water as the water content rises, and this water contains dissolved ions that increase the electrical conductivity of the soil. Higher electrical conductivity results from a more concentrated concentration of dissolved ions in the soil pore water when the soil is drier. As the soil grows wetter, the ions become more diluted, which can lead to a decrease in electrical conductivity. It's crucial to remember that, despite the typical negative relationship between soil water content and electrical conductivity, there are certain outliers. Sometimes irrigation or precipitation causes the soil's water content to rise, which allows salts to seep into the soil and raises electrical conductivity. As a result, there are many variables that might affect the link between soil water content and soil pore water electrical conductivity, such as the kinds and concentrations of ions present in the soil, the texture of the soil, and the particular environmental circumstances.

The liquid phase electrical conductivity (EC), σ_p, is used to calculate the salinity of the soil. A high concentration of soluble salts is indicated by a high EC, and vice versa. If there is a fixed link between the liquid phase electrical conductivity (σ_p), bulk electrical conductivity (σ_b), and water content (θ), then (σ_p) could be calculated. With the help of a theoretical model and the discovered linear relationship between the soil relative dielectric permittivity, ε_b, and σ_b values, Hilhorst was able to translate (σ_b) to (σ_p). Hilhorst states that σ_p may be found using the equation (Aljoumani et al., 2018):

$$\sigma_p = \frac{\varepsilon_b \sigma_b}{\varepsilon_b - \varepsilon_{\sigma_b=0}} \qquad (1.17)$$

where (σ_p) is the pore water electrical conductivity (dS/m); ε_b is the relative dielectric permittivity of the bulk soil (dimensionless), ε_p is the relative dielectric permittivity of the soil pore (dimensionless), σ_b is the bulk electrical conductivity (dS/m), $\varepsilon_{\sigma_b=0}$ is the relative dielectric permittivity of the soil when the bulk electrical conductivity is 0 (dimensionless).

1.5 Crops and Comfort Zones

Understanding the type of soil is essential for conserving water in agricultural soils using drip micro-irrigation. It is possible to identify the kinds of crops that can flourish and conserve water with more knowledge about the soil matric potential and water content. This is due to the fact that soil types like clay, sand, silt, and others all have various capacities for retaining water, therefore water content alone is not a reliable measure of a plant's comfort zone. A fine-textured clay with the same 30% water content may appear only moist and be well below the ideal comfort zone for a plant because the clay's surface will bind the water, making it less available to the plant. In contrast, sand with 30% water content will be too wet for optimal plant growth, threatening a lack of aeration to the roots, and flirting with saturation. Plant ideal runs from roughly -2 to 5 kPa, which is on the very wet side, to approximately -100 kPa, at the drier end of optimal. Unlike water content, matric potential measurements clearly show plant accessible water. Plants will experience a deficit below that point, and they begin to suffer below -1000 kPa. Matric potentials below -1000 to -2000 kPa will permanently wilt plants, depending on the species. The simple reference scale for some crop kinds is shown in Figure 1.8. If plants are kept in this Matric potential comfort zone, they will remain stress-free and produce more. From Figure 1.8, it can be observed that while some crops can do well within a wide range of matric potential (e.g. orange; -20 to -100 kPa, tomato; -80 t0 -150 kPa), others can only do well within a short range of matric potential (e.g. potatoes; -30 to -50 kPa, carrots; -55 to -65 kPa). One of the objectives of this research is to investigate the soil water retention characteristics and apply a smart micro-irrigation to determine crops comfort zones in soil types.

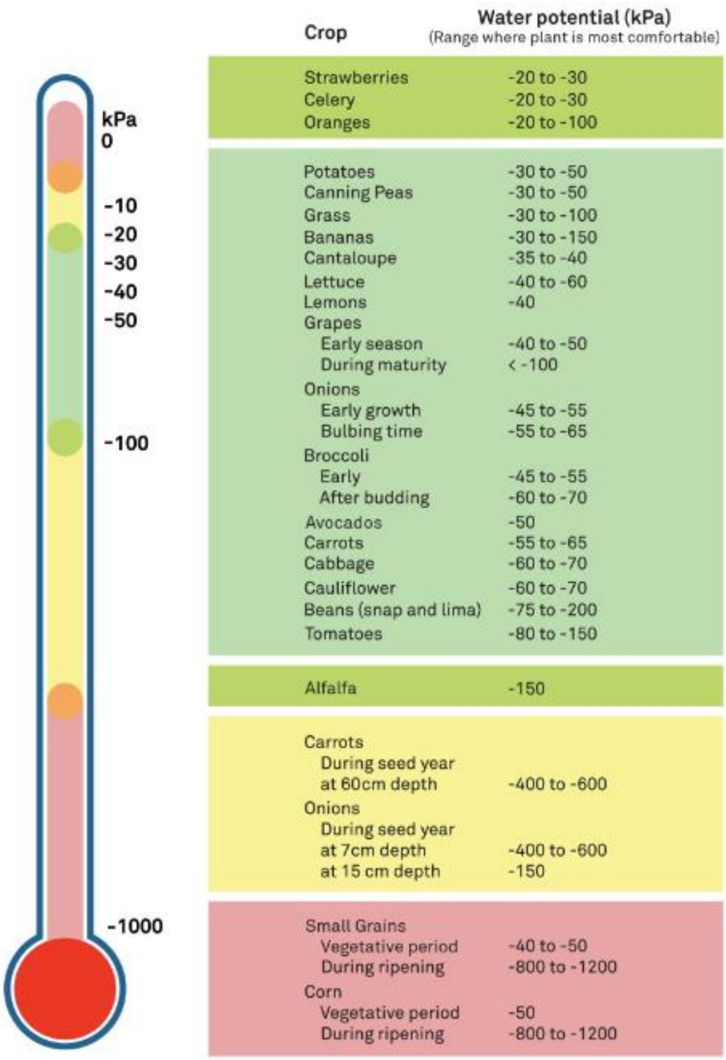

Figure 1.8. Water potential scale for some crops (Taylor & Ashcroft, 1972)

1.6 Motivation

From the previous sections, it can be clearly deduced that agricultural crop production is choked by the challenges of water and land availability. To be able to deal with the management of water availability, the concept of drip micro-irrigation is being developed. However, an efficient practice of drip micro-irrigation requires a knowledge of hydrodynamics characterization of soil subsurface flows for the water conservation purposes as the dynamics of water flow through the soil subsurface is complex. This study provides the evidence to broaden the understanding of the complex hydrodynamics of water flow through the soil subsurface. Characterization of hydraulic parameters through wetting infiltration experiments using a column of packed soil sample and monoliths of undisturbed soil samples have been carried out. The goal of this study is to give scientific evidence for the development of water-efficient irrigation systems by shedding light on the hydrodynamic behaviour of soils from two distinct locations of Nigeria: Oleh and Ivrogbo. During the infiltration studies, the water matric potential and soil moisture content were measured at various sample depths per minute. Aberdeen soil has also been obtained for comparison.

Applications for understanding the complex hydrodynamics of water flow through soil subsurface can be found in a wide range of disciplines, including hydrogeology, engineering, geosciences, and agricultural irrigation. However, in order to effectively investigate water flow through soils, flow laws must be employed, necessitating the quantification of soil hydraulic parameters. In application of flow laws for flow of water through soils, Darcy’s law is fundamental. Therefore, hydrodynamic characterization of soil subsurface flows, which involves the spatial distributions of hydraulic properties and hydraulic states in the subsurface, such as permeability, soil water content and soil water retention characteristics, hydraulic conductivity and moisture diffusivity has been approached by many researchers from different ways. Such include the use of models such as standard Single-Domain models, Double-Porosity models, Geometry-Based Mobile-Immobile Transport models, First-Order Type Mobile-Immobile Transport models, Microstructure models, Discrete Macropore models, Dual and Multiple-Permeability models. However, model-based research requires input parameters that control how long chemicals and water stay in the soil. These input parameters such as textural soil properties which involve particle size distribution and porosity are normally obtained by indirect methods such as pedotransfer functions (PTFs), many of which have been developed to predict hydraulic parameters and the corresponding hydraulic functions. But the PTFs often rely on statistical regression equations, thus making them site-specific and should be used with care.

To achieve a high-resolution characterization, direct measurement is usually employed, such as field testing or in-situ measurement of soil hydraulic properties. Although progress is being made in the direct measurement of the hydraulic characteristics, these processes are costly and thus prohibitive for most critical zones studies, as they involve the requirement of special sensors, and demand the skills of technicians. The prohibitive cost and requirement of sensors and skills of technician apply whether they are laboratory methods or field methods such as the use of tension disc infiltrometer, double ring infiltrometer, constant head permeameter or undisturbed soil core. Despite the established fact that direct methods of measurement of hydraulic properties are tedious and expensive, it should however be noted that there is no indirect method that exists without some use of direct methods because it is only direct measurement that would create the database used for the derivation and calibration of predicted hydraulic characteristics. Hence the development of indirect methods requires further research on up-to-date, accurate and efficient direct measurement techniques.

1.7 Research Aims

This research aims to characterise the complex hydrodynamic behaviour of subsurface flows in different types of soils for better management of water during irrigation of agricultural lands. These research aims are realised through a series of experimental investigations to obtain:

i. the profile of soil water content from unsaturated conditions in a packed soil column, as well as undisturbed soil columns, through the use of sophisticated moisture sensors.

ii. the profile of soil matric potential from unsaturated conditions in a packed soil column, as well as undisturbed soil columns, obtained using modern equitensiometer sensors.

iii. soil water characteristics curves, as a relationship between soil water content and soil matric potential, and provide insights into their links to crops comfort zones in different soil types.

1.8 Thesis Outline

Chapter 2 presents a detailed literature review on soil hydraulic properties to reveal knowledge gaps on soil subsurface flow characterisation. The chapter also reveals different numerical and experimental techniques in determining soil hydraulic properties, involving both field and laboratory methods of measurement for hydraulic properties dataset generation.

Chapter 3 describes the methodology used. This involves the laboratory experimental procedure, logging and data generation.

Chapter 4 presents the results of the soil water content for the packed soil column and the monolith of undisturbed soil columns experiments. It shows analysis of the data, flow profiles and their comparison, with a discussion of similarities and discrepancies.

Chapter 5 presents experimental results of the soil matric potential for the soil samples with analysis and discussion of their flow profiles, their comparison, with a discussion of similarities and discrepancies.

Chapter 6 presents the experimental results of the soil water characteristics curves for the soil samples with analysis and discussion of their flow profiles, their comparison, with a discussion of similarities and discrepancies. This chapter also discusses the intelligent application of drip micro-irrigation with respect to crops comfort zones for increased crop productivity.

Chapter 7 presents the conclusions drawn from this research and the recommendations for future work.

Chapter 2
Literature Review

This chapter is divided into 3 main sections. Section 1 considers reviews on water flow processes through saturated and unsaturated soils for the purpose of the determination of the soil subsurface flow characteristics. Section 2 discusses numerical models developed for different flow conditions. The 3rd section presents experimental investigations, which is divided into in-situ or field experiments and laboratory investigations of the flow of water through soil columns.

2.1 Water Flow Processes Through Saturated and Unsaturated Soils

(Gerke, Horst H., 2006) presented a review of model approaches for describing preferential flow through structured soils. He categorizes the soil matrix as single grained, massive and aggregated as postulated by (Hillel, 2004), and recognizes flow through soils as either uniform or nonuniform (Heber Green & Ampt, 1911; Hendrickx & Flury, 2001). In uniform flow, the wetting fronts are stable and move downward in a homogeneous front while irregular wetting profile of the soil is observed in nonuniform flow. In nonuniform flow, irregular flow patterns are noticed where water moves faster in some locations than others across the soil profile. This nonuniform flow pattern is also known as preferential flow and could be in the form of macropore flow for root channels, cracks, fissures and earthworm burrows; unstable flow for coarse-textured soils (Dekker & Ritsema, 1996); finger-like flow where part of the soil is bypassed, and funnel flow where less permeable zones are bypassed by the flow pattern.

The author presents the standard single-domain models (Ross & Smettem, 2000a), which is based on the classical Richards equation for unsaturated and variably saturated flow and the convection-dispersion equation for solute transport. He also considers the double-porosity models (Bibby, 1981; Hornung & Showalter, 1990; J.Valocchi, 1990; Molson et al., 2005; van Genuchten & Dalton, 1986), discrete macropore models (Beven, 1982), and dual- and multiple-permeability models (Gwo et al., 1995; Jarvis, N. et al., 2006; Othmer et al., 1991). He focuses the review on deterministic approaches for describing preferential flow and transport in structured soil with special emphasis on the two-domain approach and poses questions on whether water in the preferential flow paths is still influenced by capillary forces or by gravity and viscous forces, and whether the domain concept assuming a porous continuum is applicable for preferential flow paths and not only soil matrix. He avers that conceptual problems describing preferential flow domain are yet to be resolved even though progress has been made, and there is need for measurement procedures and techniques for independent parameters determination.

(de Rooij, G. H., 2000) presented a review of models approach to finger flow research with a focus on the vadose zone. Using linear stability analysis (LSA), he revealed eight theoretical expressions which have been derived for the finger radius (R_f), and further categorises them into three groups according to the ratio of infiltration rate to the soil hydraulic conductivity in the finger. The expressions are shown in table 1.

In Table 1 below, which gives a summary of the finger radius in theoretical expressions, R_f is the finger radius [L], g is the acceleration due to gravity [LT^{-2}], η is a soil characteristic parameter, ρ is the density of the fluid [ML^{-3}], θ is the soil volumetric water content, σ is the bulk water-air surface tension MT^{-2}], and the subscripts f and i represent the value in the finger and the initial value of the subscripted variable, respectively.

Table 2.1. Theoretical expression for the finger radius (Rf) derived through linear stability analysis or dimensional analysis/experimentation (de Rooij, G. H., 2000)

No.	References	Expression for R_f[L]
1	(Glass, R. J. et al., 1991; R.L. et al., 1959; Saffman & Taylor, 1958)	$R_{f,1} = 4.16\left(\frac{\sigma}{\rho g}\right)^{1/2}\left(1-\frac{P}{K_f}\right)^{-(1/2)}$
2	(Philip, 1975; White et al., 1976)	$R_{f,2} = 4.16(\theta_f-\theta_i)^{-(1/2)}\left(\frac{\sigma}{\rho g}\right)^{1/2}\left(1-\frac{P}{K_f}\right)^{-(1/2)}$
3	(Glass, R. J. et al., 1991; R.L. et al., 1959; Wang, Z. et al., 1998)	$R_{f,3} = 4.8(R^*\lvert h_{we}\rvert)^{1/2}\left(1-\frac{P}{K_f}\right)^{-(1/2)}$
4	(Glass, R. J. et al., 1991; PARLANGE & HILL, 1976)	$R_{f,4} = \frac{2.4S^2}{K_f\left(1-\frac{P}{K_f}\right)^{(\theta_f-\theta_i)}}$
5	(Liu, Y. et al., 1994)	$R_{f,5} = \frac{4.8\theta_f\left(\frac{dy}{d\theta}\right)_{\theta_f}}{\eta+1.5}$
6	(DE ROOIJ, GERRIT,H. & CHO, 1999; Glass, R. J. et al., 1991)	$R_{f,6} = \frac{4.8\theta_f}{K_f\left(1-\frac{P}{K_f}\right)(\theta_f-\theta_i)}\int_{h_i}^{h_f} K\,dh$
7	(Glass, R. J. et al., 1991; PARLANGE & HILL, 1976; Wang, Z. et al., 1998)	$R_{f,7} = 0.6\lvert h_{we}-h_{ae}\rvert\left(1-\frac{P}{K_f}\right)^{-1}$
8	(Glass, Robert J. et al., 1990)	$R_{f,8} = \frac{2.05S^2}{K_f(\theta_f-\theta_i)}\left(1-\frac{P}{K_f}\right)^{1/2}$

According to de Rooij (2000) in his review of finger growth (Flury et al., 1995; Meakin, 1991; Nieber, 1996), it is still unclear how the initial water content affects finger development. Despite the numerous publications from huge research effort at fingered flow modelling, prediction of the finger sizes cannot be said to be accurate. This is because the expressions for homogeneous profiles are definitely affected by the high level of heterogeneity in natural soils.

(Šimůnek et al., 2003a) reviewed numerous different approaches for modelling preferential and non-equilibrium flow and transport with a focus on the vadose zone. They describe the model as simple or more complex, depending on whether it is a combination of the Richard's equation with composite equation of the hydraulic properties of the soil matrix and structure (Durner, 1994; Durner et al., 1999; Mohanty et al., 1997; Othmer et al., 1991), or the model uses the Richard's or kinematic wave equation eg.   (Jarvis, N., 1994) for flow in the soil structure with an assumption of immobile water in the soil matrix.

Using different forms of dual-porosity, dual permeability, multi-porosity, and/or multi-permeability models (Gerke, H. H. & van Genuchten, 1993; Gwo et al., 1995), simunek et al. (2003) explain preferential flow in structured media. They describe the dual-porosity and dual-permeability models to assume that porous medium consists of two interactive regions, namely the fracture system or macropore, and the rock matrix or micropore. While the dual-porosity model assume flow in the macropore, with stagnant water in the matrix, the dual-permeability models assume water flow in both matrix and macropore or fracture system. According to Simunek et al. (2003), the dual-porosity and dual-permeability models have the disadvantage of requiring too many input parameters (Gerke, H. H. & van Genuchten, 1993) to characterise both pore systems in contrast to models for single pore regions, yet it is uncertain how to obtain these parameters, either by estimation or through direct measurements (Clothier et al., 1995; Jaynes et al., 1995). They explain the need for intercode comparison for models describing preferential and /or non-equilibrium flow, prompting the development of HYDRIUS-ID and HYDRIUS-2D.

(Jarvis, N. J., 2007) conducted a review of consequences, controlling factors and principles affecting non-equilibrium water flow and solute transport in soil macropores, with a focus more on agricultural soils than rock fractures. He presents macropore flow as an occurrence of heterogeneous structures which create non-uniform water pressure or solute concentration, or both, during vertical flow and transport, which invalidates the representative elementary volume concept. The study poses the question as to the pore size (Beven & Germann, 1982; Luxmoore, 1981) that is adequate for non-equilibrium water flow and solute transport, and posits that pores of equivalent cylindrical diameter which are greater than about 0.3 – 0.5mm can be categorized as macropores (Jardine et al., 1993; Jarvis, N. J. et al., 1987; Langner et al., 1999; Wilson et al., 1998). This is equivalent to water-entry pressures of -10 to -6cm of water in the Laplace equation.

The network of macropores is affected by biological activities such as root channels and earthworm burrows (Angers & Caron, 1998; Gerke, Horst H., 2006; Shipitalo & Butt, 1999; Zehe & Flühler, 2001), and chemical activities such as leaching and the deposition of elements such as phosphorus (de Jonge et al., 2004; Kleinman et al., 2005), nitrates (Larsson & Jarvis, 1999), and trace elements (Camobreco et al., 1996; Richards, B. K. et al., 1998) which can affect the clay content (Haria et al., 2003; Roulier et al., 2006). According to (Gish et al., 2004; Gjettermann et al., 1997; McLeod et al., 1998; Williams et al., 2000), leaching of surface-applied solutes is also increased with high intensities of rainfall. Although the study outlines research scope for several topics on macropore water flow and solute transport, it presents the fact that the mechanism is uncertain, and the flow configuration or geometry is very variable and will always be guessed.

(Lewis & Sjöstrom, 2010) conducted a review of modern methods of performing soil column experiments for both unsaturated and saturated columns. The study discusses disadvantages and advantages of different experimental methods with the best practises that can potentially solve column design problems in undisturbed monolith-type and repacked soil columns. Four soil column types are presented viz, unsaturated, saturated, monolith and packed soil columns. While the unsaturated and saturated types of soil columns deal with issues bordering on saturation levels, the monolith and packed soil columns are concerned with the method of construction of the soil columns.

According to (Bromly et al., 2007), packing of the soil columns for laboratory experiments promotes homogeneity and avoid preferential flow. Packing methods for soil columns laboratory experiments include damp packing (Bégin et al., 2003; Communar et al., 2004; Ghodrati et al., 1999; Hrapovic et al., 2005) which involves mechanical packing of small amounts of damp or dry soils into the soil column, slurry packing (Powelson & Mills, 2001; Sentenac et al., 2001; Simon et al., 2000) which includes settling the saturated soil at the bottom of the column, and other methods such as wetting and drying cycles to assist compaction (Corwin, 2000).

2.2 Models of Fluid Flow Through Variably Saturated Soils

Water, transported dissolved substances, suspended particles, and colloids may, in heterogeneous structured soils, bypass the majority of the soil's porous matrix, leading to nonequilibrium conditions in the concentrations of solutes and pressure heads between the pore region of the matrix and preferential flow paths. The usage of standard flow and transport models, which are mostly based on the convection-dispersion equation and Richards' equation, is significantly limited by preferential flow. To solve this issues different model approaches have been put forth. The majority of these models attempt to characterise flow and transport in sluggish or stationary pore regions and preferred flow routes independently. Some of these models are given below.

2.2.1 Single Porosity Model

The conventional Richards' equation for unsaturated or variably saturated flow and the convection-dispersion equation for solute transport are typically the foundation for macroscopic models of water and solute movement in soils (Gerke, Horst H., 2006; Hillel, 2004; Šimůnek et al., 2003b). Regarding one-dimensional (1D) vertical motion that is positive downwardly oriented, we have (Gerke, Horst H., 2006):

$$\mathrm{C}\frac{\partial \mathrm{h}}{\partial \mathrm{t}} = \frac{\partial}{\partial \mathrm{z}}\left(\mathrm{K}\frac{\partial \mathrm{h}}{\partial \mathrm{z}} - \mathrm{K}\right) \tag{2.1}$$

$$\frac{\partial(\theta \mathrm{Rc})}{\partial \mathrm{t}} = \frac{\partial}{\partial \mathrm{z}}\left(\theta \mathrm{D}\frac{\partial \mathrm{c}}{\partial \mathrm{z}} - \mathrm{qc}\right) \tag{2.2}$$

where t is time [s], Z is distance [m], K is the hydraulic conductivity [ms^{-1}] as a function of h or θ, c is the soil solution concentration [kgm^{-3}], and C is the soil water capacity, dθ/dh, θ is the volumetric water content [m^3m^{-3}], h is the soil water pressure head [m] or the matric potential, which is of negative value in unsaturated soils, D is the effective solute dispersion coefficient [m^2s^{-1}], and R is the dimensionless solute retardation factor, $R = 1 + k_d\rho_b/\theta$, with k_d the distribution coefficient [m^3kg^{-1}] reflecting linear equilibrium sorption and ρ_b is the soil bulk density [kgm^{-3}]. q is the volumetric fluid flux density [ms^{-1}] provided by Darcy's law as:

$$q = -K\frac{\partial h}{\partial z} + K \tag{2.3}$$

If the flow is steady, and the soil is homogeneous (q and θ are constant in time and space), equation 2.2 is reduced to the 1D convection-dispersion equation:

$$R\frac{\partial c}{\partial t} = D\frac{\partial^2 c}{\partial z^2} - v\frac{\partial c}{\partial z} \tag{2.4}$$

where $v = q/\theta$ is the average pore-water velocity [ms^{-1}]
The standard models, while still helpful for many applications, are unable to describe preferential flow in structured soil because, among other simplifying assumptions, they assume homogeneity and local-equilibrium conditions within a representative elementary volume (REV) (e.g., laminar flow, rigidity of the solid phase, no air phase effects). Decoupling the pressure head from the water content in the retention function, based on the single-domain model method, allowed (Ross & Smettem, 2000b) to simulate local nonequilibrium and develop an equation containing the independent variables θ and h. The real water content moving towards the equilibrium water content, θ_e, is described by a kinetic equation as follows:

$$\frac{\partial \theta}{\partial t} = f(\theta, \theta_e): \qquad f(\theta, \theta_e) = (\theta_e - \theta)/\tau \tag{2.5}$$

where τ is the equilibration time constant and a linear driving function was applied. The Richards equation's numerical solutions can simply adopt this strategy. With very few adjustments to the water content, it enables the simulation of the swift passage of nonequilibrium moisture fronts through the soil as indicated by significant changes in pressure head.

2.2.2 Dual Porosity Models

Water in the matrix, or intra-aggregate pores or the rock matrix, is assumed to be immobile by dual-porosity models, which limit water flow to the fractures (or inter-aggregate pores and macropores. Intra-aggregate pores, then, are stationary pockets that do not allow convective flow but can interchange, retain, and store water. This conception results in two-region dual-porosity type flow and transport models (Šimůnek et al., 2003b; van Genuchten & Wierenga, 1976). This divides the liquid phase into zones that are static (stagnant, intra-aggregate), θ_m, and mobile (flowing, inter-aggregate), θ_f:

$$\theta = \theta_{\mathrm{m}} + \theta_{\mathrm{f}} \tag{2.6}$$

Let subscripts f and m represent fractures, intra-aggregate pores, and macropores, and the soil matrix, intra-aggregate pores, and rock matrix, respectively. The Richard's equation (2.1), which describes water flow in the cracks, and the mass balance equation, which describes moisture dynamics in the matrix, can be combined to generate the dual-porosity formulation for water flow as follows:

$$\frac{\partial \theta_f}{\partial t} = \frac{\partial}{\partial z}\left[K(h)\left(\frac{\partial h}{\partial z} + 1\right)\right] - S_f - \Gamma_w$$

(2.7)

$$\frac{\partial \theta_m}{\partial t} = -S_m + \Gamma_w$$

while Γ_w represents the rate at which water moves from the inter- to the intra-aggregate pores, S_f and S_m represent sink terms in both zones.

2.2.3 Dual Permeability Models

According to dual-permeability models, the matrix and the fracture pore domain are two distinct interacting subsystems that can represent the entire porous media system. The fracture domain in certain soils, such as cracked clays, may be empty, which causes a major difference in the physical behaviour of the soil from capillary flow. When a system has two porous continua, or dual porosity, it means that flow can occur in both porous domains, which are distinguished by different hydraulic conductivities. This is referred to as dual-permeability. These kinds of models vary primarily in how they describe mass transfer between the matrix and fracture pore domains and flow within the macropore or fracture pore system. The flow equations for the fracture (subscript f) and matrix (subscript m) pore systems are (Gerke, H. H. & van Genuchten, 1993; Šimůnek et al., 2003a; Vogel, H. ö et al., 2023; Vogel, T. et al., 2000):

$$\frac{\partial \theta_f}{\partial t} = \frac{\partial}{\partial z}\left(K_f \frac{\partial h_f}{\partial z} + K_f\right) - S_f - \frac{\Gamma_w}{w} \tag{2.8}$$

And

$$\frac{\partial \theta_m}{\partial t} = \frac{\partial}{\partial z}\left(K_m \frac{\partial h_m}{\partial z} + K_m\right) - S_m + \frac{\Gamma_w}{1-w} \tag{2.9}$$

where w is the ratio of the volumes of the fracture (inter-aggregate) and the total pore systems, ${\theta_{fs}}/{\theta_s}$

2.2.4 Multiple Porosity/Permeability Models

Though they have extra overlapping pore regions, multiple-porosity and permeability models essentially resemble dual-porosity models. More flexibility is thus possible, but at the cost of necessitating additional criteria that might also be inadequately specified physically.

Based on the assumption of a unit hydraulic gradient and a piecewise linear approximation to the hydraulic conductivity function, (Steenhuis et al., 1990) suggest a multi-domain model of solute mobility. Before redistribution, water fractions and solutes from each pore class were mixed in a single pool to compute the solute exchange between pore classes. (Gwo et al., 1995) assumed three overlapping pore regions: primary fractures, secondary fractures, and soil matrix (i.e., macropores, mesopores, and micropores) while (Hutson & Wagenet, 1995) developing the MURF AND MURT models for multi-region flow and transport, respectively. The multi-region model TRANSMIT (Hutson & Wagenet, 1995) was built on the basis of the single-domain model LEACHM. This model takes into account n overlapping pore zones, and again uses the Richards and convection-dispersion equation to describe the flow and transport in each region. Like (Gwo et al., 1995), they used convective and first-order diffusive transfer for solutes and first-order mass-transfer terms for water to enable water and solute exchange throughout all pore areas.

2.3 Experimental Measurement of Soil Hydraulic Properties

The understanding of soil hydraulic properties is crucial for many environmental science applications: (i) diagnosing the hydrodynamic functioning of soils in relation to the applied natural and/or human constraints; and (ii) simulating physical processes to establish a prediction on the order of magnitude of the hydraulic fluxes capable of, for example, providing nutrients and water to the plant rooting system or advecting chemicals that lead to point of diffuse pollution of the groundwater table (Angulo-Jaramillo et al., 2000). The established paradigm was put to the test in the 1950s to early 1970s by fresh experimental observations of fast non-equilibrium water flow in macropores and the ensuing impact on solute displacement patterns. To determine soil parameters like temperature, water content, and soil pore pressure as well as functions like soil hydraulic conductivity function, soil water characteristics curve, and soil water diffusivity, experimental measurements of soil hydraulic properties are essentially conducted using soil columns, either outdoors or in a laboratory equipped with instrumentation. This is typically accomplished by enclosing the soil column, for structural reasons as well as to stop fluid loss, in an impermeable and stiff shell material.

According to (Lewis & Sjöstrom, 2010), since 1950, a great deal of work in the domains of hydrology, agriculture, and soil sciences has been published, most of which rely on the findings of soil column experiments. Even still, there has never been an attempt to standardize or gather the best practices for building soil columns, and a survey of the literature reveals a dizzying variety of technical methods. A few of the tiniest columns documented in the literature have a diameter of 1 cm and a length of 1.4 cm (Voegelin et al., 2003). The largest, however, weigh more than 50 tonnes and measure up to 2 m x 2 m x 5 m (Mali et al., 2007). Historically and generally speaking, soil columns that function in the unsaturated regime have been called lysimeters shown in Figure 2.1 below. Large outdoor soil columns are typically referred to by this phrase, even though there isn't a specification that specifies a minimum size. These columns are commonly used to replicate conditions found in soil between the earth's surface and the top of the groundwater table, also known as the vadose zone or unsaturated zone. These columns are characterized by having both air and water in their pore spaces. On the other hand, the pore spaces of soil columns operating in the saturated regime are devoid of any gaseous phase or air. In this case, a liquid-such as water or an oil- that is not in the aqueous phase fills the pores completely. Usually, these soil columns are employed to mimic the environmental parameters of an aquifer. There are significant design variations in the soil columns used to simulate saturated and unsaturated conditions.

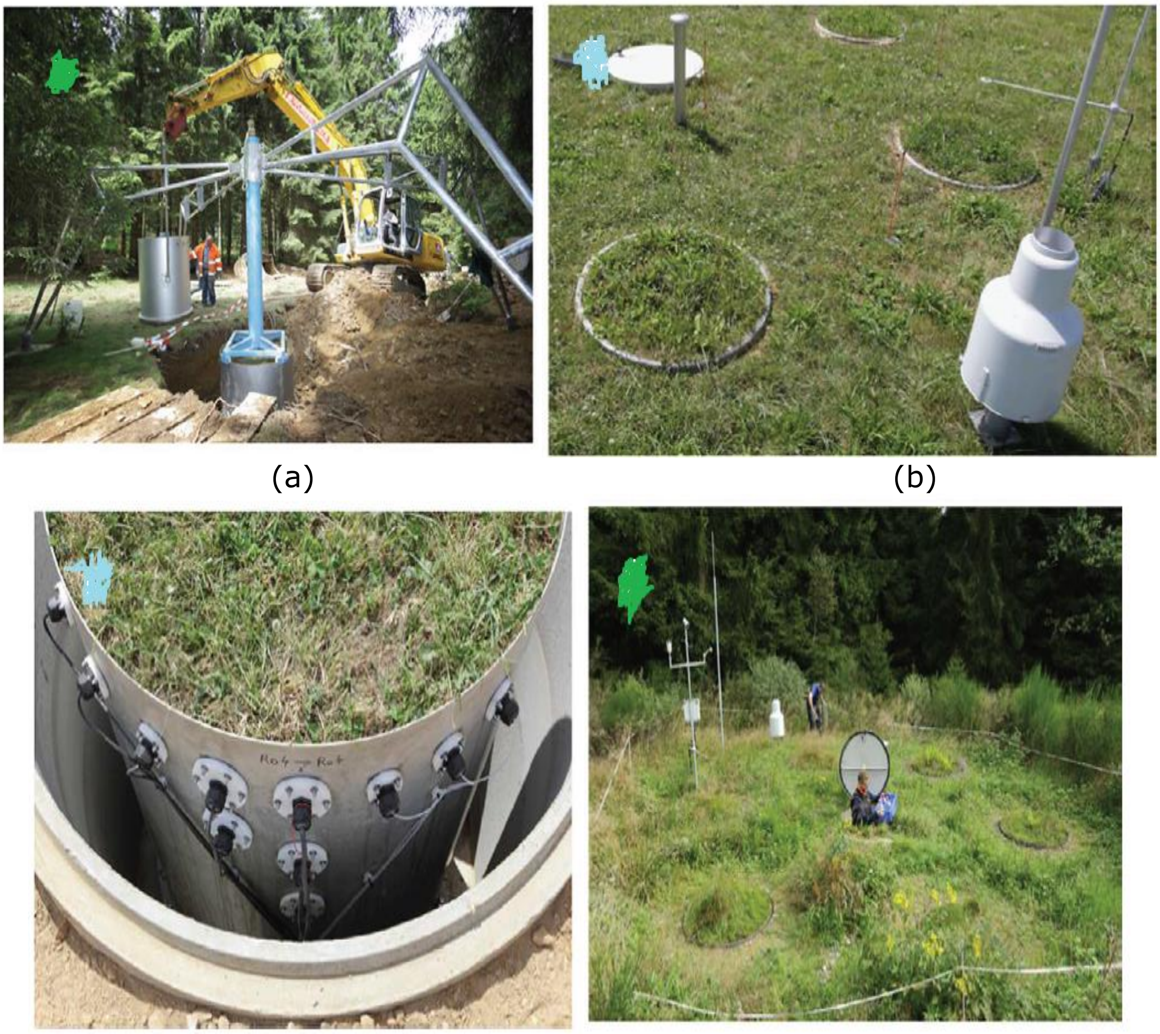

(a) (b)

(c) (d)

Figure 2.1. (a) Coring of an undisturbed lysimeter core, (b) installed lysimeter, (c) instrumentation, and (d) view of a lysimeter setup with underground access (Pütz et al., 2018)

Soil columns can be categorised based on two factors: the building method or the saturation level, as previously described. The literature has documented two main types of construction: monolith columns that employ undisturbed soil and packed columns that use disturbed soil. Excavated or “disturbed” soils are used to construct packed soil columns. The dirt is then backfilled into a rigid container and compacted. In contrast, monoliths are taken out of the natural soil whole and undamaged. Depending on the goals of the experiment, packed columns may or may not be preferred over monoliths because of their greater homogeneity. It has been demonstrated that the experimental outcomes will directly depend on whether packed or monoliths columns are used.

2.3.1 Field Measurement of Soil Hydraulic Properties

Numerous methods have been put forth for the in-situ determination of saturated hydraulic conductivity, Ks, via infiltration measurements. The undisturbed soil core method (SCM), rainfall simulator (RS), single and double ring infiltrometers (SRI and DRI), tension permeameter (TP), constant-head well permeameter (CHP), and falling-head borehole permeameter are some of the frequently used instruments. However, results from in-situ measurements of saturated hydraulic conductivity, Ks, using commonly used tools and methodologies have often been inconsistent. The double ring infiltrometer (DRI), the Guelph version of the constant-head well permeameter (GUELPH-CHP), and the CSIRO version of the tension permeameter (CSIRO-TP) were the three traditional devices whose Ks estimates were compared by (Morbidelli et al., 2017) as shown in figure 2.2. They evaluated these methods’ ability to consistently produce repeatable values and to identify the plot-scale variation of saturated hydraulic conductivity, Ks, by using steady deep flow rates, which were obtained from controlled rainfall-runoff experiments, as benchmark values of Ks at local and field-plot scales. For the DRI (Figure 2.2 (a)) measurements, two rings of 30 and 55 cm diameter on the inside and outside, respectively, were used. To establish a nearly one-dimensional flow underneath the inner ring, where the infiltrated water depth at successive time steps was monitored, they were buried at least 5 cm deep and filled with water about at the same level in both rings. The positive head CSIRO-TP measurements (Figure 2.2 (b)) were carried out using a bubbling tower, a graded water reservoir, and a disc with a radius of 20 cm. The apparatus known as GUELPH-CHP (Figure 2.2 (c)) was placed into a borehole of 8 cm in diameter and 15 cm in depth, respectively.

(a)

(b) (c)

Figure 2.2. Estimation of soil hydraulic conductivity (a) double ring infiltrometer (b) CSIRO positive-head tension permeameter, and (c) GUELPH constant head permeameter (Morbidelli et al., 2017)

When comparing the three devices' estimates of Ks to benchmark values, the authors found that the devices' estimates were not very accurate. In a lab setting, the DRI overestimates by a factor of 2, and at the plot size, by a factor of 5. While the CSIRO-TP delivers more restrained overestimates but unexpectedly substantial geographical heterogeneity of Ks in the laboratory soil, the GUELPH-

CHP produces large variations in both scenarios. They contend that before utilising these tools with confidence to evaluate both field variability and local observations, the reasons for the observed inconsistencies should still be investigated.

(Moret-Fernández et al., 2015) developed a mobile, modified hood infiltrometer (MHI) design that makes it possible to infer the hydraulic characteristics of soil from the transient cumulative infiltration curve in Zaragoza Spain. The MHI is made up of a water supply reservoir that, as seen in figure 2.3, is attached to a hat-shaped base that is positioned on the soil's surface. The transient infiltration curve analysis yielded corresponding values that were compared to the hydraulic conductivity (Ks) measured using MHI in a loam soil using the multiple head technique. The sorptivity (S) and Ks determined by the transient infiltration curve analysis were compared to the corresponding values obtained with a disc infiltrometer (DI) after the MHI was tested on three distinct soils under saturated circumstances. The results show, according to the authors, that this method enabled precise estimates of hydraulic conductivity as well as sorptivity. Additionally, they stated that research indicated that the prototype permits accurate calculations of the soil hydraulic parameters on soil surfaces that are covered.

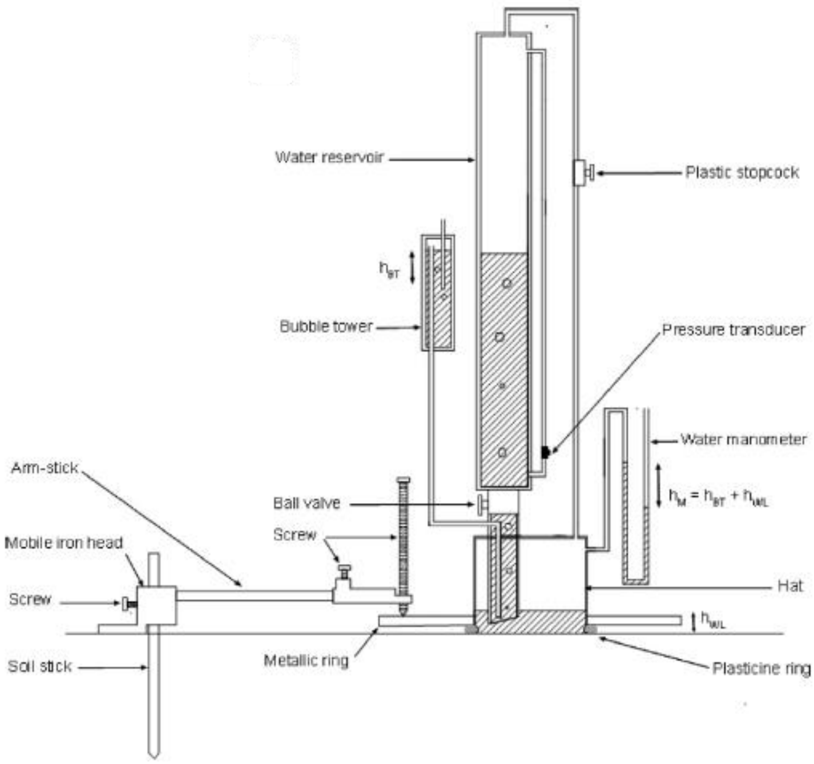

(a)

(b)

Figure 2.3. (a) Sketch (b) Picture of the modified hood infiltrometer (Moret-Fernández et al., 2015)

2.3.2 Soil Column Laboratory Measurement of Soil Hydraulic Properties.

(Gallage et al., 2013) developed a unique permeameter that measures suction (negative pore-water) values directly and uses the steady-state approach to determine the hydraulic conductivity of unsaturated soils. Two tensiometers are installed in the apparatus, as depicted in figure 2.4, to allow for the direct measurement of suction during the experiments. The hydraulic conductivity function of sandy soil can be obtained using the device across a low suction range of 0-10 kpa. Tests on two identical sandy soil specimens from Japan, Edosaki and Chiba, confirmed the measurement of unsaturated hydraulic conductivity with the novel permeameter and yielded similar results. The two soils were then subjected to drying and wetting processes, and the hydraulic conductivity functions of each were determined. Using the Fredlund equations (Fredlund & Xing, 1994), the Van Genuchten estimation (van Genuchten, 1980), and the Brooks and Corey estimation (Brooks et al., 1964), the measured unsaturated hydraulic conductivity functions were compared with the predictions. The findings imply that the various prediction techniques can fairly well describe the observed behaviour; nevertheless, the forecast produced by the Fredlund et al. (1994) method was more accurate.

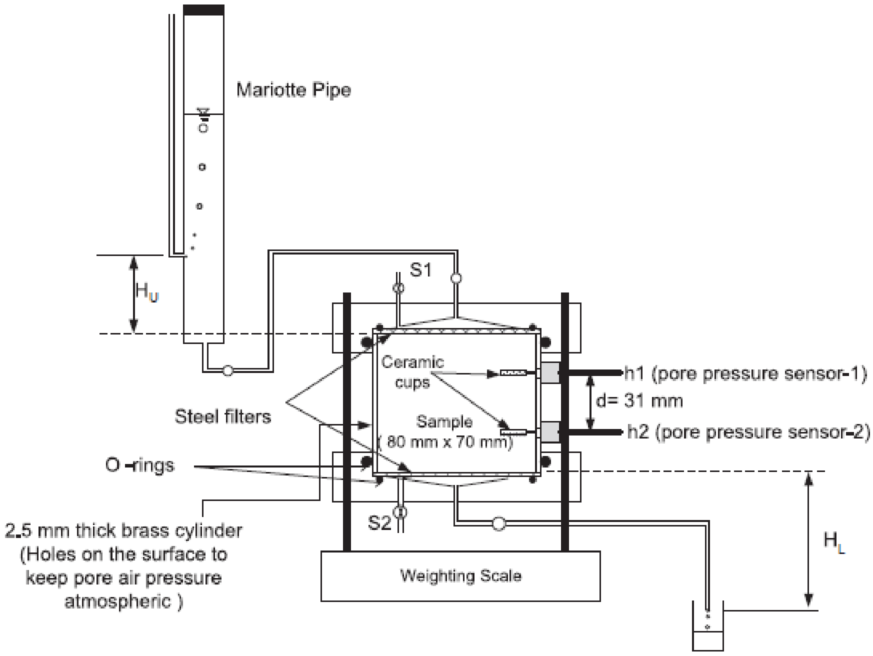

Figure 2.4. Novel permeameter for laboratory measurement of unsaturated hydraulic conductivity (Gallage et al., 2013)

A hydrogeophysical soil column system was created by (Bienvenue et al., 2022) to measure important hydraulic and electrical characteristics of regolith in critical zones. The newly designed soil column system is comprised of a cylindrical cell to contain soil samples and a unique hydrogeophysical probe that measures electrical potential and pore water pressure in soils. In both saturated and unsaturated situations, the system is capable of measuring the essential hydraulic and electrical properties of unconsolidated materials concurrently.

A sand sample that was mechanically packed in a cylindrical cell and taken from a river bank near Mores Creek in the United States of America was used to test the produced soil column, as depicted in figure 2.5. The findings indicate that while the saturated flow can produce transient responses of pore water pressure, outflow, and self-potential SP, which can be processed to estimate soil's key hydraulic and electrical properties, the saturated flow test from the system can be used to directly measure the saturated hydraulic conductivity K_{sat}, saturated complex electrical conductivity σ^*_{sat}, and saturated streaming potential coupling coefficient C_{sat}. Unfortunately, the consideration of reconstituted samples is the only one possible with the current design. When interpreting geophysical field data, care should be taken when using the properties measured from reconstituted samples because the material structure can have a significant impact on the hydraulic and electrical properties of geological materials. It is also vital to determine whether the setup is still effective for clay- or silt-rich materials because some critical zone materials contain a fair quantity of fine grains, and the related studies will take longer than the displayed sand samples. However, the established configuration represents a breakthrough in the investigation of the petrophysical characteristics of minerals in the critical zone.

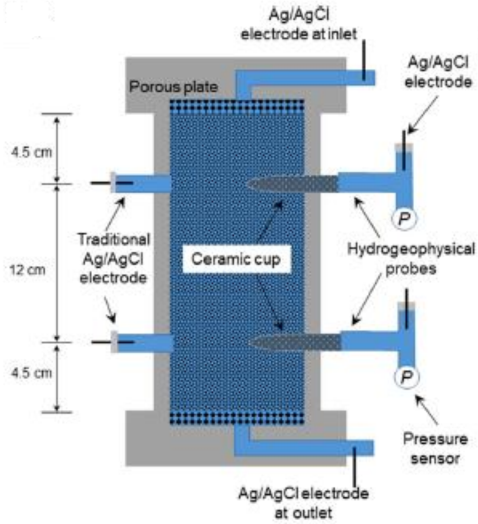

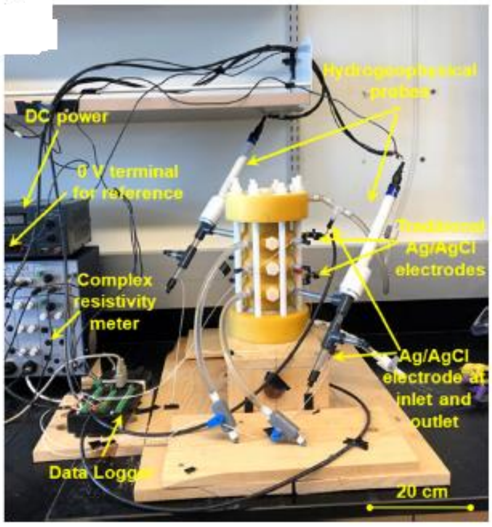

(a) (b)

Figure 2.5. (a) the schematic and (b) soil column for novel hydrogeophysical probe (Bienvenue et al., 2022)

(Hou, Xiaokun et al., 2019) looked at the movement of water in a soil column that was unsaturated and had several infiltration episodes over the course of 62 days in the lab. Figure 2.6 depicts the configuration. The dirt was held in place while sensors for suction and water content measurement were supported by a 0.236-meter-diameter, 4-meter-tall column. For the purpose of measuring water content and suction, fourteen moisture probes and five water potential probes were fitted. From the Heifangtai loess platform in Gansu Province, China, soil with a significantly elevated natural groundwater table (GWT) and a disturbed hydraulic condition due to farming over the decades was collected and used for the experiment. About 5.6% of the soil is made up of clay (<0.002 mm), while 84%

of it is made up of silt (0.002-0.05 mm). The formation of two wetting fronts, i.e., wetting front I and wetting front II, brought about by the initial and subsequent infiltration events, respectively, is highlighted by the results. Between the two fronts, a stable zone forms where the water content is roughly constant. To understand in-situ water flow, a conceptual model of the suction profile is put out that separates the unsaturated zone into four zones: the active, stable, transition, and capillary fringe zones. This classification helps to give a logical explanation for how water flows across various zones. In order to examine the flow and extend the seepage theory for unsaturated soils, 1D numerical analysis is also conducted. The wetting SWCC of compacted loess is displayed in figure 2.7. It consists of three parts: (i) measured data obtained through the axis translation technique; (ii) fitted curve utilising the equation of van Genuchten (1980) and the associated fitting parameters; and (iii) data obtained through the use of moisture probes and water potential in the column test.

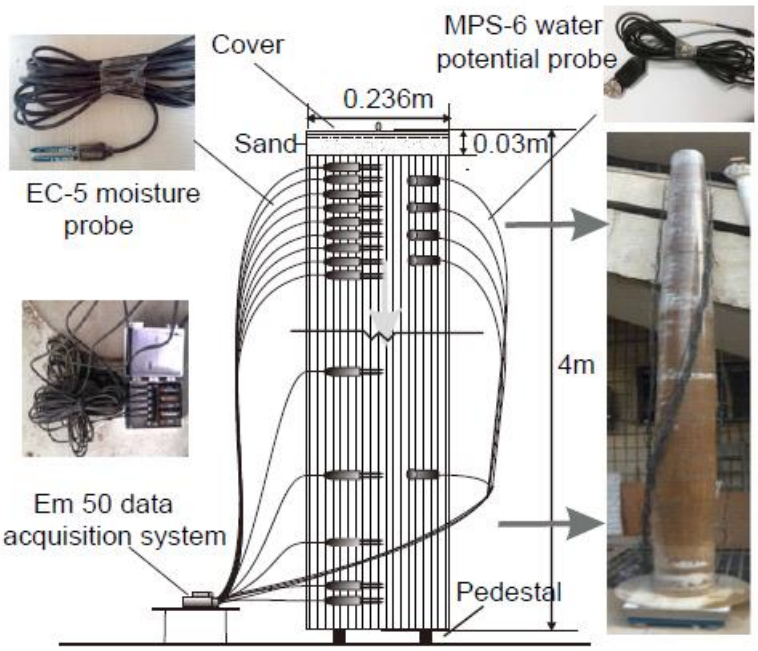

Figure 2.6. Soil column for water flow in unsaturated soil (Hou, Xiaokun et al., 2019)

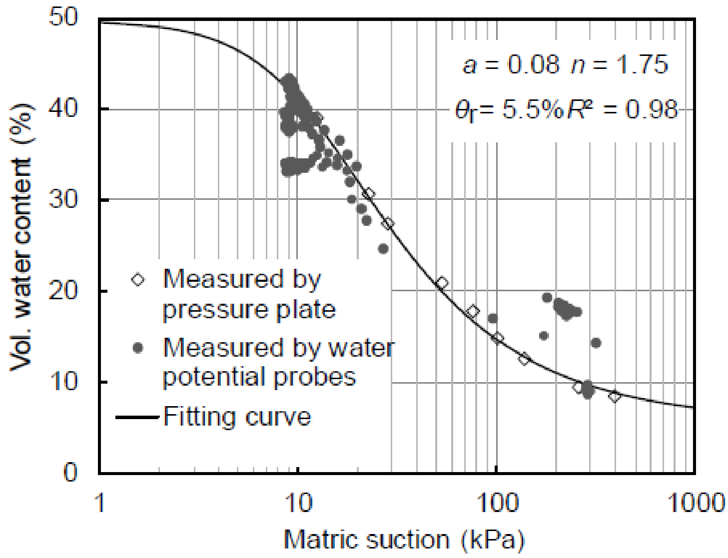

Figure 2.7. SWCC for the loess test (Hou, Xiaokun et al., 2019)

(Liu, Q. et al., 2012) created an automatic soil water retention test system that can calculate the soil water retention curve by measuring and recording volume changes during testing and by remotely controlling the entire procedure with a computer. The new system, according to the authors, offered a number of noteworthy benefits over the current systems, not the least of which is its ability to quantify volume change during testing using just one sample and automatically determine both the wetting and drying properties with high accuracy. The water retention curves for four distinct soil types, K-8, Takeda, Sasaguri, and Fukuchi, all collected from Japan and ranging in texture from sandy to silty – have been determined while accounting for volume change. The impact of volume variation on the soil water retention curves is displayed in figure 2.8. The volume change of soil specimens has an additive effect on the volumetric water content or the degree of saturation, as the volumetric water content cannot be directly measured. This means that the effect of volume change on soil water retention curves increases in the residual condition as the slope of the soil water retention decreases. However, the authors claimed that the system was constrained by the use of acrylic acid resin in the main unit, which restricted the appropriate air pressure to roughly 300 kPa. In light of this, the test system is appropriate for experiments involving silty and sandy soils. Clay soils are not suitable for it.

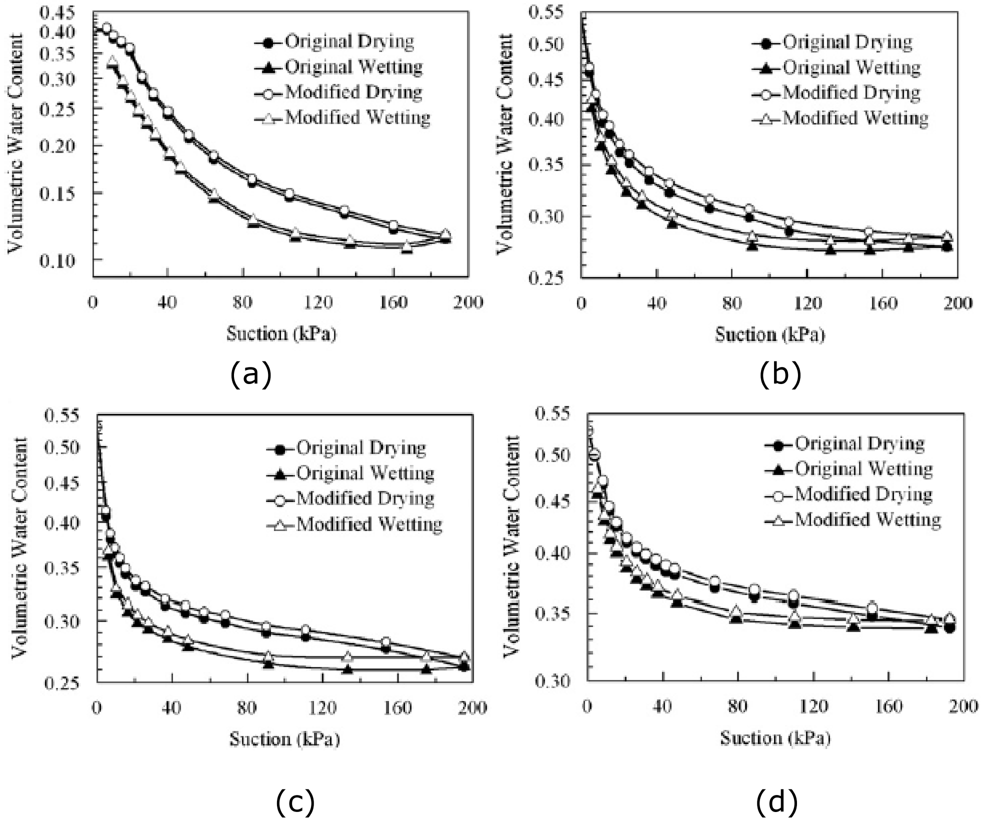

Figure 2.8. Effect of volume change on soil water retention curve. (a) K-8 (b) Takeda (c) Sasaguri (d) Fukuchi (Liu, Q. et al., 2012)

In order to propose a strategy to analyse the feasibility of several measurement strategies to detect the flow parameters from transient flow measurements, (Ritter et al., 2004) conducted irrigation experiments on a large undisturbed volcanic soil column. In the inversion problem, data on matric pressure head, soil water content, and/or bottom flux are introduced. The water flow module of the WAVE model in conjunction with GMCS and NMS method (Global Multilevel Coordinate Search combined with a Nelder Mead Simplex, GMCS-NMS) was used to inversely estimate the parameters. Using steel cylinders (θ45 x 85 x 0.4 cm), a large monolith of undisturbed volcanic soil with a sandy-clay-loam texture was removed from a field in Tenerife, Spain. It was then transported to the laboratory and instrumented with seven digital tensiometers and 21 TDR probes, as shown in figure 2.9a, inserted at seven observation depths (denoted as A-G). A compact rainfall simulator was built with a 550 x 550 x 32 mm^3 plexi-glass box fitted with 310 hypodermic needles (Θ0.3 x 6 mm placed 20 mm apart) to apply water uniformly at the top of the column. The results show that the parameters for the inverse modelling for the second experiment were chosen with the help of the water retention data at each soil depth from the first irrigation experiment. As shown in figure (2.9b), the first experiment revealed heterogeneities in the soil profile, where four layers (H1-H4) with varying water retention could be distinguished.

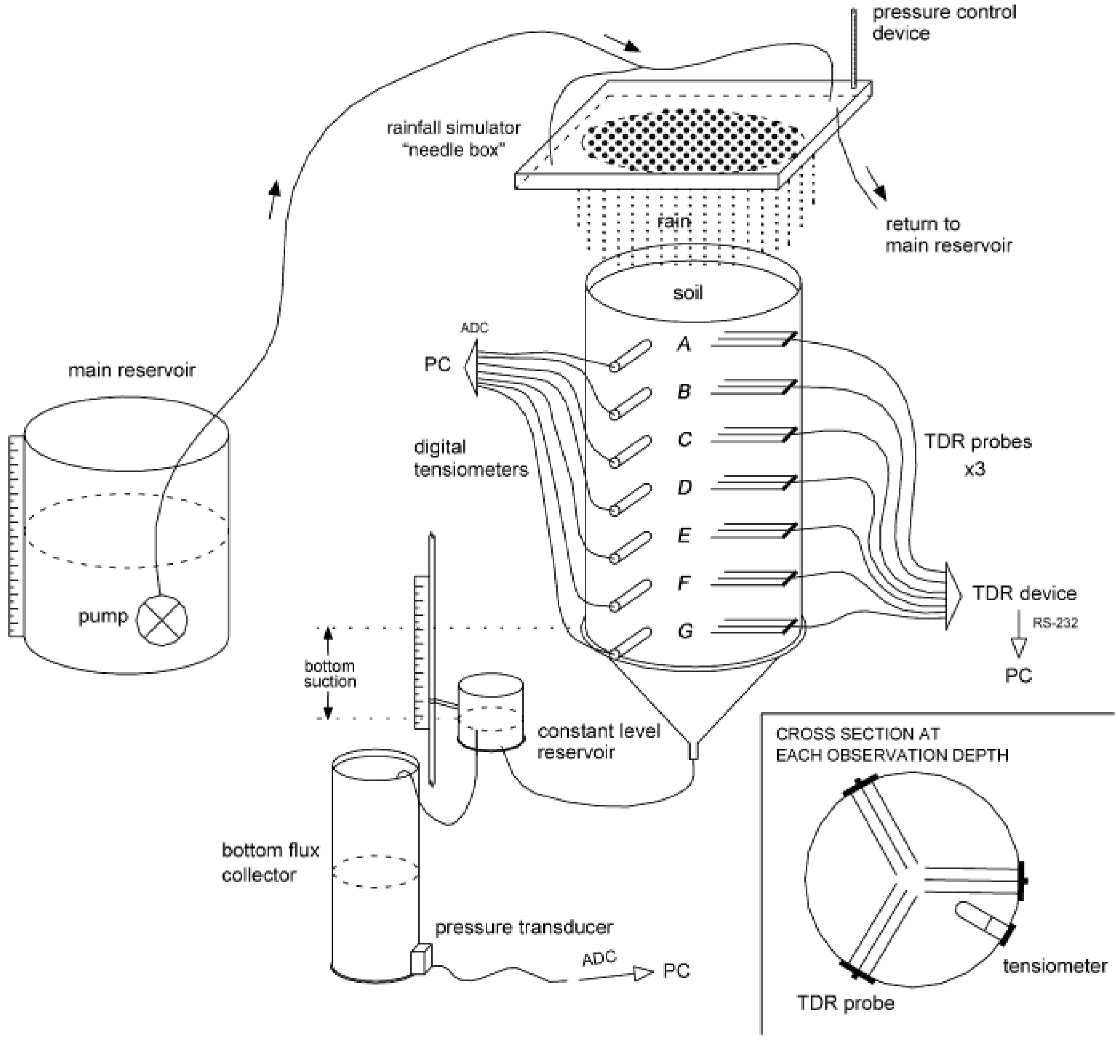

(a)

Figure 2.9. (a) Soil column laboratory set-up for volcanic soil monolith (Ritter et al., 2004)

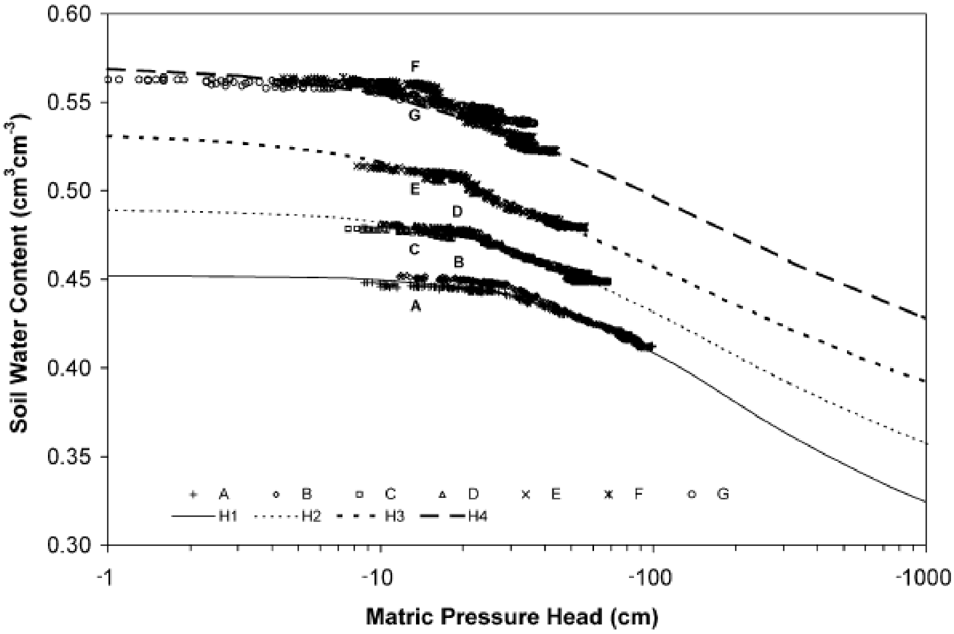

(b)

Figure 2.9. (b) Soil moisture retention curves observed in the monolith. Measured data (symbols) and fitted van Genuchten curves (lines) (Ritter et al., 2004)

Using cutting-edge measurement techniques, (Köhne, J. & Mohanty, 2005) created a unique soil column experiment that allowed for the identification of the degree of model complexity required to explain the experimental data of preferential flow in the microporous soil. These techniques also allowed for the quantification of interdomain (macropore-matrix) water transfer and the discrimination of macropore and matrix water flow. The parameters for the single- and dual-domain preferential flow models were obtained by inversely solving the pseudo-three-dimensional axisymmetric Richards' equation (ARE). A 24.4 cm diameter, 80 cm long acrylic column with a perforated PVC plate (2 holes of 0.3 cm per cm^2) at the bottom covered with a nylon membrane comprised the novel experimental set up, which is depicted in figure 2.10a. Additionally, there was a central cylindrical flow divider to reduce lower boundary effects on the water exchange flux between macropore and matrix, as well as separate outlets for macropore and matrix effluent. While the column was filled with dry-sieved, graded sandy loam from an agricultural field close to College Station, Texas, coarse sand was put into the annulus. Tensiometers and time domain reflectometry (TDR) probes were used to instrument the system once the matrix and macropore domains were established in order to record the water content and pressure head at different depths. Figure 2.10b displays the hydraulic functions for the matrix and macropore domains that were produced by fitting the infiltration drainage, and upward infiltration data using the axisymmetric Richards' equation (ARE) technique. It demonstrates how the hydraulic characteristics of a macropore and a matrix differ significantly. The results show that preferential flow is characterised by local hydraulic nonequilibrium of pressure heads, water contents, and flow velocities in matrix and macropore domains.

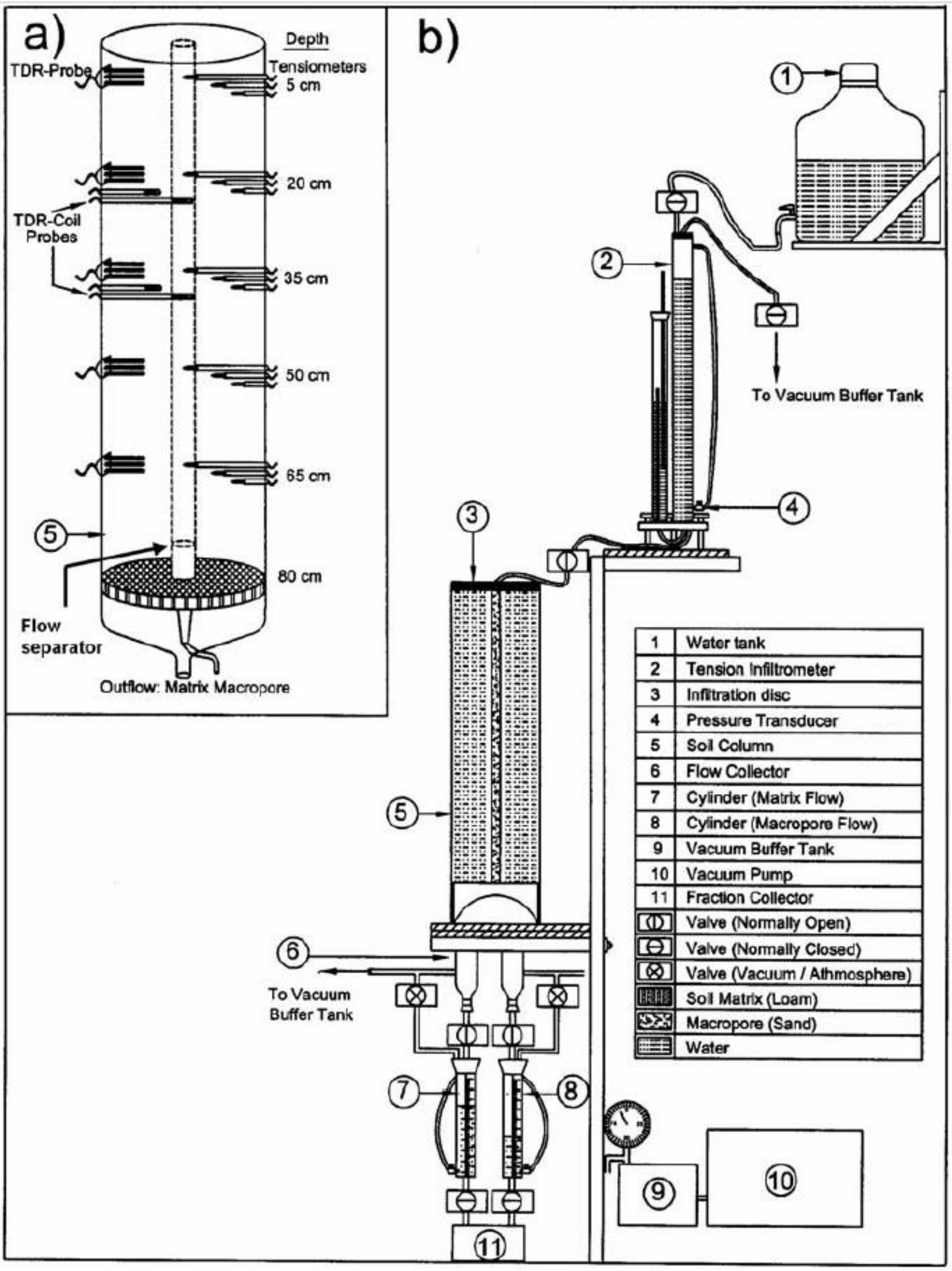

Figure 2.10a. Soil column experiment for studying macropore flow processes: (a) column with instrumentation and (b) complete setup (Köhne, J. & Mohanty, 2005)

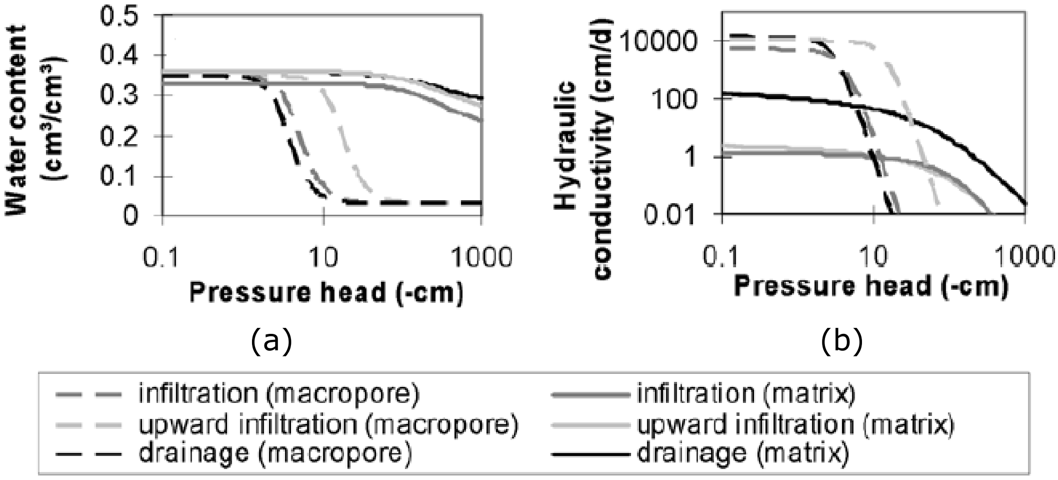

Figure 2.10b. Hydraulic van Genuchten functions for matrix and macropore obtained by inverse parameter estimation of approach ARE for drainage, infiltration, and upward infiltration experiments: (a) water retention and (b) hydraulic conductivity (Köhne, J. & Mohanty, 2005)

Basem et al. (2018) used a time-varying dynamic linear model (DLM) and the Kalman filter (Kf) to estimate the evolution of soil pore water electrical conductivity (σ_p) over time in a study conducted on a sandy soil in a lab setting. In order to convert the deterministic Hilhorst model into a stochastic model and assess the linear relationship between the relative dielectric permittivity ε_b and the bulk electrical conductivity (σ_b) in order to capture the deterministic changes to ($1/\sigma_p$), a time series of the relative dielectric permittivity ε_b and (σ_b) of the soil were measured using time domain reflectometry (TDR) at various depths in a soil column. Sand having a density of 1.4 g/cm^3 and a water content of roughly 4 m^3/m^3 was placed into the columns. In order to gather sufficient observations for modelling, TDR and soil temperature sensors were put at four different depths. The temperature, bulk electrical conductivity (σ_b), and soil relative dielectric permittivity ε_b were monitored every five minutes (Figure 2.11). The authors claim finding high positive autocorrelations between the residuals by using the Hilhorst model. Additionally, they claim that by applying and adjusting them to DLM, the predicted evolution of (σ_p) converged to its true value and the observed and modelled data ε_b obtained a considerably better fit.

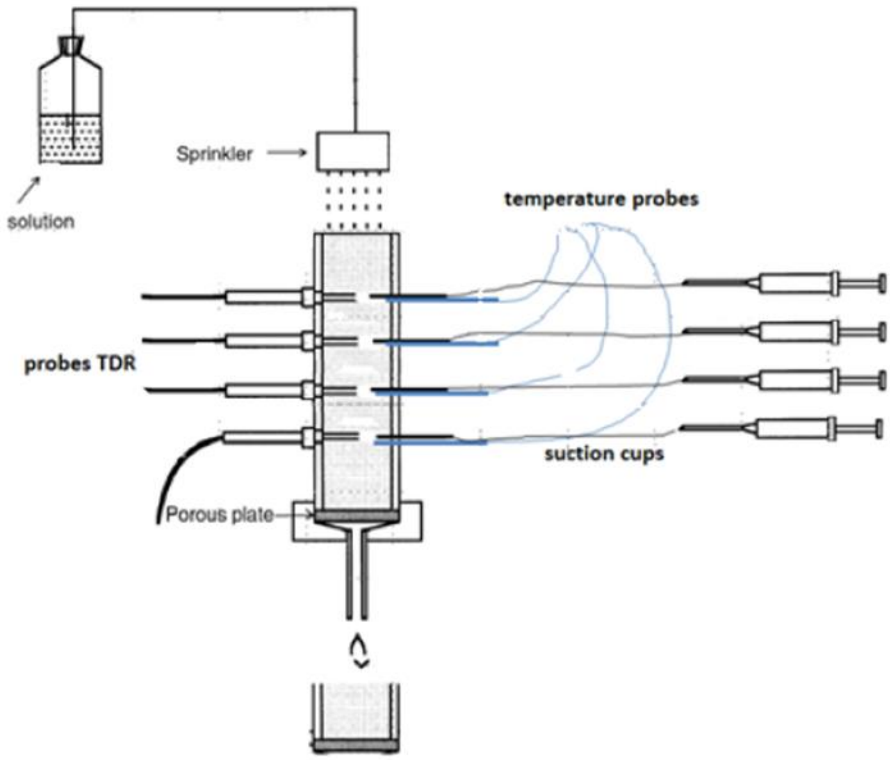

Figure 2.11. Soil column experiment for the determination of soil pore water electrical conductivity (Aljoumani et al., 2018)

Table 2.2 Summary of Literature Reports on Flow through Variably Saturated Soils							
S/N	References	Year	Research Activity	Parameters	Sensors	Findings	Location
1	(de Rooij, G. H., 2000)	2000	Review of finger flow models	Finger radius, R_f	-	Eight expressions categorised into 3 groups	-
2	(Šimůnek et al., 2003b)	2003	Review of modelling preferential and non-equilibrium flow	-	-	Explanation of preferential flow in the structured media and prompting of development of Hydrus-1D and Hydrius-2D	-
3	(Gerke, Horst H., 2006)	2006	Review of model approaches to preferential flow	-	-	Flow through soils are uniform or nonuniform	-
4	(Jarvis, N. J., 2007)	2007	Review of non-equilibrium flow.	-	-	Mechanism of macropore water flow and solute transport is uncertain and the geometry is guessed.	-
5	(Lewis & Sjöstrom, 2010)	2010	Review of methods of conducting soil column experiments	-	-	Monolith and packed soil columns affect method of soil column construction	-
6	(Bromly et al., 2007)	2007	Review of experimental methods	-	-	Packing of the soil column for lab exp. promotes homogeneity and reduces preferential flow	-
7	(Hillel, 2004)	2004	Model description	C, K, D, h, θ, t, τ	-	Single porosity, double porosity models	-

8	(van Genuchten & Wierenga, 1976)	1976	Model description	K, t, θ, θ_f, θ_m, S_f, S_m, Γ_f, Γ_m	-	Dual porosity formulation for water flow	-
9	(Vogel, H. ö et al., 2023)	2023	Model description	K, t, θ, θ_f, θ_m, S_f, S_m, Γ_f, Γ_m	-	Dual permeability	-
10	(Gwo et al., 1995)	1995	Model development	θ, S, D, ψ	-	MURF AND MURT MODELS	-
9	(van Genuchten, 1980)	1980	Model equation	θ, S, D, ψ	-	SWCC, Diffusivity, Sorptivity.	-
10	(Fredlund & Xing, 1994)	1994	Model equation	θ, S, D, ψ	-	SWCC, Diffusivity, Sorptivity.	-
11	(Brooks et al., 1964)	1964	Model equation	θ, S, D, ψ	-	SWCC, Diffusivity, Sorptivity	-
12	(Koorevaar et al., 1991)	1991	Hydraulic properties description	θ, S, D, ψ	-	SWCC, Diffusivity, Sorptivity	-
13	(Morbidelli et al., 2017)	2017	Field Experiment	θs, θi, q, ψ, Ks	DRI, GUELPH-CHP, CSIRO-TP	Devices' estimates were not accurate	Perugia in Italy
14	(Moret-Fernández et al., 2015)	2015	Field Experiment	Ks, S	MHI	Accurate calculation of soil hydraulic properties	Zaragoza in Spain
15	(Gallage et al., 2013)	2013	Laboratory Experiment	Ks	Permeameter, Tensiometers	Fredlund forecast was more accurate	Specimen from Japan
16	(Bienvenue et al., 2022)	2022	Laboratory Experiment	Ks, σ*s, Cs	Hydrogeophysical probe	Direct measurement of hydraulic properties	Specimen from Mores Creek in USA
17	(Hou, X. et al., 2019)	2019	Laboratory Experiment	θ, ψ	Moisture probes, water potential probes	Wetting SWCC is displayed.	Specimen from Gangsu Province in China.
18	(Liu, Q. et al., 2012)	2012	Laboratory Experiment	θ, ψ	Oedometer-type device, control	As slope of soil water retention curve decreases, effect of	Specimen from K-8, Sasaguri,

					software, water pressure transducer	volume change increases	Fukuchi, Takeda in Japan
19	(Ritter et al., 2004)	2004	Laboratory Experiment	θ, ψ, q	Tensiometers, TDR probes	Water retention data from first experiment was useful in selecting parameters for inverse modelling in second experiment,	Specimen from Tenerife in Spain
20	(Köhne, J. Maximilian & Mohanty, 2005a)	2005	Laboratory Experiment	θ, ψ	Tensiometers, TDR probes	Hydraulic characteristics of macropore and matrix differ significantly	Specimen from College station in Texas.
21	(Aljoumani et al., 2018)	2018	Laboratory Experiment	σ_p, σ_b, ε_b	TDR probes, temperature probes	high positive autocorrelations between the residuals by using the Hilhorst model.	Berlin, Germany

2.4 Research Gaps in Knowledge

It is evident from the review that a plethora of studies have been done on different facets of flow through variable-saturated soils in order to ascertain the hydraulic properties of the soil. The adaptation of Darcy's equation in the form of model equations dominated earlier findings. Model equations and model descriptions of water flow processes through saturated and unsaturated soils are readily found in the literature. These entail analyses of models that characterise various forms of flow in the matrix and macropore or fracture system, such as single porosity models, dual porosity models, and dual permeability models. They also discuss preferential flow model methodologies. The reviews address a number of ideas that describe the hydrodynamic flow characteristics in the subsurface soil, including soil heterogeneity and homogeneity as well as whether the flow is nonequilibrium, preferential, or uniform.

There has been a good sixty years' worth of literature produced about model description, model equations, and model development, dating back from 1964. The last 25 years are covered by the literature that was consulted for reviews. Though progress has been made, (Gerke, Horst H. 2006) asserts that measurement protocols and methodologies for independent parameter determination are still needed in order to address conceptual challenges regarding the preferential flow domain. The fact that the macropore water flow mechanism is unknown and that the flow configuration or geometry is highly variable and will always be estimated is also presented by Jarvis, N. J. (2007). Moreover, the literature review discusses the experimental determination of hydraulic parameters by laboratory or field measurements. The previous ten years have seen a greater number of studies on experimental measurement, both in the field and in the lab. These hydraulic characteristics include the soil water characteristic curve, also known as soil water retention curves, in addition to the soil matric potential, soil water diffusivity, soil hydraulic conductivity, soil pore water electrical conductivity, and soil water content. Lewis and Sjöstrom (2010) state that since 1950, a significant amount of research has been published in the fields of hydrology, agriculture, and soil sciences, the majority of which is based on the results of soil column experiments. Despite this, no attempt has ever been made to collect or standardise the best practices for creating soil columns, and a review of the literature indicates an overwhelming range of technical approaches. In addition, a great deal of research has been done on the subject of determining the soil water characteristics curve. Plotting the entire soil water characteristic on a single graph becomes difficult when the matric head is lowered to very high negative values, such as $h_m \approx -10^4$ m, unless h_m is shown on a logarithmic scale (Koorevaar, Dirksen and Menelik 1991). This is why the curve is frequently plotted on a semilogarithmic scale (van Genuchten, M. Th 1980). Nonetheless, the curve is plotted at varying scales by different sources. The purpose of this study is to broaden our understanding of the intricate hydrodynamics of water flow through subterranean soil and contribute to the body of knowledge that has been gathered to demystify these intricacies.

2.4.1 Research Objectives

Having conducted a thorough review of a large volume of published literature and identified knowledge gaps in the existing research, the following research objectives have been formulated for this study:

1. Determination of soil water content at intervals of 10 cm in soil column laboratory experiments, mimicking drip soil subsurface micro-irrigation.
2. Determination of soil matric potential at intervals of 10 cm in a soil column laboratory experiments.
3. Draw soil water characteristics curves as a relationship between the soil water content and the soil matric potential for different types of soils.
4. To provide insight into and broaden the understanding on the complex hydrodynamics of water flow through soil subsurface with a focus on water conservation using a link between the soil water content, the soil matric potential, and the crop comfort zone.

Chapter 3
Methodology

The soil column approach is used in this study's experimental investigations to achieve its goals for research. In order to perform soil hydrodynamic testing, a custom-built soil column test rig has been developed and equipped with the necessary equipment. This chapter presents the specifics of the test rig, the related instrumentation, and the methods. The research involves a series of soil column water flow tests carried out, utilizing a conceptualised and designed rig using CAD design. This chapter’s first section provides a thorough explanation of the experimental setup and its components. The second section provides a thorough description and characterization of the soil samples tested, following which the experimental procedures are described.

3.1 Apparatus for The Experiments

In this study, the experimental setup is developed for the flow of water through soil. It is designed to perform gravity-driven flow through the soil column at very low flow velocity from an elevated water supply tank with the aid of a ball valve. The experimental rig has been designed using CAD software Solidworks in this study.

The experimental setup's primary characteristics are as follows:

1. It is a portable setup, making it possible to relocate the complete setup from one laboratory to another.
2. The operational temperature is the same as the surrounding air temperature, hence thermal effect is not considered.
3. Measurements have been conducted from unsaturated conditions of the soil samples.

Figure 3.1a depicts a CAD drawing of the experimental test rig, and Figure 3.1b shows an image of the entire experimental apparatus. There are three sections to the experimental rig: the upper, middle, and lower sections. The data logging/monitoring system and the rig make up the entire experimental setup. A detailed description of the various sections and components of the entire experimental setup is provided below.

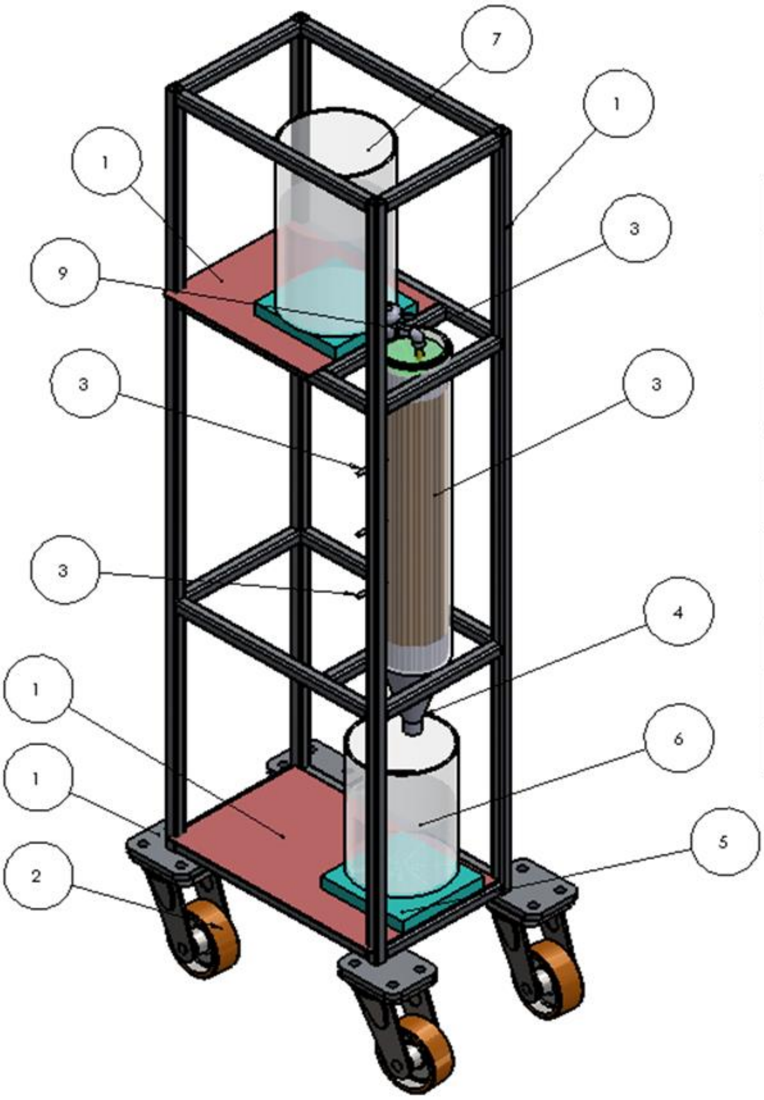

ITEM NO.	PART NUMBER
1	Rig Design Weldment
2	Caster wheel assembly
3	Porous section
4	funnel
5	Weighing scale
6	Receiver tank
7	Elevated tank
8	Part1^Irrigation assembly
9	Tap2
10	Flexible pipe

(a)

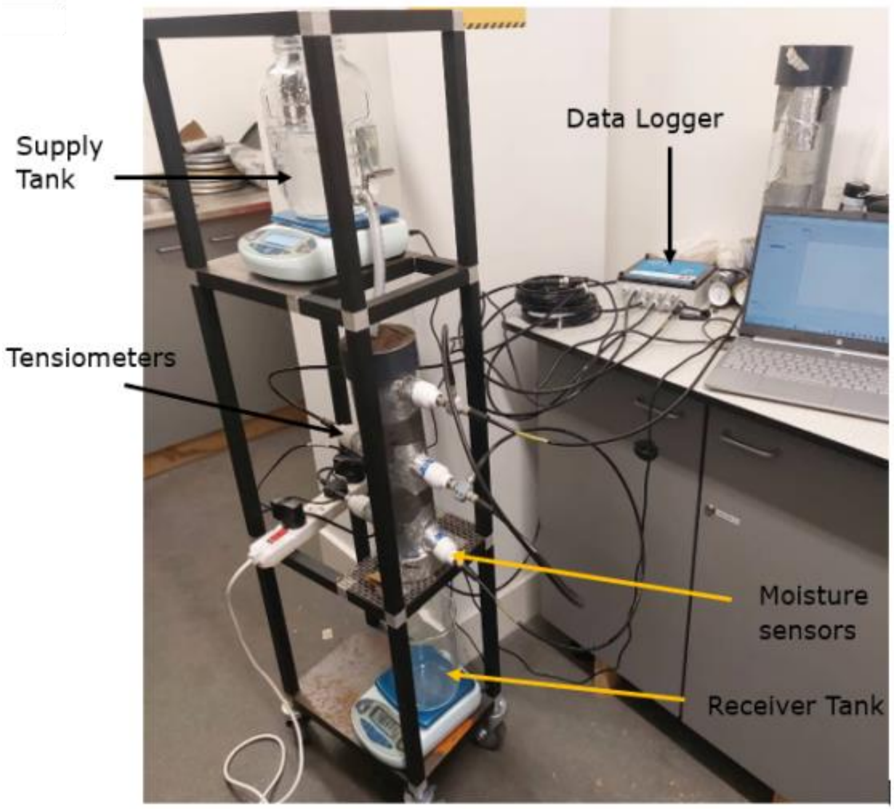

(b)

Figure 3.1 (a) CAD model of the soil column test rig (b) Fabricated experimental setup used as workstation for the soil column experiment.

3.1.1 The Aluminium Support Structure

Using an aluminium square tube, the soil column experimental test rig support structure was developed and constructed. Its complete dimensions were 1240 x 350 x 210 mm. Weighing scales and water tanks were installed on flanges made of 2mm aluminium sheet plate-6082-T6 Grade at the base of the topmost section and the bottommost section as shown in Figure (3.1b). The sections were 400 mm high at the lowest points, 500 mm high in the middle, and 340 mm high at the top. In Figure 3.2, the support structure is displayed. The CAD drawing is in (a), and the image with the Nisorpa 100 mm industrial castor wheels attached is in (b). The 4-inch 100mm Heavy Duty Castors are composed of robust steel brackets and premium polyurethane wheels that are noiseless, wear-proof, and leave no drag trace on the floor. The castor wheel has a diameter of 100mm, a width of 32mm, and a mounting height of 130mm with a total load capacity of 480kg

(120kg per castor). The experimental setup may be transported from one place to another with ease because of the kind and quality of the castor wheels.

ITEM NO.	QUANTITY
1	4
2	8
3	10
4	1
5	1
6	4

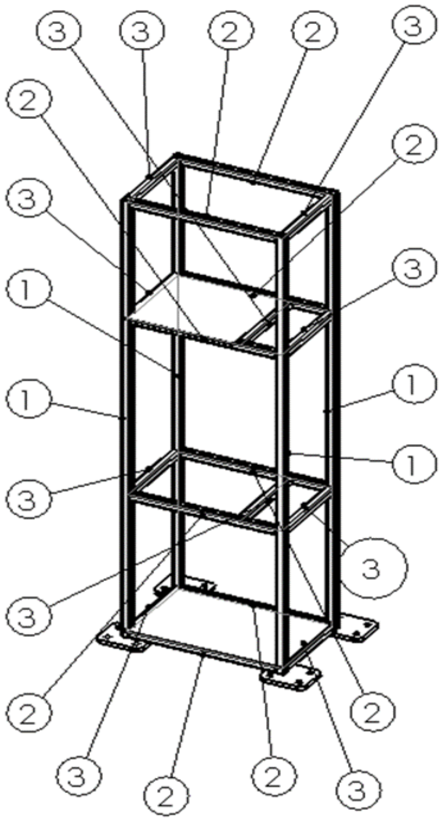

Figure 3.2. (a) CAD model of rig frame

Figure 3.2.(b) photo image of the rig frame with castor wheels

3.1.2 The Supply Tank

A weighing scale was situated atop a flange at the base of the highest section of the experimental rig. The transparent Navaris Dispenser supply tank, measuring 120L x 95W x 253H mm, with a Tap-4 Litre glass jar with stainless steel tap, as sketched in Figure (3.3), was positioned on top of the weighing scale. The tap served as a control valve to regulate the flow velocity from the supply tank and achieved drip irrigation water droplets. To simulate drip irrigation, a 5mm internal diameter flexible hose was attached from the tap to the soil column, directing the water flow from the supply tank to the soil sample as shown in Figure (3.1b).

Figure 3.3. Supply tank

3.1.3 The Soil Column

The experimental rig's central section is where the soil column is located. It includes the soil sample used in the experiment. For the purpose of fitting the sensors for measuring the soil matric potential and water content, horizontal holes with 45mm diameter were bored at intervals of 100mm spacing downward the soil column, which was 400mm high (see Figure 3.4b). The soil column which could be of different diameters is placed in the central section. Figure (3.4) displays samples from the soil column along with a transparent acrylic PVC cylindrical pipe with an internal diameter of 139.7 mm containing packed soil instrumented with sensors. To maintain its rigidity, heavy-duty 6mm wire mesh 304 stainless steel woven LPI x 1.6mm was packed into the base of the soil column. To prevent even the smallest soil particle from getting through the sieve during the water flow experiment, the base of the soil column was additionally filled with 100 GSM (gram per square meter) heavy-duty black Geotextile fabric. By doing this, the accuracy of the mass balance water flow computations was guaranteed. Depending on the diameter of the soil column being used, a premium transparent plastic Big Germ Hunters funnel was additionally fastened to the base of the column. The funnel's mouth opening was 100mm in diameter, with a 13mm spout diameter, for a soil column with an internal diameter of 100mm. The funnel was utilized to direct the water flow from the soil column into the receiver tank, just like in many previous soil column studies, such as (Ritter et al., 2004). Aluminium foil tape, which also functioned as a leak-proof sealer, kept the funnel, sieve, and sensors in place because the water flowed from a drip form under low pressure due to gravity.

(a)

(b)

Figure 3.4. (a) Samples of soil column (b) Soil column instrumented with sensors.

3.1.4 The Receiver Tank

For the purpose of computing mass balance water flow, the receiver tank, which was situated in the lowest section of the experimental rig and sat atop another weighing scale, is depicted in Figure 3.1. The recipient tank was a transparent, 155L x 155W x 190H millimetre, Borosilicate glass-graded measuring beaker for use in a laboratory or kitchen, with a capacity of 2000 millilitres. Through the funnel, water was transferred to it from the soil column.

3.1.5 Weighing Scales

The goal of installing the weighing scales was to do mass balance calculations. In order to record the weight of the water in the tank as it was gradually released into the soil during each experiment, a weighing scale was situated beneath the water supply tank in the uppermost section of the experimental rig. In order to track the weight of water collected from the soil column over the course of each experiment, a second weighing scale was positioned beneath the receiver tank at the lowest section of the experimental rig. A photo image of the scale is displayed in Figure (3.5). It was a professional electronic weighing balance weighing 5000 grammes with a backlit LCD display and five count unit conversions. It was a portable HUKOER Laboratory scale with high precision digital counting at 0.01 grammes.

Figure 3.5. photo image of the weighing scale

3.1.6 Soil Water Content Recording System

The data logger, which was linked to a PC running DELTALINK version 3.9, was coupled to sensors placed in the soil column to record the soil water content, or θ. This particular sensor was a multi-parameter Delta-T Devices Limited (UK) WET150 sensor, which could be used in soils, substrates, and other growing media. In Figure 3.6, the WET150 sensor is displayed. The pins of the WET150 were 55mm long and spaced 20mm apart. In addition to determining the soil's temperature, electrical conductivity, and water content, it evaluated the dielectric characteristics of the soil. With the highest accuracy of ±3%, the sensor turned the recorded dielectric characteristics into water content over the entire range of 0 to 100%. It also converted soil bulk conductivity from 0 to 500 mS/m to 100%. Additionally, the bulk electrical conductivity of soil (EC_b) was measured by the WET150 sensor throughout a range of 0 to 2000 mS/m, with its accuracy being best between 0 and 1200 mS/m ±(10 mS/m + 6%). Additionally, it computed the electrical conductivity of the water contained in the soil's pores, or Pore Water Conductivity (ECp). A tiny sensor included in the sensor body measured temperature. The serial digital interface at 1200 baud (SDI-12) communication protocol standard (version 1.3) was completely compliant with the WET150 sensor. Sensors that had an integrated microprocessor could share a single 3-wire cable to transmit data to a data logger thanks to the SDI-12 communication protocol. As a result, the WET150 could be used with any third-party, SDI-12-compliant logging or metering device, including the Delta-T Devices UK GP2 data logger that was utilised in the experiment. For the common soil types, the WET150 could calculate and output the soil water content directly.

Figure 3.6. WET150 sensor for soil water measurement.

3.1.7 Soil Matric Potential Recording System

The EQ3 Equitensiometer (EQ3) sensor, which detects soil matric potential and temperature, is the main component of the soil matric potential recording system. However, because the WET150 sensor already measures temperature, the EQ3 sensor's programming does not contain the temperature parameter in using it for the experiments. Additional details will be provided in section 3.4. The negative pressure, sometimes known as suction, needed to remove water from the spaces between soil particles is known as the soil matric potential, Ψ and has units of pressure, kPa. The water potential is influenced by various factors such as gravity, air pressure, osmosis, and the capillary action of soil particles. The last factor, known as the Soil Matric Potential, or Ψ_m, fluctuates from 0 kPa at field capacity to roughly -1500 kPa at the permanent wilting point and is strongly influenced by the soil's wetness. It is a crucial sign of water stress in plants. Although temperature and salinity also have an impact, the amount of water present and the composition of the soil determine the measured value of soil matric potential.

The EQ3 Equitensiometer sensor is shown in Figure 3.7. An array of stainless steel rods transmits an electromagnetic field into a porous substance (the equilibrium body). The ML3 ThetaProbe, a precision soil moisture sensor, is the component of the EQ3, and its measuring rods are implanted in the equilibrium body, a porous substance. The water content and matric potential of this substance has a well-established, consistent relationship. The matric potential inside the equilibrium body equilibrates to that of the surrounding soils when the probe is put into the soil. The EQ3 generates a 100MHz waveform (like an FM radio) when power is added. An array of stainless steel rods receives the waveform, and these rods transfers an electromagnetic field into a porous substance, which is the equilibrium body. Permittivity, a measurement of a material's reaction to polarisation in an electromagnetic field, is mostly determined by the water content of the porous substance (the equilibrium body) encircling the rods. The permittivity of air is 1, while that of water is approximately 81. As a result of the porous material's considerable influence on the applied field that the EQ3 detects, a constant voltage output serves as a straightforward and accurate indicator of the soil matric potential. The ML3 ThetaProbe measures the water content of the matric material directly; using the calibration curve included with each device, this may be translated into the matric potential of the surrounding soil.

Figure 3.7. EQ3 Equitensiometer

3.1.8 Data Logging and Monitoring Devices

The GP2 Data Logger and Controller, a research-grade logger with sophisticated feedback control and complex computed measures, is utilised for the experiment's data logging and monitoring (Figure 3.8). The GP2 data logger includes 12 differential analogue input channels in addition to a serial input channel that can accept up to 62 SDI-12 sensors or a single WET sensor. The reading speed of each sensor varies, ranging from 1 second to more than 1000 days.

Figure 3.8. GP2 Data Logger

The data logger could store over 2.5 million readings, with several recording speeds available for each combination of parameters and multiple recording kinds offered, including average, minimum, maximum, total, integral, wind-rose, and conditional. The DELTALINK 3.9 programme software, a product of Delta-T Devices, is in communication with the data logger through pre-installed software on the PC. Using the DELTALINK 3.9 software on the PC, simple programmes can be rapidly generated and then transferred to the GP2 data logger with the help of a useful user interface and sensor library. It is possible to write complex programme scripts without knowing any programming languages or inputting instructions. Complex control algorithms and new measurements can be developed mathematically using trigonometric and algebraic functions, conditional logic, and readily created instruction sequences. Personal variables, such as the number of days that moisture has been below a threshold, can also be created and manipulated. The GP2 data logger featured a simulator that is very helpful for irrigation and helps with verifying and comprehending the behaviour of logging and control programmes.

3.1.9 Application of Software

The PC software developed by Delta-T Devices for configuring and obtaining data from the GP2 data logger is called DeltaLINK 3.9. Once the GP2 Data logger is connected to a PC via a serial cable and the DeltaLINK 3.9 software is installed on the computer, the logger is detected by the software and shown in the status bar, as illustrated in Figure 3.9. The WET150 SDI-12 sensors that are in the sensor library are compatible with the software. In order to set up, control, retrieve, and display logged data, the installation programme creates a DeltaLINK 3.9 programme group in the Windows Programmes menu. With the GP2 Multifunction programme editor, which offers a comprehensive feature set, the DeltaLINK 3.9 supports the GP2 Advanced Data Logger and Controller. This includes: (a) a large library of Delta-T sensors, along with comprehensive programming and installation notes; (b) flexible recording options, such as multiple recording rates, statistics, and wind processing functions (such as direction and vector averaging, wind roses), conditional recording; and (c) scripts for complete customisation of logging and control behaviour. The GP2 simulator, which mimics the majority of meteorological and environmental sensors as well as response-applied irrigation, is also included. To import DeltaLIINK datasets into a Microsoft Excel (32-bit) spreadsheet, a dataset import wizard is also installed on the PC. All of the data that has been stored in the GP2 data logger will be retrieved and shown on the screen from the dataset window shown in Figure 3.9. These can be saved to a PC dataset file, which can then be modified to open in Excel when the dataset import wizard is utilised. The file extension can be changed to .csv.

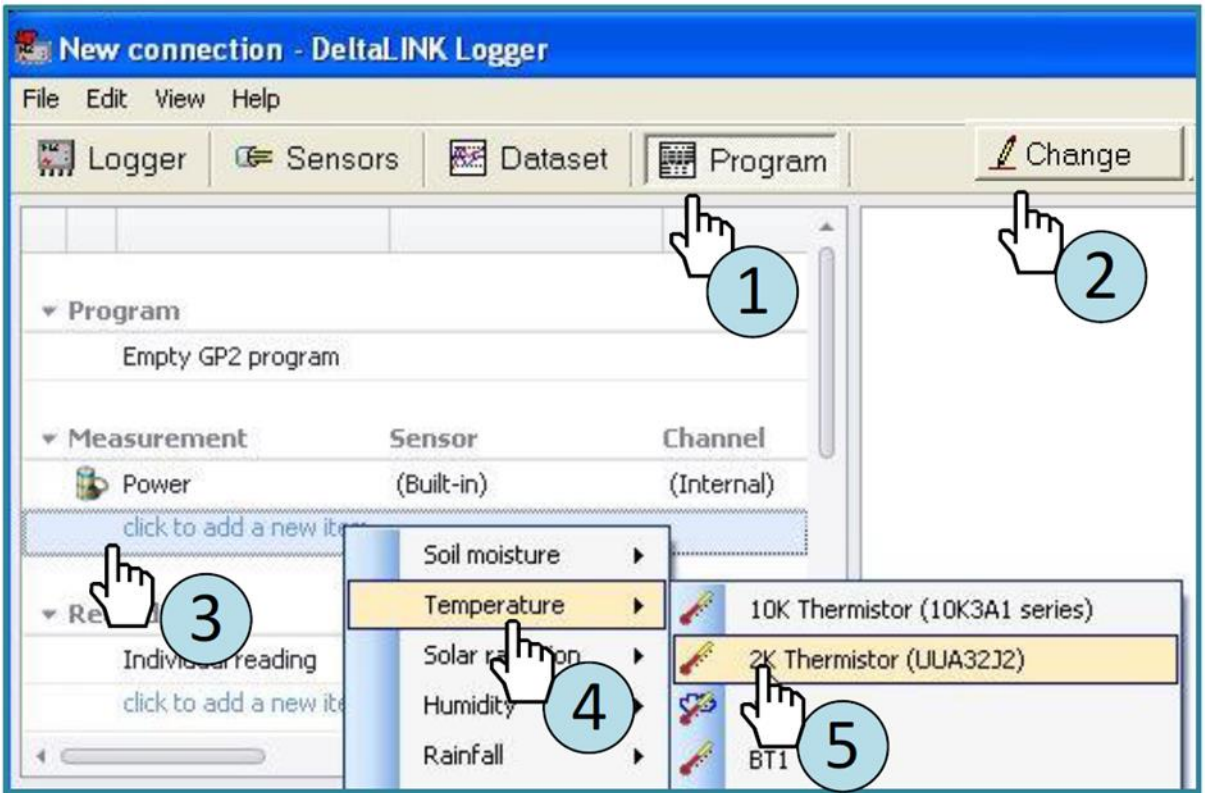

Figure 3.9. DeltaLINK 3.9 interface for the GP2 Data Logger.

3.2 Test Materials

Materials for the soil column studies were acquired from three different locations, as indicated in the sections below. Three samples were collected; two were from the inland valley soils of Nigeria's Niger Delta, while the third was from Aberdeen, UK's Garthdee area. Originally, materials from three distinct locations in the Niger Delta area's inland valley were designated for the soil column investigations; however, transborder logistics restricted the samples to two. To compare the methods used for sample preparation, the kind of soil used, and the dimensions of the cylinder column, the third sample from Aberdeen's Garthdee region had to be included.

3.2.1 Packed Soil Samples from Aberdeen

One of the soil column experiment samples is taken from a garden near the River Dee at Robert Gordon University in the Garthdee area of Aberdeen, United Kingdom (Lat/Long 56.123136N,2.134911W). The sample appears to be silty sand based on the grain size distribution. According to Hrapovic et al. (2005) and Ghodrati, Chendorain, and Chang (1999b), the sample is damp packed, which entails mechanically packing tiny volumes of damp soils into the soil column (Communar, Keren, and Li 2004). To promote homogeneity during the experiment, extra attention is taken to ensure that the grain arrangement is similar across the soil sample. With an internal diameter of 139.7 mm and a height of 400 mm, the soil column is a transparent acrylic PVC cylindrical pipe with 45 mm diameter holes bored through vertically downward at intervals of 100 mm spacing for the locations of sensors in the laboratory.

3.2.2 Monolith of Undisturbed Soil Sample from Ivrogbo

According to Ritter et al. (2004), a monolith of undisturbed soil sample is taken from a fallowed area in Ivrogbo near a branch of the river Niger (lat/long 5.41872N, 6.34359E). The property, which lies on the Nigerian Niger-Delta region's inland valley, has been used for agriculture in one way or another for more than 15 years, but at the time the sample for the experiment is taken, it is covered with weeds. After the weeds are removed from the top, a cylindrical PVC pipe is buried in the ground vertically downwards. With an internal diameter of 101.6 mm and a height of 400 mm, the cylindrical PVC pipe is smaller than the pipe utilised in the packed soil column for the Aberdeen soil. After driving the pipe vertically into the ground until it is level with the soil's surface, the earth is removed from the sides of the pipe using a shovel. The undisturbed soil sample is submitted to the laboratory after being sealed. Preliminary study is carried out to determine the bulk density, Atterberg limits, and soil particle size. To test electrical conductivity, exchangeable acidity, basic elements (magnesium, calcium, potassium, and phosphorus), total exchangeable gases, and total organic carbon (TOC), a portion of the soil sample is also transported to a chemical laboratory. Summary of the soil analysis for the soil classification of the soil sample, using the American Association of State Highway and Transportation Officials (AASHTO) and the Unified Soil Classification System (USCS) is presented. These two commonly used systems of classifying soils are based on particle size distribution and Atterberg Limits. The detail of the preliminary research is presented in chapter four under results and discussion for monolith of undisturbed soil column from Ivrogbo.

3.2.3 Monolith of Undisturbed Soil Sample from Oleh

A monolith of undisturbed soil sample is also taken from a fallowed land in a farm garden in Oleh (lat/long 5.46186N, 6.20624E), according to Ritter et al. (2004). The parcel of land, which is also located in the inland valley of the Nigerian Niger-Delta region, has been utilised for agricultural activities in one form or another for more than 20 years, but is left fallow and grown with weeds when the trial sample is obtained. A cylindrical PVC pipe is buried vertically downward in the earth after the top is cleared of weeds. The cylindrical PVC pipe is 400 mm tall and has an internal diameter of 101.6 mm, which is smaller than the pipe used in the packed soil column for the Aberdeen soil but similar to the pipe used in the monolith of undisturbed soil sample from Ivrogbo. Using a shovel, the earth is dug out from the sides of the pipe after it is driven vertically into the ground until is level with the soil's surface. After being sealed, the undisturbed soil sample is sent to the laboratory. To ascertain the bulk density, Atterberg limits, and soil particle size, preliminary research is conducted. In addition, a piece of the soil sample is sent to a chemical laboratory to measure electrical conductivity, exchangeable acidity, basic elements (magnesium, calcium, potassium, and phosphorus), total exchangeable gases, and total organic carbon (TOC). A summary of the soil analysis is provided for the purpose of of classifying the soil sample using the Unified Soil Classification System (USCS) and the American Association of State Highway and Transportation Officials (AASHTO). Particle size distribution and Atterberg limits serve as the foundation for these two widely used methods of classifying soils. The early research findings are provided in Chapter Four for the Oleh monolith soil column.

3.3 Experimental Procedure and Sequence

The dry unsaturated soil with sensors are weighed in a Seca weighing scale as indicated in Figure 3.10 below. This is to dolument the soil column's weight prior to logging. In order to monitor the amount of water retained in the soil throughout the experiment throughout the time, the weight of the soil column equipped with the sensors is also measured after the experiment (logging). Additionally, the rig's upper supply tank is filled with water, and the weight of the tank is measured using the electronic laboratory scale located beneath it.

To ascertain the amount of water that entered the soil column during each experiment, the weight is also noted afterwards. To calculate the water flux during each experiment, the lower portion of the rig's recerver tank is additionally weighed both before and after by means of the electronic weighing scaale located beneath it in the laboratory. The EQ3 GP2 logger channel can be created in DeltaLINK by choosing an EQ2x sensor type measurement and entering the special look-up table that comes with each equitensiometer sensor.

Figure 3.10. Unsaturated soil column with sensors before experiment

The experiment programme is constructed using the GP2 multifunction program in the DeltaLINK 3.9 software, validated, saved, and forwarded to the data logger. The moment logging is initiated, the experiment begins. In order to simulate drip micro-irrigation, the tap in the supply tank located in the upper section of the rig is left open, allowing water to flow in form of drip flow in slow droplets through the hose and into the soil. The amount of water released as measured over time by the electronic laboratory weighing scale is used to calculate the flow rate. The dataset is examined using the dataset window in the GP2 logger interface of the DeltaLINK 3.9 when water begins to accumulate in the receiver tank. It is observed that the pressure value decreases from a negative value to zero and moves towards a positive value. After that, the dataset import wizard is used to import the dataset into an Excel file and logging is halted. As previously mentioned, the soil column is detached from the logger and weighed once more.

3.4 Correlation of Soil Water Retention Curve

The following describes three predictions made by Brooks and Corey (1964), van Genuchten (1980), and (Fredlund & Xing, 1994) for the soil water characteristics curve. When the measured soil water characteristics curve data are available, each method's corresponding closed-form equation is typically obtained by fitting the data. The van Genuchten method, however, was used to compare the curves in this study because, as stated by Gallage et al. (2013), the integration in the (Fredlund & Xing, 1994) equation is complex, and a closed-form solution is only available in numerical software like Soil Vision (2006), SEEP/W (2004), and VADOSE/W (2004), where Simpson's rule is typically used to integrate the equation. The Brooks and Corey (1964) equation does not converge rapidly when used in numerical simulations of seepage in saturated-unsaturated soils.

3.4.1 Brooks and Corey Correlation

The (Brooks et al., 1964) that is used to best-fit the soil-water characteristic curve data is as follows (Gallage et al., 2013):

$$\theta = \theta_r + (\theta_s - \theta_r)\left(\frac{\psi_b}{\psi}\right)^{\lambda} \text{ for } \psi \geq \psi_b \tag{3.1}$$

where θ is the volumetric water content, θ_s the saturated volumetric water content, θ_r the residual volumetric water content, ψ the soil suction (kPa), ψ_b the curve fitting parameter (air-entry value), and λ the fitting parameter (pore-size distribution index).

3.4.2 Van Genuchten Correlation

An approach based on fitting soil-water characteristic data by van Genuchten's (1980) equation was proposed by (van Genuchten, M. Th 1980). The van Genuchten (1980) equation for the soil-water characteristic of unsaturated soils is presented in equation (3.2):

$$\theta = \theta_r + \frac{(\theta_s - \theta_r)}{[1 + (\alpha\psi^n)]^m} \tag{3.2}$$

where θ is the volumetric water content, θ_s is the saturated volumetric water content, θ_r is the residual volumetric water content, α and n are the curve fitting parameters, and m = 1 – 1/n.

3.4.3 Fredlund and Xing Correlation

In 1994, Fredlund and Xing introduced a technique for characterising the soil water characteristic curve. Fredlund and Xing (1994) suggested Equation 3.3 to fit the soil-water characteristic data. (Gallage, Kodikara, and Uchimura 2013) state that the complex equation has no closed-form solution:

$$\theta = \left\{1 - \frac{\ln(1+\psi/\psi_r)}{\ln(1+10^6/\psi_r)}\right\}\left\{\frac{\theta_s}{\ln[e+(\psi/a)^n]^m}\right\} \tag{3.3}$$

where θ is volumetric water, ψ is soil suction (kPa), ψ_r is residual suction (kPa), e is a natural number (2.71828…), and a, m, n = fitting parameters (parameter a has the unit of pressure (kPa)).

3.5 Technical Challenges

Despite at least three centuries of experience using soil columns, no standardisation of experimental procedures has taken place, according to Lewis and Sjöstrom 2010b. Direct comparisons of study results from multiple studies are challenging since many of the experimental methodologies and approaches that are reported in the literature are exclusive to a particular researcher or to a research team. This is required, largely, because different kinds of experiments call for drastically varied methods of conducting experiments. A number of variables, including the equipment used, the personnel's skill, and the methodology used, have contributed to the disparity in the soil column analysis findings. Soil column experiments continue to be a crucial component of research on the hydrodynamic subsurface flow of water through soils, despite the challenges associated with obtaining repeatable data. Therefore, it is imperative to standardise experimental best practices for the collection, quality assurance, and interpretation of soil column data in order to reduce data uncertainties. To design conduct and validate experimental soil column water flow studies, one must fully admit the uncertainties in the conventional approach and have a solid understanding of it. The following highlights a few sources of uncertainty, research constraints, and technical difficulties that were faced.

1. Wall effect: Water migrates to the cylinder walls during soil column water flow studies, creating preferred flow—a faster flow around the walls caused by a greater attraction between the water and the cylinder wall. Using silicon gum, the inner wall of the cylinder are rubbed to prevent this. In order to replicate drip micro-irrigation, water is also slowly injected into the soil column through a hose in the centre of the soil column, allowing the soil to be evenly moistened as it descends the column. Additionally, the column's geometry is designed to follow the cylinder height to diameter ratio of 4 to 1, as per Bromly, Hinz, and Aylmore (2007).
2. Non-repeatability of the experiments: The process is only done once for each soil sample since it is very difficult to repeat the experiments and get the same results because the soil hydraulic conductivity fluctuates with each trial.
3. Technical knowhow of the equipment: Learning how to operate the data logger and the sensors for the experiment is challenging and time-consuming, in addition to the equipment's exorbitant expenses. The programmes for the fluid flow tests and the production of the final results for analysis in Excel and other data-analysis formats are also very sophisticated.

3.6 Scope of the Research

The scope of the study is limited to the following:

i. Soil analysis of two different locations in the inland valley region of the Niger Delta area of Nigeria has been carried out.
ii. Conceptualisation, CAD design, and construction of a laboratory test rig for soil column infiltration experiments has been carried out as well.
iii. Infiltration tests have been conducted using packed soil sample from Aberdeen and monoliths of soil samples from two distinct areas of the inland valley of the Nigerian Niger Delta: Ivrogbo and Oleh. Afterwards, the packed sample from Aberdeen is disturbed to create a fourth sample that will resemble ploughing.

iv. The soil water characteristic curves, which represent a link between the soil matric potential and the soil water content, are found by analysis of the recorded data from the infiltration experiments. The Van Genuchten model of the soil water characteristics curve has been used for the verification of the experimental data. From analysis of the soil water characteristics curves of the soil samples, a smart drip micro-irrigation is suggested based on a knowledge of plant comfort zones for different crops.

Chapter 4

Soil Water Content based Hydrodynamic Characterisation of Different Soil Types

The findings from the infiltration experiments detailing the soil water content are reported in this chapter. A packed soil sample from Aberdeen, and monoliths of undisturbed soil samples from Ivrogbo and Oleh in the inland valley of the Niger Delta region of Nigeria are used, and the soil water content at different soil depths are presented and compared.

4.1 Test Conditions

A total of four experiments are conducted in this study. After drying for some weeks, the packed sample is ploughed and stones are removed which completely alters the texture and make the second Aberdeen sample. The Ivrogbo and Oleh monoliths of undisturbed soil samples make the third and fourth samples respectively. This section presents the results on the infiltration experiments carried out on the four soil samples considered in this study, critically evaluating the spatio-temporal soil water content.

4.1.1 Packed Soil Sample

Based on the grain size distribution, the Aberdeen soil sample is considered to be silty sand. It is also wet-packed, meaning that small amounts of damp soil are mechanically packed into the soil column. Extra care is taken to guarantee that the grain arrangement is consistent across the soil sample in order to support homogeneity throughout the experiment. In a second experiment, the same soil sample is disturbed to simulate ploughing after it has dried for approximately six months in the laboratory under normal pressure and temperature conditions. After removing every stone, the soil is repacked, and an infiltration experiment is carried out. The purpose of the tests is to carry out the hydrodynamic characterisation of the soil samples through the infiltration experiments, through the determination of the soil water content, the soil matric potential and the soil water characteristic curve.

4.1.2 Monolith of Undisturbed Soil Sample from Ivrogbo

Two sets of experiments are provided in this study. The first step is a preliminary examination to identify the type of soil used for the soil column experiment for the soil from Ivrogbo (lat/long 5.41872N, 6.34359E), a location close to a branch of the River Niger in the inland valley of the Nigerian Niger Delta. In order to classify the soil, the initial research is conducted using sieve analysis in the laboratory of Setraco Nigeria Limited to measure the particle size diameter, bulk density, and Atterberg limit. For gaseous analysis, samples are also brought to Golden Years Laboratory. In order to examine the properties of soil water for the purpose of water conservation activities, a monolith of undisturbed soil sample is brought to the laboratory for the study's primary experiment for the characterisation of the soil hydraulic properties. The procedure is described in section 3.2.2.

4.1.3 Monolith of Undisturbed Soil Sample from Oleh

This study also includes two sets of experiments. In order to determine the type of soil utilised for the soil column experiment, a preliminary analysis is conducted on the soil from Oleh (lat/long 5.46186N, 6.20624E), an area that is swampy and located in the inland valley of the Nigerian Niger Delta. The first step in classifying the soil is measuring the bulk density, Atterberg limit, and particle size diameter in the laboratory of Setraco Nigeria Limited utilising sieve analysis. Samples are also brought to Golden Years Laboratory for gaseous analysis. For the major experiment of the study, a monolith of undisturbed soil sample is also taken to the laboratory to analyse the properties of soil water for the purpose of water conservation operations. Section 3.2.3 provides a description of the process.

4.2 Test Results

This section presents the results of the infiltration experiments for the packed soil sample and the ploughed soil sample, as well as the Ivrogbo and Oleh samples. In addition, the section also presents the results for the sieve analysis for the determination of the soil types for the Ivrogbo and the Oleh samples.

4.2.1 Packed Soil Sample

The results of the first experiment are shown in this section. First, two EQ3 Equitensiometer sensors are integrated on one side of the 400 mm high, 139.7 mm internal diameter soil sample column through 45 mm bored holes in the cylindrical pipe, and three WET150 sensors are integrated on the other side, spaced 100 mm vertically downward. The first EQ3 tensiometer is positioned 200 mm vertically downward, while the second one is positioned 300 mm from the top, 100 mm apart. To find the amount of water in the soil before and after each infiltration experiment, the soil column and the sensors are weighed in a Seca weighing scale both prior to attachment to the GP2 data logger and again after logging is complete and the logger is disconnected. This procedure is used to compute the flow Reynolds number and determine the hose's flow velocity by taking into consideration the water that is released from the supply tank. This is required to verify whether the flow is laminar, meaning that a slow flow is preferred for drip micro-irrigation. Referring to Figure 4.4, the setup for the soil column infiltration studies carried out in the lab is the same for every sample. Table 4.1 below summarises the mass balance flow process data.

Table 4.1. Mass balance during infiltration experiment of packed soil sample

Date of Experiment	05/07/2023	06/07/2023
Supply Tank		
Initial weight (g)	3576.14	2676.14
Final weight (g)	2676.14	2061
Water released (g)	900	615.14
Time of flow (minutes)	191	97
Receiver Tank		
Initial weight (g)	482.46	482.46
Final weight (g)	482.46	490.86
Water received (g)	0	8.4
Time of flow (minutes)	191	97
Soil Column		
Initial weight of soil column (g)	8200	
Initial weight of soil column with sensors before experiment (g)	9000	
Weight of soil column with sensors after experiment (g)	9900	10500
Weight of water retained in soil (g)	900	600

Two dates for the experiments are shown in Table 4.1 because the logging is stopped on the first day and the experiment is resumed and completed on the second day. The experiment is for more than three hours on the first day and is finished after roughly one and a half hours on the second day. On the first day of the experiment, it is observed that 900g of water is held in the medium, but no water is released into the receiver tank. On the first day, the flow rate is calculated as 7.8534E-08 m^3/s; on the second day, it is calculated as 1.05694E-07 m^3/s. The two infiltration tests are averaged, and the resultant flow rate is 8.76817E-08 m^3/s. Comparably, in the first experiment, the flow velocity via the tube from the supply tank into the soil column is calculated as 4.00684E-05 m/s. In contrast, in the second experiment, it is calculated as 5.39256E-5 m/s, with an average of 4.47356E-5 m/s. According to computations, the experiment's first day's Reynolds number is 2.003419169, while the second day's is 2.696279543. The average is calculated to be 2.236778392. It is evident that both experiments, even though the first day's flow velocity is lower than the second day's, are laminar flows with low Reynolds numbers suitable for drip micro-irrigation systems. Utilising the averages to analyse the dynamics of the flow is also suitable. Appendix 2 of this report contains the logged data produced by the soil column infiltration experiment for the packed soil sample from Aberdeen.

4.2.2 Ploughed Soil Sample

The results of the second experiment, which employed a sample of ploughed soil from Aberdeen's Garthdee region, are presented in this section. First, three WET150 sensors were integrated on one side of the 400 mm high, 139.7 mm internal diameter soil sample column, spaced 100 mm vertically downward, and two EQ3 Equitensiometer sensors are inserted on the other side through 45 mm drilled holes in the cylindrical pipe. The first EQ3 tensiometer is placed 200 mm vertically downward, while the second one is placed 100 mm apart and 300 mm from the top. The soil column and the sensors are weighed in a Seca weighing scale both before and after attachment to the GP2 data logger, as well as once again after logging is finished and the logger is detached, in order to determine the amount of water in the soil before and after each infiltration experiment. Using this process, the flow Reynolds number and the hose's flow velocity are calculated while accounting for the water that is released from the supply tank. This is required to verify whether the flow is laminar, indicating that a slow flow is optimal for drip micro-irrigation. Every minute, data is logged during the 217-minute duration of the experiment. At the conclusion of the experiment, it is noted that 312.99g of water has been received in the receiver tank, despite 2,140.71g of water having been released from the supply tank. The flow velocity is determined to be 8.38863E-05 m/s, the Reynolds number to be 4.194312518, and the flow rate to be 1.64417E-07 m^3/s. As a result, the flow has low Reynolds number and laminar, making it ideal for drip micro-irrigation systems. The logged data from the soil column infiltration experiment for the ploughed soil sample from Aberdeen is included in Appendix 3 of this report. Each sample is subjected to the same setup for the soil column infiltration experiments carried out in the laboratory using Figure 4.4. The data from the mass balance flow procedure is shown in Table 4.2 below.

Table 4.2. Mass balance consideration of water flow processes for infiltration experiment of Aberdeen ploughed soil sample

Date of Experiment	23/01/2024
Supply tank	
Initial weight (g)	3745.32
Final weight (g)	1604.61
Water released (g)	2140.71
Time of flow (minutes)	224
Receiver tank	
Initial weight (g)	482.43
Final weight (g)	795.42
Water received (g)	312.99
Time of flow (minutes)	224
Soil column	
Initial weight of soil column (g)	N/A
Initial weight of soil column with sensors before experiment (g)	8600
Weight of soil column with sensors after experiment (g)	10400
Weight of water retained in soil (g)	1800

4.2.3 Test Results for Sieve Analysis of Monolith of Undisturbed Soil Sample from Ivrogbo

Table 4.3 presents the results of the sieve examination of the soil at Ivrogbo. Given that the diameter is defined as the diameter for which the percent passing in the sieve analysis is 90%, the particle diameter of the Ivrogbo sample is 0.3 mm. The test output graph is shown in Figure 4.1. The Atterberg limit test findings for the Ivrogbo soil sample are shown in Table 4.4, and the test output graph is shown in

Figure 4.2. In Table 4.5, the bulk density test yields an average bulk density of 1.64 g/cm^3 for the Ivrogbo soil. The outcomes of the gaseous analysis are shown in Table 4.6. Porosity of Soil: As paricle size increases, surface soil porosity usually increases. This results from soil biological processes causing the production of soil aggregates in surface soils with finer textures. Particulate adherence and increased resistance to compaction are two aspects of aggregation. Sandy soil typically has a bulk density of 1.50 to 1.70 g/cm^3. Porosity as a result ranges from 0.43 to 0.36. Clay soil typically has a bulk density of 1.1 to 1.3 g/cm^3. This results in a porosity that ranges from 0.58 to 0.51. The porosity of the Ivrogbo soil sample is calculated to be 0.36 based on the bulk density of 1.64 g/cm^3.

Table 4.3. Determination of Particle Size for Ivrogbo Soil Sample

Weight of sample before washing (g) 363.40

Sieve Size		Weight Retained	Percentage Retained	Percentage Passing
#	(mm)	(g)	(%)	(%)
3-in	75.00	0.00	0.0	100.0
1 1/2-in	37.50	0.00	0.0	100.0
3/4-in	19.00	0.00	0.0	100.0
3/8-in	9.50	0.00	0.0	100.0
No.4	4.75	0.00	0.0	100.0
No.10	2.00	0.00	0.0	100.0
No.16	1.18	0.00	0.0	100.0
No.30	0.600	15.40	4.2	95.8
No.40	0.425	15.40	4.2	95.8
No.50	0.300	20.30	5.6	90.2
No.100	0.150	42.70	11.8	78.4
No.200	0.075	94.30	25.9	52.5
Pan		190.70	52.5	
Total		363.40		

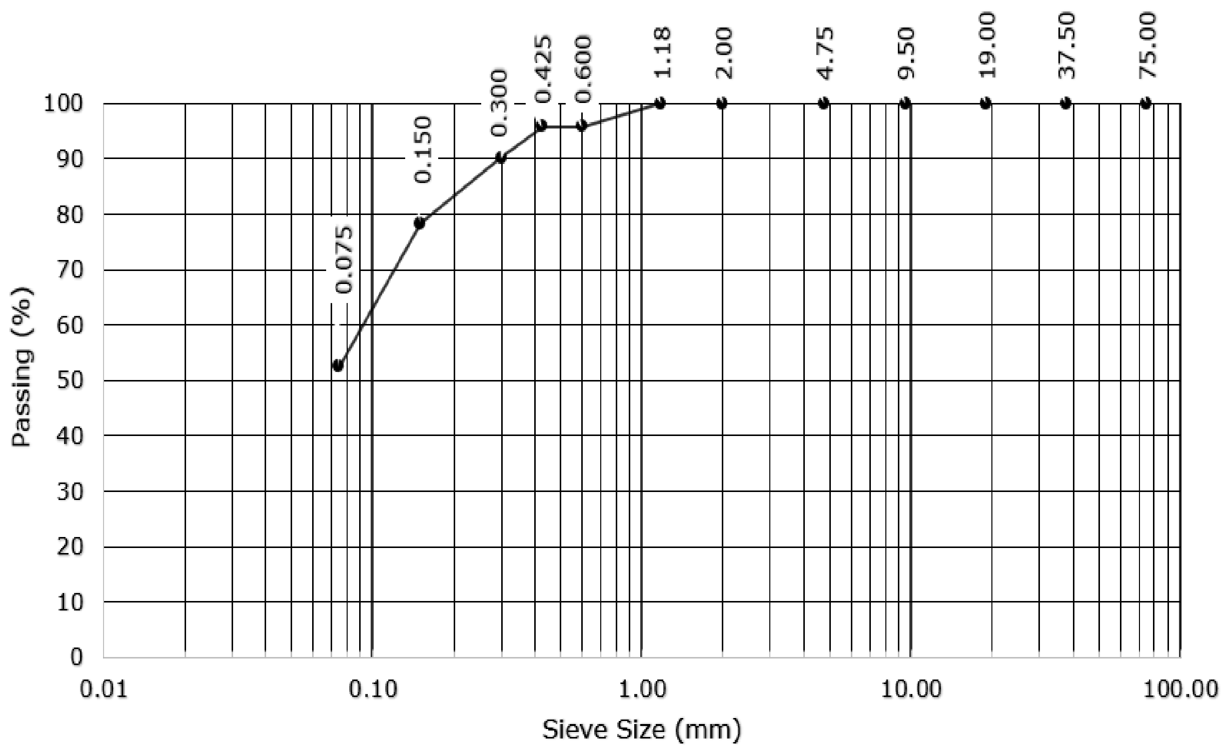

Figure 4.1. Test output graph for Ivrogbo soil

Table 4.4. Atterberg Limit for Ivrogbo Soil Sample

Topsoil 0.45m							
Description		Test					
Test Type		Liquid Limit			Plastic Limit		
Test No.		1	2	3	1	2	Average
No. of Blows (Liquid Limit Test)		13	23	34			
Container No.		F	X	A	G	J	
Weight of wet soil + Container	(g)	44.69	46.12	47.91	27.99	28.01	
Weight of drysoil + Container	(g)	35.91	37.13	38.58	25.67	25.74	
Weight of Container	(g)	16.00	15.98	15.77	16.00	15.99	
Weight of moisture (A)	(g)	8.78	8.99	9.33	2.32	2.27	
Weight of dry soil (B)	(g)	19.91	21.15	22.81	9.67	9.75	
Moisture content	(%)	44.10	42.51	40.90	23.99	23.28	23.64
Test Results							
Liquid Limit		(LL)			42.20		
Plastic Limit		(PL)			23.60		
Plasticity Index		(PI)			18.60		

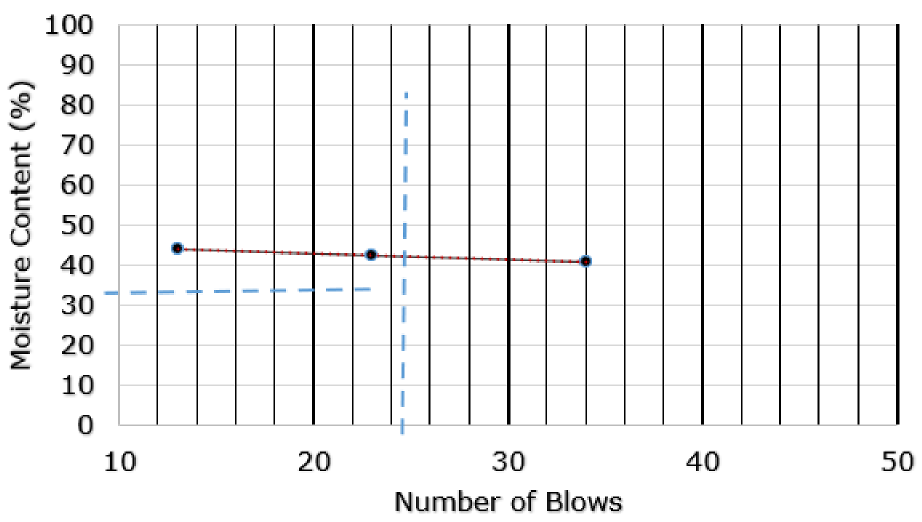

Figure 4.2. Atterberg Limit Test Output Graph for Ivrogbo

Table 4.5. Bulk density test for Ivrogbo soil sample

Type Of Material: Lateritic Material	
Container Volume (V)	3232
Container Weight Empty	186
Container weight + Sample	5500
Material Weight (W)	5314
Density = W/V	1.64
AVERAGE DENSITY =	1.64 g/cm^3

Table 4.6. Gaseous analysis for the Ivrogbo soil sample

parameters	Ivrogbo
Calcium, meq/100g	4.20
Magnesium, meq/100g	2.56
Potassium, meq/100g	1.52
Sodium, meq/100g	1.98
TOC, %	0.02
Total Nirogen, mg/kg	59.27
Total Phosphate, mg/kg	9.69
Exchangeable Acidity, meq/100g	0.25
Electrical Conductivity, μS/cm	86.30

Using the Unified Soil Classification System (USCS) and the American Association of State Highway and Transportation Officials (AASHTO (Moreno-Maroto et al., 2021b), Table 4.7 provides an overview of the soil analysis conducted for the soil classification of the Ivrogbo soil sample. These two widely used methods of soil classification are based on Atterberg Limits and particle dispersion shown above. The Unified Soil Classification System (USCS) and the American Association of State Highway and Transportation Office (AASHTO) (Table 4.7) have determined that the test material (Ivrogbo soil sample) is silty clay with low to medium plasticity, and a bulk density of 1.64g/cm3, with a calculated porosity of 0.36 is determined. This classification is based on sieve analysis and gaseous analysis.

Table 4.7. Soil Classification for Ivrogbo soil sample

Sample	% passing				% Fraction Retained No 4	Diameter D of % passing			Atterberg Limits		Classification	
	sieve	sieve	sieve	sieve		D60	D30	D10	Liquid Limit	Plasticity Index		
No	No 200	No 40	No 10	No 4			mm		(LL)	(PI)	AASHTO	Unified
Ivrogbo	52.5	95.8	100.0	100.0	0.0	0.10	–	–	42.2	18.6	A-7-6	CL

4.2.4 Test Results of Infiltration Experiment for Monolith of Soil Sample from Ivrogbo

This section presents the findings from the main experiment conducted in the laboratory using a soil sample from Ivrogbo. Initially, the 400 mm high soil sample column with an internal diameter of 101.6 mm is instrumented with two EQ3 Equitensiometers on one side through 45 mm bored holes in the cylindrical pipe, and three WET150 sensors at a spacing of 100 mm vertically downward on the other. The first EQ3 tensiometer is placed at 200 mm vertically downward, while the other is also 100 mm apart, that is at 300 mm from the top. Before attaching to the GP2 data logger and again once logging is ended and the logger is disconnected, the soil column and the sensors are weighed in a seca weighing scale as illustrated in Figure 4.3. Figure 4.4 displays how the experiment is set up. The EQ3 Equitensiometer recordings with the label Psi at 200 mm from the top of the soil column correspond to the WET150 recordings with the labels Theta(3), SoilTemp(3), and ECp(3), while the EQ3 Equitensiometer recordings with the label Psi(2) at 300 mm from the top of the soil column correspond to the WET150 recordings with the labels Theta(2), SoilTemp(2), and ECp(2). At 100 mm from the top of the soil column, there are no EQ3 Equitensiometer records that correlate to the WET150 data labelled Theta, SoilTemp, and ECp.
When logging is commenced, the tap of Figure 4.4 is opened slowly to release water from the supply tank into the soil through the hose. The tap is turned off and logging is stopped when the psi values are zero or read positive. Table 4.8 below displays the mass balance flow process data. The experiment is run for 126 minutes with data logging done every minute. It is observed that while 647.9g of water is released from the supply tank, 190.44g of water is received in the receiver tank at the end of the experiment. The flow rate is calculated as 8.57011E-08 m^3/s with a flow velocity of 4.3725E-05 m/s and Reynolds number of 2.186251485. Hence the flow is laminar with low Reynolds number suitable for drip micro-irrigation systems. Appendix 5 contains the logged data produced by the soil column infiltration experiment for the Ivrogbo soil sample.

Figure 4.3. Weight of Ivrogbo soil column and sensors before the experiment

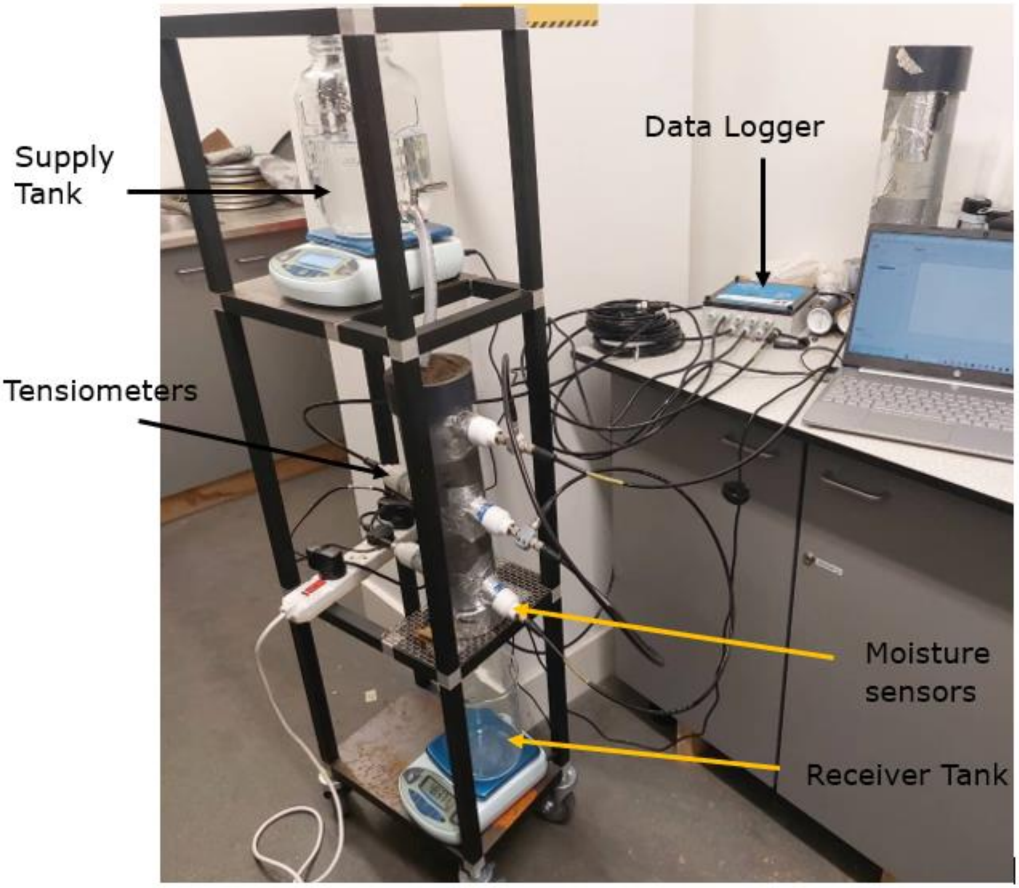

Figure 4.4. Arrangement for the experiment of the Ivrogbo soil sample

Table 4.8. Mass balance consideration of water flow processes for the infiltration experiment using the Ivrogbo soil sample

Date of Experiment	08/08/2023
Supply tank	
Initial weight (g)	3610.53
Final weight (g)	2962.63
Water released (g)	647.9
Time of flow (minutes)	126
Receiver tank	
Initial weight (g)	484.16
Final weight (g)	674.6
Water received (g)	190.44
Time of flow (minutes)	126
Soil column	
Initial weight of soil column (g)	N/A
Initial weight of soil column with sensors before experiment (g)	8000
Weight of soil column with sensors after experiment (g)	8400
Weight of water retained in soil (g)	400

4.2.5 Test Results for Sieve Analysis of Monolith of Undisturbed Soil Sample from Oleh

Table 4.9 shows the results of the sieve analysis for the Oleh soil. Since the diameter is defined as the diameter for which the percent passing is 90% in the sieve analysis, the Oleh sample's particle diameter is 0.6 mm. The test output graph is shown in Figure 4.5.

Table 4.9. Determination Of Particle Size for Oleh Soil Sample

Weight of sample before washing (g) 380.2				
Sieve Size #	(mm)	Weight Retained (g)	Percentage Retained (%)	Percentage Passing (%)
3-in	75.00	0.00	0.0	100.0
1 1/2-in	37.50	0.00	0.0	100.0
3/4-in	19.00	0.00	0.0	100.0
3/8-in	9.50	0.00	0.0	100.0
No.4	4.75	0.00	0.0	100.0
No.10	2.00	0.00	0.0	100.0
No.16	1.18	9.40	2.7	97.3
No.30	0.600	26.10	7.6	89.7
No.40	0.425	26.10	7.6	89.7
No.50	0.300	50.10	14.6	75.1
No.100	0.150	70.06	20.5	54.5
No.200	0.075	73.10	21.3	33.3
Pan		114.30	33.3	
Total		343.60		

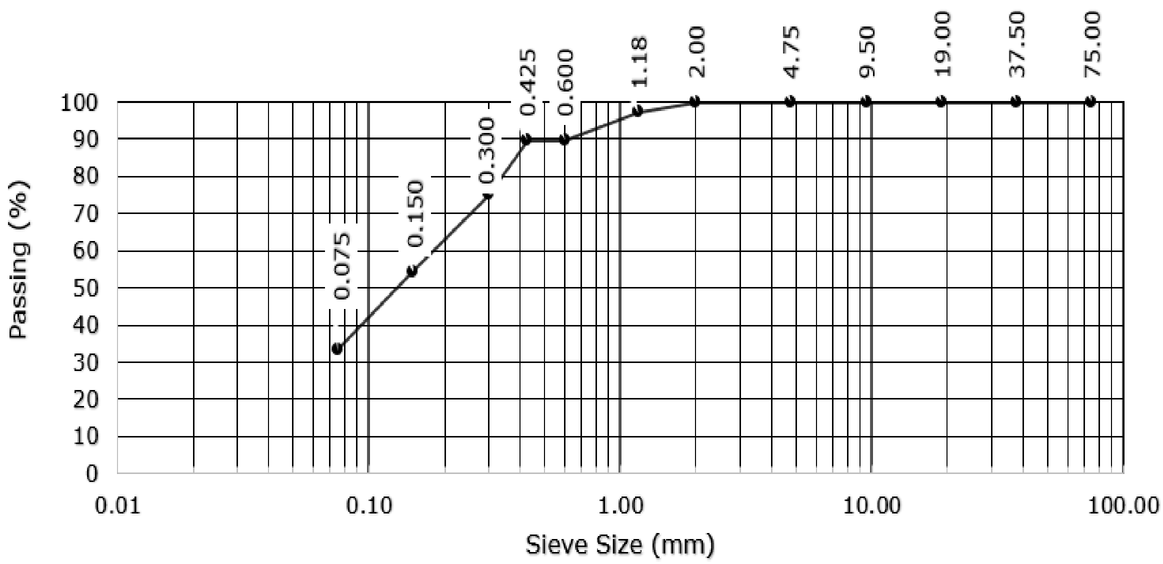

Determination of D60, D30, D10 (mm) % Passing Sieve #10 (2mm)

Figure 4.5. Test Output Graph for Oleh Soil

Table 4.10 provides the results of the Atterberg limit test for the Oleh soil sample, and Figure 4.6 depicts the test output graph. The average bulk density of the Oleh soil, as determined by the bulk density test, is 1.64 g/cm^3, as reported in Table 4.11. The outcomes of the gaseous analysis are shown in Table 4.12. The soil porosity of surface soil typically decreases as particle size increases. This happens when surface soils with finer textures produce soil aggregates due to biological processes in the soil. Particulate adhesion and enhanced resistance to compaction are two features of aggregation. The bulk density of sandy soil is usually between 1.50 and 1.70 g/cm^3. As such, porosity varies from 0.43 to 0.36. The bulk density of clay soil is usually between 1.1 and 1.3 g/cm^3. As a result, the porosity varies between 0.58 and 0.51. The bulk density of 1.64 g/cm^3 is used to compute the porosity of the Oleh soil sample, which comes out at 0.36.

Table 4.10. Atterberg Limit for Oleh Soil Sample

Topsoil 0.45m							
Description		Test					
Test Type		Liquid Limit			Plastic Limit		
Test No.		1	2	3	1	2	Average
No. of Blows (Liquid Limit Test)		13	23	34			
Container No.		N	AS	ZZ	RG	KL	
Weight of wet soil + Container	(g)	44.98	45.76	46.40	28.78	29.43	
Weight of drysoil + Container	(g)	37.09	37.77	38.45	26.55	27.00	
Weight of Container	(g)	16.22	16.00	15.99	16.00	15.98	
Weight of moisture (A)	(g)	7.89	7.99	8.00	2.23	2.43	
Weight of dry soil (B)	(g)	20.87	21.77	22.47	10.55	11.02	
Moisture content	(%)	37.81	36.70	35.60	21.14	22.05	21.59
Test Results							
Liquid Limit		(LL)			36.5		
Plastic Limit		(PL)			21.6		
Plasticity Index		(PI)			14.9		

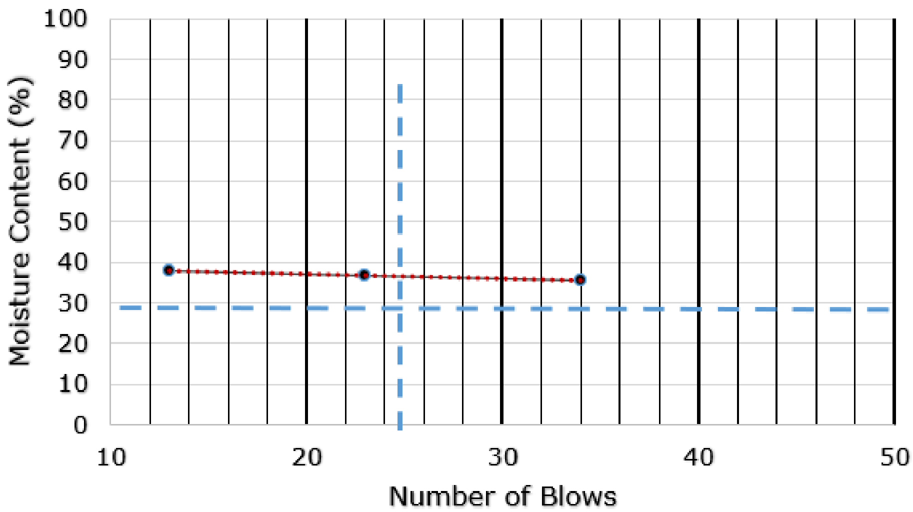

Figure 4.6. Atterberg Limit Test Output Graph for Oleh Soil

Table 4.11. Bulk Density Test For Oleh Soil Sample

TYPE OF MATERIAL: LATERITIC MATERIAL	
Container Volume (V)	3423
Container Weight Empty	188
Container weight + Sample	5814
Material Weight (W)	5626
Density = W/V	1.64
AVERAGE DENSITY	1.64 g/cm^3

Table 4.12. Gaseous analysis for the Oleh soil sample

Parameters	Oleh
Calcium, meq/100g	4.86
Magnesium, meq/100g	2.47
Potassium, meq/100g	1.39
Sodium, meq/100g	2.15
TOC, %	0.03
Total Nirogen, mg/kg	79.07
Total Phosphate, mg/kg	13.05
Exchangeable Acidity, meq/100g	0.30
Electrical Conductivity, µS/cm	104.80

Using the Unified Soil Classification System (USCS) and the American Association of State Highway and Transportation Officials (AASHTO) (Moreno-Maroto, Alonso-Azcárate and O'Kelly 2021), Table 4.13 provides an overview of the soil analysis conducted for the soil classification of the Oleh soil sample. According to the Unified Soil Classification System (USCS) and the American Association of State Highway and Transportation Office (AASHTO) (Table 4.13), the test material, or the Oleh soil sample, is a sand clay mixture with a bulk density of 1.64g/cm^3 and a computed porosity of 0.36. Gaseous analysis and sieve analysis form the basis of this categorization

Table 4.13. Soil Classification for Oleh soil sample

Sample	% passing				% Fraction Retained No 4	Diameter D of % passing			Atterberg Limits		Classification	
	sieve	sieve	sieve	sieve		D60	D30	D10	Liquid Limit	Plasticity Index		
No	No 200	No 40	No 10	No 4		mm			(LL)	(PI)	AASHTO	Unified
Oleh	33.3	89.7	100.0	100.0	0.0	0.19	–	–	36.5	14.9	A-2-6	SC

4.2.6 Test Results of Infiltration Experiment for Monolith of Soil Sample from Oleh

The results of the primary experiment employing a monolith of soil sample from Oleh are reported in this section, which is comparable to the Ivrogbo soil column experiment discussed above. Initially, three WET150 sensors spaced 100 mm vertically downward on one side and two EQ3 Equitensiometers on the other side are integrated through 45 mm bored holes in the cylindrical pipe 400 mm high soil sample column with an internal diameter of 101.6 mm. The first EQ3 tensiometer is positioned 200 mm vertically downward, while the second one is positioned 300 mm from the top, 100 mm apart. The soil column and the sensors are weighed on a Seca weighing scale, both prior to attachment to the GP2 data logger and again after logging is complete and the logger is disconnected. Table 4.14 displays the data for the mass balance flow process. The hose's flow velocity, measured when water is released from the supply tank into the soil column, is 5.16613E-05 m/s with a mass flow rate of 1.01256E-07 m^3/s. The flow Reynolds number is calculated to be 2.583065105, which is laminar flow for the hose in the magnitude of drip flow to replicate drip micro-irrigation. Table 4.14 shows that during the 148-minute experiment, 905.23g (or 905.23 cm^3) of water are released from the supply tank, whereas 536.36 cm3 of water are received in the receiver tank. Furthermore, 300g of water is held in the soil. This indicates that there is a water difference of roughly 7% that the experiment is unable to account for. Leaks in the soil column are the cause of this. Appendix 5 contains the raw data from the experiment. The logging rate is set to one minute. Consequently, the experiment takes 148 minutes to finish, as evidenced by the raw data that is generated. Additionally, the WET150 recordings labelled Theta(3), SoilTemp(3), and ECp(3) correspond to the EQ3 Equitensiometer recordings labelled Psi at 200 mm from the top of the soil column, while the EQ3 Equitensiometer recordings labelled Psi(2) at 300 mm from the top of the soil column correspond to the WET150 recordings labelled Theta(2), SoilTemp(2), and ECp(2). There are no EQ3 Equitensiometer records that correlate to the WET150 data with the labels Theta, SoilTemp, and ECp at 100 mm below the top of the soil column. The three WET 150 sensors are allocated address 1 at the top of the SDI-12 protocol to read ECp, SoilTemp, and Theta. Theta(3), SoilTemp(3), and ECp(3) are read by the sensor positioned 200 mm vertically downward at address 2, and Theta(2), SoilTemp(2), and ECp(2) are read by the bottom sensor at address 3. This is the explanation for the discrepancy.

Table 4.14. Mass balance consideration of water flow processes

Date of Experiment	10/08/2023
Supply Tank	
Initial weight (g)	2768.93
Final weight (g)	1863.7
Water released (g)	905.23
Time of flow (minutes)	149
Receiver Tank	
Initial weight (g)	482.74
Final weight (g)	1022.1
Water received (g)	539.36
Time of flow (minutes)	149
Soil Column	
Initial weight of soil column (g)	N/A
Initial weight of soil column with sensors before experiment (g)	8500
Weight of soil column with sensors after experiment (g)	8800
Weight of water retained in soil (g)	300

4.3 Soil Water Content

The soil water content profiles of the infiltration experiments for the soil samples are presented in this section. The results for the packed soil sample, the ploughed soil sample, the Ivrogbo sample, and the Oleh sample are presented for the 100 mm depth, 200 mm depth and the 300 mm depth.

4.3.1 Measured Soil Water Content for the Packed Soil Sample from Aberdeen

Figures 4.7, 4.8 and 4.9 present measurements of the infiltration at the 100mm, 200mm, and 300mm depths vertically down the soil column showing domain-specific soil water content. While the water content remains steady and minimal for the first 27 minutes before it begins to transition in the 100mm depth, it takes about 80 minutes to start rising in the 200mm depth, and 190 minutes in the 300mm depth. These minimal water content values are taken as the residual values for the unsaturated conditions at these depths. The profiles show that while the water attains steady flow around 80 minutes in the 100mm depth, the 300mm depth is still not reached in the 190th minute, hence there is no water in the receiver tank before logging is stopped on the first day, which prompts continuity in the second day. However, a discontinuity is noticed in the 190th minute due to the break in logging. This is shown in the three figures and Figure 4.10 though it is observed at the resumption of logging that the water content is higher at the 300mm depth, and least at the 100mm depth. This can be attributed to the accumulation of water at the bottom of the soil column overnight. It is noticed that on the second logging, the water content at the 100 mm depth sustains a quick rise from 13.9% and attains a steady value of 25.6% at a cumulated time of 220 minutes while the water content at the 200 mm depth rises from 17.5% at the second logging and attains a steady value of 30% at 244 minutes, the water content at the 300 mm depth rises from 18.6% on the second logging and continues to rise after attainment of 37.5% even after 287 minutes when the logging is finally stopped. The continued rise of the water content at the 300 mm depth could be attributed to nonequilibrium flow which is generated by the accumulation.

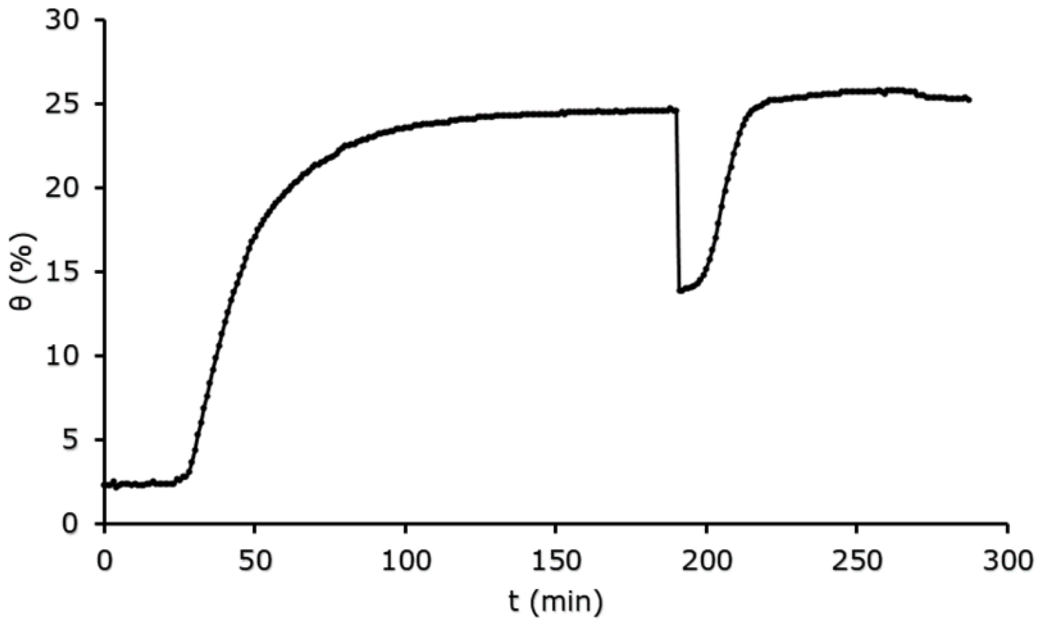

Figure 4.7. Domain-specific volumetric soil water content at 100 mm depth for Aberdeen packed soil sample

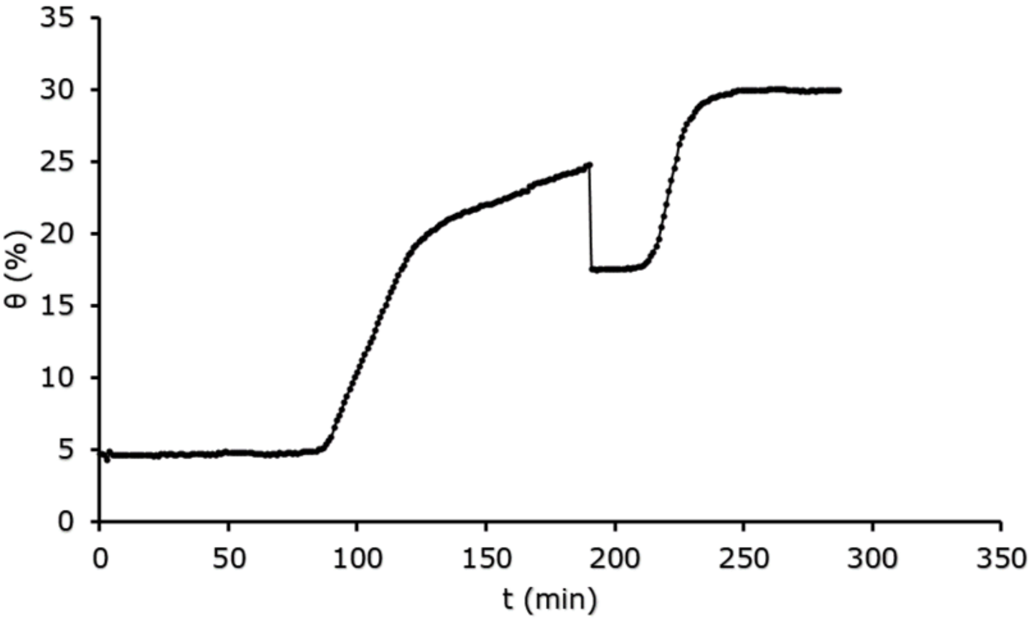

Figure 4.8. Domain-specific volumetric soil water content at 200 mm depth for Aberdeen packed soil sample

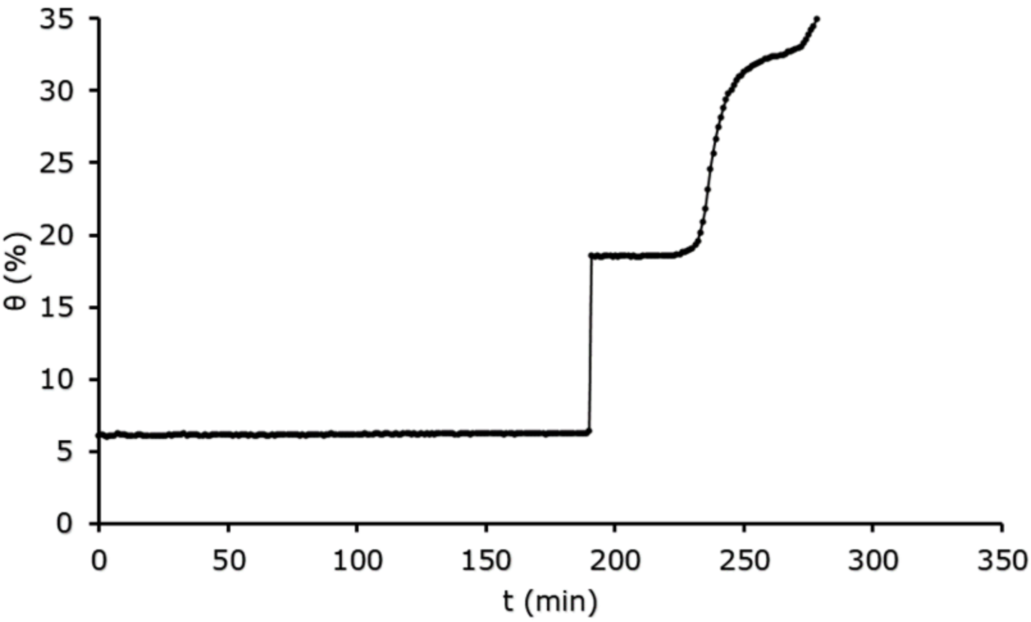

Figure 4.9. Domain-specific volumetric soil water content at 300mm depth for Aberdeen packed soil sample

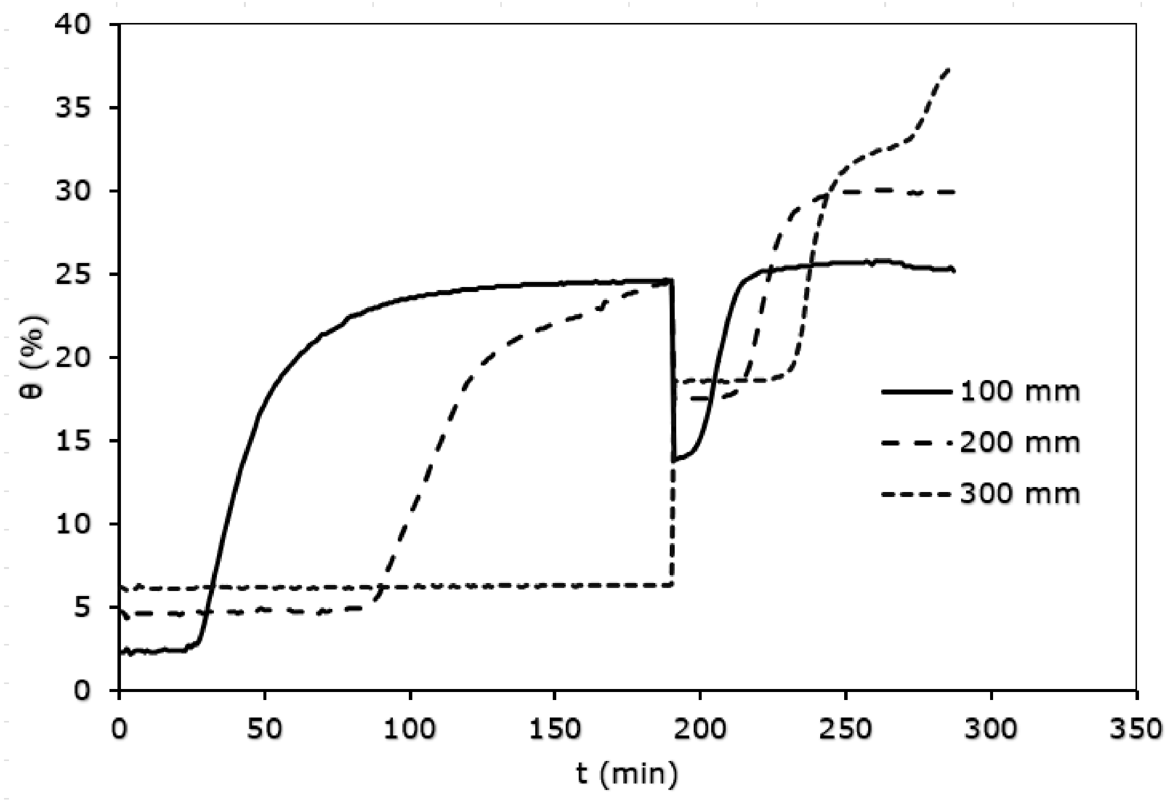

Figure 4.10. Infiltration experiment showing domain-specific water content at depths of (a) 100 mm (b) 200 mm (c) 300 mm for packed soil sample

4.3.2 Measured Soil Water Content for the Ploughed Soil Sample from Aberdeen

The measured soil water content for the ploughed soil sample is displayed in Figures 4.11 through 4.14. Based on observations, the first water content at 200 mm is 3.1%, the initial water content at 300 mm is 4%, and the driest soil is found at 100 mm. These figures describe the soil water content for the residual soil values (RSV). The water content at the 300 mm depth starts rising from 4.9% at 110 minutes after the logging commences, and it reaches 30.3% in 110 minutes when the logging is terminated. In under ninety minutes, the water content at 100 mm rises from 2.8% to a stable 32%. In 110 minutes, the water content at 200 mm deep increases from 3.4% to a constant 31%. The logging is stopped because the mass balance calculation shows that 312.99 of water has accumulated in the receiver tank, suggesting that the porous section is probably saturated. Furthermore, Figure 4.14 demonstrates how the three curves maintain the streamline flow, showing that the flow is uniform, steady, and consistent throughout the whole profile with a stable wetting front.

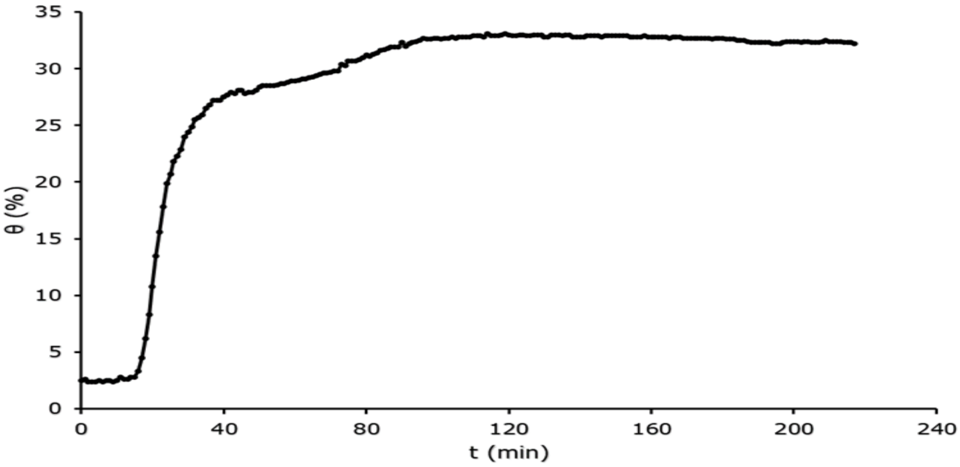

Figure 4.11. Domain-specific volumetric soil water content at 100mm depth for Aberdeen ploughed soil sample

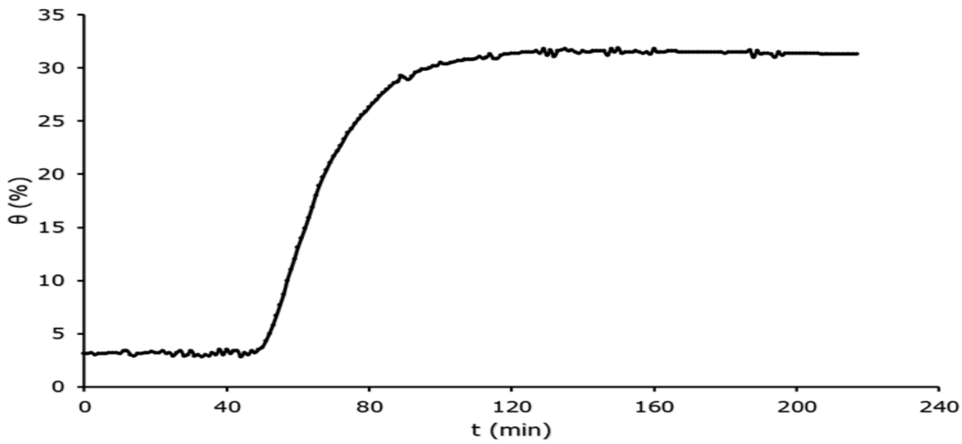

Figure 4.12. Domain-specific volumetric soil water content at 200mm depth for Aberdeen ploughed soil sample

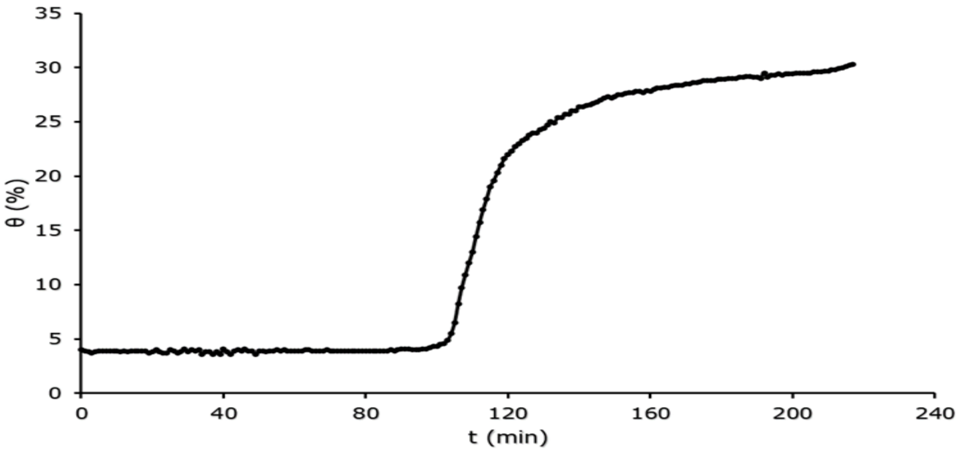

Figure 4.13. Domain-specific volumetric soil water content at 300mm depth for Aberdeen ploughed soil sample

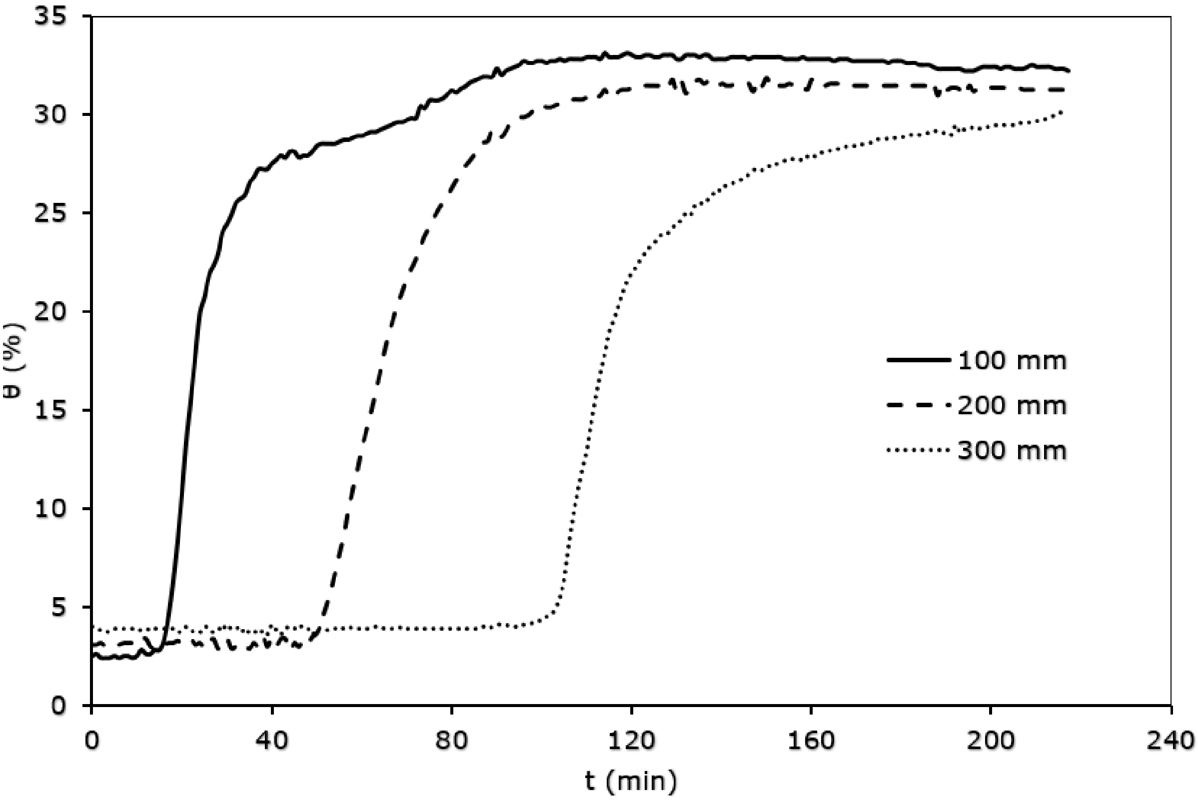

Figure 4.14. Infiltration experiment showing domain specific water content at depths of (a) 100 mm (b) 200 mm (c) 300 mm using the Aberdeen ploughed soil sample

4.3.3 Measured Soil Water Content for Monolith of Undisturbed Soil Sample from Ivrogbo

The soil water content profiles for the depths of 100 mm, 200 mm, and 300 mm, as well as the average for the 200 mm and 300 mm depths, are shown in Figures 4.15 to 4.19. The 200 mm and 300 mm depths have corresponding sensors for the soil matric suction. The soil water content is observed to stay constant at 100 mm deep for a few minutes, then it starts to rise quickly until it reaches around 35%. After that, it returns to being constant and fluctuates between 34% and 36% for the majority of the remaining period of the 126 minutes of the experiment. For roughly the first 50 minutes of the experiment, the soil water content at 200 mm depth is seen to be stable. After that, it starts to rise gradually and steadily until it reaches the same range of values as at 100 mm depth. This is represented by the curve with dashed line in Figure 4.19, which includes the depth data points of 100 mm, 200 mm, and 300 mm. This implies that as the water seeps through the soil column, a preferred flow is experienced. The flow profile at the 300 mm depth is shown by the curve in Figure 4.17 which maintains a parallel flow with the 100 mm depth profile after around 50 minutes of the experiment. We can conclude that there is either preferential flow or nonequilibrium water flow through the soil column for the sample.

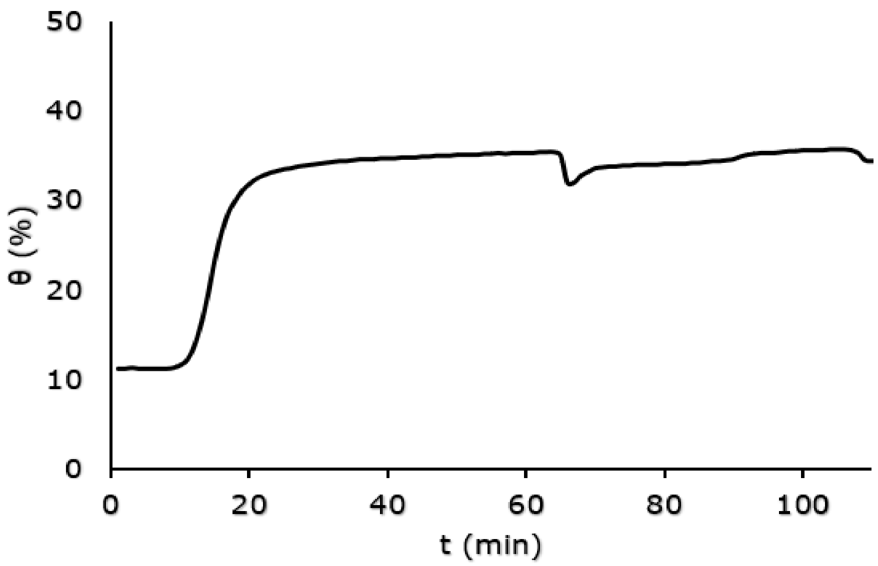

Figure 4.15. Domain-specific volumetric soil water content at 100mm depth for Ivrogbo soil sample infiltration experiment

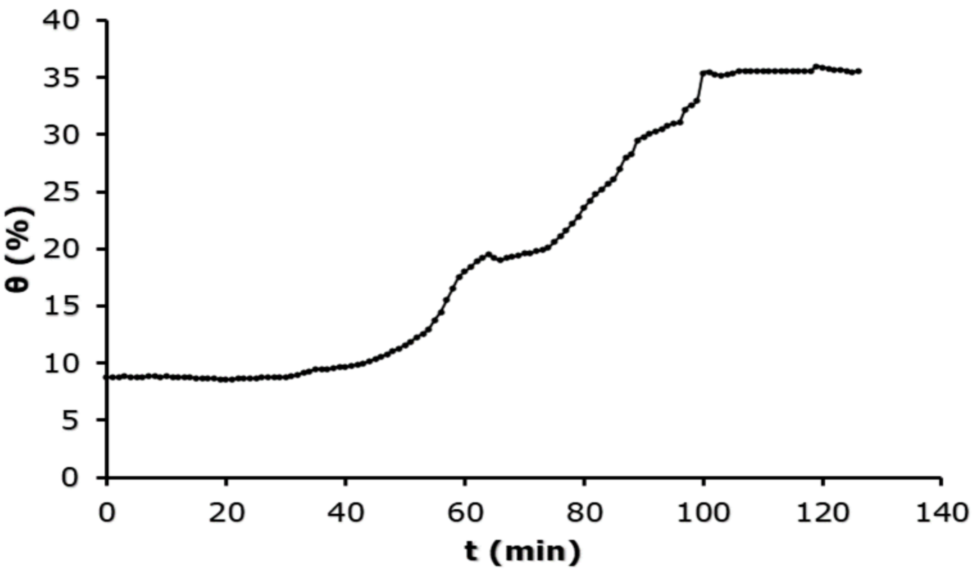

Figure 4.16. Domain-specific volumetric soil water content at 200mm depth for Ivrogbo soil sample infiltration experiment

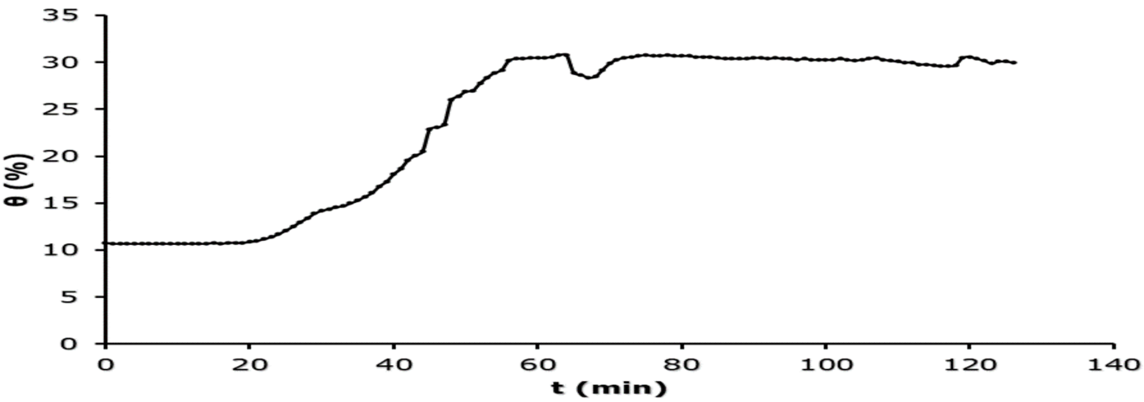

Figure 4.17. Domain-specific volumetric soil water content at 300mm depth for Ivrogbo soil sample infiltration experiment

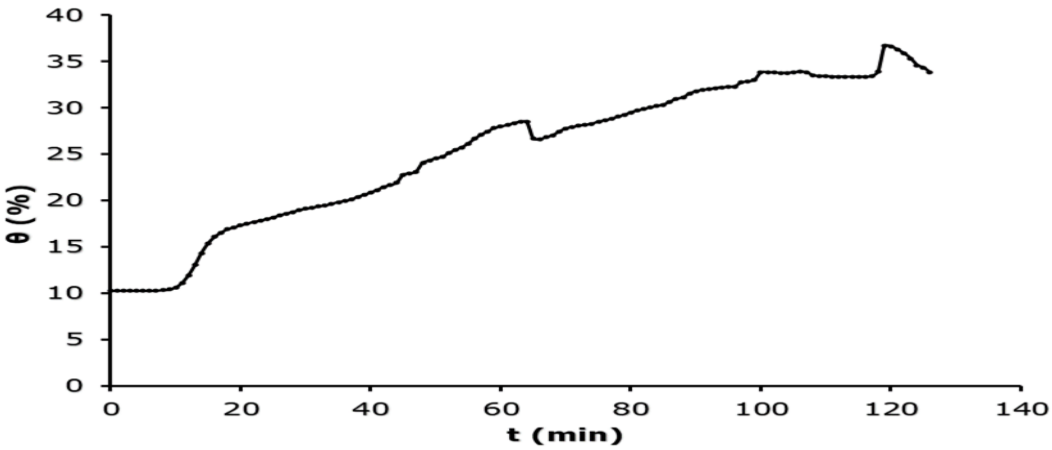

Figure 4.18. Domain-specific volumetric soil water content for average of 200mm and 300mm depth for Ivrogbo soil sample infiltration experiment

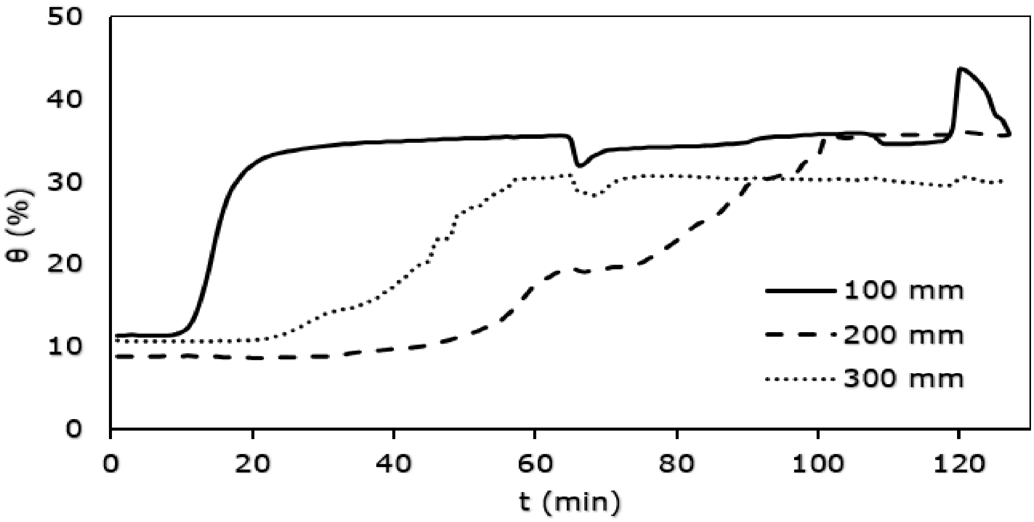

Figure 4.19. Infiltration experiment showing domain specific water content at depths of (a) 100 mm (b) 200 mm (c) 300 mm using the monolith of Ivrogbo soil sample

4.3.4 Measured Soil Water Content for Monolith of Undisturbed Soil Sample from Oleh

Figures 4.20 to 4.24 display the soil water content profiles for the depths of 100 mm, 200 mm, and 300 mm as well as the average for the 200 mm and 300 mm depths. There are equivalent sensors for the soil matric suction at 200 and 300 mm depths. For a few minutes, the soil water content is seen to remain steady at a depth of 100 mm. After that, it begins to rise swiftly and at a steep slope, reaching approximately 33%. It keeps this value for the remainder of the 148 minutes of the experiment, with minor fluctuations.

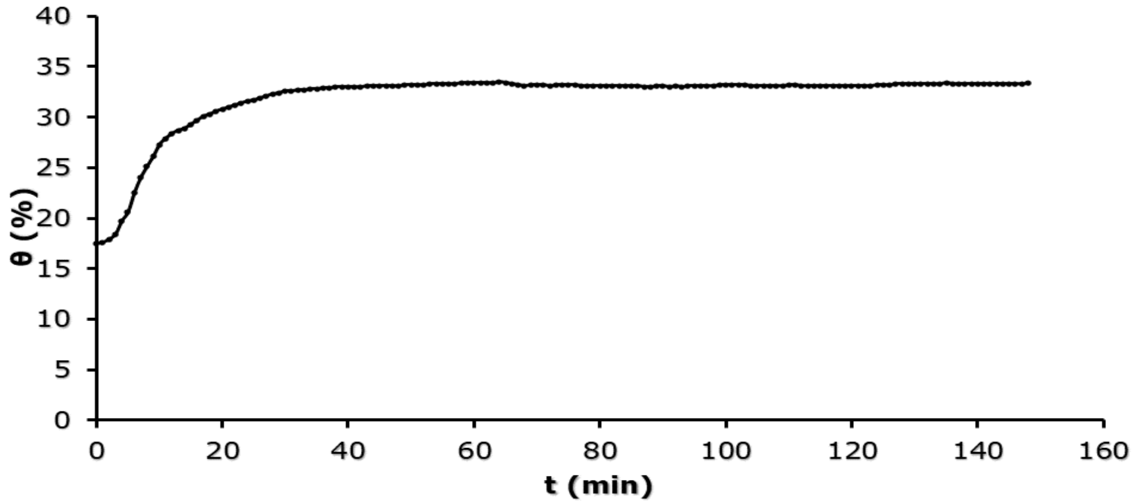

Figure 4.20. Domain-specific volumetric soil water content at 100mm depth for Oleh soil sample infiltration experiment

The soil water content at 200 mm depth in Figure 4.21 is observed to be constant at 15.9% during about the first 11 minutes of the experiment. Following that, it begins to rise quickly and consistently until it surpasses the values at 300 and 100 mm of depth. This is seen by the dashed curve in Figure 4.24, which has the 100, 200, and 300 mm depth data points. This suggests that a preferred flow is felt as the water percolates down the soil column.

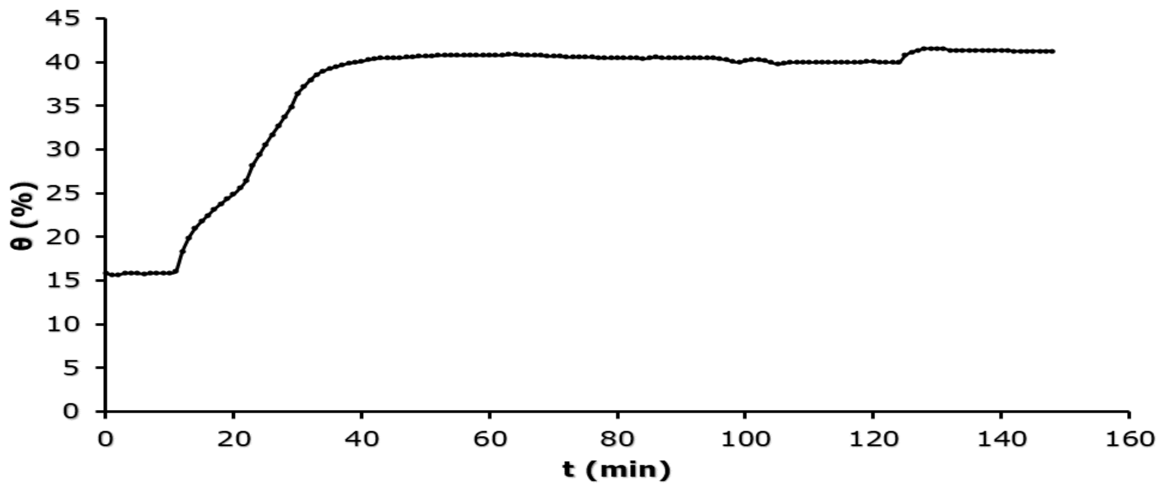

Figure 4.21. Domain-specific volumetric soil water content at 200mm depth for Oleh soil sample infiltration experiment

The curve in Figure 4.24, which begins at about 28% and increases above the water content at the 100 mm depth after about 50 minutes of the experiment, depicts the flow profile at the 300 mm depth. (Köhne, J. Maximilian and Mohanty 2005b) showed a pattern resembling this one to illustrate nonequilibrium flow.

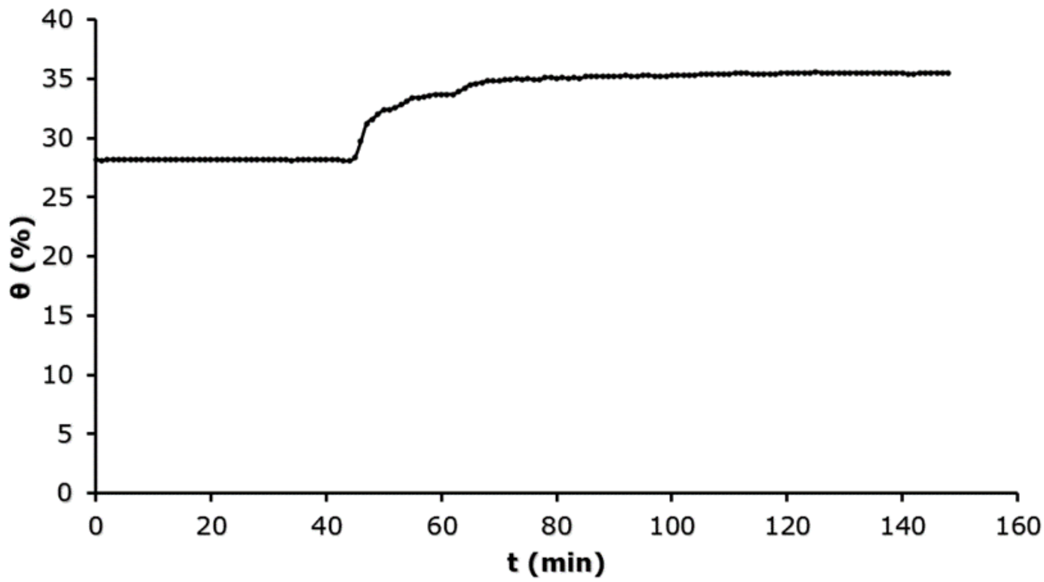

Figure 4.22. Domain-specific volumetric soil water content at 300mm depth for Oleh soil sample infiltration experiment

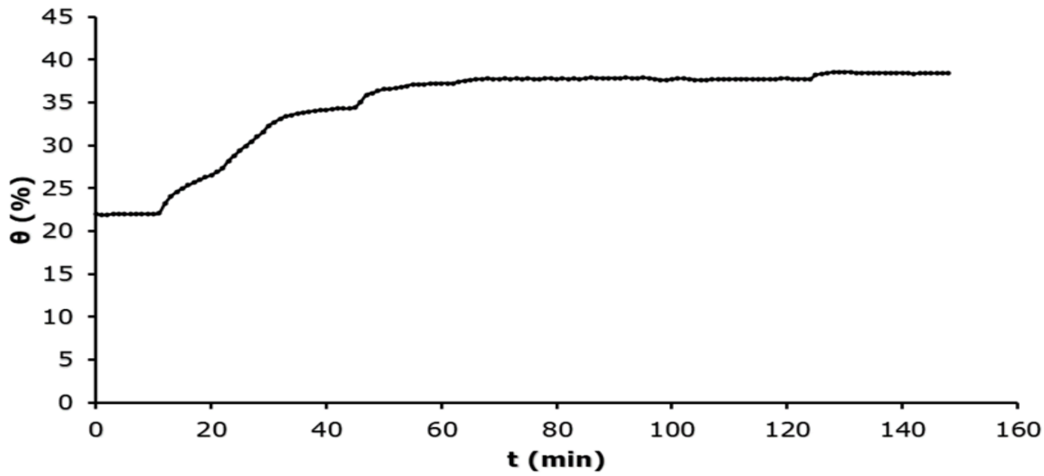

Figure 4.23. Domain-specific volumetric soil water content for average of 200mm and 300mm depth for Oleh soil sample infiltration experiment

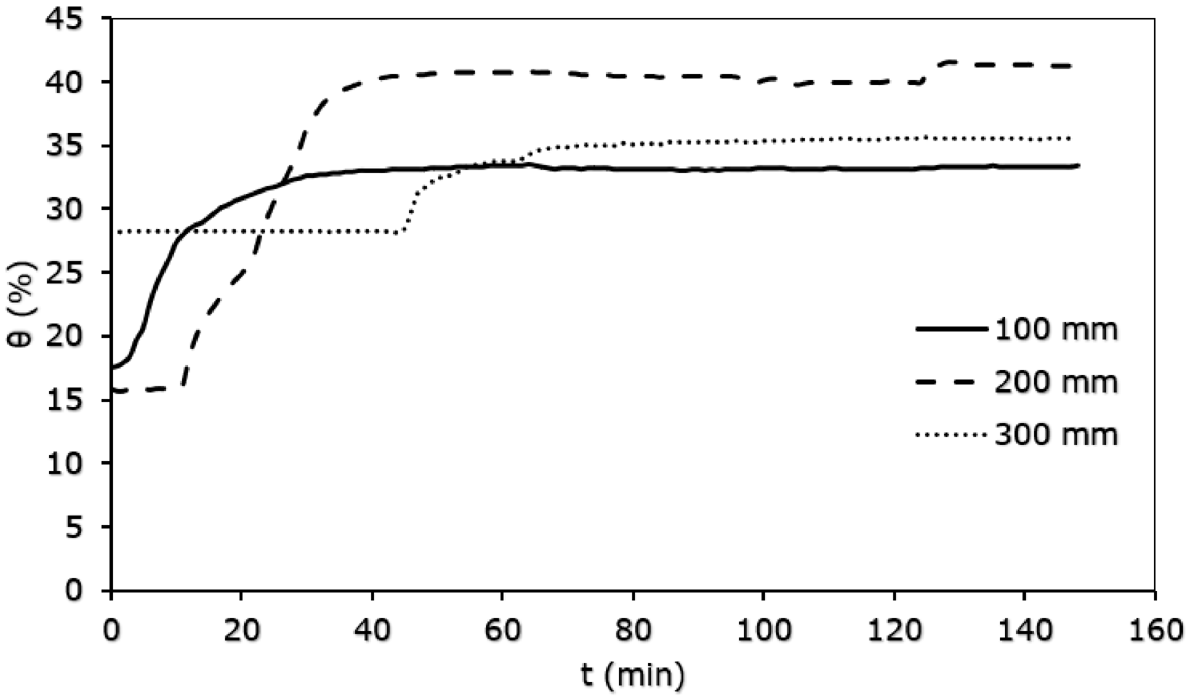

Figure 4.24. Infiltration experiment showing domain specific water content at depths of (a) 100 mm (b) 200 mm (c) 300 mm using the monolith of Oleh soil sample

4.3.5 Comparison of the Soil Water Content in the Soil Types

Figure 4.25 presents the domain-specific soil water content for the packed soil sample, the ploughed soil sample, the Ivrogbo soil sample and the Oleh soil sample at 100 mm depth (Figure 4.25a), 200 mm depth (Figure 4.25b), and 300 mm depth (Figure 4.25c). At 100 mm depth , it is noticed that the Oleh soil sample is wettest pre-experiment with 17.5% water content while the Ivrogbo sample has 11.3%. The Aberdeen packed and ploughed samples have around 2.5% water content. However, as the infiltration experiments are conducted, it is observed that each of the soil samples attained steady water content with the Ivrogbo sample having the highest water content and the Aberdeen packed sample having the the least water content. Size distribution, which determines total water storage, available water holding capacity, and water circulation in the soil, is governed by soil qualities like texture and structure. Improved plant-water connections are typically not achievable by soil texture modification; however, organic matter can be added to the soil to create meso- and macro-porosity, which increases plant accessible water holding capacity and aids in free drainage. For most land use decisions, a grasp of the interactions between soil and water is essential (Irmak et al., 2014). For instance, at 100 minutes into the experiments, the Ivrogbo soil sample has 35.7% water content while the Oleh sample has 33.2% water content. The packed sample has 23.6% water content while the ploughed sample has 32.7% water content. This is because the silty clay with low to medium plasticity texture of the Ivrogbo soil makes it fine-grained while the silty sand nature of the packed sample makes it coarse-grained. The fine-grained soils are characterised by higher available water because they possess higher number of pores, while the sandy soils hold lower available water values (Li, D. et al., 2016). It is observed that the ploughed sample has higher water content than the packed sample because it has become more fine-grained after removal of stones from the packed sample. At the 200 mm depth, it is noticed that the order of magnitude of the water content from highest to lowest after 110 minutes is Oleh Sample, Ivrogbo sample, Ploughed sample, and the packed sample. This same order of magnitude manifests at 300 mm depth. It shows that the Oleh sample is finer-grained than the Ivrogbo vertically downwards at that section.

In this study, it is observed that it is not suitable to repeat the infiltration experiments and take average values for the matric potential and soil water content for the different runs on each sample. The Ivrogbo and Oleh soils harden when dried after the first run obviously due to their clay content. The packed sample is seen to introduce preferential flow as shown in Figure 4.10 in the second logging. When attempts are made to carry out another experiment after the first run at intervals of two weeks for the ploughed soil sample, it is noticed that at 300 mm depth, the first infiltration experiment has a matric potential of -890.1 kpa and water content of 22 % at the start, and a matric potential of -22.8 kpa and water content of 27.3 % thirty minutes later. For the second infiltration experiment two weeks later, the matric potential at the start is -10.4 kpa at a water content of 24.9 %, and a matric potential of -8.2 kpa and a water content of 25.1 % after thirty minutes.

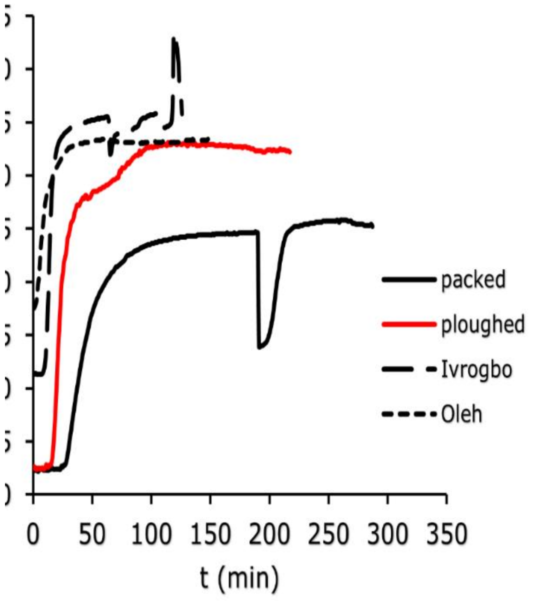

(a)

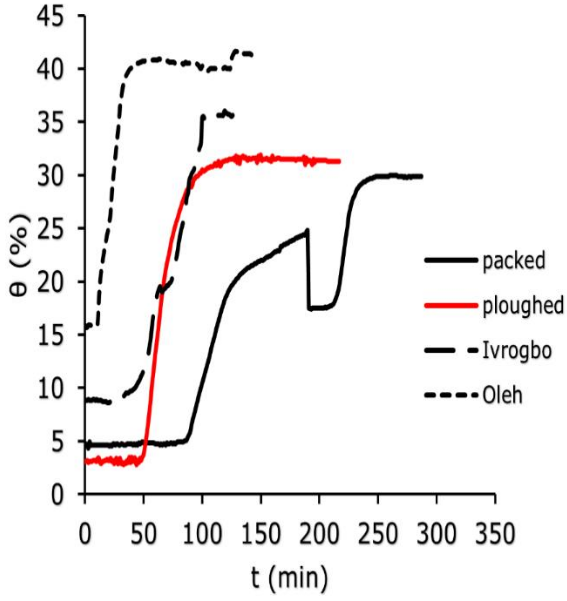

(b)

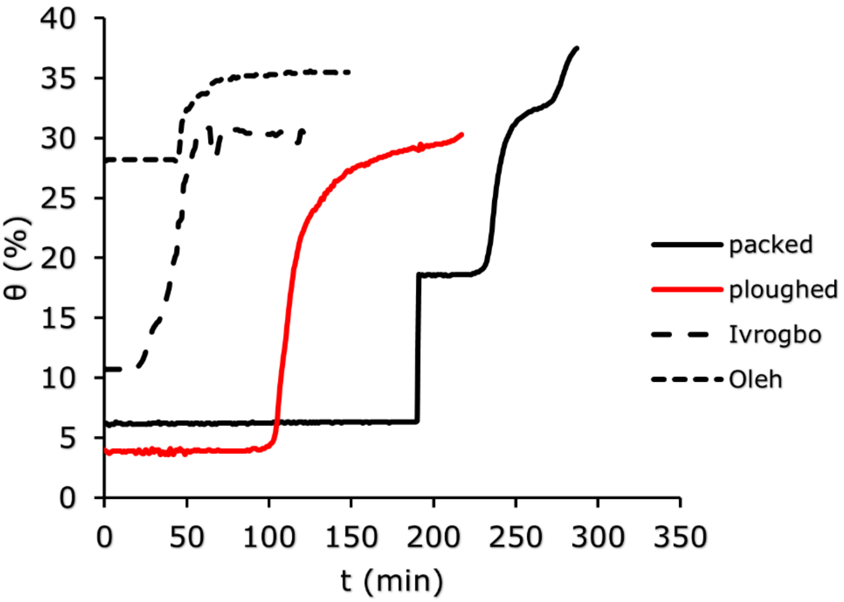

(c)

Figure 4.25 Domain-specific soil water content for the different soil types (a) 100 mm depth (b) 200 mm depth (c) 300 mm depth

4.4 Summary of Key Findings

This chapter presents a thorough examination of the findings from four infiltration tests that used a packed soil sample from Aberdeen's Garthdee district, a monolith of undisturbed soil sample from Ivrogbo and a monolith of undisturbed soil sample from Oleh, based on their soil water contents. The Aberdeen sample is further ploughed with removal of stones to make another sample with finer grains. Below is a summary of the main conclusions.

- As shown in Figure 4.25, the fine-texture samples are characterized by higher available water values, while the coarse-textured samples hold lower available water values.
- When the soil texture alters vertically downwards, the water holding capacity changes to maintain a higher value available water for the finer grained texture. For instance, in Figure 4.25 at 100 mm depth (Figure 4.25a) the Ivrogbo sample obviously with finer grains maintain higher available water value, but at 200 mm (Figure 4.25b) and 300 mm (Figure 4.25c), the Oleh sample projects higher available water values suggesting that the grains are finer than the Ivrogbo soil grains at those depths.
- Figures 4.10 (packed), 4.14 (ploughed), 4.19 (Ivrogbo), and 4.24 (Oleh) depict the profiles of the soil water content. The ploughed sample at depths of 100 mm, 200 mm, and 300 mm demonstrate uniform flow with a uniform wetting front, whereas the other three samples have faster flow at some depths more than others, indicating nonequilibrium or preferential flow.

Chapter 5

Matric Potential based Hydrodynamic Characterisation of Different Soil Types

The findings of the soil matric potential from the infiltration experiments for the packed soil sample which is further disturbed to mimic ploughing, the undisturbed soil sample from Ivrogbo, and the undisturbed soil sample from Oleh are presented in this chapter. The profiles of the soil matric potentials are analysed and compared.

5.1 Soil Matric Potential

The findings of the infiltration experiments for the Ivrogbo and Oleh samples, as well as the packed and ploughed soil samples, are shown in this section. The section begins with an examination of their soil matric potentials and ends with a comparison of them.

5.1.1 Measured Soil Matric Potential for Packed Soil Sample from Aberdeen

Measurement of the domain-specific matric potential for the 200 mm depth and 300 mm depth are shown in Figure 5.1 and Figure 5.2. For the first 99 minutes, the matric potential increases gradually to a more negative value at 200 mm depth which corresponds to the residual values of the water content but records a sharp decrease to a less negative value until around 175 minutes before it appears steady. It holds steady for a while after the discontinuity, corresponding to the water content holding steady from 190 minutes to 206 minutes, then continues a steady decrease to saturation at zero. It should be noted that the matric potential is a negative value in the unsaturated zone, hence it is taken as decreasing when the negative value reduces as the soil water content increases. On the other hand, it is observed that the matric potential at the 300 mm depth continues to have negative values beyond 280 minutes even until the logging is stopped. This could be explained by the fact that there is a nonequilibrium flow directed at the EQ3 Equitensiometer sensor at 200 mm depth more rapidly with a non-uniform wetting front which makes the matric potential decrease from -436.5 kPa to 0 in 235 minutes of the logging period, while the matric potential at the EQ3 Equitensiometer sensor at 300 mm depth records a decrease from -28.1 kPa to -12.6 kPa for more than 280 minutes of the logging period.

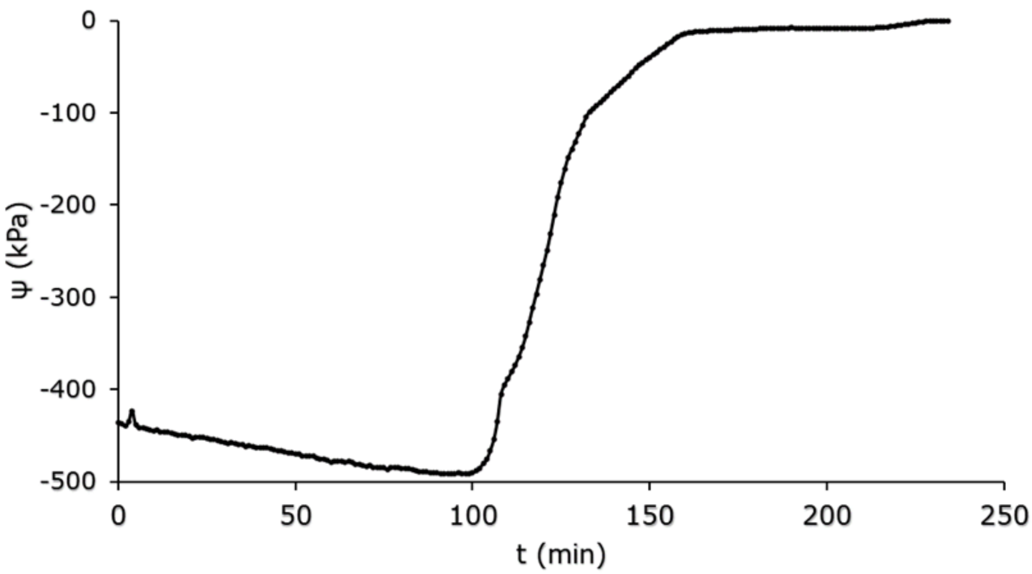

Figure 5.1. Domain-specific matric suction at 200 mm depth using Aberdeen packed soil infiltration experiment

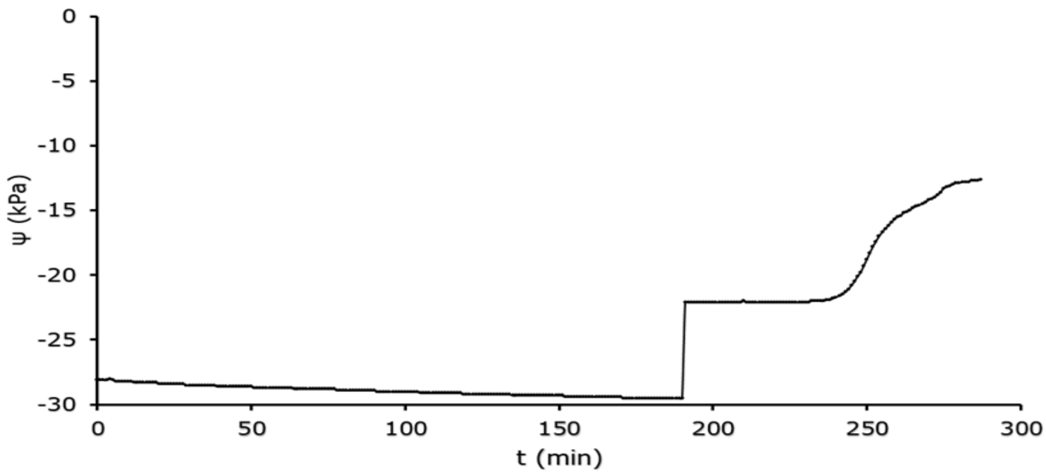

Figure 5.2. Domain-specific matric suction at 300 mm depth using Aberdeen packed soil infiltration experiment

5.1.2 Measured Soil Matric Potential for Ploughed Soil Sample from Aberdeen

According to Van Genuchten (1980), the soil water characteristics curves are often plotted on a semilogarithmic scale, but (Koorevaar et al., 1991) explained that it is to overcome the challenges of plotting the matric potential on the arithmetic scale when the value is so large. It is further explained that the literature that has been consulted reveal contradictory styles by different authors in plotting the soil water characteristics curve. While some authors plotted it on the semilogarithmic scale, others plotted it on an arithmetic scale. Also, while some authors plotted the matric potential on the abscissa in a semilogarithmic scale, others plotted the matric potential on the abscissa on the arithmetic scale, yet others plotted the matric potential on the ordinate on the arithmetic scale or semilogarithmic scale. This is further clarified using the domain-specific matric suction at 200 mm and 300 mm depths using Aberdeen ploughed soil infiltration experiment shown in Figure 5.3. The matric potential is plotted on arithmetic scale, and it appears that the values of the matric potential approaches a steady value in 125 minutes of the experiment for both the 200 mm and 300 mm depths of the soil column. However, if the same data were plotted on a semilogarithmic (not shown), and it would be observed that there is clearly a time lag between when the matric potential attained steady values at the two different depths as the experiment progressed. While the matric potential at the 200 mm depth attains steady value of about -8 kPa around 90 minutes of the experiment, the matric potential at 300 mm depth attains steady value of about -22 kPa around 150 minutes of the experiment.

As earlier stated, nevertheless, the matric potential is plotted on the arithmetic scale in this study because the generated values are in the region of -1800 kPa or less, which are conveniently accommodated in the arithmetic scale. Moreover, this is sufficient to establish a relationship between the matric potential and soil water content, which is one of the objectives of this research. The matric potential is also plotted on the ordinate according to (Koorevaar et al., 1991) which is shown in Figure 1.6.

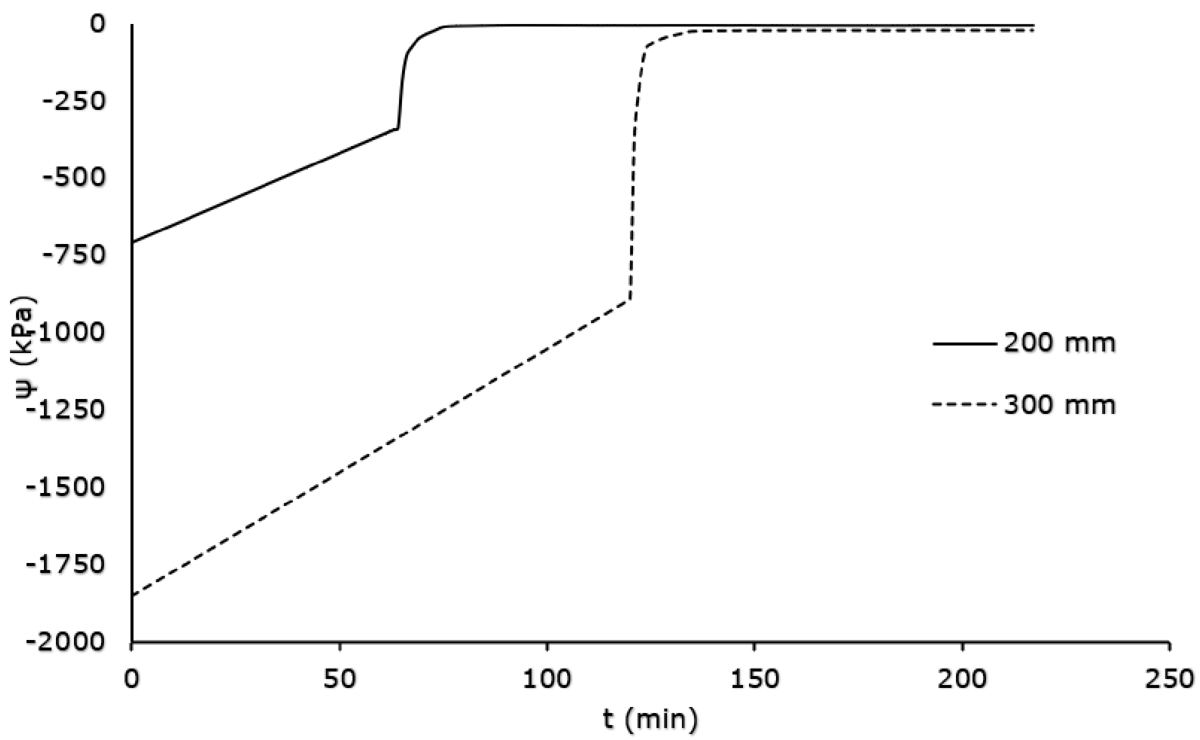

Figure 5.3. Domain-specific matric suction at 200 mm and 300 mm depths using Aberdeen ploughed soil infiltration experiment

5.1.3 Measured Soil Matric Potential for Monolith of Soil Sample from Ivrogbo

Figures 5.4 to 5.6 display the profiles of the domain-specific matric potentials at 200 mm depth, 300 mm depth, and the average of both depths during the experiment. Additionally, it is noted that the profile indicated a constant curve for the matric potential at the beginning of the experiment with low water content. It then generally follows a transition period before becoming steady at the saturation end, suggesting constant matric potential. The logging is stopped in both cases before the matric suction reaches zero. It is also possible to conclude that the sample's water flow through the soil column is either preferential or nonequilibrium. This conclusion is further supported by the mass balance data, which indicates that even if the matric potential readings at the 200mm and 300 mm levels were negative, a significant amount of the discharged water had already accumulated at the reception tank.

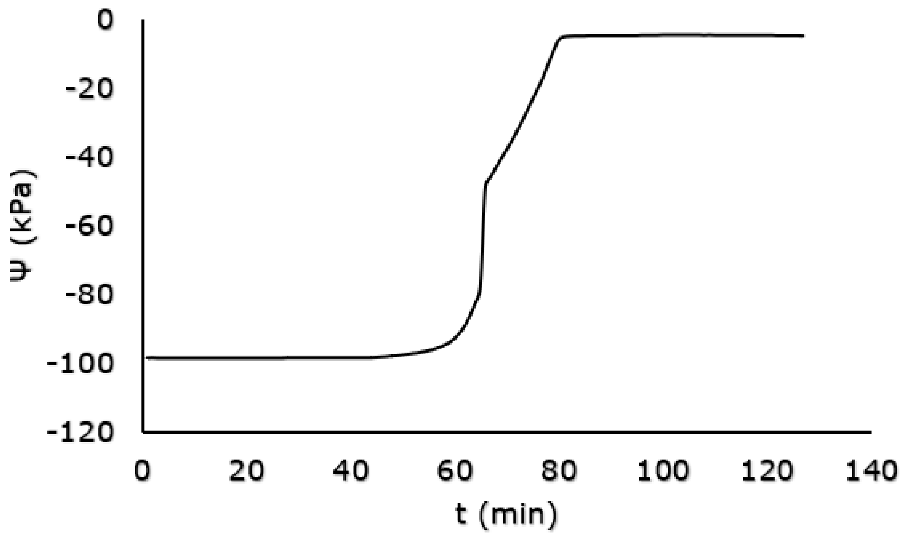

Figure 5.4. Domain-specific matric suction at 200 mm depth using monolith of soil sample from Ivrogbo in the infiltration experiment

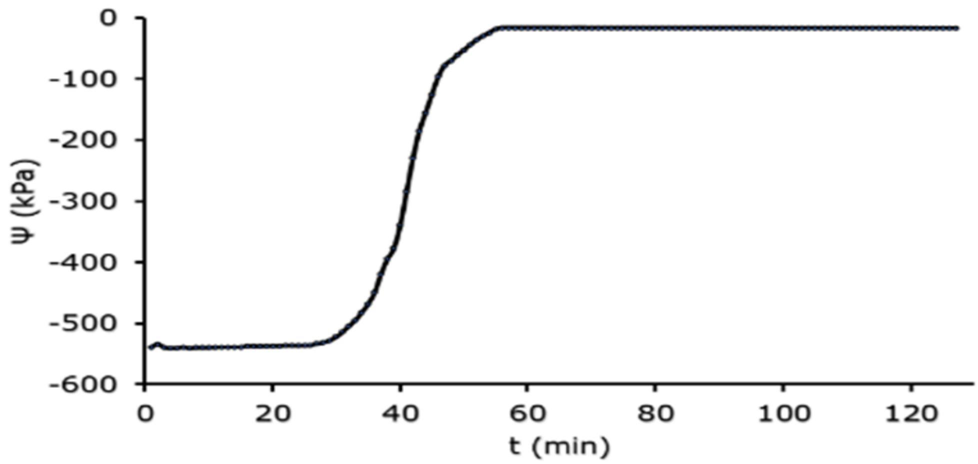

Figure 5.5. Domain-specific matric suction at 300 mm depth using monolith of soil sample from Ivrogbo in the infiltration experiment

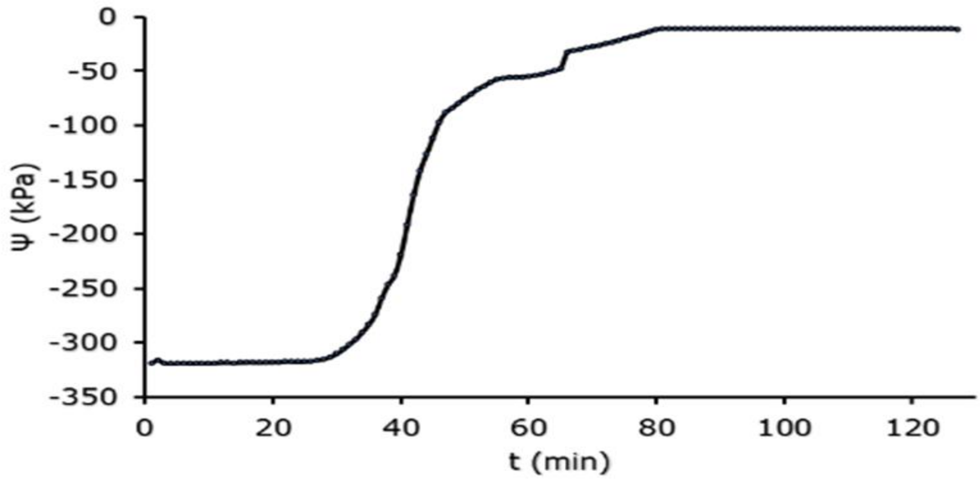

Figure 5.6. Average matric suction for 200 and 300 mm depth for Ivrogbo soil

5.1.4 Measured Soil Matric Potential for Monolith of Soil Sample from Oleh

The profiles of the domain-specific matric potentials at 200 mm depth, 300 mm depth, and the average of both depths over the course of the experiment are shown in Figures 5.7 to Figure 5.9. Furthermore, it is observed that, at the beginning of the experiment with low water content, the profile defines a constant curve for the matric potential and generally follows a transition period before becoming steady at the saturation end which suggests steady matric potential. In both instances, the logging is terminated prior to the matric suction reaching zero. We can also draw the conclusion that the water flows through the soil column for the sample was either nonequilibrium or preferential. The mass balance records, which showed that a large portion of the released water had already collected at the receiver tank despite the matric potential readings being negative at both the 200mm and 300 mm levels, further corroborate this finding.

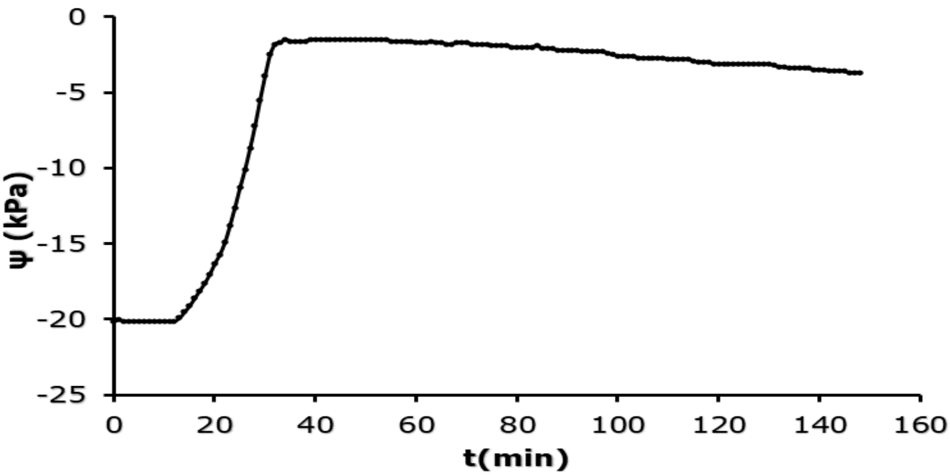

Figure 5.7. Domain-specific matric suction at 200 mm depth using monolith of soil sample from Oleh in the infiltration experiment

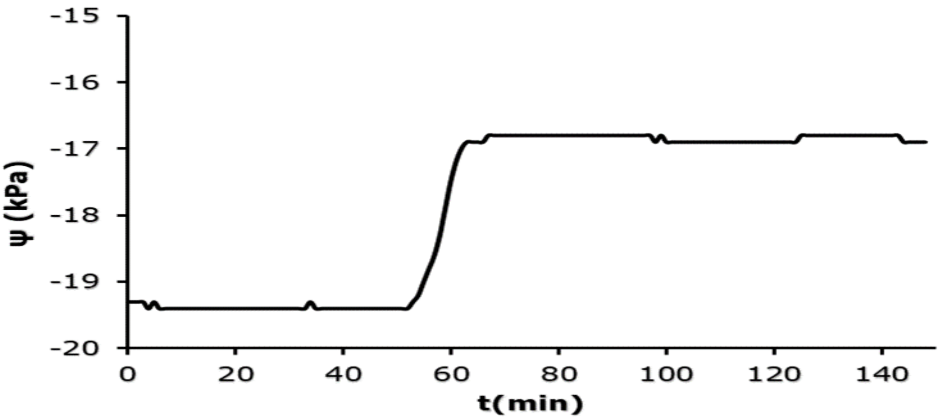

Figure 5.8. Domain-specific matric suction at 300 mm depth using monolith of soil sample from Oleh in the infiltration experiment

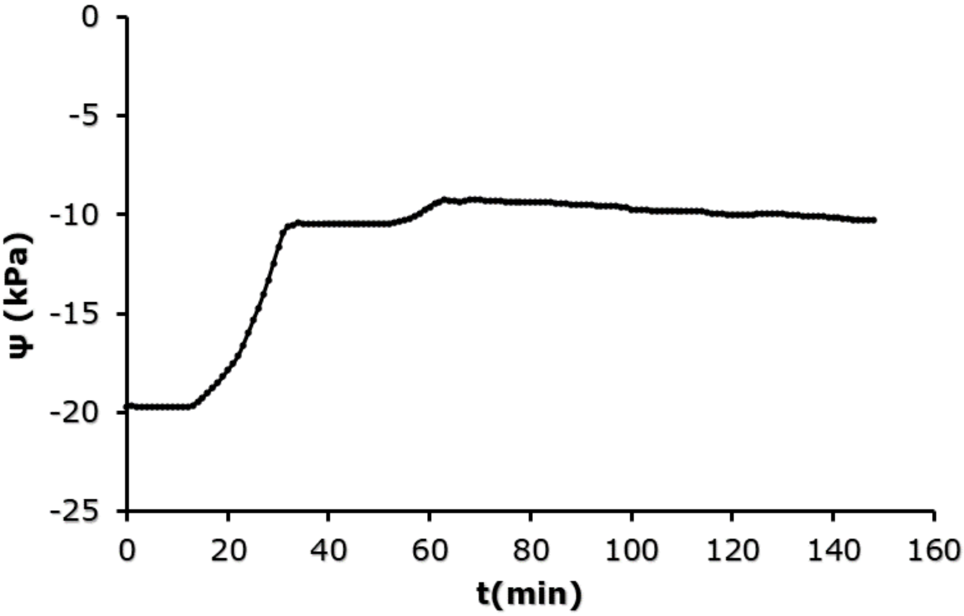

Figure 5.9. Average matric suction for 200 and 300 mm depth for Oleh soil

5.1.5 Comparison of Soil Matric Potential in the Different Soil Types

When the soil gets drier, the link between water molecules and soil pores gets even stronger. Water is drawn out of the large soil pores first and is held more firmly in the smaller pores. Water molecules that are most readily available to plants are extracted initially, followed by progressively more tightly bound water molecules. Because of this, soil matric potential steadily rises with soil dryness (its greatest value, zero, denotes extremely wet soil conditions). Soil matric potential increases adversely (greater tension) with increasing soil dryness (Irmak et al. 2014). The water-holding capacity of sandy soil is extremely low. Different soils have different irrigation trigger points when their properties, such as their saturated hydraulic conductivity (Ksat), field capacity (FC), permanent wilting point (PWP), bulk density (BD), and particle size distribution (i.e., percent sand, silt, and clay), are different.

Figure 5.10 presents the domain-specific profiles for the matric potential for the packed soil sample, the ploughed soil sample, the Ivrogbo soil sample, and the Oleh soil sample at 200 mm depth (Figure 5.10a) and at 300 mm depth (Figure 5.10b). At 200 mm depth (Figure 5.10(a)), the ploughed soil sample is initially drier than the packed soil sample and hence has a higher negative matric potential. But within the first 90 minutes, this reduces to about -8 kPa from -710 kPa giving a slope of about 7.8 kPa/min. Within the same time, the packed sample increased from -436 kPa to -490 kPa, giving a negative slope of -0.6 kPa/min. From their flow conditions, water is introduced into the packed sample from the upper tank with an average flow rate of 8.77E-08 m^3/s, flow velocity of 4.47E-5 m/s and Reynolds number of 2.24 while water is introduced into the ploughed soil sample from the upper tank with an average flow rate of 1.64E-07 m^3/s, flow velocity of 8.39 m/s and Reynolds number of 4.19. This means that both have low Reynolds numbers with laminar flow conditions. However, with the removal of stones from the packed sample to make the ploughed sample, the soil texture has been altered with the packed sample becoming sandier and the ploughed sample becoming siltier, more homogeneous, and having higher field capacity. This has made the matric potential of the ploughed sample to decrease at a higher rate compared to the packed sample under the same laminar flow conditions. It is observed that while the matric potential of the ploughed sample decreases to a constant value in about 90 minutes, it takes more than 200 minutes for the packed sample to decrease to a steady value. The Ivrogbo soil type is silty clay with low to medium plasticity which has higher field capacity than the Oleh soil which is sand clay mixture. They both have similar laminar flow conditions, but the Oleh soil is wetter pre-experiment. However, the matric potential of the Ivrogbo soil decreases from -98.2 kPa to -4.6 kPa in 90 minutes with a gradient of 0.95 before becoming steady, while the matric potential of the Oleh soil decreases from -20.1 kPa to -2.2 kPa in 90 minutes with a gradient of 0.2 before becoming steady. This also shows that the Ivrogbo soil with a texture of silty clay with low to medium plasticity has higher field capacity than the Oleh soil. The packed soil sample has an initial matric potential of -28.1 kPa at 300 mm depth (Figure 5.10b), while the ploughed soil sample is immediately at the permanent wilting threshold with a matric potential of -1850 kPa. Additionally, the Oleh soil sample starts at -19.3 kPa, while the Ivrogbo soil sample starts at -539.2 kPa. When their matric potentials are compared after 125 minutes, it is found that the packed soil sample has a negative gradient of -0.0088, whereas the matric potential of the ploughed soil sample has declined with a gradient of around 14. The matric potential of the Ivrogbo soil sample decreases from -539.2 kPa to -17.4 kPa with a gradient of 4 while the matric potential of the Oleh soil sample decreases with a gradient of 0.02 from -19.3 kPa to -17.4 kPa. As a result, there is agreement between the matric potential profiles of the 200 mm depth and the 300 mm depth. This indicates that when water is introduced to the soil, the type or texture of the soil affects the profile of the soil matric potential (K. et al. 2023; Irmak et al. 2014; O'Green 2013; Robertson et al. 1984; Taylor and Ashcroft 1972). According to this study, the ploughed soil is siltier than the packed soil, which is thought to be silty sand. The largest field capacity is found in the sand clay mixture of Oleh soil sample. The Ivrogbo soil sample (a mixture of silty clay, low to medium plasticity) come next, and this is followed by the ploughed soil sample, and the packed soil sample. This shows that the soil samples with the fine-grained textures have higher field capacity than the soil samples with the coarse-grained textures as also described in (Yang et al., 2023)

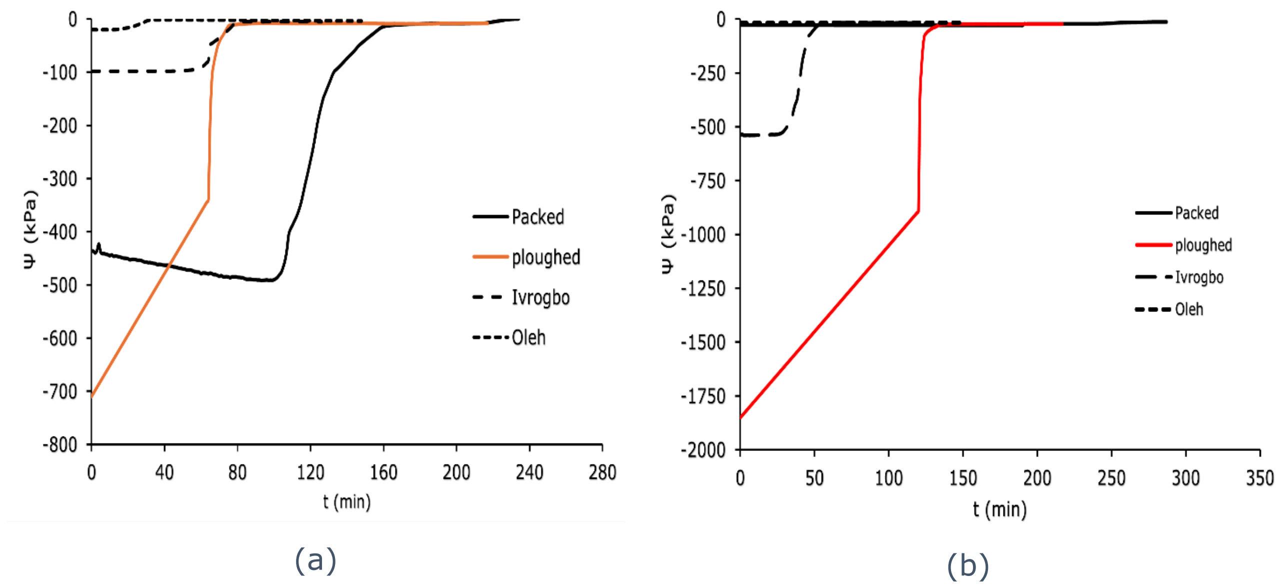

Figure 5.10 Domain-specific Soil Matric Potential in the Soil Types (a) 200 mm (b) 300 mm

5.2 Summary of key findings

This chapter presents and analyses in detail the findings of the infiltration experiment conducted using the packed soil sample, the ploughed soil sample, the Ivrogbo soil sample, and the Oleh soil sample with investigation of their matric potentials. Below is an overview of the most important findings:

- Using the Unified Soil Classification System (USCS) and the American Association of State Highway and Transportation Officials (AASHTO), the Ivrogbo soil sample is found to be silty clay with low to medium plasticity while the Oleh soil sample is found to be sand clay mixture. The packed and the ploughed soil samples are considered to be silty sand with the packed sample considered to be sandier.
- The soil texture has huge effect on the field holding capacity and matric potential. While the field holding capacity of the packed sand soil sample is least, the field holding capacity of the sand clay mixture soil sample from Oleh is highest.
- As demonstrated in Figure 5.10, the profiles of the soil samples at depths of 200 mm, and 300 mm reveal as water is added to the soils, the matric potentials decrease at different rates depending on the soil texture.
- The findings demonstrate that high matric suction values are recorded at low soil water content and low matric suction values are reported at high water content. A high water content is associated with the saturation zone, and a low water content is associated with the residual zone.

Chapter 6

Hydrodynamic Characterisation of Different Soil Types based on Soil Water Characteristics Curve

The analysis conducted to characterise the water flow through the packed soil sample and monoliths of soil samples from Ivrogbo and Oleh in the Nigerian Niger Delta is presented in this chapter, utilising the soil water characteristics curve. By establishing the relationship between the volumetric soil water content and the soil matric potential, the tests are conducted to identify the soil water characteristic curve.

6.1 Soil Water Characteristic Curve

The relationship between the soil water contents and the soil matric potentials obtained during the infiltration experiments of the various soil samples, that is,the packed soil sample, the ploughed soil sample, the Ivrogbo sample, and the Oleh sample is plotted in this section to create the soil water characteristics curves. Additionally, a comparison is drawn between the soil water characteristics curve at 200 mm depth and the predicted Van Genuchten curve.

6.1.1 Measured Soil Water Characteristic Curve (SWCC) For Packed Soil Sample

Figures 6.1-6.3 present the soil water characteristics curves (SWCC) for the packed soil sample. According to Van Genuchten (1980), the soil water characteristics curves are often plotted on a semilogarithmic scale, but (Koorevaar et al., 1991) explain that it is to overcome the challenges of plotting the matric potential on the arithmetic scale when the value is so large. However, the literature that has been consulted reveal contradictory styles by different authors in plotting the soil water characteristics curve. While some authors plotted it on the semilogarithmic scale (e.g., (Eyo et al., 2022; Hou, X. et al., 2019; Ritter et al., 2004; van Genuchten, 1980)), others plotted it on an arithmetic scale e.g., (Koorevaar et al., 1991; Liu, Q. et al., 2012). Also, while some authors plotted the matric potential on the X-axis in a semilogarithmic scale e.g., (Hou, X. et al., 2019; Köhne, J. Maximilian & Mohanty, 2005b; Ritter et al., 2004), others plotted the matric potential on the X-axis on the arithmetic scale e.g., (Liu, Q. et al., 2012), yet others plotted the matric potential on the Y-axis on the arithmetic scale or semilogarithmic scale e.g., (Koorevaar et al., 1991; van Genuchten, 1980). In this study, the matric potential is plotted on the arithmetic scale because the generated values are in the region of -1800 kPa or less, which are conveniently accommodated in the arithmetic scale. The matric potential is also plotted on the Y-axis according to (Koorevaar et al., 1991) which is shown in Figure 1.6.

Figure 6.1 shows the SWCC at 200 mm depth. The features of the Residual Suction Value (RSV) in the residual zone, the transition zone and the saturation zone are clearly defined according to (Eyo et al., 2022). The residual soil suction is reflected around Ψ= -436.5 kPa with a corresponding residual soil water content, θ, of 4.7%. The matric potential and soil water content, however, are shown to be inversely related in the unsaturation zone. This means that as soil water content rises, the matric potential decreases from a more negative value towards zero in the saturation zone, which means that the soil tends towards saturation. Figure 6.2 is a plot of the SWCC at the 300 mm depth showing a residual value in the region of 6.1%, a break and resumption of logging at 18.6% and -22.1 kPa. Although a clear transition region is observed between (26%, -22kPa) and (35%, -13kPa), it could be noticed that the soil water content continues to rise, and saturation is not attained before the logging is stopped. This is attributed to the fact that nonequilibrium flow is encountered as earlier observed.

A comparison of the experimental and simulated data is shown in this section. The predicted and measured soil water characteristic curves (a) and (b) are shown in Figure 6.3. Predicted Van Genuchten SWCC is shown in (a) while measured SWCC for the infiltration experiment using a packed soil sample at 200 mm is shown in (b). At the lowest value of the soil water content for the simulated data, the soil matric suction is notably very high, indicating that the water content is residual, and the soil was exceedingly dry. The matric pressure head drops at very low constant soil water content in the residual zone; when the water content rises quickly in the transition zone, the matric pressure head decreases at a much-reduced rate. The water content returns to its steady value at the higher end of the 50% range, producing a vertically upward and downward S-shaped (sigmoid) curve. The curve approaches saturation at this point. Similarly, the soil water characteristic curve of the packed soil sample shows a low matric potential value of -0.1 kPa at high volumetric water content of 29% and a high matric potential value of -436.5 kPa at low volumetric water content of 4.7%. Nonetheless, the range of values is smaller than the predicted curve. The value of n is noticed to be 10 with θ_r equal to 0.046 and θ_s equal to 0.23. This gives a percentage difference of 80 % when compared to n equal to 2 in the Van Genuchten curve. The pre-experiment moisture content of the soil sample is part of the cause of this, in addition to differences in the soil type. The soil column experiment for the packed soil sample also precisely describes the characteristics of the residual zone, transition zone, and saturation zone with a feature of an S-shaped curve (sigmoid curve), which compares reasonably with the literature as shown in

(Eyo et al., 2022)

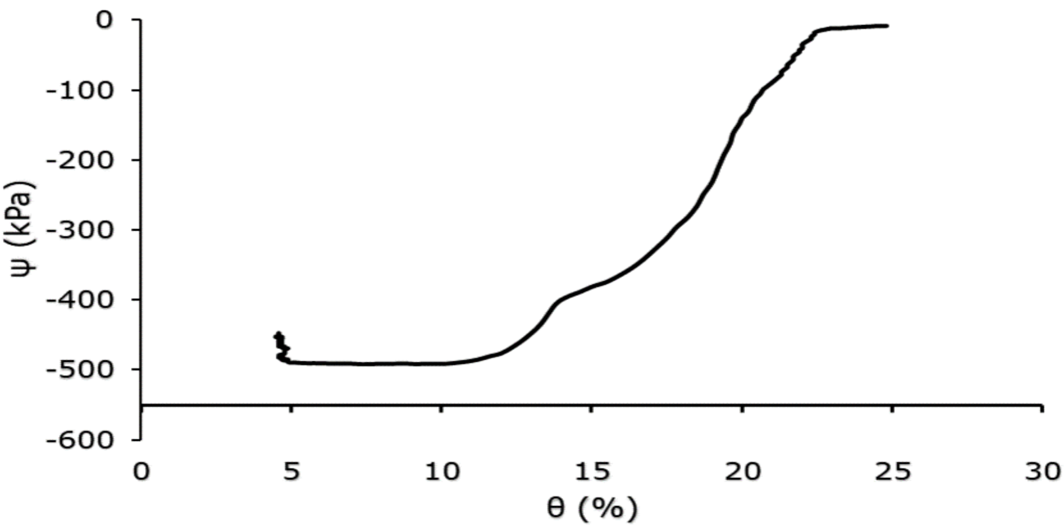

Figure 6.1. Infiltration experiment at 200 mm depth for Aberdeen packed soil column showing the soil water characteristic curve

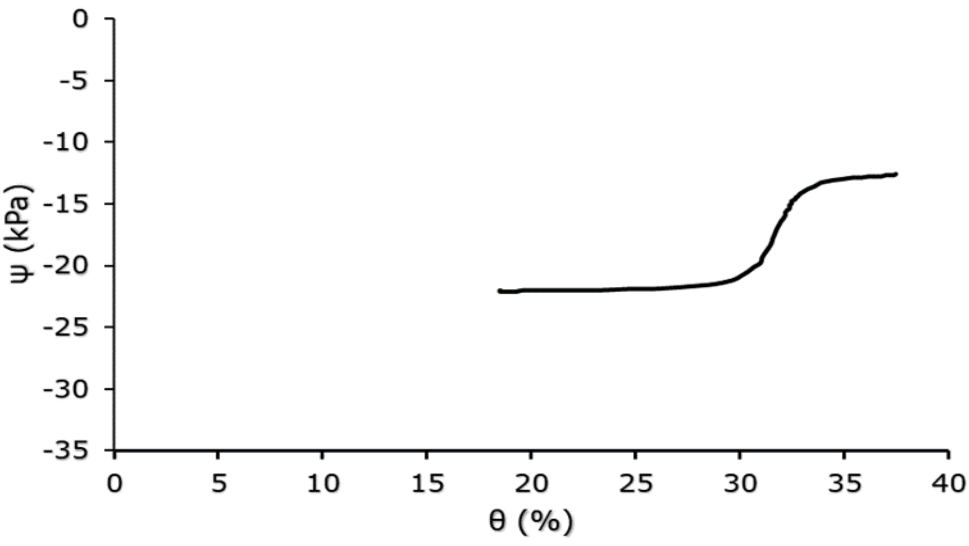

Figure 6.2. Infiltration experiment at 300 mm depth for Aberdeen packed soil column showing the soil water characteristic curve

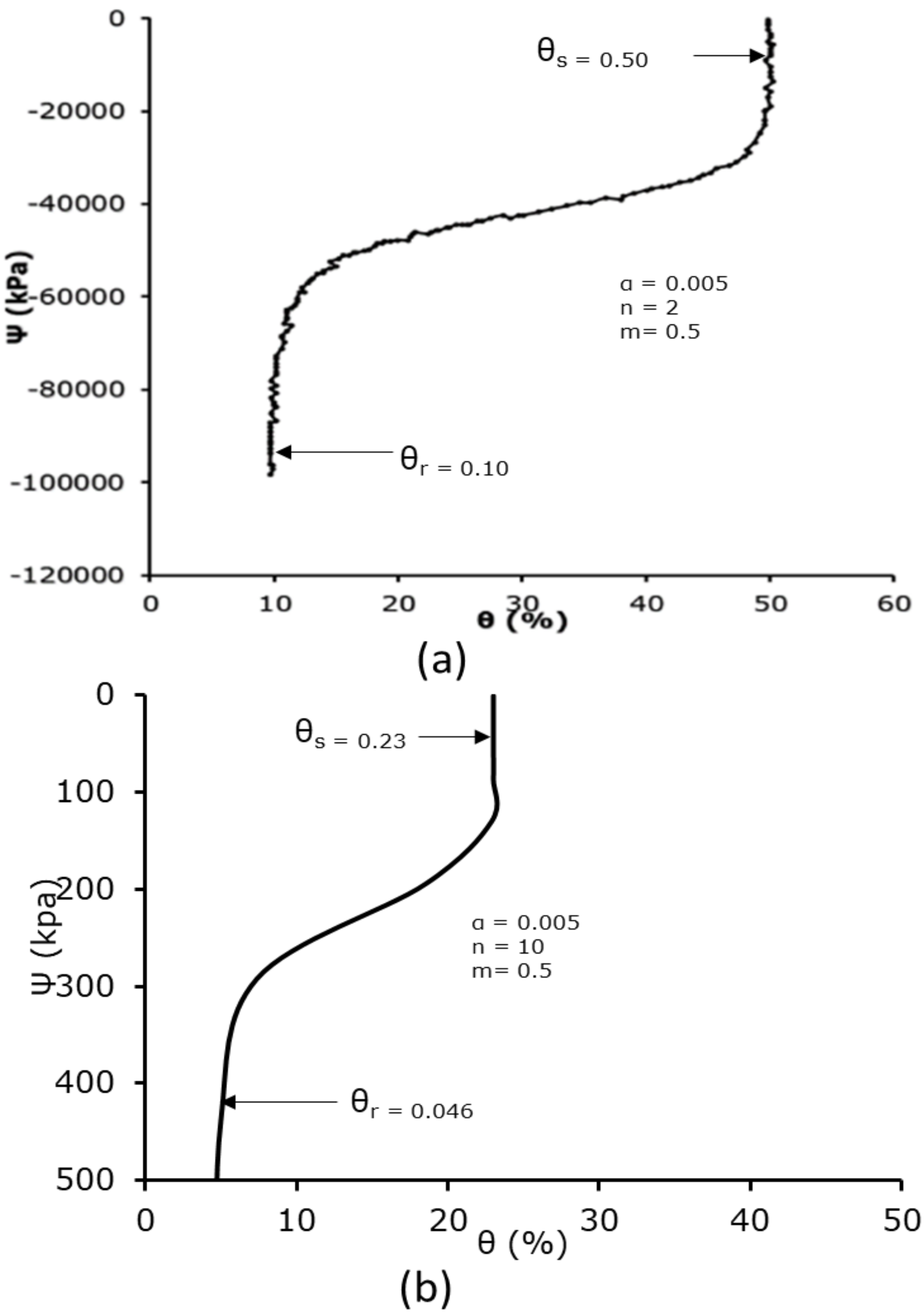

Figure 6.3. Predicted and measured soil water characteristic curve (a) Predicted Van Genuchten SWCC (b) Measured SWCC at 200 mm for the packed soil sample

6.1.2 Measured Soil Water Characteristic Curve (SWCC) for Ploughed Soil Sample from Aberdeen

Figure 6.4 shows the SWCC at 200 mm depth. The features of the residual suction value (RSV) in the residual zone, the transition zone and the saturation zone are clearly defined according to (Eyo et al., 2022). The residual soil suction is reflected around Ψ= -710 kPa with a corresponding residual soil water content, θ, of 3.1%. A very high percentage difference of 99.7 % is also noticed between the residual value of the predicted Van Genuchten curve and the residual value of the packed soil sample. The matric potential and soil water content are shown to be inversely related in the unsaturated zone. This means that as soil water content rose, the matric potential decreased from a more negative value towards zero. There is a trend here that leads to saturation. Figure 6.5 is a plot of the SWCC at the 300 mm depth showing a residual value of the soil water content in the region of 4% with a corresponding matric suction of -1850 kPa, while Figure 6.6 shows the predicted Van Genuchten SWCC (a) and measured SWCC for the infiltration experiment using the ploughed soil sample at 200 mm (b). The value of n is noticed to be 15 with θ_r equal to 0.03 and θ_s equal to 0.23. This gives a percentage difference of 86.7 % when compared to n equal to 2 in the Van Genuchten curve.

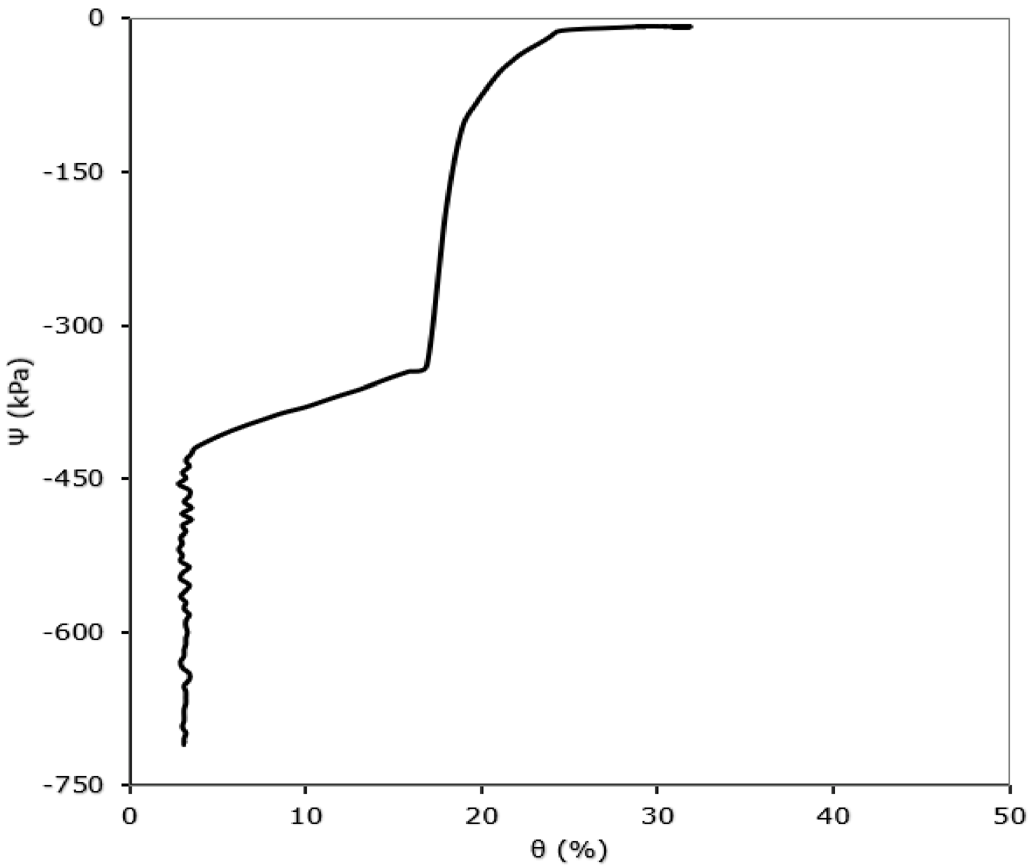

Figure 6.4. Infiltration experiment at 200 mm depth for Aberdeen ploughed soil column showing the soil water characteristic curve

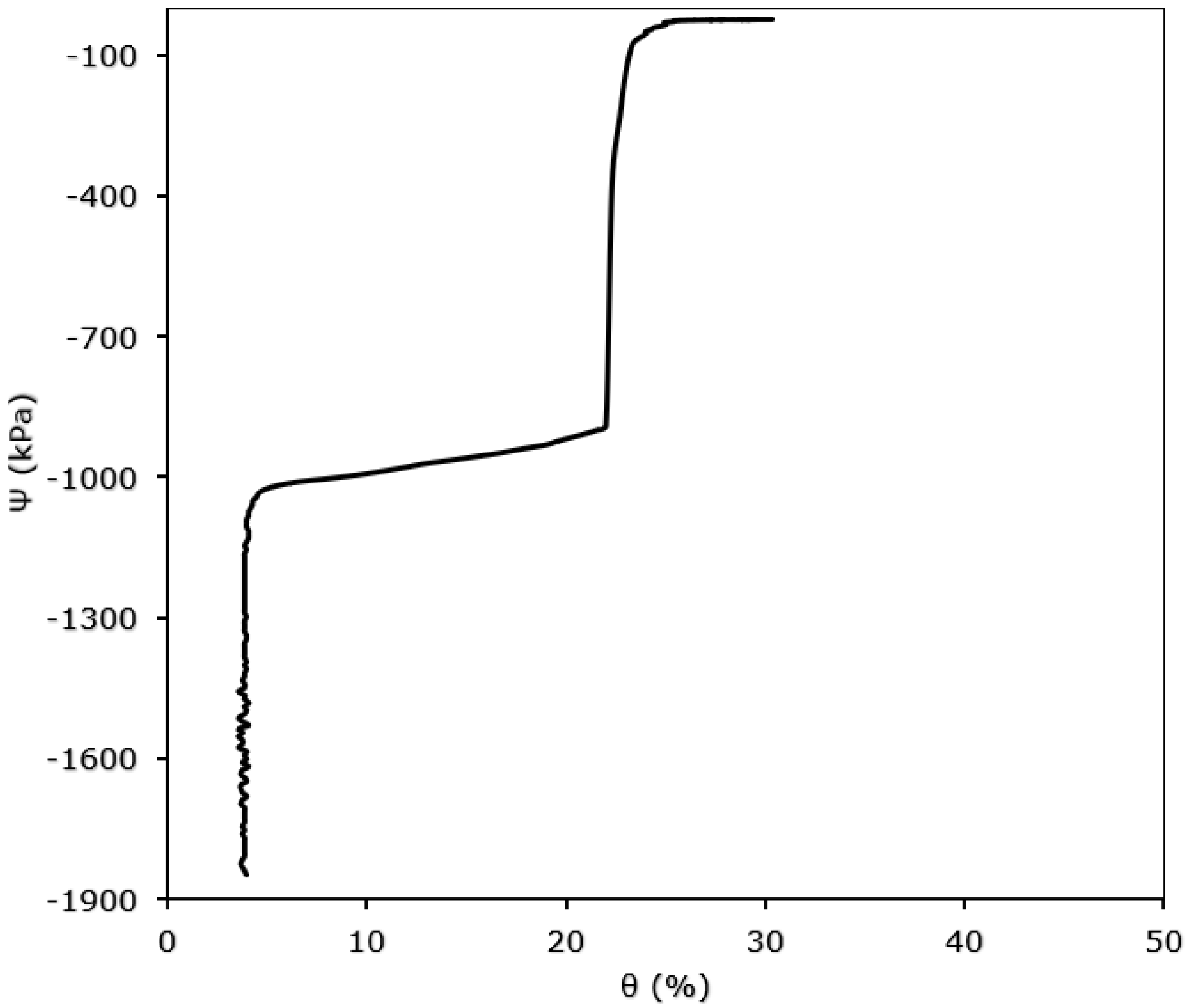

Figure 6.5. Infiltration experiment at 300 mm depth for Aberdeen ploughed soil column showing the soil water characteristic curve

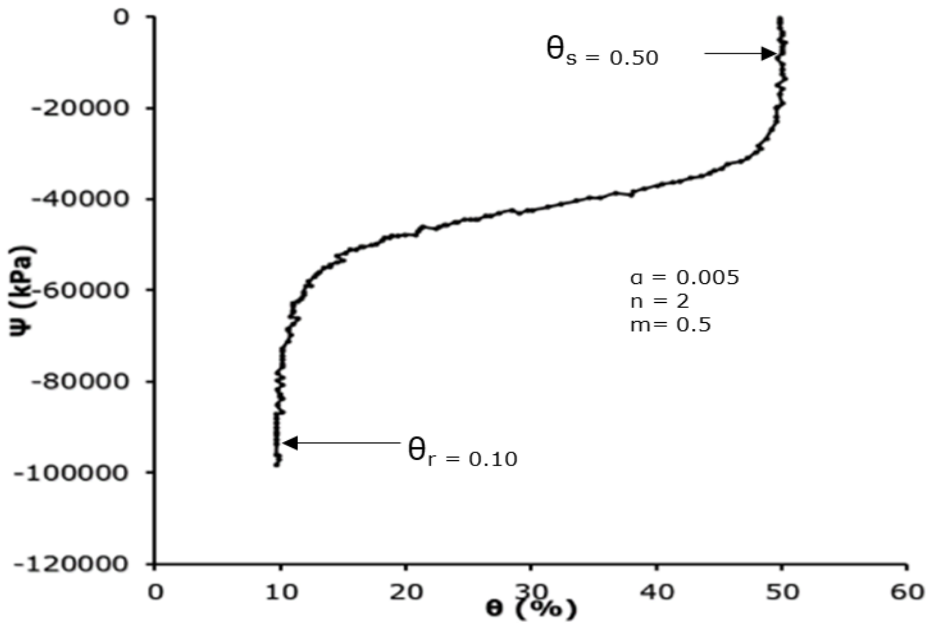

(a)

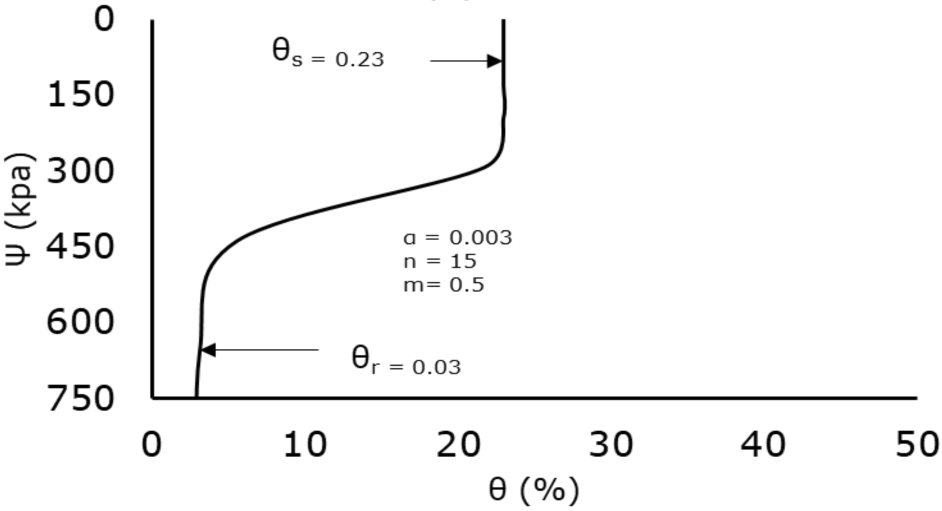

(b)

Figure 6.6. Predicted and measured soil water characteristic curve (a) Predicted Van Genuchten SWCC (b) Measured SWCC at 200 mm for the ploughed soil sample

6.1.3 Measured Soil Water Characteristic Curve (SWCC) For Monolith of Soil Sample from Ivrogbo

The soil water characteristic curve is typically described in terms of matric potential and the volumetric soil water content. In the laboratory, the wetting soil water characteristic curve (SWCC) for the Ivrogbo soil sample with a bulk density of 1640 kg/m^3 is measured at various depths using the soil column experiment and the related test protocol that has been described.

The soil water characteristic curve for the Ivrogbo soil sample at 200 mm and 300 mm depths are shown in Figures 6.7 (b) and 6.8. The average soil water characteristic curve, represented in Figure 6.9, is obtained by averaging the soil water content and the related values of the soil matric potentials. This is because there is no sensor to measure the matric potential at a depth of 100 mm. The results show that with low soil water content, high matric suction values are recorded, whereas at high water content, low matric suction values are reported. The saturation zone is correlated with a high water content, and the residual zone is correlated with a low water content. Because of the attraction force between the residual water and the matrix, high matric pressure is needed at the residual zone to release the water from the soil matrix (Eyo, Ng'ambi, and Abbey 2022b; Koorevaar, Dirksen, and Menelik 1991). It is observed that when the water content rises, there is a transition zone where the matric suction gradually decreases. The matric suction for the low water content value is above -500 kPa at 300 mm, and it is approximately -100 kPa at 200 mm below the column's top. The reason for this is that the soil sample is drier at 300 mm than it is at 200 mm. The curve's shape is basically sigmoid, and the findings are consistent with previous research.

This section also presents a comparison of the simulated and experimental data, based on the model of van Genuchten, M. Th. (1980) as previously explained, from which the simulated data is obtained. Figure 6.7 (a) illustrates this. Figure 6.7 (b) depicts the measured soil water characteristic curve for the Ivrogbo soil sample at 200 mm. The matric pressure is noticeably very high at the lower value of the soil water content for the simulated data, indicating that the soil is extremely dry and the water content is residual. In the residual zone, the matric pressure head decreases at very low constant soil water content; however, in the transition zone, the matric pressure head decreases at a substantially reduced rate when the water content rises quickly. At the upper end of the 50% range, the water content returns to its constant value, resulting in a vertically upward and downward S-shaped (sigmoid) curve. This is where the curve reaches saturation. In contrast, the Ivrogbo soil's soil water characteristic curve likewise displays a high matric potential value at low volumetric water content and a low matric potential value at high volumetric water content. The range of values is, nevertheless, less than that of the simulated curve. Consequently, a 99.9%

percentage between the residual value of the packed soil sample and the residual value of the projected Van Genuchten curve is seen.
This occurs as a result of the soil sample's pre-experiment moisture content. The soil column experiment for the Ivrogbo soil sample also clearly describes the features of the residual zone, transition zone, and saturation zone using an S-shaped curve (sigmoid curve), which compares reasonably with literature as shown in (Eyo et al., 2022; Koorevaar et al., 1991).

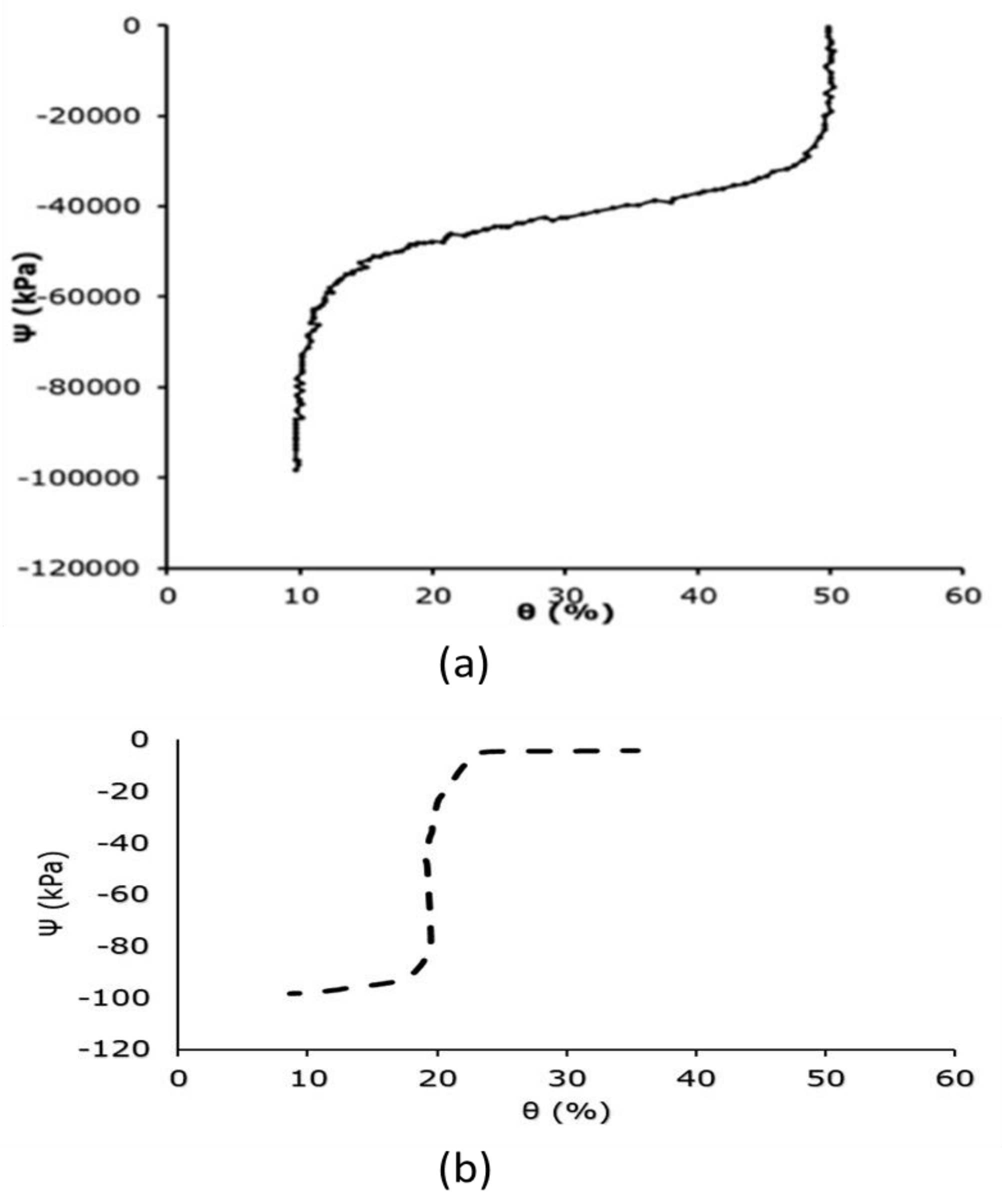

Figure 6.7. Predicted and measured soil water characteristic curve (a) Predicted Van Genuchten SWCC (b) Measured SWCC at 200 mm for the Ivrogbo soil sample infiltration experiment

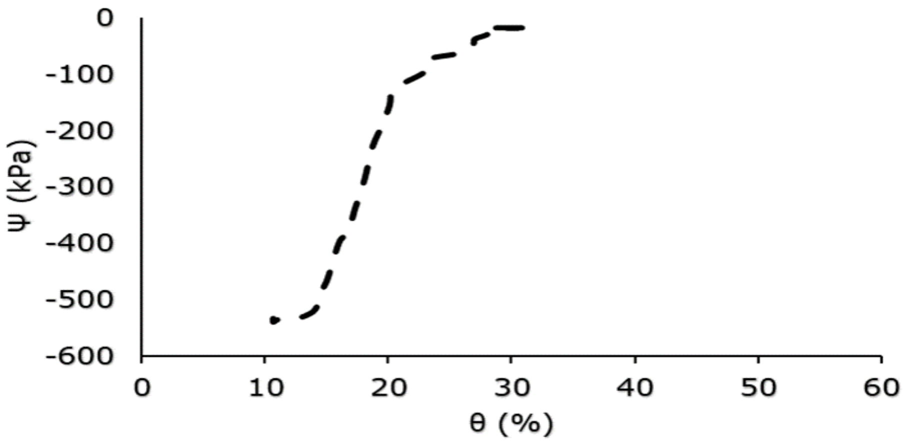

Figure 6.8. Infiltration experiment at 300 mm depth for Ivrogbo soil column showing the soil water characteristic curve

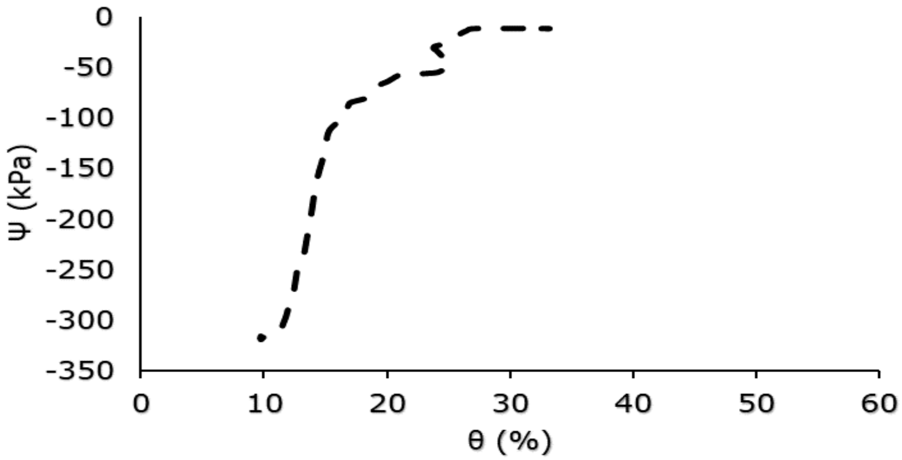

Figure 6.9. Average measured soil water characteristic curve for Ivrogbo soil

6.1.4 Measured Soil Water Characteristic Curve (SWCC) For Monolith of Soil Sample from Oleh

Using the soil column experiment and the associated test protocol that has been described, the wetting soil water characteristic curve (SWCC) for the Oleh soil sample with a bulk density of 1640 kg/m^3 is measured in the laboratory at 200 mm and 300 mm depths, as well as the average of the records for the 200 mm and 300 mm depths. Figures 6.10 and 6.11 depict the Oleh soil sample's soil water characteristic curve at 200 and 300 mm depths. By averaging the soil water content and the associated values of the soil matric potentials at both depths, the average soil water characteristic curve, shown in Figure 6.12, is produced. This is a result of the absence of a sensor that can gauge the matric potential at a 100 mm depth. The findings indicate that high matric suction values are recorded at low soil water contents, while low matric suction values are reported at high soil water contents. A high water content is associated with the saturation zone, and a low water content is associated with the residual zone. Strong matric pressure is required at the residual zone to release the water from the soil matrix due to the attraction force between the residual water and the matrix (Eyo, Ng'ambi, and Abbey 2022b; Koorevaar, Dirksen, and Menelik 1991). There appears to be a transition zone where the matric suction progressively drops as the water content rises. The low water content value's matric suction is only about -20 kPa at 300 mm and roughly -19 kPa at 200 mm below the top of the column. This is because the soil sample is already very wet when the experiment starts. Because of the soil sample's initial wetness, the majority of the curve seemed to be in the transition zone, despite the fact that the curve's shape is essentially sigmoid and the results are consistent with earlier studies.

In this part, the simulated and experimental results are also compared. Based on van Genuchten, M. Th. (1980)'s developed model, simulated data collected from a representative plot of the soil water characteristic curve are used to present Figure 6.13. Figure 6.13 (b) displays the soil water characteristic curve for the Oleh soil sample at 200 mm. The matric pressure is noticeably very high at the lowest value of the soil water content for the simulated data, suggesting that the soil is extremely dry and that the water content is residual. Moreover, soil texture for the simulated data is coarse-grained with low field capacity and high matric potential.

When the water content in the soil increases swiftly in the transition zone, the matric pressure head declines at a significantly slower rate than it does when the water content in the residual zone remains constant. At the upper end of the 50% range of the soil water content, the water content returns to its constant value, creating a vertically upward and downward S-shaped (sigmoid) curve. This is also the point at which the curve saturates. Conversely, the Oleh soil's soil water characteristic curve displays a high matric potential value at low volumetric water level and a low matric potential value at high volumetric water content. The range of values is still less than the expected curve, though. Consequently, a 99.98%

percentage between the residual value of the packed soil sample and the residual value of the projected Van Genuchten curve is seen.

Given that the soil is quite wet before the experiment begins, it is noticed that the soil water content is already 15.9% and 28.2% at 200 mm and 300 mm depth, respectively, and that the matric potential is only within the range of -20 kPa, registering a maximum of -20 kPa. Although it is not meant to be 100% exact, the soil column experiment for the Oleh soil sample also uses an S-shaped curve (sigmoid curve) to clearly depict the characteristics of the residual zone, transition zone, and saturation zone. The curve reasonably matches with the findings in the literature.

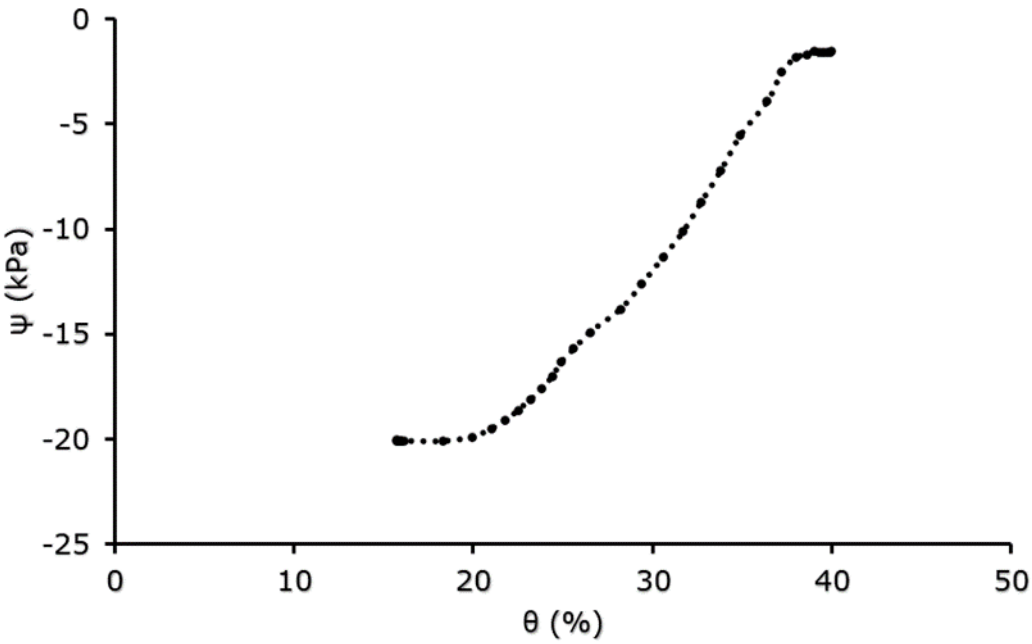

Figure 6.10. Infiltration experiment at 200 mm depth for Oleh soil column showing the soil water characteristic curve

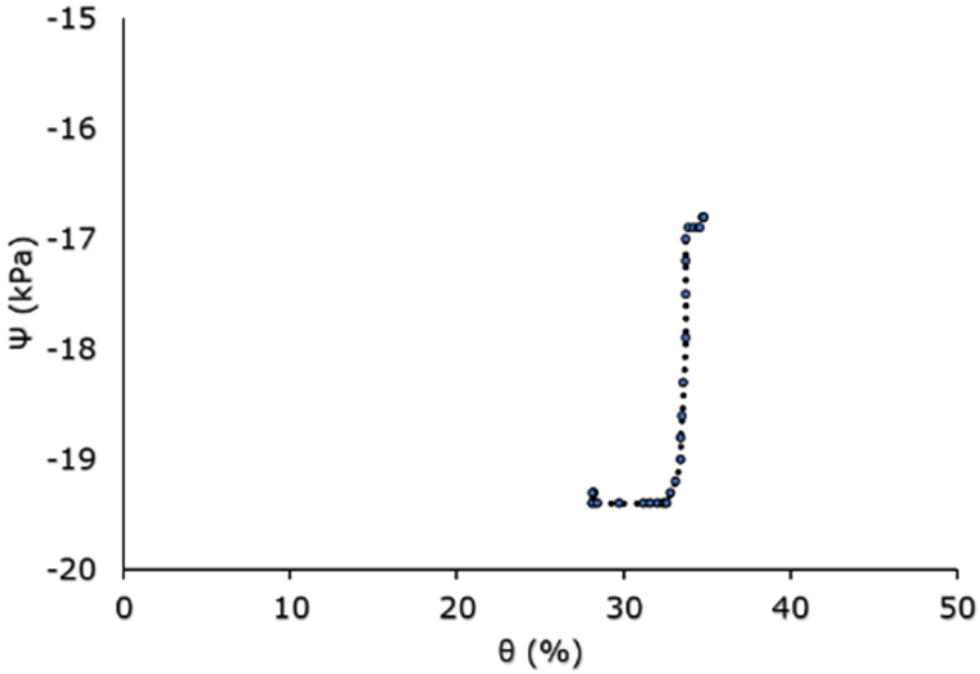

Figure 6.11. Infiltration experiment at 300 mm depth for Oleh soil column showing the soil water characteristic curve

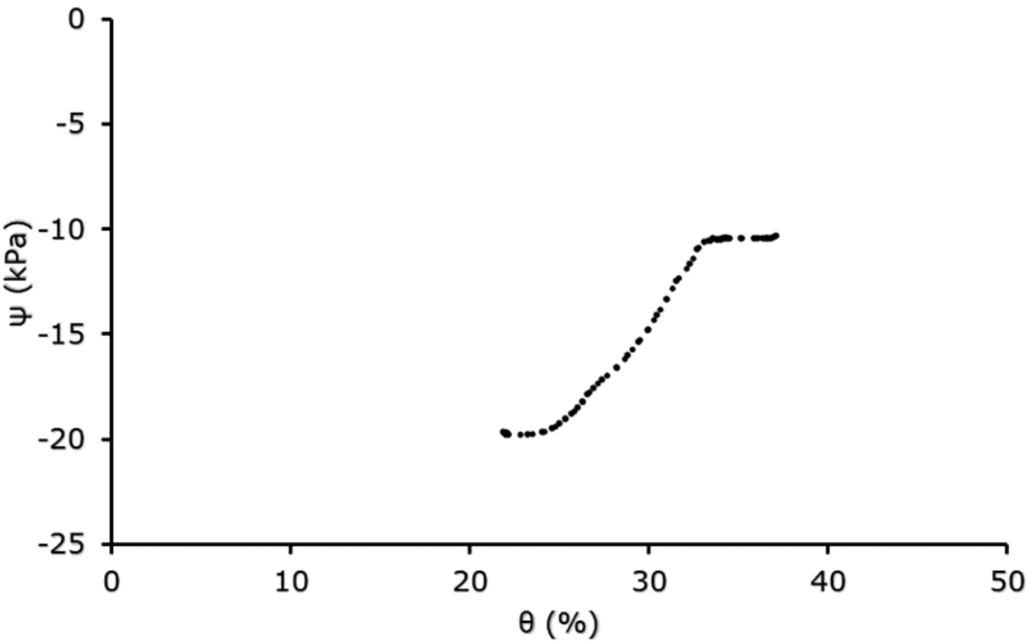

Figure 6.12. Average measured soil water characteristic curve for Oleh soil

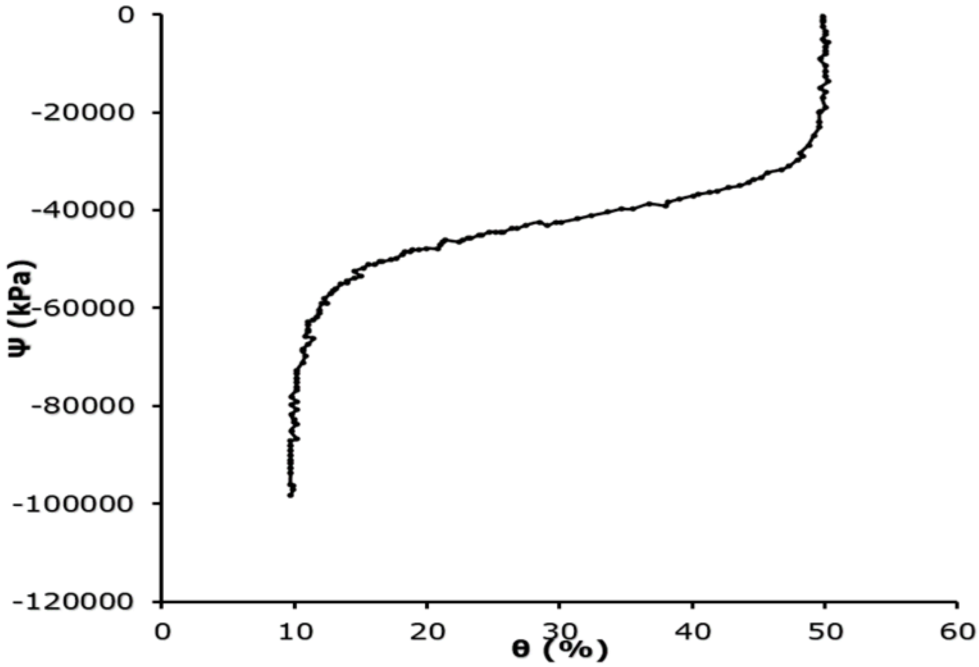

(a)

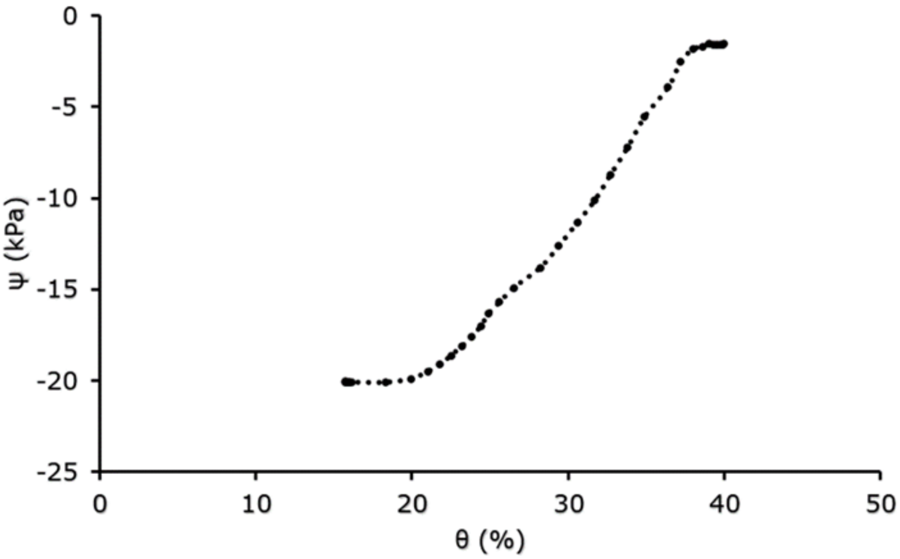

(b)

Figure 6.13. Predicted and measured soil water characteristic curve (a) Predicted Van Genuchten SWCC (b) Measured SWCC at 200 mm for the Oleh soil sample infiltration experiment

6.2 Comparison of the Soil Water Characteristics Curves in the Soil types

Figure 6.14 presents the domain-specific soil water characteristics curves for the packed soil sample, the ploughed soil sample, the Ivrogbo soil sample, and the Oleh soil sample at the 200 mm depth (Figure 6.14a) and the 300 mm depth (Figure 6.14b). Many factors, including soil texture, soil dry density, initial water content, particle size, and pore structure, have significant impact on the soil water characteristics curves of unsaturated soils (Yang et al., 2023). The fine-textured soils are characterised by higher available water values, while the sandy soils have lower available water values (Li, D. et al., 2016; Yang et al., 2023). The soil samples as explained in chapter four have the Ivrogbo soil sample classified as fine-grained, followed by the Oleh soil sample. The packed soil sample is coarser than the ploughed soil sample because stones have been removed from the former. At 200 mm depth (Figure 6.14(a)), It is observed that although the four soil types are subjected to similar condition of laminar flow as explained in chapter four, their soil water characteristic curves are significantly different. In a range of the same time of about 100 minutes, while the soil water content increases from 8.8% at a matric potential of -98 kPa to 35.3% at a matric potential of -4.4 kpa for the Ivrogbo soil sample, the soil water content of the packed soil sample increases from 4.7% at a matric potential of -436.5 kPa to 11.2% but the matric potential increases to -485.2 kPa. This is because the Ivrogbo soil is fine-grained with higher available water holding capacity than the packed soil sample which is coarsed grained. However, the soil water content of the ploughed soil sample increases from 3.1% at a matric potential of -710 kPa to a soil water content of 30.4% at a matric potential of -7.9 kPa. This is because having removed the stones and ploughed the soil, it has altered the soil texture and increased the fineness of the grains thereby increasing the soil available water holding capacity. The soil water content of the Oleh soil sample increases from 15.9% at a matric potential of -20.1 kPa to 40.3% at a matric potential of -2.6 kPa due to the fine grained clay content and the fact that the sample was already very wet pre-experiment. The same pattern is noticed at the 300 mm depth in Figure 6.14(b). In 130 minutes, the soil water content of the Ivrogbo soil sample increases from 10.8% at a matric potential of -539.2 kPa to 30% at a matric potential of -17.5 kPa but the water content of the packed sample increases from 6.1% at a matric potential of -28.1 kPa to a water content of 6.2% with the matric potential having increased to -29.2 kPa because the former is fine-grained, enhancing its water holding capacity while the latter is coarse-grained. While the ploughed soil sample is initially at permanent wilting point with a matric potential of -1850 kPa and water content of 4%, the water content increases to 23.8% at a matric potential of -58.8 kPa within the same time range because the texture has changed with the removal of the stones and condition of ploughing, then its water holding capacity has increased. At 300 mm depth, the water content of the Oleh soil sample increases from 28.2% at a matric potential of -19.3 kPa to 35.5% at a matric potential of -16.8 kPa, also because of its fine-grained nature of sand clay mixture and wetness pre-exprerimert.

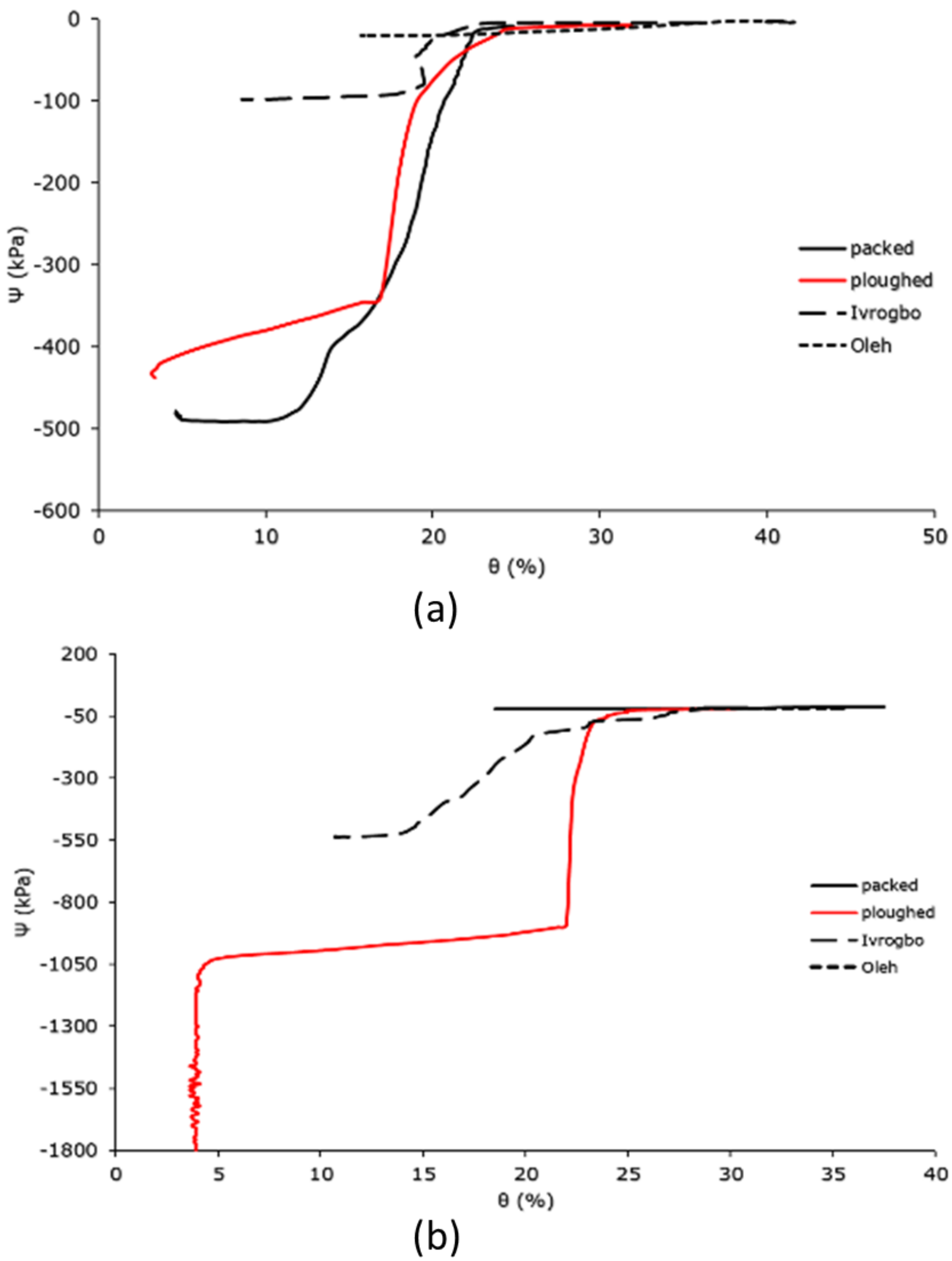

Figure 6.14 Domain-specific Soil Water Characteristics Curve for the Different Soil Types (a) 200 mm (b) 300 mm

6.3 Development of Smart Drip Micro-Irrigation System Based on Hydrodynamics Characterisation of Soils

As stated earlier in chapter one, with greater understanding of the soil matric potential and water content, it is possible to determine the types of crops that can thrive and preserve water. This is because different types of soil, such as clay, sand, silt, and others, have different capacity for holding water; so, a plant's comfort zone cannot be accurately determined by its water content. The soil water characteristic curves of soils with different textures are significantly different. This logic can be applied to the different soil types covered in this study and enable a more scientific approach to the water management strategy that can lead to increased crop productivity. The Ivrogbo sample is determined to be silty clay with low to medium plasticity, which is fine-grained while the Oleh sample is determined to be sand clay mixture, which is also fine-grained. The packed sample is silty sand and is shown to be coarse-grained, but with the removal of peds and ploughing, it significantly changes to fine-textured soil as shown in the hydrodynamic behaviour in Figure 6.14. From the data in Appendix 2 to Appendix 5 from which Figure 6.14a and Figure 6.14b are developed, it is observed that at 200 mm for the Oleh sample (Appendix 5), when the matric potential is -20 kPa, the water content is 16%, but for the Ivrogbo sample the water content is 20% at -20 kPa (Appendix 4). At -20 kPa for the packed sample for the same 200 mm depth, the water content is 22% (Appendix 2), while it is 24% for the ploughed sample (Appendix 3). At 300 mm depth, the water content for the Oleh sample is 28% when the matric potential is -20kPa, and the water content of the Ivrogbo sample is 28% when the matric potential is also -20kPa. However, the water content of the packed sample is 31% when the matric potential is -20 kPa at that depth, while the water content for the ploughed sample is around 30% when the matric potential -20 kPa. With this known conditions of the soil characteristics of the different samples, a smart drip micro-irrigation can be installed with crops of known comfort zones with minimum threshold of -20 kPa matric potential. We take the case of the orange tree from Figure 1.8 where the crop is most comfortable within a range of matric potential of -20 kPa to -100 kPa. With a smart drip micro-irrigation installed in an orange orchard planted in the Oleh soil sample, drought will trigger the smart irrigation when the water content reduces below 16%. With the smart drip irrigation in the Ivrogbo soil for the orange orchard, it will be triggered when the water content reduces below 20%. The system will be triggered when the water content reduces below 22% in the packed sample and even below 24% in the ploughed sample. This means that there is most water savings with the Oleh sample in the presented scenario.

6.4 Summary of Key Findings

This section summarizes the hydrodynamics characteristics of different soil types based on their soil water characteristics curves. The soil types include a packed and ploughed soil sample from Aberdeen, a monolith of undisturbed soil sample from Ivrogbo and a monolith of undisturbed soil sample from Oleh both in Niger Delta area of Nigeria.

- The findings demonstrate that high matric suction values are recorded at low soil water content and low matric suction values are reported at high soil water content. A high water content is associated with the saturation zone, and a low water content is associated with the residual zone. This is depicted in Figure 6.14a and Figure 6.14b.
- Soils differing greatly in texture have quite varied soil water characteristic curves. Higher available water values are seen in fine-textured soils compared to lower available water values in sandy soils.
- As seen in Figure 6.14a and Figure 6.14b, matric potential decreases to a more positive value as the water content increases.
- A plant comfort zone cannot be accurately determined by the soil water content. It is necessary to determine the soil texture and the matric potential to determine the plant comfort zone and match it with the water content.

Chapter 7
Conclusions

This chapter presents the concluding remarks on the findings that have been arrived at in this study on the concept of understanding the complex hydrodynamics of water flow through the soil subsurface. The important contributions to knowledge which this research has made are also presented. Additionally, the recommendations for future work to broaden the knowledge on subsurface flow characterisation, especially pertaining to water conservation purposes for agricultural development are made.

7.1 Research Problem Synopsis

An understanding of the complex hydrodynamics of water flow through the soil subsurface has many benefits in different fields including engineering and irrigation in agriculture. Different research studies to characterise the flow of water through the soil subsurface in the field and laboratory have been independently conducted but challenges always abound because the soil subsurface conceals much information that is invisible to the unaided eyes. A critical review of published literature reveals that flow characterisation of soil subsurface water dynamics involves hydraulic parameters including soil hydraulic conductivity, soil water diffusivity, soil water characteristics curve, soil water content, soil matric potential and soil pore water electrical conductivity. Water flow processes in the soil subsurface are affected by the soil homogeneity or heterogeneity, leading to uniform flow or preferential or nonequilibrium flow due to the presence of macropores. Despite a significant amount of research that has been published in the fields of hydrology, agriculture, and soil sciences, the majority of which is based on the results of soil column experiments, attempt has never been made to collect or standardise the best practices for creating soil columns.

This study has been carried out to broaden our understanding of the complex hydrodynamics of water flow through the soil subsurface for the purpose of conserving water especially in drip micro-irrigation activities. Gravity flow infiltration experiments were conducted using soil samples from three different regions in a soil column set up to investigate the soil water dynamics by studying the soil hydraulic parameters including the soil water content, soil matric potential, and soil water characteristics curve at domain-specific depths of the soils in the column.

7.2 Thesis Conclusion

A thorough and extensive investigation was carried out to broaden the knowledge on the understanding of the complex hydrodynamics of water flow processes through the soil subsurface for the purpose of water conservation in micro-irrigation activities. A real-world series of experiments were conducted in the laboratory using a conceptualised, designed and built soil column test rig to carry out gravity flow on packed and ploughed soil sample from Aberdeen, and monoliths of undisturbed soil samples from Ivrogbo and Oleh which are two different regions from the inland valley of the Niger Delta region of Nigeria, in order to investigate the complex hydrodynamics of soil water flow. The investigations carried out involved the behaviour of soil hydraulic properties including the soil water content, the soil matric potential, and the soil water characteristics curve. Effect of temperature was ignored in the study because the soil water diffusivity was also not considered.

Based on the formulated research objectives derived from the knowledge gap in the consulted literature and the results and discussion presented, the following conclusions are drawn from this study.

Research Objective #1: To measure the soil water content at intervals of 10 cm in a soil column laboratory experiment mimicking drip soil subsurface micro-irrigation.

Conclusion #1: Having generated large volumes of data from appropriate measurement of the soil hydraulic parameters, the data are curated to provide understanding of the flow dynamics of water in the soil subsurface. When the soil texture alters vertically downwards, the water holding capacity changes to maintain a higher value of available water for the finer grained texture. For instance, at 100 mm depth the Ivrogbo sample obviously with finer grains maintain higher available water value of 35.7% while the Oleh sample has 33.2%, but at 200 mm, the Oleh sample projects higher available water value of 40% while the Ivrogbo sample has 35% suggesting that the grains are finer than the Ivrogbo soil grains at that depth. A general trend is established for the movement of the soil water content in the unsaturated zone, also known as the vadose zone. As water was initially added to the soil in the vadose zone, the water content appeared constant before beginning to increase rapidly over time with the steady addition of the water. Thereafter, the flow profile appeared steady again. The initial constant appearance described the residual zone while the region of rapid increase described the transition zone, with the next steady phase indicating that the soil was becoming saturated. The undisturbed monolith of the soil column generally showed a behaviour of nonequilibrium flow or preferential flow when compared with the profiles for the packed soil column, but the ploughed soil displayed uniform flow. This could be used as a guide in micro-irrigation systems. The fine-texture samples are characterised by higher available water values, while the coarse-textured samples hold lower available water values.

Research Objective #2: To measure the soil matric potential at intervals of 10 cm in a soil column laboratory experiment mimicking drip soil surface micro-irrigation.

Conclusion #2: The soil texture has huge effect on the field holding capacity and matric potential. As water is added to the soils, the matric potentials decrease at different rates depending on the soil texture. A high water content is associated with the saturation zone, and a low water content is associated with the residual zone. When water is applied to the various soil samples over a period of approximately 100 minutes at a depth of 200 mm, the matric potential of the Oleh soil sample is -2.6 kpa, but the Ivrogbo soil sample records a matric potential of -4.4 kpa. The matric potential of the ploughed soil sample is -7.9 kPa, but the matric potential of the packed soil sample is -485.2 kPa. It takes less water to reach field capacity (i.e., the EU standard for crop comfort zone) and has the lowest negative matric potential (great water retention capabilities) of any soil sample from the Oleh area. Based on these results, farmers in the Oleh region can readily implement drip micro-irrigation.

Research Objective #3: To analyse the soil water characteristics curve as a relationship between the soil water content and the soil matric potential.

Conclusion #3: The experimental data has been verified using the Van Genuchten model of the soil water characteristics curve. Comparing the four samples' volumetric soil water contents and soil matric potentials at various depths reveals a significant variation in their behaviour. However, compared to the predicted curve, the range of values is narrower.

At 200 mm depth, the value of n is noticed to be 15 with θ_r of 0.0046 and θ_s of 0.23 for the packed soil sample, giving a percentage difference of 86.7 % compared to n equal to 2 in the Van Genuchten curve. Also, for the ploughed sample, n equals 10 giving a percentage difference of 80 % but θ_r = 0.03 while θ_s = 0.23. For the Ivrogbo sample and Oleh samples, the range of the matric potential is relatively too small for the comparism. In addition to variations in soil type, one contributing factor to this is the soil sample's pre-experiment moisture content.

7.3 Contribution to Knowledge

This study has been conducted to contribute to the body of knowledge in soil subsurface flows by providing a better understanding of experimental approaches to flow characterisation and determination of soil water retention curve. During this research, the author did the following:

i. Carried out data analysis to derive the soil water retention curve (SWRC) which compares with published numerical data.
ii. Demonstrated a simplified method of hydrodynamic characterisation of soil subsurface flows through the use of modern digital instruments which generate enormous data with a flexibility that is devoid of the complexity associated with indirect predictive modelling methods.
iii. Presented a quantitative and qualitative evaluation of the soil water retention curve as a soil hydraulic property derived from a simplified experimental method.
iv. A better insight into the understanding of flow dynamics was provided, with a focus on water conservation using a link between the soil water content, the soil matric potential, and the crop comfort zone, which when implemented can improve micro-irrigation activities for better crop yield.

The findings in this study establish a better understanding of the complexity of soil subsurface flow dynamics in the determination of soil hydraulic properties.

7.4 Recommendations for Future Work

This study has provided the knowledge to broaden the understanding of the complex hydrodynamics of water flow through the soil subsurface. Flow characterization of hydraulic parameters of water flow through wetting infiltration experiments in the laboratory using a column of packed soil sample and monoliths of undisturbed soil samples have been carried out. Based on the findings, a recommendation for further investigation is made as follows:

Recommendation #1: Further investigation should be carried out with different set of samples from other defined geographical locations using the same product of sensors and data logger. However, the cylindrical pipe for the soil column should be standardized at 139.7 – 152.4 mm internal diameter to enable the pins of the wet 150 and the steel rods of the EQ3 Equitensiometer sit well at any depth in the soil column without creating interference during logging. Furthermore, appropriate sealing device should be used, and the interior walls of the container should be rubbed with a good gel to create a good bond between the cylinder wall and the soil and avoid preferential flow of water along the cylinder wall.

Recommendation #2: The real-world experiments have generated a large volume of dataset which should be curated and used to develop models for pedotransfer functions for predicting soil hydraulic properties.

Recommendation #3: A similar research should be undertaken with a focus on soil hydraulic conductivity and soil water diffusivity.

References

ABBASI, Y. et al., 2011. Evaluation of Pedotransfer Functions for Estimating Soil Water Retention Curve of Saline and Saline-Alkali Soils of Iran. *Pedosphere,* 21(2), pp. 230–237.

ABD EL-GHANY, B.F. et al., 2010. Effect of some soil microorganisms on soil properties and wheat production under North Sinai conditions. *Journal of Applied Sciences Research,* 4(5), pp. 559–579.

ALJOUMANI, B., SANCHEZ-ESPIGARES, J. and WESSOLEK, G., 2018. Estimating Pore Water Electrical Conductivity of Sandy Soil from Time Domain Reflectometry Records Using a Time-Varying Dynamic Linear Model. *Sensors,* 18(12),

ANGERS, D. and CARON, J., 1998. Plant-Induced Changes in Soil Structure: Processes and Feedbacks. *Biogeochemistry,* 42, pp. 55–72.

ANGULO-JARAMILLO, R. et al., 2000. Field measurement of soil surface hydraulic properties by disc and ring infiltrometers: A review and recent developments. *Soil and Tillage Research,* 55(1), pp. 1–29.

ATANGANA, A., 2018. Chapter 2 - Principle of Groundwater Flow. In: A. ATANGANA ed.*Fractional Operators with Constant and Variable Order with Application to Geo-Hydrology.* Academic Press. pp. 15–47.

BATES, B. et al., 2008. *Climate change and water. technical paper of the intergovernmental panel on climate change.*

BAYAT, H. et al., 2013. Combination of artificial neural networks and fractal theory to predict soil water retention curve. *Computers and Electronics in Agriculture,* 92, pp. 92–103.

BÉGIN, L., FORTIN, J. and CARON, J., 2003. Evaluation of the Fluoride Retardation Factor in Unsaturated and Undisturbed Soil Columns. *Soil Science Society of America Journal,* 67(6), pp. 1635–1646.

BEVEN, K., 1982. On subsurface stormflow: Predictions with simple kinematic theory for saturated and unsaturated flows. *Water Resources Research,* 18(6), pp. 1627–1633.

BEVEN, K. and GERMANN, P., 1982. Macropores and water flow in soils. *Water Resources Research,* 18(5), pp. 1311–1325.

BIBBY, R., 1981. Mass transport of solutes in dual-porosity media. *Water Resources Research,* 17(4), pp. 1075–1081.

BIENVENUE, T., XIE, J. and NIU, Q., 2022. Developing a soil column system to measure hydrogeophysical properties of unconsolidated sediment. *Vadose zone journal,* 21(2), pp. n/a.

BROMLY, M., HINZ, C. and AYLMORE, L.A.G., 2007. Relation of dispersivity to properties of homogeneous saturated repacked soil columns. *European Journal of Soil Science,* 58(1), pp. 293–301.

BROOKS, R.H., COREY, A.T. and COLORADO STATE UNIVERSITY HYDROLOGY AND WATER, RESOURCES PROGRAM, 1964. *Hydraulic properties of porous media.* Fort Collins: Colorado State University Hydrology and Water Resources Program] Fort Collins.

CAMOBRECO, V. et al., 1996. Movement of Heavy Metals Through Undisturbed and Homogenized Soil Columns. *Soil Science,* 161, pp. 740–750.

CARMAN, P.C., 1997. Fluid flow through granular beds. *Chemical Engineering Research and Design,* 75, pp. S32–S48.

CLAISSE, P.A., 2016. Chapter 9 - Transport of fluids in solids. In: P.A. CLAISSE ed.*Civil Engineering Materials.* Boston: Butterworth-Heinemann. pp. 83–90.

CLARKE, B. et al., 2022. Extreme weather impacts of climate change: an attribution perspective. *Environmental Research: Climate,* 1(1), pp. 012001.

CLOTHIER, B.E. et al., 1995. The measured mobile-water content of an unsaturated soil as a function of hydraulic regime. *Soil Research,* 33(3), pp. 397–414.

COMMUNAR, G., KEREN, R. and LI, F., 2004. Deriving Boron Adsorption Isotherms from Soil Column Displacement Experiments. *Soil Science Society of America Journal - SSSAJ,* 68

CORWIN, D.L., 2000. Evaluation of a simple lysimeter-design modification to minimize sidewall flow. *Journal of contaminant hydrology,* 42(1), pp. 35–49.

DARYATI, D. et al., 2019. Soil characteristics analysis based on the unified soil classification system. *Journal of Physics: Conference Series,* 1402(2), pp. 022028.

DE JONGE, L. et al., 2004. Particle Leaching and Particle-Facilitated Transport of Phosphorus at Field Scale. *Vadose Zone Journal - VADOSE ZONE J,* 3, pp. 462–470.

DE ROOIJ, G.H., 2000. Modeling fingered flow of water in soils owing to wetting front instability: a review. *Journal of Hydrology,* 231-232, pp. 277–294.

DE ROOIJ, G.,H. and CHO, H., 1999. Modelling solute leaching during fingered flow by integrating and expanding various theoretical and empirical concepts. *Hydrological Sciences Journal,* 44(3), pp. 447–465.

DEKKER, L.W. and RITSEMA, C.J., 1996. Variation in water content and wetting patterns in Dutch water repellent peaty clay and clayey peat soils. *Catena,* 28(1), pp. 89–105.

DUKHAN, N., BAĞCI, Ö and ÖZDEMIR, M., 2014. Experimental flow in various porous media and reconciliation of Forchheimer and Ergun relations. *Experimental Thermal and Fluid Science,* 57, pp. 425–433.

DURNER, W., 1994. Hydraulic conductivity estimation for soils with heterogeneous pore structure. *Water Resources Research,* 30(2), pp. 211–223.

DURNER, W., et al., 1999. Determination of parameters for flexible hydraulic functions by inverse modeling. In: Anonymous pp. 817–829.

EYO, E.U., NG'AMBI, S. and ABBEY, S.J., 2022. An overview of soil–water characteristic curves of stabilised soils and their influential factors. *Journal of King Saud University - Engineering Sciences,* 34(1), pp. 31–45.

FLURY, M. et al., 1995. Transport of Anions and Herbicides in a Loamy and a Sandy Field Soil. *Water Resources Research,* 31(4), pp. 823–835.

FREDLUND, D. and XING, A., 1994. Equations for the Soil–Water Characteristic Curve. *Canadian Geotechnical Journal - CAN GEOTECH J,* 31, pp. 521–532.

FU, Y. et al., 2021. Estimating soil water retention curves from soil thermal conductivity measurements. *Journal of Hydrology,* 603, pp. 127171.

GALLAGE, C., KODIKARA, J. and UCHIMURA, T., 2013. Laboratory measurement of hydraulic conductivity functions of two unsaturated sandy soils during drying and wetting processes. *Soils and Foundations,* 53(3), pp. 417–430.

GERKE, H.H. and VAN GENUCHTEN, M.T., 1993. A dual-porosity model for simulating the preferential movement of water and solutes in structured porous media. *Water Resources Research,* 29(2), pp. 305–319.

GERKE, H.H., 2006. Preferential flow descriptions for structured soils. *Journal of plant nutrition and soil science; Z.Pflanzenernähr.Bodenk,* 169(3), pp. 382–400.

GHODRATI, M., CHENDORAIN, M. and CHANG, Y.J., 1999. Characterization of Macropore Flow Mechanisms in Soil by Means of a Split Macropore Column. *Soil Science Society of America Journal,* 63(5), pp. 1093–1101.

GISH, T.J. et al., 2004. Impact of Preferential Flow at Varying Irrigation Rates by Quantifying Mass Fluxes. *Journal of environmental quality,* 33(3), pp. 1033–1040.

GJETTERMANN, B. et al., 1997. Preferential flow in sandy loam soils as affected by irrigation intensity. *Soil Technology,* 11(2), pp. 139–152.

GLASS, R.J., PARLANGE, J.-. and STEENHUIS, T.S., 1991. Immiscible Displacement in Porous Media: Stability Analysis of Three-Dimensional, Axisymmetric Disturbances With Application to Gravity-Driven Wetting Front Instability. *Water Resources Research,* 27(8), pp. 1947–1956.

GLASS, R.J. et al., 1990. Wetting front instability in unsaturated porous media: A three-dimensional study in initially dry sand. *Transport in Porous Media,* 5(3), pp. 247–268.

GWO, J.P. et al., 1995. A multiple-pore-region concept to modeling mass transfer in subsurface media. *Journal of Hydrology,* 164(1), pp. 217–237.

HAGHVERDI, A., CORNELIS, W.M. and GHAHRAMAN, B., 2012. A pseudo-continuous neural network approach for developing water retention pedotransfer functions with limited data. *Journal of Hydrology,* 442-443, pp. 46–54.

HAGHVERDI, A., ÖZTÜRK, H.S. and DURNER, W., 2018. Measurement and estimation of the soil water retention curve using the evaporation method and the pseudo continuous pedotransfer function. *Journal of Hydrology,* 563, pp. 251–259.

HARIA, A.H., HODNETT, M.G. and JOHNSON, A.C., 2003. Mechanisms of groundwater recharge and pesticide penetration to a chalk aquifer in southern England. *Journal of Hydrology,* 275(1), pp. 122–137.

HE, H. et al., 2021. Chapter Three - A review of time domain reflectometry (TDR) applications in porous media. *Advances in Agronomy,* 168, pp. 83–155.

HEBER GREEN, W. and AMPT, G.A., 1911. Studies on Soil Phyics. *The Journal of Agricultural Science,* 4(1), pp. 1–24.

HENDRICKX, J. and FLURY, M., 2001. Uniform and preferential flow mechanisms in the vadose zone. In: Anonymous pp. 149–187.

HILLEL, D., *Introduction to environmental soil physics.* Amsterdam: Elsevier Academic Press Amsterdam.

HORNUNG, U. and SHOWALTER, R.E., 1990. Diffusion models for fractured media. *Journal of Mathematical Analysis and Applications,* 147(1), pp. 69–80.

HOU, X., VANAPALLI, S.K. and LI, T., 2019. Water Flow in Unsaturated Soils Subjected to Multiple Infiltration Events. *Canadian Geotechnical Journal,* 57(3), pp. 389.

HOU, X., VANAPALLI, S. and LI, T., 2019. Water flow in unsaturated soils subjected to multiple infiltration events. *Canadian Geotechnical Journal,* 57

HRAPOVIC, L. et al., 2005. Laboratory Study of Treatment of Trichloroethene by Chemical Oxidation Followed by Bioremediation. *Environmental science & technology,* 39, pp. 2888–97.

HUTSON, J.L. and WAGENET, R.J., 1995. A Multiregion Model Describing Water Flow and Solute Transport in Heterogeneous Soils. *Soil Science Society of America Journal,* 59(3), pp. 743–751.

IRMAK, S. et al., 2014. Principles and Operational Characteristics of Watermark Granular Matrix Sensor to Measure Soil Water Status and Its Practical Applications for Irrigation Management in Various Soil Textures.

J.VALOCCHI, A., 1990. Use of temporal moment analysis to study reactive solute transport in aggregated porous media. *Geoderma,* 46(1), pp. 233–247.

JARDINE, P.M., JACOBS, G.K. and O'DELL, J.D., 1993. Unsaturated Transport Processes in Undisturbed Heterogeneous Porous Media: II. Co-Contaminants. *Soil Science Society of America Journal,* 57(4), pp. 954–962.

JARVIS, N., 1994. *The MACRO model (version 3.1): Technical description and sample simulations.* Swedish University of Agricultural Sciences, Department of Soil Sciences.

JARVIS, N.J., 2007. A review of non-equilibrium water flow and solute transport in soil macropores: principles, controlling factors and consequences for water quality. *European Journal of Soil Science,* 58(3), pp. 523–546.

JARVIS, N.J., LEEDS-HARRISON, P. and DOSSER, J.M., 1987. The use of tension infiltrometers to assess routes and rates of infiltration in a clay soil. *Journal of Soil Science,* 38(4), pp. 633–640.

JARVIS, N. et al., 2006. Modelling water and solute transport in macroporous soil. I. Model description and sensitivity analysis. *Journal of Soil Science,* 42, pp. 59–70.

JARVIS, N. et al., 2013. Influence of soil, land use and climatic factors on the hydraulic conductivity of soil. *Hydrology and Earth System Sciences,* 17(12), pp. 5185–5195.

JAYNES, D.B., LOGSDON, S.D. and HORTON, R., 1995. Field Method for Measuring Mobile/Immobile Water Content and Solute Transfer Rate Coefficient. *Soil Science Society of America Journal,* 59(2), pp. 352–356.

KARGAS, G., KOKA, D. and LONDRA, P.A., 2022. Determination of Soil Hydraulic Properties from Infiltration Data Using Various Methods. *Land,* 11(6),

KARUP, D. et al., 2017. Prediction of the soil water retention curve for structured soil from saturation to oven-dryness. *European Journal of Soil Science,* 68(1), pp. 57–65.

KELLER, J.M. and SIMMONS, C.S., 2005. *The Influence of Selected Liquid and Soil Properties on the Propagation of Spills over Flat Permeable Surfaces.* United States:

KLEINMAN, P. et al., 2005. Phosphorus leaching through intact soil columns before and after poultry manure application. *Soil Science,* 170

KÖHNE, J.M. and MOHANTY, B.P., 2005a. Water flow processes in a soil column with a cylindrical macropore: Experiment and hierarchical modeling. *Water Resources Research,* 41(3),

KÖHNE, J.M. and MOHANTY, B.P., 2005b. Water flow processes in a soil column with a cylindrical macropore: Experiment and hierarchical modeling. *Water Resources Research; Water Resour.Res,* 41(3), pp. W03010–n/a.

KÖHNE, J. and MOHANTY, B., 2005. Water flow processes in a soil column with a cylindrical macropore: Experiment and hierarchical modeling. *Water Resources Research - WATER RESOUR RES,* 41

KOOL, D. et al., 2019. Soil water retention and hydraulic conductivity dynamics following tillage. *Soil and Tillage Research,* 193, pp. 95–100.

KOOREVAAR, P., DIRKSEN, C. and MENELIK, G., 1991. *Elements of soil physics.* 3. ed., 3. impr ed. Amsterdam u.a: Elsevier Amsterdam u.a.

KOZENY, J., 1927. Uber Kapillare Leitung der Wasser in Boden. *Royal Academy of Science, Vienna, Proc.Class I,* 136, pp. 271–306.

KUTILEK, M. and JENDELE, L., 2008. The structural porosity in soil hydraulic functions - A review. *Soil and Water Research,* 3, pp. S7–S20.

LANGNER, H.W. et al., 1999. Preferential Flow through Intact Soil Cores Effects of Matric Head. *Soil Science Society of America Journal,* 63(6), pp. 1591–1598.

LARSSON, M.H. and JARVIS, N.J., 1999. A Dual-Porosity Model to Quantify Macropore Flow Effects on Nitrate Leaching. *Journal of environmental quality,* 28(4), pp. 1298–1307.

LEWIS, J. and SJÖSTROM, J., 2010. Optimizing the experimental design of soil columns in saturated and unsaturated transport experiments. *Journal of contaminant hydrology,* 115(1), pp. 1–13.

LI, D. et al., 2016. Predicting available water of soil from particle-size distribution and bulk density in an oasis–desert transect in northwestern China. *Journal of Hydrology,* 538, pp. 539–550.

LI, J. et al., 2022. A new method of estimating soil water diffusivity based on variation in the wetting front position and on the principle of stationary action. *Journal of Hydrology,* 612, pp. 128290.

LIU, Q. et al., 2012. Automatic soil water retention test system with volume change measurement for sandy and silty soils. *Soils and Foundations,* 52(2), pp. 368–380.

LIU, Y., STEENHUIS, T.S. and PARLANGE, J.-., 1994. Closed-form solution for finger width in sandy soils at different water contents. *Water Resources Research,* 30(4), pp. 949–952.

LU, N., 2019. Linking Soil Water Adsorption to Geotechnical Engineering Properties. In: Anonymous pp. 93–139.

LUO, S. et al., 2022a. Soil water potential: A historical perspective and recent breakthroughs. *Vadose Zone Journal,* 21(4), pp. e20203.

LUO, S. et al., 2022b. Soil water potential: A historical perspective and recent breakthroughs. *Vadose Zone Journal,* 21(4), pp. e20203.

LUXMOORE, R.J., 1981. Micro-, Meso-, and Macroporosity of Soil. *Soil Science Society of America Journal,* 45(3), pp. 671–672.

MACDONALD, M.J. et al., 1991. A generalized Blake-Kozeny equation for multisized spherical particles. *AIChE Journal,* 37(10), pp. 1583–1588.

MALI, N., URBANC, J. and LEIS, A., 2007. Tracing of water movement through the unsaturated zone of a coarse gravel aquifer by means of dye and deuterated water. *Environmental Geology,* 51, pp. 1401–1412.

MCLEOD, M., SCHIPPER, L.A. and TAYLOR, M.D., 1998. Preferential flow in a well drained and a poorly drained soil under different overhead irrigation regimes. *Soil Use and Management,* 14(2), pp. 96–100.

MEAKIN, P., 1991. Fractal aggregates in geophysics. *Reviews of Geophysics,* 29(3), pp. 317–354.

MOHANTY, B.P. et al., 1997. New piecewise-continuous hydraulic functions for modeling preferential flow in an intermittent-flood-irrigated field. *Water Resources Research,* 33(9), pp. 2049–2063.

MOLSON, J.W. et al., 2005. Numerical simulations of pyrite oxidation and acid mine drainage in unsaturated waste rock piles. *Journal of contaminant hydrology,* 78(4), pp. 343–371.

MORBIDELLI, R. et al., 2017. In-Situ Measurements of Soil Saturated Hydraulic Conductivity: Assessment of Reliability Through Rainfall-Runoff Experiments: In-Situ Measurements of Soil Saturated Hydraulic Conductivity. *Hydrological Processes,* 31

MORENO-MAROTO, J.M., ALONSO-AZCÁRATE, J. and O'KELLY, B.C., 2021a. Review and critical examination of fine-grained soil classification systems based on plasticity. *Applied Clay Science,* 200, pp. 105955.

MORENO-MAROTO, J.M., ALONSO-AZCÁRATE, J. and O'KELLY, B.C., 2021b. Review and critical examination of fine-grained soil classification systems based on plasticity. *Applied Clay Science,* 200, pp. 105955.

MORET-FERNÁNDEZ, D. et al., 2015. A modified hood infiltrometer to estimate the soil hydraulic properties from the transient water flow measurements. *Journal of Hydrology,* 530, pp. 554–560.

MUALEM, Y., 1976. A new model for predicting the hydraulic conductivity of unsaturated porous media. *Water Resources Research,* 12(3), pp. 513–522.

NIEBER, J.L., 1996. Modeling finger development and persistence in initially dry porous media. *Geoderma,* 70(2), pp. 207–229.

OBI, J.C. et al., 2014. Development of pedotransfer functions for coastal plain soils using terrain attributes. *Catena,* 123, pp. 252–262.

OR, D. and TULLER, M., 1999. Liquid retention and interfacial area in variably saturated porous media: Upscaling from single-pore to sample-scale model. *Water Resources Research,* 35(12), pp. 3591–3605.

OTHMER, H., DIEKKRUGER, B. and KUTILEK, M., 1991. BIMODAL POROSITY AND UNSATURATED HYDRAULIC CONDUCTIVITY. *Soil Science,* 152(3),

PARLANGE, J.-. and HILL, D.E., 1976. THEORETICAL ANALYSIS OF WETTING FRONT INSTABILITY IN SOILS. *Soil Science,* 122(4),

PASSIOURA, J.B., 1980. The Meaning of Matric Potential. *Journal of experimental botany,* 31(123), pp. 1161–1169.

PHILIP, J.R., 1975. Stability Analysis of Infiltration. *Soil Science Society of America Journal,* 39(6), pp. 1042–1049.

POWELSON, D. and MILLS, A., 2001. Transport of Escherichia coli in sand columns with constant and changing water contents. *Journal of environmental quality,* 30, pp. 238–45.

PRAKASH, K. and SRIDHARAN, A., 2012. Classification of Non-Plastic Soils. *Indian Geotechnical Journal,* 42(2), pp. 118–123.

PÜTZ, T., FANK, J. and FLURY, M., 2018. Lysimeters in Vadose Zone Research. *Vadose Zone Journal,* 17(1), pp. 180035.

R.L., C., VAN MEURS, P. and VAN DER POEL, C., 1959. The Instability of Slow, Immiscible, Viscous Liquid-Liquid Displacements in Permeable Media. *Transactions of the AIME,* 216(01), pp. 188–194.

RADINJA, M. et al., 2019. Determination of Spatial and Temporal Variability of Soil Hydraulic Conductivity for Urban Runoff Modelling. *Water,* 11(5),

RICHARDS, B.K. et al., 1998. Metal mobility at an old, heavily loaded sludge application site. *Environmental Pollution,* 99(3), pp. 365–377.

RICHARDS, L.A., *Capillary Conduction of Liquids Through Porous Mediums.*

RICHARDSON, J.F. et al., 2002. *Coulson and richardson's chemical engineering. vol. 2, particle technology and separation processes.* 5th ed. ed. Oxford: Butterworth-Heinemann Oxford.

RITTER, A. et al., 2004. Analysis of alternative measurement strategies for the inverse optimization of the hydraulic properties of a volcanic soil. *Journal of Hydrology,* 295(1), pp. 124–139.

ROSS, P.J. and SMETTEM, K.R.J., 2000a. A Simple Treatment of Physical Nonequilibrium Water Flow in Soils. *Soil Science Society of America Journal,* 64(6), pp. 1926–1930.

ROSS, P.J. and SMETTEM, K.R.J., 2000b. A Simple Treatment of Physical Nonequilibrium Water Flow in Soils. *Soil Science Society of America Journal,* 64(6), pp. 1926–1930.

ROULIER, S. et al., 2006. Controls on atrazine leaching through a soil-unsaturated fractured limestone sequence at Brévilles, France. *Journal of contaminant hydrology,* 84, pp. 81–105.

RUDIYANTO et al., 2021. Pedotransfer functions for estimating soil hydraulic properties from saturation to dryness. *Geoderma,* 403, pp. 115194.

SAFFMAN, P.G. and TAYLOR, G., 1958. The Penetration of a Fluid into a Porous Medium or Hele-Shaw Cell Containing a More Viscous Liquid. *Proceedings of the Royal Society of London Series A,* 245, pp. 312–329.

SCHEIDEGGER, A.E., 1974. *The physics of flow through porous media (3rd edition).* University of Toronto Press.

SCHUHMANN, R., et al., 2011. Determination of Hydraulic Conductivity Based on (Soil) - Moisture Content of Fine Grained Soils. In: Anonymous

SELIM, T. et al., 2013. Soil Water and Salinity Distribution under Different Treatments of Drip Irrigation. *Soil Science Society of America Journal,* 77(4), pp. 1144–1156.

SENTENAC, P., LYNCH, R.J. and BOLTON, M., 2001. Measurement of a side-wall boundary effect in soil columns using fibre-optics sensing. *International Journal of Physical Modelling in Geotechnics,* 1, pp. 35–41.

SHACKELFORD, C.D., 2013. Geoenvironmental Engineering☆. In: Anonymous *Reference Module in Earth Systems and Environmental Sciences.* Elsevier.

SHIPITALO, M. and BUTT, K., 1999. Occupancy and geometrical properties of Lumbricus terrestris L. burrows affecting infiltration. *Pedobiologia,* 43, pp. 782–794.

SIMON, R. et al., 2000. Effect of Redox Zonation on the Reductive Transformation of p-Cyanonitrobenzene in a Laboratory Sediment Column. *Environmental science & technology,* 34(17), pp. 3617–3622.

ŠIMŮNEK, J. et al., 2003a. Review and comparison of models for describing non-equilibrium and preferential flow and transport in the vadose zone. *Journal of Hydrology,* 272(1), pp. 14–35.

ŠIMŮNEK, J. et al., 2003b. Review and comparison of models for describing non-equilibrium and preferential flow and transport in the vadose zone. *Journal of Hydrology,* 272(1), pp. 14–35.

STEENHUIS, T.S., PARLANCE, J.-. and ANDREINI, M.S., 1990. A numerical model for preferential solute movement in structured soils. *Geoderma,* 46(1), pp. 193–208.

TAYLOR, S.A. and ASHCROFT, G.L., 1972. *Physical edaphology: The physics of irrigated and nonirrigated soils.* W.H. Freeman.

TIAB, D. and DONALDSON, E.C., 2016. Chapter 3 - Porosity and Permeability. In: D. TIAB and Erle C. Donaldson eds. *Petrophysics (Fourth Edition).* Boston: Gulf Professional Publishing. pp. 67–186.

TIAN, Z. et al., 2021. New pedotransfer functions for soil water retention curves that better account for bulk density effects. *Soil and Tillage Research,* 205, pp. 104812.

TOMASELLA, J., HODNETT, M.G. and ROSSATO, L., 2000. Pedotransfer Functions for the Estimation of Soil Water Retention in Brazilian Soils. *Soil Science Society of America Journal,* 64(1), pp. 327–338.

TULLER, M., OR, D. and DUDLEY, L.M., 1999. Adsorption and capillary condensation in porous media: Liquid retention and interfacial configurations in angular pores. *Water Resources Research,* 35(7), pp. 1949–1964.

UNESCO WORLD WATER ASSESSMENT PROGRAMME, 2022. *UN World Water Development Report 2022.* United Nations.

UNESCO WORLD WATER ASSESSMENT PROGRAMME, 2023. *The united nations world water development report 2023: Partnerships and cooperation for water.* Paris : UNESCO.

VAN GENUCHTEN, M.T., 1980. A Closed-form Equation for Predicting the Hydraulic Conductivity of Unsaturated Soils. *Soil Science Society of America Journal,* 44(5), pp. 892–898.

VAN GENUCHTEN, M.T. and DALTON, F.N., 1986. Models for simulating salt movement in aggregated field soils. *Geoderma,* 38(1), pp. 165–183.

VAN GENUCHTEN, M.T. and WIERENGA, P.J., 1976. Mass Transfer Studies in Sorbing Porous Media I. Analytical Solutions. *Soil Science Society of America Journal,* 40(4), pp. 473–480.

VANAPALLI, S.K. et al., 1996. Model for the prediction of shear strength with respect to soil suction. *Canadian Geotechnical Journal,* 33(3), pp. 379–392.

VEREECKEN, H. et al., 1989. Estimating the soil moisture retention characteristic from texture, bulk density, and carbon content. *Soil Science,* 148(6), pp. 389–403.

VILLARREAL, R. et al., 2019. Diffusivity and sorptivity determination at different soil water contents from horizontal infiltration. *Geoderma,* 338, pp. 88–96.

VOEGELIN, A., BARMETTLER, K. and KRETZSCHMAR, R., 2003. Heavy metal release from contaminated soils: Comparison of column leaching and batch extraction results. *Journal of environmental quality,* 32, pp. 865–75.

VOGEL, H.Ö et al., 2023. Soil hydraulic conductivity in the state of nonequilibrium. *Vadose Zone Journal,* 22(2), pp. e20238.

VOGEL, T. et al., 2000. Modeling flow and transport in a two-dimensional dual-permeability system with spatially variable hydraulic properties. *Journal of Hydrology,* 238(1), pp. 78–89.

WANG, X. et al., 2020. Effects of schedules of subsurface drip irrigation with air injection on water consumption, yield components and water use efficiency of tomato in a greenhouse in the North China Plain. *Scientia Horticulturae,* 269, pp. 109396.

WANG, Z., FEYEN, J. and ELRICK, D.E., 1998. Prediction of fingering in porous media. *Water Resources Research,* 34(9), pp. 2183–2190.

WHALLEY, W.R., OBER, E.S. and JENKINS, M., 2013. Measurement of the matric potential of soil water in the rhizosphere. *Journal of experimental botany,* 64(13), pp. 3951–3963.

WHITE, I., COLOMBERA, P.M. and PHILIP, J.R., 1976. Experimental Study of Wetting Front Instability Induced by Sudden Change of Pressure Gradient. *Soil Science Society of America Journal,* 40(6), pp. 824–829.

WILLIAMS, A. et al., 2000. Investigating preferential flow in a large intact soil block under pasture. *Soil Use and Management,* 16(4), pp. 264–269.

WILSON, G.V. et al., 1998. Tillage and Cover Crop Effects on Saturated and Unsaturated Transport of Fluometuron. *Soil Science Society of America Journal,* 62(1), pp. 46–55.

WOESSNER, W. and POETER, E., 2020. *Hydrogeologic properties of earth materials and principles of groundwater flow.*

YANG, C. et al., 2023. Evaluation of Soil-Water Characteristic Curves for Different Textural Soils Using Fractal Analysis. *Water,* 15(4),

ZEHE, E. and FLÜHLER, H., 2001. Preferential transport of Isoproturon at a plot scale and a field scale tile-drained site. *Journal of Hydrology,* 247, pp. 100–115.

ZHANG, C. and LU, N., 2019. Unitary Definition of Matric Suction. *Journal of Geotechnical and Geoenvironmental Engineering,* 145, pp. 02818004.

Appendix 1. Simulated data for soil water characteristic curve (Van Genuchten 1980)

Minutes	θ (%)	Ψ (-kPa)	Minutes	θ (%)	Ψ (-kPa)	Minutes	θ (%)	Ψ (-kPa)	Minutes	θ (%)	Ψ (-kPa)
1	9.72355	98341.2	**44**	12.0822	-59102.7	**87**	29.08158	-43052.3	**130**	50.05342	-7367.28
2	9.933255	97010.36	**45**	12.496	-59100.4	**88**	29.70368	-42384.1	**131**	50.05482	-6702.44
3	9.934657	96345.52	**46**	12.2912	-58104.2	**89**	30.11748	-42381.8	**132**	50.26383	-5704.02
4	9.72846	96014.24	**47**	12.7071	-57104.7	**90**	31.36027	-41710	**133**	50.05693	-5705.17
5	9.733369	93687.28	**48**	12.91541	-56438.7	**91**	32.39617	-41039.5	**134**	49.85143	-5041.47
6	9.735473	92690.01	**49**	13.12301	-56105.1	**92**	33.63897	-40367.7	**135**	50.06043	-4043.05
7	9.737577	91692.74	**50**	13.53891	-55105.6	**93**	34.67486	-39697.2	**136**	50.06184	-3378.21
8	9.73898	91027.89	**51**	13.95341	-54770.8	**94**	35.50246	-39692.6	**137**	49.85704	-2382.08
9	9.741084	90030.62	**52**	13.95411	-54438.4	**95**	36.74596	-38688.4	**138**	49.85915	-1384.81
10	9.743188	89033.35	**53**	14.57621	-53770.1	**96**	37.98665	-39014	**139**	49.85985	-1052.39
11	9.745292	88036.08	**54**	14.99071	-53435.4	**97**	38.19495	-38348	**140**	49.86125	-387.543
12	9.747396	87038.81	**55**	14.57901	-52440.4	**98**	39.02395	-37678.5	**141**	49.86265	277.3034
13	10.1619	86704.1	**56**	15.20111	-51772.1	**99**	40.05985	-37008		50.05342	-7367.28
14	9.751604	85044.27	**57**	15.61631	-51105	**100**	40.47435	-36673.3			
15	10.16821	83712.29	**58**	16.03011	-51102.7	**101**	41.30265	-36336.2			
16	9.96201	83381.01	**59**	16.44531	-50435.6	**102**	41.92404	-36000.4			
17	9.963413	82716.16	**60**	16.65221	-50434.4	**103**	42.75304	-35331			
18	9.758618	81720.04	**61**	17.27361	-50098.6	**104**	43.58134	-34993.9			
19	10.17452	80720.48	**62**	17.68811	-49763.9	**105**	44.20344	-34325.7			
20	9.762826	79725.5	**63**	18.10331	-49096.7	**106**	44.61864	-33658.5			
21	10.17803	79058.36	**64**	18.31161	-48430.7	**107**	45.24004	-33322.7			
22	9.766333	78063.39	**65**	18.72541	-48428.4	**108**	45.65594	-32323.1			
23	10.18294	76731.4	**66**	18.93301	-48094.9	**109**	46.69184	-31652.5			
24	10.18434	76066.55	**67**	19.34681	-48092.6	**110**	47.31394	-30984.2			
25	10.18644	75069.28	**68**	19.96821	-47756.7	**111**	47.93744	-29651.1			
26	10.18785	74404.44	**69**	20.7958	-47752.1	**112**	48.35264	-28984			
27	10.18995	73407.17	**70**	21.0041	-47086.1	**113**	48.14714	-28320.3			
28	10.19135	72742.32	**71**	21.2124	-46420.1	**114**	48.77135	-26654.7			
29	10.60866	71077.91	**72**	21.42	-46086.6	**115**	49.18935	-24657.9			
30	10.81836	69747.07	**73**	22.4538	-46413.3	**116**	49.60666	-22993.5			

31	10.61357	68750.95	**74**	22.6614	-46079.7	**117**	49.60876	-21996.2
32	10.61427	68418.53	**75**	23.0759	-45745	**118**	49.61367	-19669.2
33	11.03017	67418.96	**76**	23.2828	-45743.8	**119**	49.61297	-20001.7
34	11.44677	66086.98	**77**	23.9049	-45075.5	**120**	50.02887	-19002.1
35	10.82678	65758	**78**	24.1118	-45074.4	**121**	49.82618	-17008.7
36	11.03578	64759.58	**79**	24.7339	-44406.1	**122**	50.03589	-15677.9
37	11.03648	64427.16	**80**	25.14769	-44403.8	**123**	49.62349	-15015.3
38	11.03859	63429.89	**81**	25.56149	-44401.5	**124**	50.24699	-13682.2
39	11.03999	62765.04	**82**	25.76839	-44400.4	**125**	50.0422	-12686.1
40	11.45449	62430.32	**83**	26.39049	-43732.1	**126**	50.0443	-11688.8
41	11.66279	61764.33	**84**	26.80429	-43729.8	**127**	50.04711	-10359.1
42	11.87109	61098.34	**85**	27.42639	-43061.5	**128**	49.63611	-9031.69
43	11.87249	60433.49	**86**	28.46228	-42390.9	**129**	50.05202	-8032.13

Appendix 2. Logged Data Generated from the soil column infiltration experiment for the Aberdeen packed soil sample

Label Units	Power V	Psi kPa	Theta %	SoilTemp deg C	ECp mS.m-1	Theta(2) %	SoilTemp(2) deg C	ECp(2) mS.m-1	Theta(3) %	SoilTemp(3) deg C	ECp(3) mS.m-1	Psi(2) kPa
05/07/2023 13:19	9.3	-436.5	2.3	19.8	#-INF	6.1	19.5	371	4.7	19.6	#-INF	-28.1
05/07/2023 13:20	9.3	-436.6	2.3	19.8	#-INF	6.2	19.5	374	4.7	19.6	#-INF	-28.1
05/07/2023 13:21	9.3	-439.9	2.3	19.8	#-INF	6.1	19.5	412	4.6	19.6	#-INF	-28.1
05/07/2023 13:22	9.3	-435.3	2.5	19.8	#-INF	6	19.5	492	4.3	19.6	#-INF	-28.1
05/07/2023 13:23	9.3	-423.1	2.2	19.8	0	6.1	19.5	552	4.9	19.6	#-INF	-28
05/07/2023 13:24	9.4	-438.6	2.3	19.8	#-INF	6.1	19.5	370	4.6	19.6	#-INF	-28.1
05/07/2023 13:25	9.4	-441.1	2.4	19.8	#-INF	6.1	19.5	407	4.6	19.6	#-INF	-28.2
05/07/2023 13:26	9.4	-441.3	2.4	19.8	#-INF	6.3	19.5	342	4.6	19.6	#-INF	-28.2
05/07/2023 13:27	9.4	-442.5	2.4	19.8	#-INF	6.2	19.5	379	4.6	19.6	#-INF	-28.2
05/07/2023 13:28	9.4	-443.4	2.3	19.8	#-INF	6.2	19.5	421	4.6	19.6	#-INF	-28.2
05/07/2023 13:29	9.4	-445.2	2.4	19.8	#-INF	6.2	19.5	370	4.6	19.6	#-INF	-28.2
05/07/2023 13:30	9.4	-443.4	2.3	19.8	#-INF	6.1	19.5	391	4.6	19.6	#-INF	-28.2
05/07/2023 13:31	9.4	-446.2	2.3	19.8	#-INF	6.1	19.5	402	4.6	19.6	#-INF	-28.3
05/07/2023 13:32	9.4	-445.9	2.3	19.8	#-INF	6.1	19.5	383	4.6	19.6	#-INF	-28.3
05/07/2023 13:33	9.4	-446.2	2.4	19.8	#-INF	6.1	19.5	401	4.6	19.6	#-INF	-28.3
05/07/2023 13:34	9.4	-447.2	2.4	19.8	#-INF	6.2	19.5	369	4.6	19.6	#-INF	-28.3
05/07/2023 13:35	9.4	-448	2.5	19.8	#-INF	6.2	19.5	388	4.6	19.5	#-INF	-28.3
05/07/2023 13:36	9.4	-449.3	2.4	19.8	#-INF	6.1	19.5	369	4.6	19.6	#-INF	-28.3
05/07/2023 13:37	9.4	-449.7	2.4	19.8	#-INF	6.1	19.5	390	4.6	19.6	#-INF	-28.3
05/07/2023 13:38	9.4	-450.1	2.4	19.8	#-INF	6.1	19.5	379	4.6	19.6	#-INF	-28.3
05/07/2023 13:39	9.4	-450.9	2.4	19.8	#-INF	6.1	19.5	394	4.6	19.6	#-INF	-28.4
05/07/2023 13:40	9.4	-452.8	2.4	19.8	#-INF	6.1	19.4	411	4.5	19.6	#-INF	-28.4
05/07/2023 13:41	9.4	-452.1	2.4	19.8	#-INF	6.1	19.4	399	4.6	19.6	#-INF	-28.4
05/07/2023 13:42	9.4	-451.9	2.4	19.8	#-INF	6.1	19.4	445	4.5	19.6	#-INF	-28.4
05/07/2023 13:43	9.4	-452.3	2.7	19.8	#-INF	6.1	19.4	425	4.7	19.6	#-INF	-28.4
05/07/2023 13:44	9.4	-453.4	2.6	19.8	#-INF	6.1	19.4	406	4.7	19.5	#-INF	-28.4
05/07/2023 13:45	9.4	-453.6	2.8	19.8	#-INF	6.1	19.4	403	4.6	19.6	#-INF	-28.4
05/07/2023 13:46	9.4	-453.8	2.8	19.8	#-INF	6.2	19.4	397	4.7	19.6	#-INF	-28.4
05/07/2023 13:47	9.4	-455.4	3.1	19.8	#-INF	6.1	19.4	362	4.7	19.6	#-INF	-28.4

05/07/2023 13:48	9.4	-456.9	3.7	19.8	#-INF	6.2	19.4	366	4.6	19.5	#-INF	-28.5
05/07/2023 13:49	9.4	-457.1	4.4	19.8	#-INF	6.2	19.4	359	4.6	19.5	#-INF	-28.5
05/07/2023 13:50	9.4	-458.2	5.3	19.8	2284	6.2	19.4	353	4.7	19.5	#-INF	-28.5
05/07/2023 13:51	9.4	-458	6	19.8	477	6.2	19.4	374	4.7	19.6	#-INF	-28.5
05/07/2023 13:52	9.4	-458.9	6.9	19.8	251	6.3	19.4	320	4.6	19.5	#-INF	-28.5
05/07/2023 13:53	9.4	-459.6	7.6	19.8	182	6.1	19.4	380	4.6	19.6	#-INF	-28.5
05/07/2023 13:54	9.4	-459.9	8.4	19.8	147	6.2	19.4	368	4.6	19.6	#-INF	-28.5
05/07/2023 13:55	9.4	-461.8	9.2	19.8	123	6.2	19.4	352	4.7	19.6	#-INF	-28.5
05/07/2023 13:56	9.4	-461.3	9.9	19.8	98	6.2	19.4	388	4.7	19.6	#-INF	-28.5
05/07/2023 13:57	9.4	-461.7	10.6	19.8	84	6.2	19.4	362	4.7	19.6	#-INF	-28.5
05/07/2023 13:58	9.4	-462.6	11.3	19.8	66	6.1	19.4	382	4.7	19.6	#-INF	-28.6
05/07/2023 13:59	9.4	-463	12	19.8	59	6.1	19.4	391	4.7	19.5	#-INF	-28.6
05/07/2023 14:00	9.4	-463.1	12.6	19.8	51	6.2	19.4	361	4.6	19.6	#-INF	-28.6
05/07/2023 14:01	9.4	-463	13.3	19.8	44	6.1	19.4	418	4.7	19.6	#-INF	-28.6
05/07/2023 14:02	9.4	-464.2	13.8	19.8	33	6.1	19.4	396	4.6	19.6	#-INF	-28.6
05/07/2023 14:03	9.4	-465.2	14.3	19.8	33	6.2	19.4	366	4.7	19.6	#-INF	-28.6
05/07/2023 14:04	9.4	-466.2	14.8	19.8	29	6.2	19.4	372	4.6	19.5	#-INF	-28.6
05/07/2023 14:05	9.4	-466.6	15.3	19.8	27	6.2	19.4	386	4.8	19.6	#-INF	-28.6
05/07/2023 14:06	9.4	-467.7	15.8	19.8	26	6.2	19.4	353	4.7	19.6	#-INF	-28.6
05/07/2023 14:07	9.4	-468.4	16.4	19.8	26	6.2	19.4	374	4.8	19.6	#-INF	-28.6
05/07/2023 14:08	9.4	-469.1	16.8	19.8	29	6.2	19.4	353	4.9	19.6	#-INF	-28.6
05/07/2023 14:09	9.4	-469.9	17.1	19.8	29	6.2	19.4	354	4.8	19.6	#-INF	-28.6
05/07/2023 14:10	9.4	-470.3	17.5	19.8	30	6.2	19.4	392	4.8	19.6	#-INF	-28.7
05/07/2023 14:11	9.4	-471.7	17.8	19.8	29	6.1	19.4	380	4.8	19.6	#-INF	-28.7
05/07/2023 14:12	9.4	-472.1	18.1	19.8	28	6.2	19.4	375	4.8	19.6	#-INF	-28.7
05/07/2023 14:13	9.4	-472.2	18.4	19.8	31	6.1	19.4	365	4.8	19.6	#-INF	-28.7
05/07/2023 14:14	9.4	-472.7	18.6	19.8	30	6.2	19.4	368	4.8	19.6	#-INF	-28.7
05/07/2023 14:15	9.4	-474.3	18.9	19.8	31	6.2	19.4	371	4.8	19.6	#-INF	-28.7
05/07/2023 14:16	9.4	-475.1	19.1	19.8	32	6.2	19.4	400	4.8	19.6	#-INF	-28.7
05/07/2023 14:17	9.4	-475.9	19.3	19.8	31	6.1	19.4	396	4.8	19.6	#-INF	-28.7
05/07/2023 14:18	9.4	-476.2	19.5	19.8	31	6.2	19.4	375	4.8	19.6	#-INF	-28.7

05/07/2023 14:19	9.4	-479	19.7	19.7	30	6.1	19.4	380	4.7	19.5	#-INF	-28.7
05/07/2023 14:20	9.4	-477.5	19.9	19.8	31	6.1	19.4	378	4.7	19.5	#-INF	-28.7
05/07/2023 14:21	9.4	-477.6	20.1	19.8	31	6.2	19.4	374	4.7	19.6	#-INF	-28.7
05/07/2023 14:22	9.4	-478.2	20.3	19.8	30	6.2	19.4	403	4.7	19.6	#-INF	-28.7
05/07/2023 14:23	9.4	-479.2	20.4	19.8	31	6.2	19.4	373	4.6	19.6	#-INF	-28.8
05/07/2023 14:24	9.4	-477.9	20.6	19.7	30	6.1	19.4	404	4.7	19.6	#-INF	-28.8
05/07/2023 14:25	9.4	-478.9	20.8	19.8	31	6.1	19.4	409	4.6	19.6	#-INF	-28.8
05/07/2023 14:26	9.4	-480.8	20.9	19.7	30	6.2	19.4	345	4.7	19.6	#-INF	-28.8
05/07/2023 14:27	9.4	-480.9	21	19.7	29	6.1	19.4	362	4.7	19.6	#-INF	-28.8
05/07/2023 14:28	9.4	-482.1	21.2	19.7	30	6.2	19.4	377	4.6	19.6	#-INF	-28.8
05/07/2023 14:29	9.4	-483.9	21.4	19.7	30	6.2	19.4	373	4.8	19.6	#-INF	-28.8
05/07/2023 14:30	9.4	-482.6	21.4	19.7	29	6.2	19.4	374	4.7	19.6	#-INF	-28.8
05/07/2023 14:31	9.4	-484.6	21.5	19.7	30	6.2	19.4	373	4.7	19.6	#-INF	-28.8
05/07/2023 14:32	9.4	-484.7	21.6	19.7	29	6.2	19.4	382	4.8	19.6	#-INF	-28.8
05/07/2023 14:33	9.4	-484.5	21.7	19.7	29	6.2	19.4	377	4.8	19.6	#-INF	-28.8
05/07/2023 14:34	9.4	-485.1	21.8	19.7	29	6.2	19.4	333	4.7	19.6	#-INF	-28.8
05/07/2023 14:35	9.4	-486.5	21.9	19.7	29	6.2	19.4	401	4.8	19.6	#-INF	-28.8
05/07/2023 14:36	9.4	-484.7	22	19.7	30	6.2	19.4	394	4.7	19.6	#-INF	-28.8
05/07/2023 14:37	9.4	-484.9	22.2	19.7	30	6.1	19.4	410	4.8	19.6	#-INF	-28.9
05/07/2023 14:38	9.4	-484.7	22.4	19.7	31	6.2	19.4	386	4.9	19.6	#-INF	-28.9
05/07/2023 14:39	9.4	-485.7	22.5	19.7	31	6.1	19.4	442	4.9	19.6	#-INF	-28.9
05/07/2023 14:40	9.4	-485.9	22.5	19.7	31	6.2	19.4	361	4.9	19.6	#-INF	-28.9
05/07/2023 14:41	9.4	-486.3	22.6	19.7	31	6.2	19.4	375	4.9	19.6	#-INF	-28.9
05/07/2023 14:42	9.4	-486.8	22.6	19.7	32	6.2	19.4	413	4.9	19.6	#-INF	-28.9
05/07/2023 14:43	9.4	-488.4	22.7	19.7	31	6.2	19.4	346	4.9	19.6	#-INF	-28.9
05/07/2023 14:44	9.4	-489.5	22.8	19.7	31	6.2	19.4	376	5	19.6	#-INF	-28.9
05/07/2023 14:45	9.4	-489.5	22.9	19.7	31	6.2	19.4	400	5	19.6	#-INF	-28.9
05/07/2023 14:46	9.4	-489.3	22.9	19.7	31	6.1	19.4	408	5.1	19.6	#+INF	-28.9
05/07/2023 14:47	9.4	-490	23	19.7	31	6.2	19.4	346	5.4	19.6	1240	-28.9
05/07/2023 14:48	9.4	-490.3	23	19.7	30	6.2	19.4	331	5.6	19.6	661	-28.9
05/07/2023 14:49	9.4	-490.3	23.1	19.7	31	6.3	19.4	362	5.9	19.6	404	-28.9

05/07/2023 14:50	9.4	-490.9	23.2	19.7	31	6.2	19.4	387	6.5	19.6	143	-29
05/07/2023 14:51	9.4	-490.9	23.2	19.7	31	6.2	19.4	394	7	19.6	80	-29
05/07/2023 14:52	9.4	-491.7	23.3	19.7	31	6.2	19.4	380	7.4	19.6	43	-29
05/07/2023 14:53	9.4	-491.4	23.3	19.7	31	6.2	19.4	367	7.8	19.6	54	-29
05/07/2023 14:54	9.4	-491.3	23.4	19.7	31	6.2	19.4	349	8.3	19.6	15	-29
05/07/2023 14:55	9.4	-490.6	23.4	19.7	31	6.2	19.4	346	8.7	19.6	27	-29
05/07/2023 14:56	9.4	-491.5	23.5	19.7	32	6.2	19.4	368	9.2	19.6	6	-29
05/07/2023 14:57	9.4	-491.1	23.5	19.7	31	6.2	19.4	405	9.6	19.6	0	-29
05/07/2023 14:58	9.4	-491.4	23.5	19.7	31	6.2	19.4	350	10	19.6	0	-29
05/07/2023 14:59	9.4	-490.2	23.6	19.7	32	6.2	19.4	382	10.4	19.6	0	-29
05/07/2023 15:00	9.4	-488.2	23.6	19.7	32	6.2	19.4	374	10.8	19.6	0	-29
05/07/2023 15:01	9.4	-485.2	23.6	19.7	31	6.2	19.4	385	11.2	19.6	0	-29
05/07/2023 15:02	9.4	-480.5	23.7	19.7	31	6.3	19.4	364	11.6	19.6	0	-29
05/07/2023 15:03	9.4	-476	23.7	19.7	31	6.2	19.4	326	12	19.6	0	-29
05/07/2023 15:04	9.4	-466.4	23.7	19.7	31	6.2	19.4	370	12.4	19.6	0	-29.1
05/07/2023 15:05	9.4	-454.3	23.8	19.7	32	6.2	19.4	350	12.8	19.6	0	-29.1
05/07/2023 15:06	9.4	-434.7	23.8	19.7	31	6.3	19.4	364	13.3	19.6	0	-29.1
05/07/2023 15:07	9.4	-406	23.8	19.7	32	6.3	19.4	341	13.8	19.6	0	-29.1
05/07/2023 15:08	9.4	-395.1	23.8	19.7	32	6.2	19.4	381	14.2	19.6	0	-29.1
05/07/2023 15:09	9.4	-388.5	23.9	19.7	32	6.2	19.4	348	14.6	19.6	0	-29.1
05/07/2023 15:10	9.4	-381	23.9	19.7	32	6.3	19.4	352	15	19.6	0	-29.1
05/07/2023 15:11	9.4	-374	23.9	19.7	32	6.3	19.4	359	15.5	19.6	0	-29.1
05/07/2023 15:12	9.4	-365.3	23.9	19.7	31	6.2	19.4	367	15.9	19.6	0	-29.1
05/07/2023 15:13	9.4	-355.1	23.9	19.7	31	6.2	19.4	369	16.3	19.6	0	-29.1
05/07/2023 15:14	9.4	-342.6	24	19.7	32	6.3	19.4	343	16.7	19.6	0	-29.1
05/07/2023 15:15	9.4	-327.3	24	19.7	32	6.2	19.4	404	17.1	19.6	0	-29.1
05/07/2023 15:16	9.4	-311.3	24	19.7	32	6.2	19.4	393	17.5	19.6	3	-29.1
05/07/2023 15:17	9.4	-296.5	24.1	19.7	32	6.3	19.4	342	17.8	19.6	5	-29.1
05/07/2023 15:18	9.4	-281.3	24.1	19.7	32	6.3	19.4	337	18.2	19.6	6	-29.2
05/07/2023 15:19	9.4	-265.4	24.1	19.7	32	6.3	19.4	360	18.5	19.6	8	-29.2
05/07/2023 15:20	9.4	-249.5	24.1	19.7	32	6.2	19.4	348	18.7	19.6	9	-29.2

05/07/2023 15:21	9.4	-231.5	24.1	19.7	31	6.3	19.4	312	19	19.6	10	-29.2
05/07/2023 15:22	9.4	-211	24.1	19.7	31	6.2	19.4	347	19.2	19.6	10	-29.2
05/07/2023 15:23	9.4	-191.8	24.2	19.7	32	6.2	19.4	351	19.4	19.6	16	-29.2
05/07/2023 15:24	9.4	-175.9	24.2	19.7	31	6.3	19.4	361	19.6	19.6	11	-29.2
05/07/2023 15:25	9.4	-161.6	24.2	19.7	32	6.2	19.4	370	19.7	19.6	10	-29.2
05/07/2023 15:26	9.4	-148.5	24.2	19.7	33	6.3	19.4	317	19.9	19.6	11	-29.2
05/07/2023 15:27	9.4	-139.7	24.2	19.7	31	6.2	19.4	346	20	19.6	9	-29.2
05/07/2023 15:28	9.4	-131.2	24.2	19.7	32	6.3	19.4	357	20.2	19.6	9	-29.2
05/07/2023 15:29	9.4	-122.6	24.3	19.7	33	6.2	19.4	350	20.3	19.6	9	-29.2
05/07/2023 15:30	9.4	-114.1	24.3	19.7	33	6.3	19.4	353	20.4	19.6	9	-29.2
05/07/2023 15:31	9.4	-105.1	24.3	19.7	33	6.3	19.4	356	20.6	19.6	9	-29.2
05/07/2023 15:32	9.4	-98.6	24.3	19.7	33	6.3	19.4	323	20.7	19.6	9	-29.2
05/07/2023 15:33	9.4	-95.4	24.3	19.7	33	6.3	19.4	361	20.8	19.6	9	-29.2
05/07/2023 15:34	9.4	-92.1	24.3	19.7	33	6.3	19.4	339	20.9	19.6	7	-29.3
05/07/2023 15:35	9.4	-88.7	24.3	19.7	33	6.3	19.4	351	21	19.6	7	-29.3
05/07/2023 15:36	9.4	-85.2	24.3	19.7	33	6.3	19.4	356	21.1	19.6	9	-29.3
05/07/2023 15:37	9.4	-81.5	24.3	19.7	33	6.2	19.4	371	21.2	19.6	7	-29.3
05/07/2023 15:38	9.4	-77.7	24.4	19.7	32	6.2	19.4	376	21.3	19.6	8	-29.3
05/07/2023 15:39	9.4	-73.9	24.4	19.7	33	6.3	19.4	382	21.3	19.6	7	-29.3
05/07/2023 15:40	9.4	-70.3	24.4	19.7	33	6.3	19.5	361	21.4	19.6	10	-29.3
05/07/2023 15:41	9.4	-67	24.4	19.7	33	6.3	19.4	343	21.5	19.6	8	-29.3
05/07/2023 15:42	9.4	-63.7	24.4	19.7	33	6.3	19.4	365	21.5	19.6	7	-29.3
05/07/2023 15:43	9.4	-60	24.4	19.7	35	6.2	19.5	377	21.6	19.6	9	-29.3
05/07/2023 15:44	9.4	-55.9	24.4	19.7	35	6.3	19.4	341	21.7	19.6	8	-29.3
05/07/2023 15:45	9.4	-51.6	24.4	19.7	35	6.3	19.4	332	21.7	19.6	7	-29.3
05/07/2023 15:46	9.4	-48.2	24.4	19.7	35	6.3	19.4	341	21.8	19.6	7	-29.3
05/07/2023 15:47	9.4	-45.4	24.4	19.7	35	6.3	19.5	339	21.9	19.6	7	-29.3
05/07/2023 15:48	9.4	-42.5	24.4	19.7	34	6.3	19.4	350	21.9	19.6	6	-29.3
05/07/2023 15:49	9.4	-39.7	24.4	19.7	34	6.3	19.4	351	22	19.6	7	-29.3
05/07/2023 15:50	9.4	-36.8	24.4	19.7	34	6.3	19.5	336	22	19.6	6	-29.3
05/07/2023 15:51	9.4	-34	24.5	19.7	35	6.3	19.4	365	22	19.6	6	-29.4

05/07/2023 15:52	9.4	-31.2	24.4	19.7	33	6.3	19.5	338	22.1	19.6	7	-29.4
05/07/2023 15:53	9.4	-28.6	24.5	19.7	33	6.3	19.5	365	22.2	19.6	6	-29.4
05/07/2023 15:54	9.4	-25.9	24.5	19.7	34	6.3	19.4	335	22.3	19.6	7	-29.4
05/07/2023 15:55	9.4	-23	24.5	19.7	33	6.3	19.5	322	22.3	19.6	4	-29.4
05/07/2023 15:56	9.4	-20.2	24.5	19.7	33	6.2	19.4	398	22.4	19.6	7	-29.4
05/07/2023 15:57	9.4	-17.7	24.5	19.7	33	6.3	19.5	387	22.4	19.6	7	-29.4
05/07/2023 15:58	9.4	-15.7	24.5	19.7	33	6.3	19.5	355	22.5	19.6	7	-29.4
05/07/2023 15:59	9.4	-14.3	24.5	19.7	32	6.3	19.5	363	22.6	19.6	9	-29.4
05/07/2023 16:00	9.4	-13.4	24.5	19.7	32	6.2	19.5	332	22.7	19.6	8	-29.4
05/07/2023 16:01	9.4	-12.8	24.5	19.7	32	6.3	19.5	314	22.8	19.6	10	-29.4
05/07/2023 16:02	9.4	-12.4	24.5	19.7	32	6.3	19.5	335	22.8	19.6	8	-29.4
05/07/2023 16:03	9.4	-12.1	24.6	19.7	32	6.3	19.5	335	22.9	19.6	8	-29.4
05/07/2023 16:04	9.4	-11.8	24.5	19.7	32	6.3	19.5	338	22.9	19.6	7	-29.4
05/07/2023 16:05	9.4	-11.6	24.5	19.7	34	6.3	19.5	340	22.9	19.6	9	-29.4
05/07/2023 16:06	9.4	-11.3	24.5	19.7	33	6.3	19.5	374	23.3	19.6	10	-29.4
05/07/2023 16:07	9.4	-11.1	24.5	19.7	34	6.3	19.5	339	23.3	19.6	10	-29.4
05/07/2023 16:08	9.4	-10.9	24.5	19.7	34	6.3	19.5	359	23.4	19.6	9	-29.4
05/07/2023 16:09	9.4	-10.7	24.6	19.7	35	6.3	19.5	364	23.5	19.6	9	-29.4
05/07/2023 16:10	9.4	-10.5	24.5	19.7	34	6.3	19.5	342	23.5	19.6	8	-29.5
05/07/2023 16:11	9.4	-10.4	24.5	19.7	34	6.3	19.5	370	23.6	19.6	9	-29.5
05/07/2023 16:12	9.4	-10.2	24.5	19.7	35	6.2	19.5	392	23.6	19.6	9	-29.5
05/07/2023 16:13	9.4	-10	24.6	19.7	39	6.3	19.5	395	23.7	19.6	10	-29.5
05/07/2023 16:14	9.4	-9.9	24.6	19.7	35	6.3	19.5	346	23.8	19.6	9	-29.5
05/07/2023 16:15	9.4	-9.7	24.6	19.7	35	6.3	19.5	368	23.8	19.6	9	-29.5
05/07/2023 16:16	9.4	-9.6	24.6	19.7	35	6.3	19.5	379	23.9	19.6	10	-29.5
05/07/2023 16:17	9.4	-9.4	24.6	19.7	36	6.3	19.5	365	23.9	19.6	9	-29.5
05/07/2023 16:18	9.4	-9.2	24.6	19.7	34	6.3	19.5	384	24	19.6	10	-29.5
05/07/2023 16:19	9.4	-9.1	24.6	19.7	34	6.3	19.5	376	24.1	19.6	10	-29.5
05/07/2023 16:20	9.4	-8.9	24.6	19.7	36	6.3	19.5	388	24.1	19.6	10	-29.5
05/07/2023 16:21	9.4	-8.8	24.6	19.7	35	6.3	19.5	398	24.2	19.6	10	-29.5
05/07/2023 16:22	9.4	-8.7	24.6	19.7	35	6.3	19.5	367	24.2	19.6	10	-29.5

05/07/2023 16:23	9.4	-8.6	24.6	19.7	35	6.3	19.5	380	24.3	19.6	10	-29.5
05/07/2023 16:24	9.3	-8.5	24.6	19.7	34	6.3	19.5	383	24.3	19.6	12	-29.5
05/07/2023 16:25	9.4	-8.3	24.6	19.7	35	6.3	19.5	386	24.4	19.6	10	-29.5
05/07/2023 16:26	9.3	-8.2	24.6	19.7	35	6.3	19.5	368	24.4	19.6	12	-29.5
05/07/2023 16:27	9.3	-8.1	24.7	19.7	35	6.3	19.5	372	24.4	19.6	11	-29.5
05/07/2023 16:28	9.3	-8	24.6	19.7	34	6.3	19.5	375	24.7	19.6	14	-29.5
05/07/2023 16:29	9.3	-7.9	24.6	19.7	36	6.4	19.5	325	24.8	19.6	16	-29.5
06/07/2023 10:34	9.3	-8.8	13.9	19.2	38	18.6	18.8	0	17.5	18.9	31	-22.1
06/07/2023 10:35	9.3	-8.8	13.9	19.2	33	18.5	18.8	0	17.5	18.9	24	-22.1
06/07/2023 10:36	9.3	-8.8	14	19.2	35	18.6	18.8	0	17.4	18.9	27	-22.1
06/07/2023 10:37	9.3	-8.8	14	19.2	35	18.5	18.8	0	17.5	19	25	-22.1
06/07/2023 10:38	9.3	-8.8	14.1	19.2	32	18.5	18.8	0	17.5	18.9	25	-22.1
06/07/2023 10:39	9.3	-8.8	14.2	19.2	39	18.6	18.8	0	17.5	19	31	-22.1
06/07/2023 10:40	9.3	-8.8	14.3	19.2	38	18.6	18.8	0	17.5	19	27	-22.1
06/07/2023 10:41	9.3	-8.8	14.5	19.2	35	18.6	18.8	0	17.5	19	27	-22.1
06/07/2023 10:42	9.3	-8.8	14.8	19.2	36	18.5	18.8	0	17.5	19	29	-22.1
06/07/2023 10:43	9.3	-8.8	15.2	19.2	35	18.6	18.8	0	17.5	19	27	-22.1
06/07/2023 10:44	9.3	-8.8	15.7	19.2	33	18.5	18.8	0	17.5	19	27	-22.1
06/07/2023 10:45	9.3	-8.8	16.3	19.2	34	18.6	18.8	0	17.5	19	27	-22.1
06/07/2023 10:46	9.3	-8.8	17	19.2	34	18.6	18.8	0	17.5	19	25	-22.1
06/07/2023 10:47	9.3	-8.8	17.9	19.2	41	18.6	18.8	0	17.5	19	25	-22.1
06/07/2023 10:48	9.3	-8.7	18.9	19.2	45	18.6	18.8	0	17.6	19	29	-22.1
06/07/2023 10:49	9.3	-8.7	19.8	19.2	47	18.5	18.8	0	17.5	19	25	-22.1
06/07/2023 10:50	9.3	-8.7	20.5	19.2	47	18.6	18.8	0	17.6	19	27	-22.1
06/07/2023 10:51	9.3	-8.5	21.2	19.2	45	18.5	18.9	0	17.6	19	27	-22.1
06/07/2023 10:52	9.3	-8.5	22	19.2	46	18.5	18.9	0	17.7	19	27	-22.1
06/07/2023 10:53	9.3	-8.4	22.6	19.2	41	18.5	18.9	0	17.7	19	25	-22
06/07/2023 10:54	9.3	-8.4	23.2	19.2	45	18.6	18.9	0	17.8	19	28	-22.1
06/07/2023 10:55	9.3	-8.3	23.7	19.2	46	18.6	18.9	0	17.9	19	28	-22.1
06/07/2023 10:56	9.3	-8.1	24.1	19.2	50	18.6	18.9	0	18.1	19	31	-22.1
06/07/2023 10:57	9.3	-7.9	24.4	19.2	49	18.6	18.9	0	18.4	19	34	-22.1

06/07/2023 10:58	9.3	-7.7	24.6	19.2	48	18.6	18.9	0	18.7	19	43	-22.1
06/07/2023 10:59	9.3	-7.4	24.7	19.2	48	18.6	18.9	0	19.1	19	46	-22.1
06/07/2023 11:00	9.3	-7	24.8	19.2	49	18.6	18.9	0	19.6	19	49	-22.1
06/07/2023 11:01	9.3	-6.5	24.9	19.2	52	18.6	18.9	0	20.4	19	55	-22.1
06/07/2023 11:02	9.3	-6	25	19.2	50	18.6	18.9	0	21.2	19	53	-22.1
06/07/2023 11:03	9.3	-5.4	25.1	19.2	49	18.6	18.9	0	22	19	54	-22.1
06/07/2023 11:04	9.3	-4.8	25.2	19.2	49	18.6	18.9	0	22.9	19	55	-22.1
06/07/2023 11:05	9.3	-4.3	25.2	19.2	48	18.6	18.9	0	23.7	19	52	-22.1
06/07/2023 11:06	9.3	-3.8	25.2	19.2	44	18.6	18.9	0	24.5	19	51	-22.1
06/07/2023 11:07	9.3	-3.3	25.2	19.2	44	18.7	18.9	0	25.2	19	52	-22.1
06/07/2023 11:08	9.3	-2.7	25.2	19.2	43	18.7	18.9	0	26.2	19	52	-22.1
06/07/2023 11:09	9.3	-2	25.3	19.2	43	18.8	18.9	0	26.7	19	51	-22.1
06/07/2023 11:10	9.3	-1.2	25.3	19.2	42	18.8	18.9	0	27.2	19	51	-22.1
06/07/2023 11:11	9.3	-1	25.3	19.2	43	18.9	18.9	0	27.6	19	51	-22.1
06/07/2023 11:12	9.3	-0.7	25.4	19.2	47	19	18.9	0	27.9	19	50	-22.1
06/07/2023 11:13	9.3	-0.5	25.4	19.2	46	19.1	18.9	0	28.1	19	50	-22.1
06/07/2023 11:14	9.3	-0.3	25.4	19.2	47	19.3	18.9	0	28.4	19	48	-22.1
06/07/2023 11:15	9.3	-0.2	25.4	19.2	47	19.6	18.9	3	28.7	19	49	-22
06/07/2023 11:16	9.3	-0.1	25.4	19.2	46	20.2	18.9	8	28.8	19	49	-22
06/07/2023 11:17	9.3	-0.1	25.5	19.2	46	20.9	18.9	9	29	19	48	-22
06/07/2023 11:18	9.3	0	25.5	19.2	46	21.8	18.9	5	29.1	19	47	-22
06/07/2023 11:19	9.3	0	25.5	19.2	46	23.2	18.9	3	29.2	19	48	-22
06/07/2023 11:20	9.3	0	25.5	19.2	45	24.6	18.9	6	29.3	19	47	-21.9
06/07/2023 11:21	9.3	0.1	25.5	19.2	46	25.7	18.9	6	29.4	19	47	-21.9
06/07/2023 11:22	9.3	0.1	25.6	19.2	45	26.7	18.9	11	29.4	19	47	-21.8
06/07/2023 11:23	9.3	0.1	25.6	19.2	49	27.5	18.9	15	29.5	19	48	-21.7
06/07/2023 11:24	9.3	0.1	25.6	19.2	50	28.2	18.9	16	29.6	19	48	-21.6
06/07/2023 11:25	9.3	0.1	25.6	19.2	50	28.8	18.9	18	29.6	19	47	-21.5
06/07/2023 11:26	9.3	0.1	25.6	19.2	50	29.4	18.9	20	29.7	19	48	-21.3
06/07/2023 11:27	9.3	0.1	25.6	19.2	49	29.8	18.9	20	29.7	19	47	-21.1
06/07/2023 11:28	9.3	0.1	25.7	19.2	49	30.1	19	20	29.7	19	47	-20.8

06/07/2023 11:29	9.3	0.1	25.7	19.2	48	30.4	19	21	29.8	19	45	-20.5
06/07/2023 11:30	9.3	0.1	25.7	19.3	48	30.7	19	22	29.8	19	45	-20.1
06/07/2023 11:31	9.3	0.1	25.7	19.3	48	31	19	23	29.9	19	46	-19.8
06/07/2023 11:32	9.3	0.1	25.7	19.3	48	31.1	19	23	29.9	19	46	-19.3
06/07/2023 11:33	9.3	0.1	25.7	19.3	48	31.3	19	23	29.9	19	45	-18.8
06/07/2023 11:34	9.3	0.1	25.7	19.3	47	31.5	19	23	29.9	19	46	-18.3
06/07/2023 11:35	9.3	0.1	25.7	19.3	48	31.6	19	23	29.9	19	44	-17.8
06/07/2023 11:36	9.3	0.1	25.7	19.3	48	31.7	19	24	29.9	19	45	-17.4
06/07/2023 11:37	9.3	0.1	25.7	19.3	45	31.8	19	24	29.9	19.1	44	-17
06/07/2023 11:38	9.3	0.1	25.7	19.3	45	31.9	19	24	29.9	19.1	44	-16.7
06/07/2023 11:39	9.3	0.1	25.7	19.3	46	32	19	25	29.9	19.1	44	-16.4
06/07/2023 11:40	9.3	0.1	25.8	19.3	48	32.1	19	25	29.9	19.1	44	-16.2
06/07/2023 11:41	9.3	0.1	25.7	19.3	44	32.2	19	25	29.9	19.1	44	-15.9
06/07/2023 11:42	9.3	0.1	25.6	19.3	43	32.2	19	26	29.9	19.1	44	-15.7
06/07/2023 11:43	9.3	0.1	25.8	19.3	51	32.3	19	26	30	19.1	47	-15.5
06/07/2023 11:44	9.3	0.1	25.8	19.3	52	32.4	19	26	30	19.1	47	-15.4
06/07/2023 11:45	9.3	0.1	25.8	19.3	52	32.4	19	27	30	19.1	47	-15.2
06/07/2023 11:46	9.3	0.1	25.8	19.3	51	32.4	19	27	30	19.1	47	-15.1
06/07/2023 11:47	9.3	0.1	25.8	19.3	49	32.5	19	27	30	19.1	46	-15
06/07/2023 11:48	9.3	0.1	25.8	19.3	52	32.5	19.1	27	30	19.1	48	-14.8
06/07/2023 11:49	9.3	0.1	25.7	19.3	43	32.6	19.1	26	30	19.1	45	-14.7
06/07/2023 11:50	9.3	0.1	25.7	19.3	45	32.7	19.1	26	29.9	19.1	44	-14.6
06/07/2023 11:51	9.3	0.1	25.7	19.3	44	32.7	19.1	26	29.9	19.1	44	-14.5
06/07/2023 11:52	9.3	0.1	25.7	19.3	44	32.8	19.1	26	29.9	19.1	45	-14.4
06/07/2023 11:53	9.3	0.1	25.5	19.3	43	32.9	19.1	26	29.9	19.1	46	-14.2
06/07/2023 11:54	9.3	0.1	25.5	19.3	42	33	19.1	26	29.9	19.1	47	-14.1
06/07/2023 11:55	9.3	0.1	25.5	19.3	43	33.1	19.1	26	29.8	19.1	45	-14
06/07/2023 11:56	9.3	0.1	25.4	19.3	43	33.3	19.1	27	29.9	19.1	46	-13.8
06/07/2023 11:57	9.3	0.1	25.4	19.3	42	33.6	19.1	26	29.8	19.1	46	-13.6
06/07/2023 11:58	9.3	0.1	25.4	19.3	42	33.9	19.1	27	29.8	19.1	46	-13.3
06/07/2023 11:59	9.3	0.1	25.4	19.3	43	34.2	19.1	27	29.9	19.1	45	-13.2

06/07/2023 12:00	9.3	0.1	25.4	19.3	42	34.5	19.1	27	29.9	19.1	45	-13.1
06/07/2023 12:01	9.3	0.1	25.4	19.3	42	35	19.1	28	29.8	19.1	45	-13
06/07/2023 12:02	9.3	0.1	25.4	19.3	42	35.4	19.1	30	29.9	19.1	45	-12.9
06/07/2023 12:03	9.3	0.1	25.3	19.3	40	35.8	19.1	29	29.9	19.1	45	-12.9
06/07/2023 12:04	9.3	0.1	25.3	19.3	41	36.2	19.1	31	29.9	19.1	47	-12.8
06/07/2023 12:05	9.3	0.1	25.3	19.3	41	36.5	19.1	32	29.9	19.1	46	-12.8
06/07/2023 12:06	9.3	0.1	25.3	19.3	41	36.8	19.1	32	29.9	19.1	47	-12.8
06/07/2023 12:07	9.3	0.1	25.3	19.3	41	37	19.1	32	29.9	19.1	47	-12.7
06/07/2023 12:08	9.3	0.1	25.3	19.3	40	37.2	19.1	31	29.9	19.1	46	-12.7
06/07/2023 12:09	9.3	0.1	25.4	19.3	42	37.4	19.1	31	29.9	19.1	45	-12.7
06/07/2023 12:10	9.3	0.1	25.2	19.3	41	37.5	19.1	32	29.9	19.1	46	-12.6

Appendix 3. Logged Data Generated from ploughed Aberdeen Soil Column Experiment

Label	Power	Psi	Theta	SoilTemp	ECp	Theta(2)	SoilTemp(2)	ECp(2)	Theta(3)	SoilTemp(3	ECp(3)	Psi(2)
Units	V	kPa	%	deg C	mS.m-1	%	deg C	mS.m-1	%	deg C	mS.m-1	kPa
23/01/2024 10:23	7.7	#-INF	2.5	19.1	#-INF	4	18.9	#-INF	3.1	18.9	#-INF	#-INF
23/01/2024 10:24	7.7	#-INF	2.6	19.1	#-INF	3.9	18.9	#-INF	3.1	19	#-INF	#-INF
23/01/2024 10:25	7.5	#-INF	2.4	19.2	#-INF	3.8	18.9	#-INF	3.2	19	#-INF	#-INF
23/01/2024 10:26	7.5	#-INF	2.4	19.2	#-INF	3.7	19	#-INF	3	19	#-INF	#-INF
23/01/2024 10:27	7.7	#-INF	2.4	19.2	#-INF	3.8	19	#-INF	3.1	19	#-INF	#-INF
23/01/2024 10:28	7.7	#-INF	2.5	19.2	#-INF	3.9	19	#-INF	3.1	19	#-INF	#-INF
23/01/2024 10:29	7.7	#-INF	2.4	19.2	#-INF	3.9	19	#-INF	3.1	19	#-INF	#-INF
23/01/2024 10:30	7.7	#-INF	2.5	19.2	#-INF	3.9	19	#-INF	3.2	19	#-INF	#-INF
23/01/2024 10:31	7.7	#-INF	2.5	19.2	#-INF	3.9	19	#-INF	3.2	19	#-INF	#-INF
23/01/2024 10:32	7.7	#-INF	2.4	19.2	#-INF	3.9	19	#-INF	3.2	19	#-INF	#-INF
23/01/2024 10:33	7.7	#-INF	2.5	19.2	#-INF	3.9	19	#-INF	3.1	19	#-INF	#-INF
23/01/2024 10:34	7.6	#-INF	2.8	19.2	#-INF	3.8	19	#-INF	3.4	19	#-INF	#-INF
23/01/2024 10:35	7.6	#-INF	2.6	19.3	#-INF	3.9	19	#-INF	3.4	19.1	0	#-INF
23/01/2024 10:36	7.7	#-INF	2.6	19.3	#-INF	3.8	19	#-INF	3	19.1	#-INF	#-INF
23/01/2024 10:37	7.5	#-INF	2.8	19.3	#-INF	3.9	19	#-INF	2.9	19.1	#-INF	#-INF
23/01/2024 10:38	7.7	#-INF	2.8	19.3	#-INF	3.9	19	#-INF	3.1	19.1	#-INF	#-INF
23/01/2024 10:39	7.7	#-INF	3.3	19.3	#-INF	3.9	19	#-INF	3.1	19.1	#-INF	#-INF
23/01/2024 10:40	7.7	#-INF	4.5	19.3	#-INF	3.9	19	#-INF	3.2	19.1	#-INF	#-INF
23/01/2024 10:41	7.7	#-INF	6.2	19.4	1027	3.9	19	#-INF	3.2	19.1	#-INF	#-INF
23/01/2024 10:42	7.6	#-INF	8.3	19.4	377	3.7	19	#-INF	3.3	19.1	#-INF	#-INF
23/01/2024 10:43	7.5	#-INF	10.8	19.5	229	3.8	19.1	#-INF	3.2	19.1	#-INF	#-INF
23/01/2024 10:44	7.5	#-INF	13.5	19.6	162	4	19.1	#-INF	3.2	19.1	0	#-INF
23/01/2024 10:45	7.4	#-INF	15.6	19.7	123	3.8	19.1	#-INF	3.4	19.2	0	#-INF
23/01/2024 10:46	7.4	#-INF	17.8	19.8	142	3.7	19.1	#-INF	3.1	19.2	#-INF	#-INF
23/01/2024 10:47	7.4	#-INF	19.9	19.9	133	3.7	19.1	#-INF	3.2	19.2	#-INF	#-INF
23/01/2024 10:48	7.4	#-INF	20.7	20	129	4	19.1	#-INF	2.9	19.2	#-INF	#-INF
23/01/2024 10:49	7.4	#-INF	21.8	20.2	121	3.9	19.2	#-INF	3.2	19.2	#-INF	#-INF
23/01/2024 10:50	7.3	#-INF	22.3	20.3	113	3.7	19.2	#-INF	3.4	19.2	#-INF	#-INF

23/01/2024 10:51	7.4	#-INF	22.9	20.4	108	3.8	19.2	#-INF	2.9	19.2	#-INF	#-INF
23/01/2024 10:52	7.4	#-INF	24	20.5	98	4.1	19.2	#-INF	3	19.2	#-INF	#-INF
23/01/2024 10:53	7.3	#-INF	24.4	20.6	96	3.8	19.2	#-INF	3.4	19.3	#-INF	#-INF
23/01/2024 10:54	7.3	#-INF	24.9	20.7	95	4	19.2	#-INF	2.9	19.3	#-INF	#-INF
23/01/2024 10:55	7.3	#-INF	25.5	20.8	89	3.9	19.2	#-INF	3	19.3	#-INF	#-INF
23/01/2024 10:56	7.3	#-INF	25.7	20.9	84	4	19.2	#-INF	2.8	19.3	#-INF	#-INF
23/01/2024 10:57	7.3	#-INF	25.9	21	76	3.6	19.2	#-INF	3	19.3	#-INF	#-INF
23/01/2024 10:58	7.3	#-INF	26.5	21.1	79	3.8	19.2	#-INF	2.9	19.3	#-INF	#-INF
23/01/2024 10:59	7.3	#-INF	26.8	21.2	78	3.8	19.2	#-INF	3.2	19.3	#-INF	#-INF
23/01/2024 11:00	7.3	#-INF	27.2	21.3	77	3.6	19.2	#-INF	3	19.3	#-INF	#-INF
23/01/2024 11:01	7.3	#-INF	27.2	21.4	76	3.8	19.2	#-INF	3.5	19.3	0	#-INF
23/01/2024 11:02	7.3	#-INF	27.2	21.5	75	3.6	19.2	#-INF	3	19.3	#-INF	#-INF
23/01/2024 11:03	7.3	#-INF	27.5	21.5	76	4.1	19.2	#-INF	3.5	19.3	0	#-INF
23/01/2024 11:04	7.3	#-INF	27.7	21.6	78	3.8	19.2	#-INF	3.1	19.4	#-INF	#-INF
23/01/2024 11:05	7.3	#-INF	27.9	21.7	71	3.6	19.3	#-INF	3.4	19.4	#-INF	#-INF
23/01/2024 11:06	7.3	#-INF	27.8	21.8	77	3.9	19.3	#-INF	3.4	19.4	#-INF	#-INF
23/01/2024 11:07	7.3	#-INF	28.1	21.8	71	4	19.3	#-INF	2.8	19.4	#-INF	#-INF
23/01/2024 11:08	7.3	#-INF	28.1	21.9	73	3.9	19.3	#-INF	3.2	19.4	#-INF	#-INF
23/01/2024 11:09	7.3	#-INF	27.8	22	65	4.1	19.3	#-INF	3	19.4	#-INF	#-INF
23/01/2024 11:10	7.3	#-INF	27.9	22.1	64	3.9	19.3	#-INF	3.4	19.4	#-INF	#-INF
23/01/2024 11:11	7.3	#-INF	27.9	22.1	68	3.9	19.3	#-INF	3.2	19.5	#-INF	#-INF
23/01/2024 11:12	7.3	#-INF	28.1	22.2	63	3.6	19.3	#-INF	3.5	19.5	#-INF	#-INF
23/01/2024 11:13	7.4	#-INF	28.4	22.2	69	3.9	19.3	#-INF	3.7	19.4	#-INF	#-INF
23/01/2024 11:14	7.4	#-INF	28.5	22.2	65	3.9	19.3	#-INF	4.3	19.4	#-INF	#-INF
23/01/2024 11:15	7.5	#-INF	28.5	22.2	66	3.8	19.2	#-INF	5	19.4	#-INF	#-INF
23/01/2024 11:16	7.5	#-INF	28.5	22.3	67	3.9	19.2	#-INF	5.8	19.4	1025	#-INF
23/01/2024 11:17	7.5	#-INF	28.5	22.3	66	3.9	19.2	#-INF	6.7	19.4	512	#-INF
23/01/2024 11:18	7.5	#-INF	28.6	22.3	65	4	19.2	#-INF	7.7	19.4	376	#-INF
23/01/2024 11:19	7.5	#-INF	28.7	22.4	66	3.9	19.2	#-INF	8.7	19.4	265	#-INF
23/01/2024 11:20	7.5	#-INF	28.7	22.4	66	4	19.2	#-INF	10	19.4	185	#-INF
23/01/2024 11:21	7.5	#-INF	28.8	22.5	66	3.9	19.2	#-INF	11	19.4	167	#-INF

23/01/2024 11:22	7.5	#-INF	28.9	22.5	65	3.9	19.2	#-INF	12	19.4	139	#-INF
23/01/2024 11:23	7.5	#-INF	28.9	22.5	65	3.9	19.2	#-INF	13.1	19.5	116	#-INF
23/01/2024 11:24	7.5	#-INF	29	22.6	64	3.9	19.2	#-INF	14	19.5	101	#-INF
23/01/2024 11:25	7.5	#-INF	29.1	22.6	61	3.9	19.2	#-INF	14.9	19.5	89	#-INF
23/01/2024 11:26	7.5	#-INF	29.1	22.6	64	4	19.2	#-INF	15.9	19.5	81	#-INF
23/01/2024 11:27	7.5	-339.5	29.2	22.7	63	4	19.2	#-INF	16.9	19.5	73	#-INF
23/01/2024 11:28	7.5	-186.4	29.3	22.7	63	3.9	19.2	#-INF	18	19.6	69	#-INF
23/01/2024 11:29	7.5	-107.8	29.4	22.7	64	3.9	19.2	#-INF	18.9	19.6	69	#-INF
23/01/2024 11:30	7.5	-83.2	29.5	22.8	63	3.9	19.2	#-INF	19.7	19.6	71	#-INF
23/01/2024 11:31	7.5	-66.4	29.6	22.8	62	3.9	19.2	#-INF	20.4	19.6	74	#-INF
23/01/2024 11:32	7.6	-51.7	29.6	22.8	61	4	19.2	#-INF	21.1	19.6	75	#-INF
23/01/2024 11:33	7.6	-42.8	29.7	22.8	62	3.9	19.2	#-INF	21.7	19.7	74	#-INF
23/01/2024 11:34	7.6	-35.8	29.8	22.9	61	3.9	19.2	#-INF	22.2	19.7	73	#-INF
23/01/2024 11:35	7.6	-30.4	29.8	22.9	62	3.9	19.2	#-INF	22.7	19.7	73	#-INF
23/01/2024 11:36	7.6	-24.6	30.4	22.9	61	3.9	19.2	#-INF	23.3	19.7	74	#-INF
23/01/2024 11:37	7.4	-18.3	30.3	22.9	58	3.9	19.2	#-INF	23.9	19.7	74	#-INF
23/01/2024 11:38	7.5	-13.1	30.7	23	60	3.9	19.3	#-INF	24.3	19.8	69	#-INF
23/01/2024 11:39	7.6	-11.6	30.7	23	61	3.9	19.3	#-INF	24.8	19.8	69	#-INF
23/01/2024 11:40	7.6	-11	30.7	23	60	3.9	19.3	#-INF	25.2	19.8	69	#-INF
23/01/2024 11:41	7.6	-10.6	30.8	23	60	3.9	19.3	#-INF	25.6	19.8	67	#-INF
23/01/2024 11:42	7.6	-10.3	31	23	58	3.9	19.3	#-INF	25.9	19.9	64	#-INF
23/01/2024 11:43	7.6	-10	31.2	23	57	3.9	19.3	#-INF	26.3	19.9	64	#-INF
23/01/2024 11:44	7.6	-9.8	31.1	23.1	59	3.9	19.3	#-INF	26.7	19.9	64	#-INF
23/01/2024 11:45	7.6	-9.6	31.3	23.1	59	3.9	19.3	#-INF	27	19.9	63	#-INF
23/01/2024 11:46	7.6	-9.3	31.4	23.1	59	3.9	19.3	#-INF	27.4	20	63	#-INF
23/01/2024 11:47	7.6	-9.1	31.6	23.1	58	3.9	19.3	#-INF	27.7	20	62	#-INF
23/01/2024 11:48	7.6	-8.9	31.7	23.1	58	3.9	19.3	#-INF	28	20	61	#-INF
23/01/2024 11:49	7.6	-8.6	31.8	23.2	58	3.9	19.3	#-INF	28.3	20.1	60	#-INF
23/01/2024 11:50	7.6	-8.5	31.9	23.2	58	4	19.3	#-INF	28.6	20.1	61	#-INF
23/01/2024 11:51	7.4	-8.2	31.9	23.2	54	3.9	19.4	#-INF	28.7	20.2	60	#-INF
23/01/2024 11:52	7.4	-8.1	31.9	23.3	57	4	19.4	#-INF	29.3	20.2	64	#-INF

23/01/2024 11:53	7.4	-7.9	32.3	23.3	57	4.1	19.4	#-INF	29.1	20.3	67	#-INF
23/01/2024 11:54	7.3	-7.8	32	23.3	54	4.1	19.4	#-INF	28.9	20.3	55	#-INF
23/01/2024 11:55	7.3	-7.7	32.2	23.3	54	4.1	19.5	#-INF	29.2	20.3	53	#-INF
23/01/2024 11:56	7.5	-7.7	32.3	23.3	56	4	19.5	#-INF	29.6	20.4	57	#-INF
23/01/2024 11:57	7.5	-7.7	32.4	23.3	56	4	19.4	#-INF	29.7	20.3	57	#-INF
23/01/2024 11:58	7.5	-7.7	32.5	23.3	56	4	19.4	#-INF	29.9	20.3	57	#-INF
23/01/2024 11:59	7.5	-7.7	32.7	23.3	56	4.1	19.4	#-INF	29.9	20.4	57	#-INF
23/01/2024 12:00	7.5	-7.8	32.6	23.3	57	4.1	19.4	#-INF	30	20.4	58	#-INF
23/01/2024 12:01	7.5	-7.8	32.6	23.3	57	4.2	19.4	#-INF	30.2	20.4	59	#-INF
23/01/2024 12:02	7.5	-7.8	32.7	23.3	56	4.3	19.4	#-INF	30.2	20.4	57	#-INF
23/01/2024 12:03	7.4	-7.8	32.7	23.3	54	4.3	19.4	#-INF	30.5	20.4	55	#-INF
23/01/2024 12:04	7.5	-7.8	32.6	23.3	55	4.5	19.5	#-INF	30.4	20.5	57	#-INF
23/01/2024 12:05	7.5	-7.9	32.7	23.3	55	4.6	19.5	#-INF	30.4	20.5	58	#-INF
23/01/2024 12:06	7.5	-8	32.7	23.3	55	4.9	19.4	#-INF	30.5	20.5	58	#-INF
23/01/2024 12:07	7.5	-8	32.8	23.3	55	5.5	19.5	1586	30.6	20.5	57	#-INF
23/01/2024 12:08	7.5	-8	32.7	23.3	55	6.5	19.5	592	30.7	20.5	58	#-INF
23/01/2024 12:09	7.5	-8	32.8	23.3	55	8.2	19.4	328	30.7	20.5	57	#-INF
23/01/2024 12:10	7.5	-8	32.8	23.3	55	9.7	19.5	234	30.8	20.5	57	#-INF
23/01/2024 12:11	7.5	-8.1	32.8	23.3	54	10.9	19.5	189	30.8	20.6	57	#-INF
23/01/2024 12:12	7.5	-8.2	32.8	23.3	55	12	19.5	170	30.8	20.6	56	#-INF
23/01/2024 12:13	7.6	-8.3	32.9	23.3	55	13	19.5	142	30.9	20.6	56	#-INF
23/01/2024 12:14	7.4	-8.2	32.9	23.3	57	14.4	19.5	141	31.1	20.6	58	#-INF
23/01/2024 12:15	7.5	-8.3	32.9	23.3	55	15.7	19.6	72	30.9	20.7	56	#-INF
23/01/2024 12:16	7.5	-8.4	32.8	23.3	54	16.9	19.6	61	31	20.7	55	#-INF
23/01/2024 12:17	7.4	-8.2	33.1	23.3	54	17.9	19.6	39	31.3	20.7	52	#-INF
23/01/2024 12:18	7.4	-8.2	32.9	23.3	52	19	19.6	41	30.9	20.8	45	#-INF
23/01/2024 12:19	7.3	-8.2	32.9	23.3	52	19.6	19.6	65	30.9	20.8	53	#-INF
23/01/2024 12:20	7.5	-8.3	32.9	23.3	54	20.3	19.7	56	31.2	20.8	56	#-INF
23/01/2024 12:21	7.5	-8.2	33	23.3	54	21	19.6	59	31.3	20.8	55	#-INF
23/01/2024 12:22	7.5	-8.3	33.1	23.3	54	21.6	19.6	61	31.3	20.8	55	#-INF
23/01/2024 12:23	7.5	-8.3	33	23.3	54	22	19.6	68	31.4	20.8	55	-890.1

23/01/2024 12:24	7.5	-8.3	32.9	23.3	54	22.3	19.7	69	31.4	20.8	56	-373.5
23/01/2024 12:25	7.5	-8.4	32.9	23.3	54	22.7	19.7	63	31.4	20.9	56	-227.7
23/01/2024 12:26	7.5	-8.2	33	23.3	54	23	19.7	64	31.5	20.9	55	-132
23/01/2024 12:27	7.5	-8.2	33	23.3	54	23.3	19.7	64	31.5	20.9	56	-77.8
23/01/2024 12:28	7.5	-8.2	32.9	23.3	54	23.5	19.7	63	31.5	20.9	57	-67
23/01/2024 12:29	7.5	-8.2	32.9	23.2	55	23.8	19.7	62	31.5	20.9	57	-58.8
23/01/2024 12:30	7.4	-8.2	33	23.2	54	24	19.7	60	31.6	20.9	59	-53.2
23/01/2024 12:31	7.4	-8	33	23.3	53	24	19.8	54	31.4	21	62	-48.1
23/01/2024 12:32	7.3	-8	33	23.3	56	24.3	19.8	60	31.8	21	58	-43.4
23/01/2024 12:33	7.3	-8	32.8	23.3	51	24.4	19.8	59	31.2	21.1	46	-39.6
23/01/2024 12:34	7.3	-8	32.8	23.3	53	24.7	19.8	59	31.7	21.1	55	-37.2
23/01/2024 12:35	7.3	-8	33	23.3	54	25	19.9	67	31.1	21.1	49	-34.2
23/01/2024 12:36	7.3	-8	33	23.3	53	24.9	19.9	50	31.6	21.1	57	-29.5
23/01/2024 12:37	7.3	-8.1	33	23.3	52	25.4	19.9	62	31.7	21.2	54	-26.8
23/01/2024 12:38	7.3	-7.9	32.9	23.3	53	25.4	19.9	50	31.8	21.2	58	-25.5
23/01/2024 12:39	7.3	-7.9	33	23.3	55	25.7	19.9	55	31.6	21.2	57	-24.8
23/01/2024 12:40	7.3	-7.9	33	23.3	56	25.7	19.9	61	31.7	21.2	55	-24.5
23/01/2024 12:41	7.3	-7.9	32.8	23.3	52	26	20	56	31.5	21.2	60	-24.2
23/01/2024 12:42	7.2	-8	32.8	23.3	53	26	20	48	31.4	21.2	58	-23.9
23/01/2024 12:43	7.2	-8	32.8	23.3	51	26.4	20	63	31.6	21.3	54	-23.8
23/01/2024 12:44	7.4	-8	32.8	23.3	53	26.4	20	56	31.5	21.3	54	-23.7
23/01/2024 12:45	7.4	-8.1	32.9	23.2	54	26.5	20	56	31.5	21.3	55	-23.6
23/01/2024 12:46	7.4	-8.2	32.9	23.2	53	26.6	19.9	54	31.6	21.2	54	-23.5
23/01/2024 12:47	7.4	-8.2	32.9	23.2	53	26.7	19.9	53	31.6	21.2	53	-23.4
23/01/2024 12:48	7.5	-8.2	32.9	23.1	54	26.8	19.9	53	31.6	21.2	54	-23.3
23/01/2024 12:49	7.3	-8	32.8	23.1	51	27	19.9	50	31.6	21.2	53	-23.2
23/01/2024 12:50	7.3	-7.9	32.9	23.2	54	27.2	20	57	31.2	21.3	51	-23
23/01/2024 12:51	7.3	-7.9	32.9	23.2	55	27.3	20	55	31.8	21.3	51	-23
23/01/2024 12:52	7.3	-7.9	32.9	23.2	55	27.2	20.1	46	31.5	21.3	56	-22.9
23/01/2024 12:53	7.3	-8.2	32.9	23.2	52	27.3	20.1	53	31.9	21.4	55	-22.8
23/01/2024 12:54	7.2	-8.2	32.9	23.2	54	27.5	20.1	49	31.4	21.4	51	-22.8

23/01/2024 12:55	7.4	-8.3	32.9	23.2	53	27.5	20.1	51	31.5	21.4	53	-22.8
23/01/2024 12:56	7.4	-8.4	32.9	23.1	53	27.6	20.1	52	31.5	21.3	53	-22.8
23/01/2024 12:57	7.4	-8.3	32.8	23.1	53	27.7	20.1	52	31.5	21.3	52	-22.7
23/01/2024 12:58	7.4	-8.3	32.8	23.1	53	27.7	20.1	51	31.6	21.3	52	-22.7
23/01/2024 12:59	7.5	-8.4	32.8	23	54	27.8	20.1	51	31.5	21.3	52	-22.6
23/01/2024 13:00	7.3	-8.5	32.8	23	51	27.8	20.1	55	31.4	21.3	45	-22.6
23/01/2024 13:01	7.3	-8.5	32.9	23	55	27.7	20.1	44	31.5	21.4	52	-22.4
23/01/2024 13:02	7.3	-8.5	32.8	23.1	53	27.9	20.1	51	31.3	21.4	50	-22.4
23/01/2024 13:03	7.3	-8.6	32.8	23.1	51	27.8	20.2	45	31.8	21.4	55	-22.3
23/01/2024 13:04	7.4	-8.7	32.8	23	53	28	20.2	50	31.5	21.4	52	-22.4
23/01/2024 13:05	7.4	-8.7	32.8	23	53	28.1	20.2	49	31.5	21.4	51	-22.4
23/01/2024 13:06	7.4	-8.7	32.8	23	53	28.1	20.1	49	31.5	21.4	51	-22.4
23/01/2024 13:07	7.5	-8.7	32.8	22.9	53	28.2	20.1	50	31.6	21.4	51	-22.4
23/01/2024 13:08	7.5	-8.7	32.7	22.9	53	28.2	20.1	50	31.6	21.4	51	-22.4
23/01/2024 13:09	7.5	-8.6	32.8	22.9	53	28.3	20.1	50	31.6	21.4	51	-22.4
23/01/2024 13:10	7.5	-8.7	32.8	22.9	53	28.4	20.2	49	31.5	21.4	50	-22.5
23/01/2024 13:11	7.5	-8.7	32.8	22.9	54	28.4	20.2	49	31.5	21.4	51	-22.5
23/01/2024 13:12	7.5	-8.7	32.7	22.9	53	28.4	20.2	50	31.5	21.4	50	-22.5
23/01/2024 13:13	7.5	-8.7	32.7	22.9	53	28.5	20.2	50	31.5	21.4	50	-22.5
23/01/2024 13:14	7.5	-8.7	32.7	22.9	54	28.5	20.2	50	31.5	21.4	50	-22.5
23/01/2024 13:15	7.5	-8.8	32.7	22.8	54	28.6	20.2	50	31.5	21.4	50	-22.5
23/01/2024 13:16	7.5	-8.8	32.7	22.8	54	28.6	20.2	49	31.5	21.4	50	-22.4
23/01/2024 13:17	7.5	-8.8	32.7	22.8	54	28.7	20.2	50	31.5	21.4	50	-22.4
23/01/2024 13:18	7.5	-8.8	32.7	22.8	54	28.8	20.2	50	31.5	21.4	50	-22.5
23/01/2024 13:19	7.5	-8.8	32.7	22.8	54	28.8	20.2	49	31.5	21.4	50	-22.6
23/01/2024 13:20	7.5	-8.8	32.6	22.8	53	28.8	20.2	50	31.5	21.4	50	-22.5
23/01/2024 13:21	7.5	-8.9	32.7	22.8	53	28.8	20.2	50	31.5	21.4	49	-22.6
23/01/2024 13:22	7.5	-8.9	32.7	22.8	53	28.9	20.3	49	31.5	21.4	49	-22.7
23/01/2024 13:23	7.5	-8.8	32.7	22.8	53	28.9	20.3	49	31.4	21.4	49	-22.7
23/01/2024 13:24	7.5	-8.9	32.6	22.7	53	28.9	20.3	49	31.5	21.4	49	-22.7
23/01/2024 13:25	7.5	-8.9	32.6	22.7	54	29	20.3	49	31.5	21.4	49	-22.6

23/01/2024 13:26	7.5	-8.9	32.6	22.7	54	29	20.3	49	31.5	21.5	49	-22.6
23/01/2024 13:27	7.5	-8.8	32.5	22.7	54	29	20.3	50	31.5	21.5	50	-22.6
23/01/2024 13:28	7.5	-8.8	32.5	22.7	54	29.1	20.3	50	31.5	21.5	49	-22.7
23/01/2024 13:29	7.5	-8.9	32.5	22.7	54	29.1	20.3	49	31.5	21.5	49	-22.6
23/01/2024 13:30	7.4	-8.8	32.4	22.7	56	29.2	20.3	47	31.7	21.5	50	-22.6
23/01/2024 13:31	7.3	-8.8	32.3	22.7	51	29.2	20.4	51	31	21.5	42	-22.6
23/01/2024 13:32	7.3	-8.5	32.3	22.7	52	29.1	20.4	45	31.6	21.6	52	-22.1
23/01/2024 13:33	7.3	-8.5	32.3	22.7	51	29.1	20.4	52	31.3	21.6	49	-22.1
23/01/2024 13:34	7.3	-8.4	32.3	22.7	53	29	20.5	45	31.4	21.6	40	-22.1
23/01/2024 13:35	7.3	-8.4	32.3	22.7	52	29.5	20.5	56	31.4	21.6	48	-22.1
23/01/2024 13:36	7.3	-8.4	32.3	22.7	50	29.1	20.5	51	31.3	21.6	41	-22.1
23/01/2024 13:37	7.3	-8.4	32.2	22.7	50	29.3	20.5	55	31	21.6	41	-22.1
23/01/2024 13:38	7.3	-8.4	32.2	22.7	52	29.3	20.5	50	31.5	21.6	46	-22
23/01/2024 13:39	7.2	-8.4	32.2	22.7	51	29.4	20.5	50	31.2	21.6	47	-22
23/01/2024 13:40	7.4	-8.5	32.3	22.7	54	29.3	20.5	49	31.4	21.6	48	-22
23/01/2024 13:41	7.4	-8.5	32.4	22.6	54	29.4	20.5	49	31.4	21.6	49	-22.1
23/01/2024 13:42	7.4	-8.5	32.4	22.6	53	29.4	20.5	49	31.4	21.6	49	-22.1
23/01/2024 13:43	7.4	-8.5	32.4	22.6	53	29.4	20.5	50	31.4	21.5	48	-22.1
23/01/2024 13:44	7.5	-8.6	32.4	22.5	53	29.5	20.5	50	31.4	21.5	49	-22.1
23/01/2024 13:45	7.5	-8.2	32.3	22.5	54	29.5	20.5	50	31.4	21.5	48	-22.1
23/01/2024 13:46	7.5	-8.1	32.4	22.5	54	29.5	20.5	50	31.4	21.5	47	-22.1
23/01/2024 13:47	7.5	-8.1	32.4	22.5	54	29.5	20.5	49	31.4	21.5	47	-22.1
23/01/2024 13:48	7.5	-8.1	32.3	22.5	54	29.5	20.5	49	31.4	21.5	47	-22.1
23/01/2024 13:49	7.5	-8.1	32.3	22.5	54	29.6	20.5	49	31.4	21.5	47	-22.1
23/01/2024 13:50	7.5	-8.1	32.3	22.5	53	29.6	20.5	49	31.3	21.5	48	-22.1
23/01/2024 13:51	7.5	-8.2	32.4	22.4	54	29.6	20.5	48	31.3	21.5	47	-22.1
23/01/2024 13:52	7.5	-8.2	32.5	22.4	54	29.7	20.5	48	31.3	21.5	46	-22.1
23/01/2024 13:53	7.5	-8.2	32.4	22.4	54	29.7	20.5	48	31.3	21.5	45	-22.1
23/01/2024 13:54	7.5	-8.2	32.4	22.4	53	29.8	20.5	47	31.3	21.5	46	-22.1
23/01/2024 13:55	7.5	-8.2	32.4	22.4	54	29.8	20.5	48	31.3	21.5	46	-22.1
23/01/2024 13:56	7.5	-8.2	32.4	22.4	55	29.9	20.5	48	31.3	21.5	46	-22.1

23/01/2024 13:57	7.5	-8.2	32.3	22.4	54	30	20.5	48	31.3	21.5	46	-22.1
23/01/2024 13:58	7.5	-8.2	32.3	22.4	54	30.1	20.5	48	31.3	21.5	46	-22.1
23/01/2024 13:59	7.5	-8.2	32.3	22.4	54	30.2	20.5	48	31.3	21.5	46	-22.1
23/01/2024 14:00	7.5	-8.2	32.2	22.3	54	30.3	20.5	49	31.3	21.5	46	-22.1

Appendix 4. Logged Data Generated from the Ivrogbo Soil Column Experiment

Label	Power	Psi	Theta	SoilTemp	ECp	Theta(2)	SoilTemp(2)	ECp(2)	Theta(3)	SoilTemp(3)	ECp(3)	Psi(2)
Units	V	kPa	%	deg C	mS.m-1	%	deg C	mS.m-1	%	deg C	mS.m-1	kPa
08/08/2023 10:20	9.2	-98.2	11.3	17.8	85	10.8	17.6	0	8.8	17.7	0	-539.2
08/08/2023 10:21	9.2	-98.1	11.3	17.8	73	10.7	17.7	0	8.8	17.7	0	-533.5
08/08/2023 10:22	9.2	-98.2	11.4	17.8	73	10.7	17.6	0	8.8	17.7	0	-539.1
08/08/2023 10:23	9.2	-98.2	11.3	17.8	73	10.7	17.6	0	8.9	17.7	0	-539.8
08/08/2023 10:24	9.2	-98.2	11.3	17.8	78	10.7	17.6	0	8.8	17.7	0	-539.7
08/08/2023 10:25	9.2	-98.2	11.3	17.8	74	10.7	17.6	0	8.8	17.7	0	-538.5
08/08/2023 10:26	9.2	-98.2	11.3	17.8	74	10.7	17.6	0	8.8	17.7	0	-539.9
08/08/2023 10:27	9.2	-98.2	11.3	17.8	78	10.7	17.6	0	8.9	17.6	0	-539.5
08/08/2023 10:28	9.2	-98.2	11.4	17.8	80	10.7	17.6	0	8.9	17.7	0	-539.4
08/08/2023 10:29	9.2	-98.2	11.7	17.8	80	10.7	17.6	0	8.8	17.6	0	-539.4
08/08/2023 10:30	9.2	-98.2	12.3	17.8	89	10.7	17.6	0	8.9	17.7	0	-539
08/08/2023 10:31	9.2	-98.2	13.8	17.8	95	10.7	17.6	0	8.8	17.7	0	-538.2
08/08/2023 10:32	9.2	-98.2	16.3	17.8	94	10.7	17.6	0	8.8	17.7	0	-538.2
08/08/2023 10:33	9.2	-98.2	19.6	17.8	102	10.7	17.6	0	8.8	17.7	0	-538.5
08/08/2023 10:34	9.2	-98.2	23.5	17.9	101	10.7	17.6	0	8.8	17.7	0	-538.1
08/08/2023 10:35	9.2	-98.2	26.6	17.9	93	10.8	17.6	0	8.7	17.7	0	-537.1
08/08/2023 10:36	9.2	-98.2	28.8	17.9	86	10.7	17.6	0	8.7	17.7	0	-537.4
08/08/2023 10:37	9.2	-98.2	30.1	17.9	83	10.8	17.6	0	8.7	17.7	0	-537.6
08/08/2023 10:38	9.2	-98.2	31.2	17.9	79	10.8	17.6	0	8.7	17.7	0	-537.1
08/08/2023 10:39	9.2	-98.2	31.9	18	79	10.8	17.6	0	8.6	17.7	7	-536.9
08/08/2023 10:40	9.2	-98.2	32.5	18	77	10.9	17.6	0	8.6	17.7	0	-536.7
08/08/2023 10:41	9.2	-98.2	32.9	18	76	11	17.6	0	8.6	17.7	0	-535.9
08/08/2023 10:42	9.2	-98.2	33.2	18	74	11.2	17.6	0	8.7	17.7	0	-535.9
08/08/2023 10:43	9.2	-98.2	33.4	18.1	73	11.4	17.7	0	8.7	17.7	0	-536.4
08/08/2023 10:44	9.2	-98.2	33.6	18.1	72	11.7	17.6	0	8.7	17.7	0	-535.8
08/08/2023 10:45	9.2	-98.2	33.7	18.1	71	12.1	17.7	0	8.7	17.7	0	-535.1
08/08/2023 10:46	9.2	-98.2	33.9	18.1	70	12.5	17.7	0	8.8	17.7	0	-533.3
08/08/2023 10:47	9.2	-98.1	34	18.2	69	13	17.7	0	8.8	17.7	0	-531.1

08/08/2023 10:48	9.2	-98.1	34.1	18.2	69	13.4	17.7	0	8.8	17.7	0	-527.7
08/08/2023 10:49	9.2	-98.1	34.2	18.2	68	13.9	17.7	0	8.8	17.7	0	-521.8
08/08/2023 10:50	9.2	-98.1	34.3	18.2	67	14.2	17.7	0	8.8	17.7	0	-513.7
08/08/2023 10:51	9.2	-98.1	34.4	18.3	66	14.4	17.7	0	8.9	17.7	0	-503.8
08/08/2023 10:52	9.2	-98.1	34.5	18.3	66	14.6	17.7	0	9	17.7	0	-494.6
08/08/2023 10:53	9.2	-98.1	34.5	18.3	64	14.7	17.7	0	9.2	17.7	0	-481.6
08/08/2023 10:54	9.2	-98.1	34.6	18.3	64	15	17.7	0	9.3	17.7	0	-468
08/08/2023 10:55	9.2	-98.1	34.7	18.4	64	15.3	17.7	0	9.5	17.8	0	-449.1
08/08/2023 10:56	9.2	-98.1	34.7	18.4	63	15.7	17.7	0	9.5	17.8	0	-419.2
08/08/2023 10:57	9.2	-98.1	34.7	18.4	62	16.1	17.7	4	9.5	17.8	0	-394.7
08/08/2023 10:58	9.2	-98.1	34.8	18.4	62	16.8	17.7	8	9.6	17.8	0	-377.6
08/08/2023 10:59	9.2	-98.1	34.8	18.5	61	17.3	17.7	12	9.7	17.8	0	-339.3
08/08/2023 11:00	9.2	-98.1	34.8	18.5	60	18.1	17.7	20	9.7	17.8	0	-284.8
08/08/2023 11:01	9.2	-98.1	34.9	18.5	60	18.7	17.7	23	9.8	17.8	0	-229.8
08/08/2023 11:02	9.2	-98.1	34.9	18.5	59	19.6	17.7	33	9.9	17.8	0	-185.2
08/08/2023 11:03	9.2	-98.1	34.9	18.5	59	20.1	17.7	35	10	17.8	0	-155
08/08/2023 11:04	9.2	-98	35	18.6	59	20.5	17.7	37	10.2	17.8	0	-124.9
08/08/2023 11:05	9.2	-97.9	35	18.6	58	22.9	17.7	55	10.4	17.8	0	-95.8
08/08/2023 11:06	9.2	-97.8	35.1	18.6	58	23.1	17.7	55	10.6	17.8	0	-77.9
08/08/2023 11:07	9.2	-97.6	35.1	18.6	57	23.4	17.7	56	10.8	17.8	0	-70.4
08/08/2023 11:08	9.2	-97.5	35.1	18.7	56	26	17.7	66	11.1	17.8	0	-61
08/08/2023 11:09	9.2	-97.3	35.2	18.7	56	26.4	17.7	66	11.3	17.8	0	-52.9
08/08/2023 11:10	9.2	-97.1	35.2	18.7	56	26.9	17.7	65	11.6	17.8	0	-44.2
08/08/2023 11:11	9.2	-96.9	35.2	18.7	56	27	17.7	67	11.9	17.8	0	-36.4
08/08/2023 11:12	9.2	-96.7	35.2	18.7	56	27.8	17.7	68	12.3	17.8	0	-30.2
08/08/2023 11:13	9.2	-96.4	35.3	18.7	55	28.4	17.7	68	12.6	17.8	0	-24.2
08/08/2023 11:14	9.2	-96.1	35.3	18.7	54	28.9	17.7	68	13	17.8	0	-18.5
08/08/2023 11:15	9.2	-95.7	35.4	18.8	54	29.2	17.7	68	13.8	17.8	0	-16.5
08/08/2023 11:16	9.2	-95.2	35.3	18.8	54	30.2	17.7	68	14.5	17.8	0	-16.4
08/08/2023 11:17	9.2	-94.6	35.4	18.8	53	30.4	17.7	67	15.5	17.8	0	-16.5
08/08/2023 11:18	9.2	-93.8	35.4	18.8	52	30.4	17.7	69	16.5	17.8	0	-16.5

08/08/2023 11:19	9.2	-92.7	35.4	18.8	52	30.5	17.7	69	17.5	17.8	0	-16.5
08/08/2023 11:20	9.2	-91.1	35.4	18.8	52	30.5	17.8	69	18	17.8	5	-16.5
08/08/2023 11:21	9.2	-89	35.5	18.8	51	30.5	17.7	68	18.4	17.8	6	-16.5
08/08/2023 11:22	9.2	-86.1	35.5	18.8	51	30.6	17.8	69	18.9	17.8	12	-16.5
08/08/2023 11:23	9.2	-82.5	35.5	18.8	51	30.8	17.8	69	19.2	17.8	18	-16.5
08/08/2023 11:24	9.2	-78.1	35.1	18.9	52	30.8	17.8	68	19.5	17.8	22	-16.5
08/08/2023 11:30	9.2	-48.4	32	18.9	47	28.9	17.8	66	19.2	17.9	18	-16.6
08/08/2023 11:31	9.2	-45.7	32.1	18.9	44	28.7	17.8	66	19	17.9	15	-16.5
08/08/2023 11:32	9.1	-43	32.9	19	48	28.4	17.8	70	19.2	17.9	25	-16.5
08/08/2023 11:33	9.2	-40.4	33.3	19	46	28.5	17.8	67	19.3	18	19	-16.5
08/08/2023 11:34	9.2	-37.9	33.7	19	47	29.2	17.8	67	19.4	17.9	22	-16.6
08/08/2023 11:35	9.2	-35.3	33.8	19	46	29.9	17.8	68	19.6	17.9	22	-16.6
08/08/2023 11:36	9.2	-32.5	33.9	18.9	46	30.3	17.8	68	19.6	17.9	22	-16.6
08/08/2023 11:37	9.2	-29.5	33.9	18.9	46	30.5	17.8	68	19.8	17.9	23	-16.6
08/08/2023 11:38	9.2	-26.4	34	18.9	45	30.6	17.8	69	19.9	17.9	25	-16.6
08/08/2023 11:39	9.2	-23.2	34	18.9	45	30.7	17.8	69	20.1	17.9	25	-16.6
08/08/2023 11:40	9.2	-20.1	34.1	18.9	45	30.8	17.8	69	20.6	17.9	27	-16.6
08/08/2023 11:41	9.2	-16.9	34.1	18.9	45	30.7	17.8	69	21.1	17.9	25	-16.6
08/08/2023 11:42	9.2	-13	34.1	18.9	45	30.7	17.8	69	21.6	17.9	26	-16.7
08/08/2023 11:43	9.2	-9.3	34.1	18.9	45	30.8	17.8	69	22.2	17.9	26	-16.7
08/08/2023 11:44	9.2	-6	34.2	18.9	44	30.7	17.8	69	22.8	17.9	28	-16.7
08/08/2023 11:45	9.2	-5	34.2	18.9	44	30.7	17.8	69	23.6	18	31	-16.7
08/08/2023 11:46	9.2	-4.8	34.2	18.9	44	30.7	17.8	69	24.2	18	30	-16.7
08/08/2023 11:47	9.2	-4.7	34.2	18.9	44	30.6	17.8	70	24.8	18	30	-16.7
08/08/2023 11:48	9.2	-4.7	34.3	18.9	44	30.6	17.8	69	25.2	18	32	-16.7
08/08/2023 11:49	9.2	-4.7	34.3	18.9	44	30.6	17.8	69	25.7	18	31	-16.7
08/08/2023 11:50	9.2	-4.6	34.4	18.9	43	30.5	17.8	69	26.1	18	32	-16.8
08/08/2023 11:51	9.2	-4.6	34.5	18.9	43	30.4	17.8	69	27	18	37	-16.8
08/08/2023 11:52	9.2	-4.6	34.5	18.9	43	30.4	17.8	68	28	18	40	-16.8
08/08/2023 11:53	9.2	-4.6	34.6	18.9	43	30.4	17.8	69	28.3	18	40	-16.8
08/08/2023 11:54	9.2	-4.6	34.7	18.9	43	30.4	17.8	69	29.5	18	43	-16.8

08/08/2023 11:55	9.2	-4.6	35	18.9	43	30.5	17.8	70	29.8	18	43	-16.8
08/08/2023 11:56	9.2	-4.6	35.2	18.9	44	30.5	17.8	69	30.1	18	45	-16.8
08/08/2023 11:57	9.2	-4.6	35.3	18.9	44	30.4	17.8	69	30.3	18	45	-16.8
08/08/2023 11:58	9.2	-4.6	35.4	18.9	44	30.5	17.8	70	30.5	18	46	-16.8
08/08/2023 11:59	9.2	-4.6	35.4	18.9	44	30.4	17.8	69	30.8	18	47	-16.8
08/08/2023 12:00	9.2	-4.5	35.4	18.9	44	30.4	17.8	69	31	18	47	-16.9
08/08/2023 12:01	9.2	-4.5	35.5	18.9	43	30.3	17.8	69	31.1	18	47	-16.9
08/08/2023 12:02	9.2	-4.5	35.6	18.9	43	30.4	17.8	69	32.2	18	49	-16.9
08/08/2023 12:03	9.2	-4.5	35.6	18.9	43	30.3	17.8	69	32.6	18	50	-17
08/08/2023 12:04	9.2	-4.4	35.7	18.9	43	30.3	17.8	69	33	18	50	-17
08/08/2023 12:05	9.2	-4.4	35.7	18.9	42	30.3	17.8	69	35.4	18	54	-17
08/08/2023 12:06	9.2	-4.4	35.7	18.9	42	30.3	17.8	70	35.5	18	54	-17
08/08/2023 12:07	9.2	-4.4	35.7	18.9	42	30.4	17.8	69	35.3	18	53	-17.1
08/08/2023 12:08	9.2	-4.4	35.8	18.9	42	30.3	17.8	69	35.2	18.1	54	-17.1
08/08/2023 12:09	9.2	-4.4	35.8	18.9	42	30.2	17.8	68	35.3	18.1	52	-17.1
08/08/2023 12:10	9.2	-4.4	35.8	18.9	41	30.3	17.8	68	35.4	18.1	52	-17.1
08/08/2023 12:11	9.2	-4.4	35.7	18.9	42	30.4	17.8	69	35.6	18.1	52	-17.1
08/08/2023 12:12	9.2	-4.5	35.4	18.9	42	30.5	17.8	70	35.6	18.1	53	-17.1
08/08/2023 12:13	9.2	-4.4	34.6	18.9	40	30.3	17.8	69	35.6	18.1	51	-17.1
08/08/2023 12:14	9.2	-4.5	34.5	18.9	40	30.2	17.8	69	35.6	18.1	51	-17.2
08/08/2023 12:15	9.2	-4.5	34.5	18.9	40	30.1	17.7	69	35.6	18.1	51	-17.2
08/08/2023 12:16	9.2	-4.5	34.5	18.9	40	30	17.8	69	35.6	18.1	51	-17.2
08/08/2023 12:17	9.2	-4.5	34.5	18.9	40	30	17.7	69	35.6	18.1	52	-17.2
08/08/2023 12:18	9.2	-4.5	34.6	18.9	39	29.8	17.7	69	35.6	18.1	51	-17.2
08/08/2023 12:19	9.2	-4.5	34.6	18.9	39	29.8	17.7	68	35.6	18.1	51	-17.2
08/08/2023 12:20	9.2	-4.5	34.7	18.9	39	29.7	17.7	68	35.6	18.1	52	-17.2
08/08/2023 12:21	9.2	-4.5	34.8	18.9	39	29.6	17.7	68	35.6	18.1	51	-17.2
08/08/2023 12:22	9.2	-4.5	35	18.9	39	29.6	17.7	68	35.6	18.1	51	-17.2
08/08/2023 12:23	9.2	-4.5	36.4	18.9	40	29.7	17.7	68	35.6	18.1	50	-17.3
08/08/2023 12:24	9.2	-4.5	43.5	19	39	30.5	17.7	69	36	18.1	51	-17.3
08/08/2023 12:25	9.2	-4.5	43.3	19	38	30.6	17.7	69	35.9	18.1	53	-17.3

08/08/2023 12:26	9.2	-4.6	42.6	19	38	30.4	17.7	70	35.8	18.1	53	-17.4
08/08/2023 12:27	9.2	-4.6	41.7	19	37	30.2	17.7	69	35.7	18.1	53	-17.4
08/08/2023 12:28	9.2	-4.6	40.4	19	36	29.9	17.6	69	35.7	18.1	53	-17.4
08/08/2023 12:29	9.2	-4.6	38.1	19	33	30.1	17.6	68	35.6	18.1	53	-17.4
08/08/2023 12:30	9.2	-4.6	37.4	19	33	30.1	17.6	69	35.5	18	53	-17.4
08/08/2023 12:31	9.2	-4.7	35.8	19	37	30	17.5	70	35.6	18	53	-17.5

Appendix 5. Logged Data Generated from the Oleh Soil Column Experiment

Label	Power	Psi	Theta	SoilTemp	ECp	Theta(2)	SoilTemp(2)	ECp(2)	Theta(3)	SoilTemp(3)	ECp(3)	Psi(2)
Units	V	kPa	%	deg C	mS.m-1	%	deg C	mS.m-1	%	deg C	mS.m-1	kPa
10/08/2023 11:25	9.1	-20.1	17.5	18.9	49	28.2	18.8	122	15.9	18.7	40	-19.3
10/08/2023 11:26	9.1	-20	17.6	18.9	51	28.1	18.8	124	15.7	18.7	51	-19.3
10/08/2023 11:27	9.1	-20.1	17.9	18.9	49	28.2	18.8	123	15.7	18.7	51	-19.3
10/08/2023 11:28	9.1	-20.1	18.4	18.9	44	28.2	18.8	124	15.9	18.7	36	-19.3
10/08/2023 11:29	9.1	-20.1	19.7	18.9	38	28.2	18.8	123	15.9	18.7	44	-19.4
10/08/2023 11:30	9.1	-20.1	20.6	18.9	39	28.2	18.8	123	15.9	18.7	43	-19.3
10/08/2023 11:31	9.1	-20.1	22.5	18.9	47	28.2	18.8	125	15.8	18.7	43	-19.4
10/08/2023 11:32	9.1	-20.1	24	18.9	52	28.2	18.8	124	15.9	18.7	44	-19.4
10/08/2023 11:33	9.1	-20.1	25.1	18.9	56	28.2	18.8	124	15.9	18.7	42	-19.4
10/08/2023 11:34	9.1	-20.1	26.1	18.9	59	28.2	18.8	124	15.9	18.7	40	-19.4
10/08/2023 11:35	9.1	-20.1	27.3	18.9	63	28.2	18.8	123	15.9	18.7	40	-19.4
10/08/2023 11:36	9.1	-20.1	27.9	18.9	64	28.2	18.8	124	16.1	18.7	41	-19.4
10/08/2023 11:37	9.1	-20.1	28.4	18.9	65	28.2	18.8	123	18.3	18.7	55	-19.4
10/08/2023 11:38	9.1	-19.9	28.7	18.9	65	28.2	18.8	123	19.9	18.7	69	-19.4
10/08/2023 11:39	9.1	-19.5	28.9	18.9	65	28.2	18.8	124	21	18.7	78	-19.4
10/08/2023 11:40	9.1	-19.1	29.3	18.9	66	28.2	18.8	125	21.8	18.7	78	-19.4
10/08/2023 11:41	9.1	-18.6	29.7	18.9	66	28.2	18.8	124	22.5	18.7	77	-19.4
10/08/2023 11:42	9.1	-18.1	30.1	18.9	64	28.2	18.8	125	23.2	18.7	73	-19.4
10/08/2023 11:43	9.1	-17.6	30.3	18.9	64	28.2	18.8	124	23.8	18.7	73	-19.4
10/08/2023 11:44	9.1	-17	30.6	18.9	64	28.2	18.8	125	24.4	18.7	70	-19.4
10/08/2023 11:45	9.1	-16.3	30.8	18.9	65	28.2	18.8	124	24.9	18.7	69	-19.4
10/08/2023 11:46	9.1	-15.7	31	18.9	65	28.2	18.8	124	25.6	18.7	67	-19.4
10/08/2023 11:47	9.1	-14.9	31.2	18.9	64	28.2	18.8	123	26.5	18.7	65	-19.4
10/08/2023 11:48	9.1	-13.8	31.4	18.9	64	28.2	18.8	125	28.2	18.7	64	-19.4
10/08/2023 11:49	9.1	-12.6	31.6	18.9	63	28.2	18.8	124	29.4	18.7	64	-19.4
10/08/2023 11:50	9.1	-11.3	31.7	18.9	64	28.2	18.8	124	30.6	18.7	61	-19.4
10/08/2023 11:51	9.1	-10.1	31.9	18.9	63	28.2	18.8	124	31.7	18.7	57	-19.4
10/08/2023 11:52	9.1	-8.7	32.1	18.9	62	28.2	18.8	125	32.7	18.7	54	-19.4
10/08/2023 11:53	9.1	-7.2	32.3	18.9	62	28.2	18.8	124	33.8	18.7	52	-19.4

10/08/2023 11:54	9.1	-5.5	32.4	18.9	62	28.2	18.8	123	34.9	18.7	48	-19.4
10/08/2023 11:55	9.1	-3.9	32.6	18.9	62	28.2	18.8	122	36.4	18.8	43	-19.4
10/08/2023 11:56	9.1	-2.5	32.6	18.9	61	28.2	18.8	122	37.2	18.8	42	-19.4
10/08/2023 11:57	9.1	-1.8	32.7	18.9	61	28.2	18.8	123	38	18.8	41	-19.4
10/08/2023 11:58	9.1	-1.7	32.7	18.9	61	28.2	18.8	122	38.6	18.8	39	-19.4
10/08/2023 11:59	9.1	-1.5	32.8	18.9	62	28.1	18.8	123	39	18.8	38	-19.3
10/08/2023 12:00	9.1	-1.6	32.8	18.9	61	28.2	18.8	122	39.3	18.8	37	-19.4
10/08/2023 12:01	9.1	-1.6	32.9	18.9	61	28.2	18.8	124	39.5	18.8	37	-19.4
10/08/2023 12:02	9.1	-1.6	32.9	18.9	62	28.2	18.8	123	39.7	18.8	38	-19.4
10/08/2023 12:03	9.1	-1.6	33	18.9	62	28.2	18.8	122	39.9	18.8	37	-19.4
10/08/2023 12:04	9.1	-1.5	33	18.9	61	28.2	18.8	122	40	18.8	37	-19.4
10/08/2023 12:05	9.1	-1.5	33	18.9	61	28.2	18.8	122	40.1	18.8	36	-19.4
10/08/2023 12:06	9.1	-1.5	33	18.9	61	28.2	18.8	123	40.3	18.8	36	-19.4
10/08/2023 12:07	9.1	-1.5	33	18.9	61	28.2	18.8	124	40.4	18.8	38	-19.4
10/08/2023 12:08	9.1	-1.5	33.1	18.9	62	28.1	18.8	124	40.5	18.8	38	-19.4
10/08/2023 12:09	9.1	-1.5	33.1	19	62	28.1	18.8	124	40.5	18.8	38	-19.4
10/08/2023 12:10	9.1	-1.5	33.1	18.9	62	28.4	18.8	123	40.5	18.8	37	-19.4
10/08/2023 12:11	9.1	-1.5	33.1	18.9	62	29.7	18.8	121	40.5	18.8	38	-19.4
10/08/2023 12:12	9.1	-1.5	33.1	19	62	31.2	18.8	116	40.6	18.8	39	-19.4
10/08/2023 12:13	9.1	-1.5	33.1	19	62	31.6	18.8	115	40.6	18.8	39	-19.4
10/08/2023 12:14	9.1	-1.5	33.2	19	62	32	18.8	114	40.7	18.8	39	-19.4
10/08/2023 12:15	9.1	-1.5	33.2	19	62	32.4	18.8	113	40.7	18.8	39	-19.4
10/08/2023 12:16	9.1	-1.5	33.2	19	62	32.4	18.8	112	40.7	18.8	37	-19.4
10/08/2023 12:17	9.1	-1.5	33.2	19	62	32.6	18.8	111	40.8	18.8	37	-19.4
10/08/2023 12:18	9.1	-1.5	33.3	19	62	32.8	18.8	112	40.8	18.8	37	-19.3
10/08/2023 12:19	9.1	-1.5	33.3	19	62	33.1	18.8	110	40.8	18.8	37	-19.2
10/08/2023 12:20	9.1	-1.6	33.3	19	62	33.4	18.7	109	40.8	18.8	36	-19
10/08/2023 12:21	9.1	-1.6	33.3	19	62	33.4	18.7	110	40.8	18.8	36	-18.8
10/08/2023 12:22	9.1	-1.6	33.3	19	63	33.5	18.7	109	40.8	18.8	36	-18.6
10/08/2023 12:23	9.1	-1.6	33.4	19	63	33.6	18.7	109	40.8	18.8	36	-18.3
10/08/2023 12:24	9.1	-1.6	33.4	19	62	33.7	18.7	109	40.8	18.8	36	-17.9

10/08/2023 12:25	9.1	-1.7	33.4	19	62	33.7	18.6	109	40.8	18.8	36	-17.5
10/08/2023 12:26	9.1	-1.7	33.4	19	62	33.7	18.6	109	40.8	18.8	36	-17.2
10/08/2023 12:27	9.1	-1.7	33.4	19	62	33.7	18.6	110	40.8	18.8	36	-17
10/08/2023 12:28	9	-1.6	33.4	19	62	33.9	18.6	108	40.9	18.8	36	-16.9
10/08/2023 12:29	9.1	-1.7	33.5	19	62	34.2	18.6	108	40.9	18.8	36	-16.9
10/08/2023 12:30	9.1	-1.7	33.4	19	62	34.5	18.6	110	40.8	18.8	36	-16.9
10/08/2023 12:31	9.1	-1.8	33.3	19	62	34.6	18.6	110	40.8	18.8	36	-16.9
10/08/2023 12:32	9.1	-1.8	33.2	19	62	34.7	18.6	109	40.8	18.8	35	-16.8
10/08/2023 12:33	9.1	-1.7	33.1	19	62	34.8	18.6	110	40.8	18.8	35	-16.8
10/08/2023 12:34	9.1	-1.7	33.2	19	62	34.8	18.5	110	40.7	18.8	35	-16.8
10/08/2023 12:35	9.1	-1.7	33.2	19	62	34.8	18.5	110	40.7	18.8	35	-16.8
10/08/2023 12:36	9.1	-1.8	33.2	19	62	34.9	18.5	110	40.7	18.8	35	-16.8
10/08/2023 12:37	9.1	-1.8	33.1	19	62	34.9	18.5	110	40.6	18.8	35	-16.8
10/08/2023 12:38	9.1	-1.8	33.2	19	63	35	18.5	110	40.6	18.8	35	-16.8
10/08/2023 12:39	9.1	-1.8	33.2	19.1	63	34.9	18.5	110	40.6	18.8	35	-16.8
10/08/2023 12:40	9.1	-1.9	33.2	19.1	63	35	18.5	110	40.6	18.8	35	-16.8
10/08/2023 12:41	9.1	-1.9	33.2	19.1	63	34.9	18.5	110	40.6	18.8	36	-16.8
10/08/2023 12:42	9.1	-1.9	33.1	19.1	63	34.9	18.5	111	40.5	18.8	35	-16.8
10/08/2023 12:43	9.1	-1.9	33.1	19.1	62	35.1	18.5	110	40.5	18.8	36	-16.8
10/08/2023 12:44	9.1	-2	33.1	19.1	62	35.1	18.5	111	40.5	18.8	35	-16.8
10/08/2023 12:45	9.1	-2	33.1	19.1	62	35	18.5	111	40.5	18.8	36	-16.8
10/08/2023 12:46	9.1	-2	33.1	19.1	62	35.1	18.5	109	40.5	18.8	35	-16.8
10/08/2023 12:47	9.1	-2	33.1	19.1	62	35	18.5	110	40.5	18.8	35	-16.8
10/08/2023 12:48	9.1	-2	33.1	19.1	62	35.1	18.5	110	40.5	18.8	35	-16.8
10/08/2023 12:49	9	-1.9	33.1	19.1	62	35	18.5	109	40.4	18.8	36	-16.8
10/08/2023 12:50	9.1	-2.1	33.1	19.1	62	35.2	18.5	109	40.5	18.8	35	-16.8
10/08/2023 12:51	9.1	-2.1	33.1	19.1	62	35.2	18.5	110	40.6	18.8	35	-16.8
10/08/2023 12:52	9.1	-2.1	33	19.1	62	35.2	18.5	109	40.5	18.8	34	-16.8
10/08/2023 12:53	9.1	-2.2	33	19.1	62	35.2	18.5	109	40.5	18.8	35	-16.8
10/08/2023 12:54	9.1	-2.2	33.1	19.1	62	35.2	18.5	110	40.5	18.8	34	-16.8
10/08/2023 12:55	9.1	-2.2	33.1	19.1	62	35.2	18.5	110	40.5	18.8	34	-16.8

10/08/2023 12:56	9.1	-2.2	33	19.1	62	35.2	18.5	110	40.5	18.8	35	-16.8
10/08/2023 12:57	9.1	-2.2	33.1	19.1	62	35.3	18.5	110	40.5	18.9	34	-16.8
10/08/2023 12:58	9.1	-2.3	33	19.1	62	35.2	18.5	109	40.5	18.8	34	-16.8
10/08/2023 12:59	9.1	-2.3	33.1	19.1	62	35.2	18.5	110	40.5	18.8	34	-16.8
10/08/2023 13:00	9.1	-2.3	33.1	19.1	62	35.3	18.5	110	40.5	18.8	34	-16.8
10/08/2023 13:01	9.1	-2.3	33.1	19.1	62	35.3	18.5	110	40.4	18.8	34	-16.8
10/08/2023 13:02	9.1	-2.3	33.1	19.1	62	35.2	18.5	109	40.3	18.8	34	-16.8
10/08/2023 13:03	9.1	-2.4	33.1	19.1	62	35.2	18.5	109	40.1	18.8	34	-16.9
10/08/2023 13:04	9.1	-2.5	33.2	19.1	63	35.2	18.5	109	40	18.8	34	-16.8
10/08/2023 13:05	9.1	-2.6	33.2	19.1	63	35.3	18.5	110	40.2	18.8	34	-16.9
10/08/2023 13:06	9.1	-2.6	33.2	19.1	63	35.3	18.5	109	40.3	18.8	35	-16.9
10/08/2023 13:07	9.1	-2.6	33.2	19.2	62	35.3	18.5	110	40.3	18.8	34	-16.9
10/08/2023 13:08	9.1	-2.6	33.2	19.2	63	35.3	18.5	110	40.2	18.8	35	-16.9
10/08/2023 13:09	9.1	-2.7	33.1	19.2	62	35.3	18.5	109	40	18.8	34	-16.9
10/08/2023 13:10	9.1	-2.7	33.1	19.2	62	35.4	18.5	109	39.8	18.9	35	-16.9
10/08/2023 13:11	9.1	-2.7	33.1	19.2	62	35.4	18.5	109	39.9	18.9	35	-16.9
10/08/2023 13:12	9.1	-2.7	33.1	19.2	62	35.4	18.5	110	40	18.9	35	-16.9
10/08/2023 13:13	9.1	-2.7	33.1	19.2	62	35.4	18.5	109	40	18.9	35	-16.9
10/08/2023 13:14	9.1	-2.7	33.1	19.2	62	35.4	18.5	109	40	18.9	34	-16.9
10/08/2023 13:15	9.1	-2.8	33.2	19.2	62	35.4	18.5	109	40	18.9	35	-16.9
10/08/2023 13:16	9.1	-2.8	33.2	19.2	62	35.5	18.5	110	40	18.9	34	-16.9
10/08/2023 13:17	9.1	-2.8	33.1	19.2	62	35.5	18.5	110	40	18.9	34	-16.9
10/08/2023 13:18	9.1	-2.8	33.1	19.2	62	35.5	18.5	110	40	18.9	34	-16.9
10/08/2023 13:19	9.1	-2.8	33.1	19.2	62	35.4	18.5	109	40	18.9	35	-16.9
10/08/2023 13:20	9.1	-2.9	33.1	19.2	62	35.4	18.5	110	40	18.9	34	-16.9
10/08/2023 13:21	9.1	-3	33.1	19.2	62	35.4	18.5	110	40	18.9	35	-16.9
10/08/2023 13:22	9.1	-3	33.1	19.2	61	35.4	18.5	110	40	18.9	35	-16.9
10/08/2023 13:23	9.1	-3	33.1	19.2	61	35.4	18.5	110	40	18.9	34	-16.9
10/08/2023 13:24	9.1	-3.1	33.1	19.2	62	35.5	18.5	110	40.1	18.9	34	-16.9
10/08/2023 13:25	9.1	-3.1	33.1	19.2	62	35.5	18.5	110	40.1	18.9	35	-16.9
10/08/2023 13:26	9.1	-3.1	33.1	19.2	62	35.5	18.5	110	40	18.9	34	-16.9

10/08/2023 13:27	9.1	-3.1	33.1	19.2	61	35.5	18.5	111	40	18.9	35	-16.9
10/08/2023 13:28	9.1	-3.1	33.1	19.2	63	35.5	18.5	110	40	18.9	36	-16.9
10/08/2023 13:29	9.1	-3.1	33.2	19.2	62	35.5	18.5	110	40	18.9	35	-16.9
10/08/2023 13:30	9.1	-3.1	33.2	19.2	62	35.6	18.5	109	40.8	18.9	35	-16.8
10/08/2023 13:31	9.1	-3.1	33.2	19.2	62	35.5	18.5	111	41.2	18.9	36	-16.8
10/08/2023 13:32	9.1	-3.1	33.3	19.2	61	35.5	18.5	110	41.4	18.9	34	-16.8
10/08/2023 13:33	9.1	-3.1	33.3	19.2	61	35.5	18.5	109	41.6	18.9	34	-16.8
10/08/2023 13:34	9.1	-3.1	33.3	19.2	61	35.5	18.5	109	41.6	18.9	34	-16.8
10/08/2023 13:35	9.1	-3.1	33.3	19.2	61	35.5	18.6	109	41.6	18.9	34	-16.8
10/08/2023 13:36	9.1	-3.2	33.3	19.2	61	35.5	18.6	109	41.6	18.9	34	-16.8
10/08/2023 13:37	9.1	-3.3	33.3	19.2	61	35.5	18.5	107	41.4	18.9	35	-16.8
10/08/2023 13:38	9.1	-3.3	33.3	19.3	61	35.5	18.5	107	41.4	18.9	35	-16.8
10/08/2023 13:39	9.1	-3.4	33.3	19.2	61	35.5	18.5	107	41.4	18.9	35	-16.8
10/08/2023 13:40	9.1	-3.4	33.4	19.3	61	35.5	18.5	107	41.4	18.9	36	-16.8
10/08/2023 13:41	9.1	-3.4	33.3	19.3	61	35.5	18.5	107	41.4	18.9	35	-16.8
10/08/2023 13:42	9.1	-3.4	33.3	19.3	61	35.5	18.5	107	41.4	18.9	35	-16.8
10/08/2023 13:43	9.1	-3.4	33.3	19.3	61	35.5	18.5	108	41.4	18.9	35	-16.8
10/08/2023 13:44	9.1	-3.5	33.3	19.3	61	35.5	18.5	107	41.4	18.9	35	-16.8
10/08/2023 13:45	9.1	-3.5	33.3	19.3	61	35.5	18.5	107	41.4	18.9	36	-16.8
10/08/2023 13:46	9.1	-3.5	33.3	19.3	61	35.4	18.5	107	41.4	18.9	36	-16.8
10/08/2023 13:47	9.1	-3.6	33.3	19.3	61	35.4	18.5	107	41.3	19	36	-16.8
10/08/2023 13:48	9.1	-3.6	33.3	19.3	61	35.5	18.5	107	41.3	19	36	-16.8
10/08/2023 13:49	9.1	-3.6	33.3	19.3	61	35.5	18.5	107	41.3	19	36	-16.9
10/08/2023 13:50	9.1	-3.6	33.3	19.3	61	35.5	18.5	107	41.3	19	36	-16.9
10/08/2023 13:51	9.1	-3.7	33.3	19.3	61	35.5	18.5	107	41.3	19	36	-16.9
10/08/2023 13:52	9.1	-3.7	33.3	19.3	61	35.5	18.5	107	41.3	19	36	-16.9
10/08/2023 13:53	9.1	-3.7	33.4	19.3	61	35.5	18.5	107	41.3	19	35	-16.9

w